

SIGNALING DYNAMICS IN *PSEUDOMONAS SYRINGAE* PV. TOMATO DC3000

A Dissertation

Presented to the Faculty of the Graduate School

of Cornell University

In Partial Fulfillment of the Requirements for the Degree of

Doctor of Philosophy

by

Max Fishman

May 2018

© 2018 Max Fishman

SIGNALING DYNAMICS IN *PSEUDOMONAS SYRINGAE* PV. TOMATO DC3000

Max Fishman, Ph. D.

Cornell University 2018

Pseudomonas syringae pv. tomato DC3000 (*Pto*) is thought to encounter disparate environments during epiphytic and endophytic growth. In order to be successful during pathogenesis, *Pto* must recognize when it enters the leaf apoplast and then regulate the appropriate genes. In bacteria, two-component systems (TCSs) commonly sense environmental changes and modulate gene regulation to suit that environment. The leaf apoplast is relatively abundant in Ca^{2+} in comparison to the leaf surface. The TCS, CvsSR, in *Pto* is a regulatory system that is induced by Ca^{2+} and regulates virulence of *Pto* in tomato and *Arabidopsis*. The global virulence regulators *hrpR*, *hrpS*, and *hrpL* are among the genes that CvsSR regulate. Its role in virulence is partially explained through its regulation of these genes and also through its regulation of the gene PSPTO_5255, which encodes a carbonic anhydrase. Deletion of PSPTO_5255 reduces virulence of *Pto* on tomato and also delays the hypersensitive response caused by *Pto* on *Nicotiana benthamiana*. PSPTO_5255 was a previously uncharacterized virulence gene in *Pto* and the mechanism by which it affects virulence is still unclear.

Bacteria may induce precipitation of calcium upon exposure to increases in external Ca^{2+} concentration. Several *Pseudomonas* species and strains induce precipitation of calcium phosphate in the external environment surrounding the bacterial colony. Calcium phosphate precipitation on the surface of bacterial cells was variable among *Pseudomonas* strains. *Pto* is among the strains that does not normally

precipitate calcium phosphate on the surface of cells. Multiple genes are involved in *Pto* calcium phosphate precipitation, including ones that suppress surface-associated calcium phosphate precipitation in *Pto*. The genes *cvsS* and *cvsR* are among the genes that suppress surface-associated calcium phosphate precipitation in *Pto*. In the $\Delta cvsS$ and $\Delta cvsR$ strains, this process is partially dependent on the CvsSR regulated genes PSPTO_5255 and PSPTO_5256. Constitutive expression of PSPTO_5255 and PSPTO_5256 in the $\Delta cvsS$ and $\Delta cvsR$ strains suppress surface-associated calcium phosphate precipitation. This suggests that *Pto* utilizes secretion of bicarbonate or carbonic acid to keep calcium phosphate from accumulating on the surface of cells.

BIOGRAPHICAL SKETCH

Max Fishman was born on September 21st, 1986 in Oakland, California. He spent the early years of his childhood in the California bay area before moving to San Diego, California with his family when he was 11. After living in San Diego for seven years he moved back to the California bay area to pursue a Bachelor's Degree at the University of California, Berkeley. It was at UC Berkeley where he first engaged in and enjoyed academic research. He graduated from UC Berkeley in 2009 with a Bachelor's of Science in Chemical Biology.

Max's informal education into the lives of plants began at home while caring for his family's fruit trees with his father. This education later found firm footing during the time he worked on a farm after he graduated college. It was in these environments where he first engaged with plant pathogens.

To my father, mother, brother, and sister who have all been supportive and
encouraging.

To my friends who have made my time in Ithaca memorable and enjoyable.

ACKNOWLEDGMENTS

I would like to thank my advisor Melanie Filiatrault for providing me support and guidance throughout my degree. Melanie has allowed me to pursue ideas and propose experiments that have allowed me to dabble in physical chemistry, explore biochemistry, and immerse myself in molecular biology and plant pathology. I would also like to thank past and present members of the Filiatrault lab and Swingle lab that have been pleasure to work with for the past several years. In particular, I would like to thank Bronwyn Butcher for helping teach me the ins and outs of working with *Pseudomonas syringae* pv. tomato DC3000 when I first started in the Filiatrault lab. I would also like to thank Paul Stodghill for his tremendous help in analyzing the RNA-seq and ChIP-seq data that I generated. Lastly, my conversations with Eric Markel were engaging and enlightening. His presence in the lab has been missed.

The plant pathology and plant-microbe biology section has been a supportive and helpful community for me throughout my time at Cornell. Members of the Collmer lab have always been willing and able to help me when I come in need of a *Pseudomonas* strain from their strain collection. Hai Lei Wei and Suma Chakravarthy in particular were extremely helpful whenever I came to them with a question or a problem. Advice from Fabio Rinaldi of the Bogdanove lab was essential for the success of various biochemical experiments that I performed throughout my tenure. Several members of the Cornell community outside the plant pathology and plant-microbe biology section have also been ever so helpful in introducing and training me in previously unknown techniques. John Grazul from CCMR has been patient and helpful in all things relating to electron microscopy. Jenny Russ Kunitake introduced me to Raman spectroscopy and was helpful with initial analysis of my samples.

My work has been partially funded by the United States Department of Agriculture Agricultural Research Service (USDA-ARS).

Lastly, I would like to thank my friends at Cornell who have made my time here fun and memorable and my family who have been supportive of me throughout my degree.

TABLE OF CONTENTS

CHAPTER 1	1
THE ROLE CA²⁺ PLAYS IN PSEUDOMONAS SYRINGAE PV. TOMATO DC3000 SIGNALING DYNAMICS	1
Introduction to <i>Pseudomonas syringae</i> and plant-pathogen interactions	1
Introduction to two-component systems of bacteria	3
Ca ²⁺ signaling in bacteria	4
Bacterial carbonic anhydrases	6
Microbially induced calcium precipitation and calcium dissolution	7
Dual RNA-seq during host-microbe interactions	9
Thesis overview	11
CHAPTER 2	12
THE CA²⁺ INDUCED TWO-COMPONENT SYSTEM, CVSSR, REGULATES THE TYPE III SECRETION SYSTEM AND THE EXTRACYTOPLASMIC FUNCTION SIGMA-FACTOR ALGU IN <i>PSEUDOMONAS SYRINGAE</i> PV. TOMATO DC3000	12
Abstract	12
Introduction	13
Results	17
Discussion	58
Materials and Methods	66
Acknowledgements	85
CHAPTER 3	86
CVSSR REGULATES PREVENTION OF SURFACE-ASSOCIATED CALCIUM PRECIPITATION IN <i>PSEUDOMONAS SYRINGAE</i> PV. TOMATO DC3000	86
Abstract	86
Introduction	87
Materials and Methods	89
Results	97
Discussion	118
Acknowledgements	123
CHAPTER 4	124
PSPTO_5255 IS A NOVEL VIRULENCE ASSOCIATED GENE IN <i>PSEUDOMONAS SYRINGAE</i> PV. TOMATO DC3000	124
Abstract	124
Introduction	125
Materials and Methods	127
Results	134

Discussion	148
Acknowledgements	152
CHAPTER 5	154
CALCIUM PRECIPITATION IN <i>PSEUDOMONAS</i>: DIFFERENCES, COMMONALITIES, AND THE GENES INVOLVED	154
Abstract	154
Introduction	155
Results	157
Discussion	197
Materials and Methods	208
Acknowledgements	213
CHAPTER 6	214
UNRAVELING THE INTERACTION BETWEEN <i>PSEUDOMONAS SYRINGAE</i> PV. TOMATO DC3000 AND <i>NICOTIANA BENTHAMIANA</i> USING DUAL-RNA SEQ	214
Abstract	214
Background	215
Results	219
Discussion	271
Materials and Methods	276
Acknowledgements	280
CHAPTER 7	281
CONCLUSIONS AND FUTURE DIRECTIONS	281
Introduction	281
Activators of CvsSR	281
Identifying the role of CvsSR <i>in planta</i>	282
Identifying the function of PSPTO_5255 in <i>Pto</i>	283
Calcium precipitation and its role in <i>Pto</i>	283
Dual RNA-seq	284
REFERENCES	288

LIST OF FIGURES

Figure 2.1.....	18
Figure 2.2.....	20
Figure 2.3.....	21
Figure 2.4.....	24
Figure 2.5.....	26
Figure 2.6.....	29
Figure 2.7.....	30
Figure 2.8.....	31
Figure 2.9.....	33
Figure 2.10.....	43
Figure 2.11.....	44
Figure 2.12.....	46
Figure 2.13.....	47
Figure 2.14.....	48
Figure 2.15.....	50
Figure 2.16.....	51
Figure 2.17.....	53
Figure 2.18.....	54
Figure 2.19.....	56
Figure 2.20.....	57
Figure 2.21.....	59
Figure 2.22.....	60
Figure 3.1.....	90
Figure 3.2.....	98
Figure 3.3.....	100
Figure 3.4.....	101
Figure 3.5.....	102
Figure 3.6.....	104
Figure 3.7.....	106
Figure 3.8.....	107
Figure 3.9.....	108
Figure 3.10.....	112
Figure 3.11.....	114
Figure 3.12.....	116
Figure 3.13.....	117
Figure 3.14.....	120

Figure 4.1.....	135
Figure 4.2.....	137
Figure 4.3.....	138
Figure 4.4.....	140
Figure 4.5.....	141
Figure 4.6.....	143
Figure 4.7.....	144
Figure 4.8.....	146
Figure 4.9.....	147
Figure 4.10.....	149
Figure 5.1.....	158
Figure 5.2.....	160
Figure 5.3.....	163
Figure 5.4.....	166
Figure 5.5.....	167
Figure 5.6.....	168
Figure 5.7.....	169
Figure 5.8.....	171
Figure 5.9.....	172
Figure 5.10.....	173
Figure 5.11.....	178
Figure 5.12.....	181
Figure 5.13.....	183
Figure 5.14.....	185
Figure 5.15.....	187
Figure 5.16.....	188
Figure 5.17.....	198
Figure 5.18.....	200
Figure 6.1.....	258
Figure 6.2.....	267
Figure 6.3.....	270

LIST OF TABLES

Table 2.1	23
Table 2.4	34
Table 2.5	39
Table 2.6	40
Table 2.7	67
Table 2.8	72
Table 3.1	92
Table 3.2	93
Table 3.3	111
Table 4.1	128
Table 4.2	129
Table 5.1	192
Table 5.2	203
Table 5.3	207
Table 5.4	211
Table 6.2	221
Table 6.3	226
Table 6.4	227
Table 6.5	228
Table 6.6	230
Table 6.7	232
Table 6.8	234
Table 6.9	235
Table 6.10	236
Table 6.11	237
Table 6.12	238
Table 6.13	240
Table 6.14	246
Table 6.15	247
Table 6.17	253
Table 6.18	263
Table 7.2	287

CHAPTER 1

THE ROLE Ca^{2+} PLAYS IN PSEUDOMONAS SYRINGAE PV. TOMATO DC3000 SIGNALING DYNAMICS

Introduction to *Pseudomonas syringae* and plant-pathogen interactions

Pseudomonas syringae is a foliar hemibiotrophic bacterial plant pathogen that infects a large variety of plants (1). The species is divided into more than 50 pathovars to designate the host range of each *P. syringae* pathovar (1). Typical symptoms caused by *P. syringae* are foliar chlorosis or necrosis and, in the case of woody plants, cankers on trunks or branches (2). *P. syringae* pv. tomato causes bacterial speck of tomato and is further classified into several strains. The most well studied of these strains is *P. syringae* pv. tomato DC3000 (*Pto*) because it can infect the model plant *Arabidopsis thaliana* (3). Deletion of the type III effector (T3E) *hopQ1-1* from the genome of *Pto* expands the host range of *Pto* to *Nicotiana benthamiana* as well (4). The infection cycle for *Pto* begins as an epiphyte on the surface of leaves. Under the appropriate conditions it travels through stomata or wounds into the leaf apoplast where it colonizes the plant, replicates, and causes disease.

Pto must fulfill several conditions in order to properly colonize a host. Those conditions include *Pto* being able to defend against and overcome the plant defense response. Plants have a two-tiered immune response to pathogens, with the first line of defense being called pattern-triggered immunity (PTI) and the second line of defense being called effector triggered immunity (ETI) (5). PTI is triggered by pattern

recognition receptors (PRRs) that recognize microbial associated molecular patterns (MAMPs) that are common to all microbes and were originally characterized in pathogens (6). In the case of *P. syringe*, MAMPs include flagellin, elongation factor Tu, lipid A, and cold-shock protein (7-10). The initiation of PTI is characterized by the rapid release of reactive oxygen species (ROS), callose deposition, increased expression of defense related genes like *PR-1*, stomatal closure, and the release of phytoalexins (11). *Pto* initially defends against PTI through the expression of various genes, including ROS detoxifying genes like catalase (12). It fully subverts PTI through the deployment of T3Es using the type III secretion system (T3SS) and secretion of the phytotoxin coronatine (3). There are 36 known T3E genes, including several pseudogenes, within the *Pto* genome (13). T3Es can be recognized by proteins coded for by plant disease resistance genes (*R*-genes). A majority of the proteins coded for by *R*-genes are nucleotide binding leucine rich repeat proteins (NLRs) (6). When an effector is directly or indirectly recognized by an NLR, ETI is triggered. ETI is characterized by localized plant cell death called the hypersensitive response (HR) (5). When ETI occurs, this is called a non-compatible interaction. Alternatively, successful infection by a plant pathogen is called a compatible interaction.

T3Es and the T3SS are regulated by the extra cytoplasmic function (ECF) sigma factor, HrpL (14). HrpL is regulated by the sigma factor RpoN and the helper proteins HrpR and HrpS (15). *Pto* relies on particular environmental conditions to activate HrpL and produce the T3SS and T3Es. Certain aspects of the plant apoplast have been replicated *in vitro* to produce medium that stimulates HrpL and production of the T3SS (16, 17). Lowering the pH of the medium to 5.0, adding fructose as a

carbon source, and also adding Fe^{3+} to the medium stimulate *hrpL* expression and production of the T3SS. However, even when using medium that stimulates production of the T3SS most T3Es are not secreted (18). Identifying transcriptional regulators or post-transcriptional regulators that are upstream of HrpL would help in deciphering conditions *Pto* requires for T3SS production and T3E deployment. These upstream regulators are likely to be stimulated or induced by environmental conditions unique to the plant leaf apoplast.

Introduction to two-component systems of bacteria

Bacteria have developed signaling transduction systems called two-component systems (TCSs) that are used to sense and respond to changes in the environment (19). TCSs are normally composed of a transmembrane histidine kinase (HK) and a cytoplasmic response regulator (RR) (19). When the HK senses a specific signal, it will autophosphorylate a conserved histidine residue in the cytoplasmic portion of the HK and then transfer that phosphate to a conserved aspartate residue on a RR recognition domain (19). HKs can respond to a single signal or to multiple signals. In bacteria, the HK EnvZ solely senses changes in environmental osmolarity and the HK PhoB solely senses when environmental phosphate levels are low (20, 21). In comparison, the HK PhoP senses Ca^{2+} and Mg^{2+} concentrations, the presence of cationic antimicrobial peptides, and acidic conditions and the HK ColS senses Fe^{3+} , Cd^{2+} , Zn^{2+} , and Mn^{2+} (22, 23). RRs have a conserved recognition domain but can vary in their output domain. The most common output domain is a DNA-binding output domain, however other output domains such as enzymatic domains, RNA-binding domains, or protein binding domains have been described (24). RR DNA-binding

domains fall into several different families, including OmpR family RRs. OmpR family RRs typically bind direct repeats as homodimers but can bind as monomers as well (25, 26). The genes that DNA-binding RRs regulate are specific to the signal that activates the HK and reflect the adaptations bacteria need to make to adapt to a given condition. The TCS PmrAB in *Salmonella enterica* senses Fe^{3+} , but is also induced by the TCS PhoPQ and the genes that PmrAB regulates will differ depending on how it is activated (22).

The *Pto* genome encodes 69 HKs and 95 RRs and many of these HKs and RRs have yet to be characterized (27). The few TCSs in *Pto* that have been characterized are involved in positively or negatively regulating virulence factors. Positive regulators include the thermo-sensing non-canonical TCS CorSRP and the TCS GacSA (28, 29). CorSRP regulates coronatine production and *hrpL* transcription and GacSA regulates production of the T3SS and *hrpR* and *hrpS* transcription. Characterized negative regulators of *Pto* virulence factors are the TCSs RhpRS and a light activated LOV-HK (30, 31). Both of these TCSs negatively regulate the T3SS in *Pto*. Chapter 2 of this thesis describes the characterization of a TCS in *Pto* called CvsSR, which is induced by Ca^{2+} and involved in regulating virulence.

Ca^{2+} signaling in bacteria

Internal and external Ca^{2+} concentrations in bacteria can differ by orders of magnitude. Much like eukaryotic cells the internal $[\text{Ca}^{2+}]$ in bacteria is kept at the nanomolar to low micromolar level (32). However, the periplasm of gram negative bacteria $[\text{Ca}^{2+}]$ is the same as or can be higher than the $[\text{Ca}^{2+}]$ or the external environment (32-34). Changes in cytoplasmic $[\text{Ca}^{2+}]$ regulates a variety of bacterial

signaling events. In *Escherichia coli* $[Ca^{2+}]$ regulates chemotaxis and is involved in regulating cell division (35). Changes in Ca^{2+} homeostasis are used by *Bacillus subtilis* during its response to hydrogen peroxide (36). Thus, internal $[Ca^{2+}]$ controls signaling events involved in some of the core functions of bacteria

Changes in external $[Ca^{2+}]$ are also important signals for bacteria and can signal pathogenic bacteria to produce various virulence factors. Several animal pathogens, including *Vibrio parahaemolyticus*, *Yersinia pestis*, and *Pseudomonas aeruginosa*, use low environmental $[Ca^{2+}]$ as a signal for production of the T3SS (37-39). *P. aeruginosa* also increases alginate production, forms thicker biofilms, and releases several virulence factors when grown in medium supplemented with 10 mM Ca^{2+} (40). However, in the case of plant pathogens, little is known about the how external $[Ca^{2+}]$ affects virulence factor production. During infection, hemibiotrophic bacterial plant pathogens live outside cells in the apoplast. The apoplast can have as much as 10 mM Ca^{2+} (41). The apoplastic $[Ca^{2+}]$ is dynamic and can change upon pathogen infection. The $[Ca^{2+}]$ of *Phaeseolus vulgaris* increases around four-fold during compatible interaction with *P. syringae* pv. *phaeseolicola* RJ3 and seven-fold during an incompatible interaction with *P. syringae* pv. *phaeseolicola* 1302a (42). Likewise $[Ca^{2+}]$ in leaves of tobacco increases 13% during infection with *Xylella fastidiosa* over a course of days (43). Such high and changing $[Ca^{2+}]$ in the apoplast make it plausible that *Pto* could use $[Ca^{2+}]$ as a signal for inducing expression and production of virulence factors in *Pto*. This thesis provides evidence for $[Ca^{2+}]$ concentrations at 5 mM or higher as an inducer of virulence factors in *Pto*. This is mainly demonstrated in chapter two and chapter four through the characterization of

the Ca²⁺-induced TCS, CvsSR, and the characterization of the CvsSR regulated carbonic anhydrase PSPTO_5255.

Bacterial carbonic anhydrases

Carbonic anhydrases are metalloenzymes that catalyze the hydration of CO₂ to H⁺ and HCO₃⁻ and vice versa (44). These enzymes are found in all forms of biological life including bacteria. There are currently six known families of carbonic anhydrases that have independently evolved (45, 46). Bacterial genomes typically encode genes for the production of α and β -carbonic anhydrases (47). Carbonic anhydrases are involved in pH homeostasis, metabolism, fatty acid biosynthesis in bacteria and CO₂ accumulation in cyanobacteria and carboxysome-bearing chemolithotrophic bacteria (48-51). Deletion or inhibition of carbonic anhydrases in *E. coli*, *Streptococcus pneumoniae*, *Ralstonia eutropha*, *Mycobacterium tuberculosis*, and *P. aeruginosa* results in a growth defect under atmospheric conditions (47, 48, 52-54). This growth defect can typically be resolved if carbonic anhydrase mutants are grown in high CO₂ environments.

Carbonic anhydrases can have specific functions in bacteria that are independent of overall metabolism. One of the first carbonic anhydrases characterized was the cyanate inducible carbonic anhydrase CynT in *E. coli* that is specifically used during cyanate degradation to replenish bicarbonate levels in the cell (55). Carbonic anhydrases are also utilized by several pathogenic bacteria during pathogen-host interactions. *Helicobacter pylori* use carbonic anhydrases to maintain a neutral intracellular pH during growth in the stomach (56). Bicarbonate is used by *Vibrio cholerae* as a signal for virulence gene expression and intracellular levels of

bicarbonate used for signaling are produced by carbonic anhydrases (57). Carbonic anhydrases are also potential virulence factors in plant pathogens. *Pectobacterium carotovorum* encodes an α -carbonic anhydrase that is a putative virulence factor (58). The *Phytophthora infestans* genome encodes several secreted carbonic anhydrases that are considered putative virulence factors (59). The genome of *Pto* encodes genes for three different β -carbonic anhydrases, PSPTO_5255, PSPTO_0994, and PSPTO_1340 (60). Chapter four of this thesis will identify and characterize PSPTO_5255 as a virulence-associated gene in *Pto*.

Microbially induced calcium precipitation and calcium dissolution

Precipitation of calcium is one reaction bacteria can have when encountering high environmental $[Ca^{2+}]$. Calcium is normally precipitated as either calcium carbonate or calcium phosphate by bacteria. This is typically thought to be through a passive process called microbially induced calcium precipitation (MICP) that produces amorphous, indistinct calcium precipitate (61). The form of calcium that bacteria precipitate during MICP depends on both the bacterial strain and growth conditions (62-64). In the case of calcium phosphate precipitation, bacterial release of phosphate from internal stores of polyphosphate is thought to be partially responsible for calcium phosphate precipitation (65). Other studies have pointed to specific enzymes having a role in microbial calcium phosphate precipitation. In certain bacteria alkaline phosphatase play a role in microbial calcium phosphate precipitation (66). In a *Serratia* sp. an acid phosphatase functions in microbial calcium phosphate precipitation (67). Overall, the exact mechanism behind microbial calcium phosphate precipitation is still up for debate. Part of the reason for the poor understanding of

microbial calcium phosphate precipitation is that little is known about the genetic regulation controlling microbial calcium phosphate precipitation. Chapter five of this thesis increases the knowledge of calcium precipitation in the genus *Pseudomonas* by characterizing calcium precipitation in multiple *Pseudomonas* species and also increases the knowledge of the genetic regulation involved in microbial calcium precipitation by identifying genes in *Pto* that are involved in regulating calcium precipitation.

In contrast to MICP, microbial calcium dissolution is the act through which microbes dissolve calcium precipitates or minerals. Calcium dissolution has several different names, one of which is phosphate solubilization. Phosphate solubilization occurs when microbes, commonly bacteria, dissolve mineral phosphates (like calcium phosphate) by secreting enzymes, like acid phosphatases, or specific compounds (68). During phosphate solubilization microbes will commonly lower the pH of medium *in vitro* and suggests that organic acids, like acetic acid, malic acid, oxalic acid and gluconic acid, rather than organic anions are secreted by microbes when solubilizing mineral phosphate (69). Gluconic acid is one of the most common organic acids secreted by bacteria during phosphate solubilization and is produced through the oxidation of glucose by pyrroloquinolone quinone (PQQ) dependent glucose dehydrogenase (70, 71). PQQ is best utilized by glucose dehydrogenase by the addition of a metal cation cofactor like Ca^{2+} (72). Phosphate solubilization has been demonstrated in a large number of bacteria, including various *Pseudomonas* species (71, 73). The extent of a bacteria's ability to solubilize calcium phosphate varies according to different species and strains and also the environment. Environments

limited in phosphate or that incorporate glucose as a carbon source increase phosphate solubilization activity among microbes (70, 73). Microbes can also use inorganic acids to solubilize calcium phosphate, but inorganic acids are less efficient than organic acids at solubilizing calcium phosphate (69). Carbonic anhydrases catalyze the hydration of CO₂ to a proton and bicarbonate and are utilized by fungi to dissolve limestone (74, 75). There is evidence that bacteria likely use carbonic anhydrases to dissolve calcium minerals as both *Bacillus mucilaginosus* and *Brevibacterium linens* BS258 upregulate expression of genes that code for carbonic anhydrases during calcium dissolution (76, 77). Chapters three and four of this thesis will include characterization of the carbonic anhydrase, PSPTO_5255, in *Pto* and provide supporting evidence for its role in calcium dissolution and virulence.

Dual RNA-seq during host-microbe interactions

The use of next generation sequencing on an organism's transcriptional profile (RNA-seq) has allowed scientists to map transcriptional changes in a multitude of organisms grown under specific conditions. In the case of pathogens, RNA-seq has typically been employed under *in vitro* conditions that mimic a part of the host environment. More recently, dual RNA-seq has been employed to profile transcriptional changes of animal hosts and a pathogen over a designated time period of infection (78). Though many of these studies are descriptive in nature they offer considerable insight into host-pathogen interactions. Dual RNA-seq of *Chlamydia trachomatis* and infected epithelial cells led to new insights into metabolic behavior of *C. trachomatis* during infection and identified a dampening of immune signaling in epithelial cells that had previously been unseen during a microarray study (79).

Likewise, dual RNA-seq of *H. influenzae* and infected mucosal epithelium over the course of 72 hours led to tremendous insight into the genes and regulatory small RNAs (sRNAs) *H. influenzae* uses during host infection (80). Dual RNA-seq of *S. enterica* serovar Typhimurium and infected host cells led to identification of a novel sRNA that regulates virulence (81). As is the case with animal pathogens, dual RNA-seq of plant pathogenic bacteria and their hosts could lead to tremendous insight into the genes involved in the infection cycle.

Dual RNA-seq with plant pathogens, especially bacterial plant pathogens, is technically challenging. Bacterial plant pathogens live extracellularly in the apoplast and produce far less RNA than their host plants. Enrichment of bacterial pathogen RNA during dual RNA-seq of animal hosts and pathogens has mainly relied on techniques optimized for cell culture and intracellular pathogens (78). These techniques cannot be utilized for dual RNA-seq of plant hosts and bacterial pathogens. There have been studies on the bacterial transcriptome during plant infection 24 to 72 hours post inoculation (82, 83). These studies have revealed novel insight into the transcriptome of plant pathogenic bacteria during infection. However, they have focused only on the pathogen and have not captured early timepoints of infection. The first few hours after inoculation of a plant by a pathogen could be considered the most important for understanding gene regulation of bacterial plant pathogens involved in adapting to the apoplast and overcoming PTI. A recent paper has investigated the *Pto* transcriptome at six hours post inoculation during *Pto-Arabidopsis* interactions in order to better understand how *Pto* responds during early timepoints to compatible or incompatible interactions and PTI induced plants (84). Chapter six of this thesis

describes notable findings from dual RNA-seq between the $\Delta hopQ1-1$ *Pto* strain and *N. benthamiana* comparing the first hour and sixth hour of infection. This method allows one to identify genes in *Pto* and *N. benthamiana* that are simultaneously differentially regulated at early timepoints during a compatible interaction.

Thesis overview

This thesis increases current knowledge on conditions *Pto* senses and uses in the plant apoplast to induce transcription of *hrpL* and other virulence factors. This information will mainly be found in chapter two of this thesis through the characterization of the Ca^{2+} induced two-component system CvsSR in *Pto*. Additional insight into genes necessary for induction of the T3SS were made during characterization of the carbonic anhydrase PSPTO_5255 in chapter four of this thesis. Characterization of calcium precipitation across several *Pseudomonas* species and identification of genes in *Pto* involved in calcium precipitation and dissolution are described in chapter three and chapter five of this thesis. Lastly, this thesis increases the knowledge of genes found to be differentially expressed in *Pto* at early points of infection using high-throughput transcriptional sequencing by next generation technologies of *Pto* and a host at the same time (dual RNA-seq).

CHAPTER 2

THE Ca^{2+} INDUCED TWO-COMPONENT SYSTEM, CVSSR, REGULATES THE TYPE III SECRETION SYSTEM AND THE EXTRACYTOPLASMIC FUNCTION SIGMA-FACTOR ALGU IN *PSEUDOMONAS SYRINGAE* PV. TOMATO DC3000¹

Abstract

Two-component systems (TCSs) of bacteria regulate many different aspects of the bacterial life cycle including pathogenesis. Most TCSs remain uncharacterized with no information about the signal(s) or regulatory targets and/or role in bacterial pathogenesis. Here, we characterized a TCS in the plant-pathogenic bacterium *Pseudomonas syringae* pv. *tomato* DC3000 (*Pto*) composed of the histidine kinase, CvsS, and the response regulator, CvsR. CvsSR is necessary for virulence of *Pto*, since ΔcvsS and ΔcvsR strains produced fewer symptoms and demonstrated reduced growth on multiple hosts as compared to WT. We discovered that the expression of *cvsSR* is induced by Ca^{2+} concentrations found in leaf apoplastic fluid. Thus, Ca^{2+} can be added to the list of signals that promote pathogenesis of *Pto* during host colonization. Through chromatin immunoprecipitation followed by next generation sequencing (ChIP-seq) and global transcriptome analysis (RNA-seq) we discerned the CvsR regulon. CvsR directly activated expression of the type III secretion system

¹ Maxwell R. Fishman, Johnson Zhang, Paul Stodghill, Melanie J. Filiatrault. The Ca^{2+} induced two-component system, CvsSR, regulates the type III secretion system and the extracytoplasmic function sigma factor AlgU in *Pseudomonas syringae* pv. *tomato* DC3000. *Journal of Bacteriology* 200:e00538-00517

regulators, *hrpR* and *hrpS*, that regulates *Pto* virulence in a type III secretion system dependent manner. CvsR also indirectly repressed transcription of the extracytoplasmic sigma factor *algU* and production of alginate. Phenotypic analysis determined that CvsSR inversely regulated biofilm formation, swarming motility, and cellulose production in a Ca^{2+} -dependent manner. Overall, our results show that CvsSR is a key regulatory hub critical for interaction with host plants.

Importance

Pathogenic bacteria must be able to react and respond to the surrounding environment, make use of available resources, and avert or counter host immune responses. Often, these abilities rely on two-component systems (TCS) composed of interacting proteins that modulate gene expression. We identified a TCS in the plant-pathogenic bacterium *Pseudomonas syringae* that responds to the presence of calcium, which is an important signal during the plant defense response. We showed that when *P. syringae* is grown in the presence of calcium this TCS regulates expression of disease contributing factors. Overall, our results provide a better understanding of how bacterial pathogens respond to plant signals and control systems necessary for eliciting disease.

Introduction

Pseudomonas syringae is a hemibiotrophic plant-pathogenic bacterial species composed of approximately 50 pathovars that differ in their host range (1, 85). This species causes significant economic losses to a number of crops, with certain pathovars being responsible for severe outbreaks of disease worldwide. Recent

outbreaks include bleeding canker disease on horse chestnut caused by *P. syringae* pv. *aesculi* and bleeding canker disease on kiwi caused *P. syringae* pv. *actinidiae* (86, 87). *P. syringae* pv. *tomato* DC3000 (*Pto*) causes bacterial speck of tomato and was one of the first bacterial plant pathogens to be sequenced (60). *Pto* is frequently used for deciphering molecular plant-pathogen interactions due to its ability to infect both tomato and *Arabidopsis thaliana*. Research on *Pto* has provided insights into the role of the type III secretion system (T3SS) in host/non-host interactions and the role type III effectors (T3Es) play in triggering the hypersensitive response (HR) in non-hosts (88). *Pto* has a well-annotated genome making it an ideal candidate for understanding the physiology of plant-pathogenic bacteria and understanding host-pathogen interactions.

Pto requires a T3SS to deliver effectors into host cells and become pathogenic. Hypersensitive response and pathogenicity (*hrp*) genes and *hrp* conserved (*hrc*) genes code for the structural components of the T3SS, while *hrp* outer protein (*hop*) genes and avirulence (*avr*) genes code for the secreted T3Es (3, 89). Both T3SS and T3E genes are in turn regulated by a subset of *hrp* genes. The extracytoplasmic function (ECF) sigma factor HrpL directly regulates both *hrc* and *hop* genes (90, 91). The enhancer binding proteins (EBPs), HrpR and HrpS, form a heterohexameric complex that binds and activates sigma⁵⁴ and allows for transcription of *hrpL* (92). In addition to regulating transcription of *hrpL*, HrpR and HrpS regulate transcription of many genes that are not in the HrpL-regulon (93). No direct transcriptional activators have been described for *hrpR* and *hrpS*; however the two-component system (TCS) RhpRS has been shown to be a direct repressor of *hrpR* and *hrpS* (94).

In *Pto*, multiple sensory systems regulate the T3SS and *hrp* genes, including GacA and AlgU (28, 95). The response regulator, GacA, regulates expression of the small RNAs (sRNAs) *rsmX*, *rsmY*, *rsmZ*, and five additional *rsmX* paralogs in *Pto* (96). The *rsmZ* and *rsmY* sRNAs in turn bind and sequester the global regulator RsmA, while it is still unclear whether the *rsmX* sRNAs bind RsmA as well (28, 96). RsmA regulates a variety of genes post-transcriptionally in *P. syringae*, including genes that code for components of the T3SS, phytoalexins, and pyoverdine (97). The ECF sigma factor AlgU has been primarily characterized as the regulator of production of the negatively charged exopolysaccharide (EPS) alginate in *Pseudomonas* (95, 98). In *Pto*, AlgU also regulates genes involved in osmotolerance, reactive oxygen species (ROS) tolerance, motility, and pathogenicity (95). In the case of pathogenicity, AlgU regulates *hrpR*, *hrpS*, and *hrpL* (95). Regulation of the T3SS through sensory systems highlights the importance of environmental signals during *Pto* pathogenesis.

Ca^{2+} is abundant in the apoplast and little is known about its role as an environmental signal for *Pto* (41). During a compatible interaction between *P. syringae* and the common bean, *Phaseolus vulgaris*, the concentration of Ca^{2+} increases within the apoplast (42). Similar increases in Ca^{2+} concentration occurs in the leaves of *Nicotiana tabacum* infected with *Xylella fastidiosa* (43). Bacteria strictly regulate Ca^{2+} concentrations in the cytoplasm at a much lower concentration than Ca^{2+} concentrations found extracellularly (33). This difference in concentration allows bacteria to use Ca^{2+} as an environmental signal (32, 33, 99). Changes in extracellular Ca^{2+} concentrations modulate several bacterial virulence traits for animal pathogens

including biofilm formation, motility, EPS production, T3SS deployment, and quorum sensing (37, 40, 100-105). Changes in Ca^{2+} concentration also affect pectinolytic enzyme production in the necrotrophic plant pathogen *Pectobacterium carotovorum* and affect biofilm formation in the xylem-limited plant pathogen *Xylella fastidiosa* (105, 106). However, in many hemibiotrophic bacterial plant pathogens—such as *Pseudomonas syringae*, *Xanthomonas*, and *Ralstonia*—there is little known about how these pathogens respond to changes in Ca^{2+} concentration and whether there are regulatory systems induced by Ca^{2+} . Given the abundance of Ca^{2+} in the plant apoplast, it is possible that Ca^{2+} represents an important signaling molecule for this group of plant pathogens.

Bacteria have evolved TCSs and ECF sigma factors to react to changes in the extracellular environment. TCSs transform signals perceived by bacteria into a cellular response using a signal relay that is commonly made up of a transmembrane histidine kinase (HK) and an intracellular response regulator (RR). During signal transduction, an HK will typically transfer a phosphate group to an RR. Following phosphorylation the RR will perform its designated function, such as binding DNA to regulate the expression of genes (19). The genome of *Pto* encodes a large number of HKs and RRs (69 HKs and 95 RRs), many of which remain uncharacterized (27). We have previously reported that expression of a TCS in *Pto* encoded by PSPTO_3380 (HK) and PSPTO_3381 (RR) is induced by Fe^{3+} (16). The expression pattern is similar to the expression pattern of HrpL-regulated genes (16). However, PSPTO_3380 and PSPTO_3381 are not considered to be part of the HrpL regulon (90, 91). We also found that PSPTO_3380 and PSPTO_3381 are directly regulated by the Ferric uptake

regulator (107). In the current study, we show that PSPTO_3380 and PSPTO_3381 represent a Ca²⁺ induced, virulence-associated TCS in *Pto*. We also identify the PSPTO_3381 regulon using chromatin immunoprecipitation followed by next-generation sequencing (ChIP-seq) and transcriptome analysis (RNA-seq). In reference to the phenotype of PSPTO_3380 and PSPTO_3381, we suggest naming this TCS the calcium, virulence, and swarming sensor (CvsS) and regulator (CvsR) and will refer to it as such throughout the manuscript.

Results

CvsS and CvsR affect virulence of *Pto*. In order to determine if *cvsS* and *cvsR* affect the ability of *Pto* to cause disease, tomato plants were dip-inoculated with Δ *cvsS* and Δ *cvsR* *Pto* strains. At 6 days post inoculation (DPI), tomato plants inoculated with either the Δ *cvsS* or Δ *cvsR* strains produced fewer symptoms than those inoculated with the WT strain (Figure 2.1A). The Δ *cvsS* and Δ *cvsR* strains also showed reduced growth on tomato plants compared to WT at 4 DPI and 6 DPI (Figure 2.1B). Both symptoms and growth of the Δ *cvsR* strain could be partially restored with a single-copy chromosomal complementation of *cvsR* (*cvsRc*) (Figures 2.1A, B). In addition, *A. thaliana* was vacuum-infiltrated with either WT, Δ *cvsS*, or Δ *cvsR* *Pto* strains to determine whether CvsSR was involved in virulence for multiple hosts. Similar to tomato plants, *A. thaliana* plants inoculated with the Δ *cvsS* and Δ *cvsR* strains showed a reduction in symptom development as well as a reduction in growth as compared to those inoculated with WT (Figures 2.1C and 2.1D). These results demonstrate that

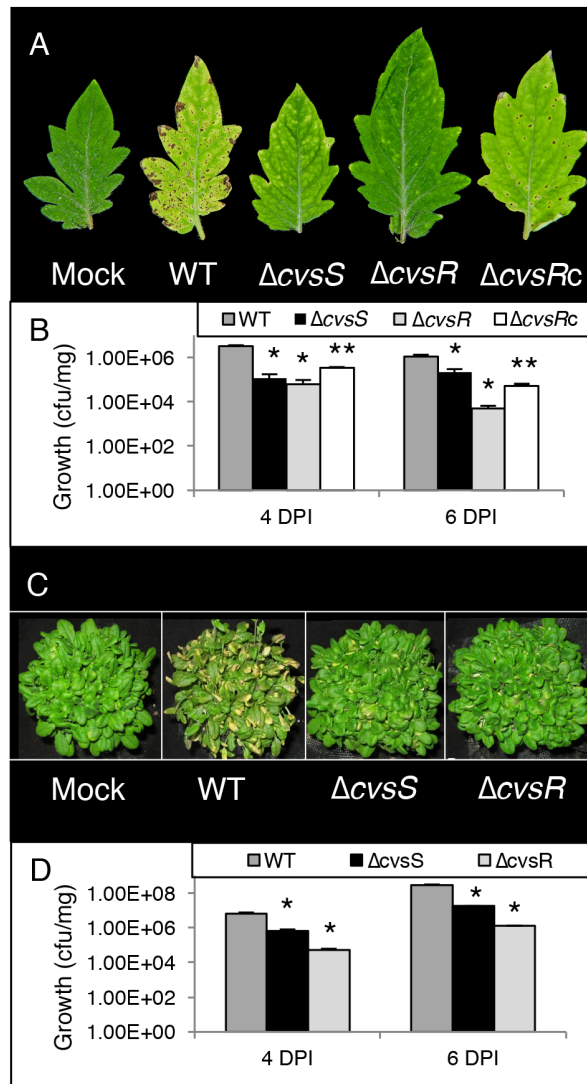


Figure 2.1: Growth and symptoms of WT, ΔcvS and ΔcvR strains on tomato and *A. thaliana*. (A) Image of symptoms at 6 DPI of tomato dip inoculated with *Pto* strains (B) Growth over time in cfu/mg are shown for WT, ΔcvS , ΔcvR , and $\Delta cvRc$ infecting tomato at 4 DPI and 6 DPI. The strains were inoculated at 2×10^7 cfu/mL. Average bacterial growth in three plants with the error bars representing the standard error between the three replicates. (C) Image of symptoms at 4 DPI on *A. thaliana* vacuum-infiltrated with *Pto* strains. (D) Growth over time in cfu/mg are shown for WT, ΔcvS , ΔcvR infecting *A. thaliana* at 4 DPI and 6 DPI that had been inoculated at 3×10^4 cfu/mL. Average bacterial growth in three plants was used with the error bars representing the standard error between the three replicates. In figures 1B and 1D * denotes a statistically significant difference with a p-value < 0.01 between growth of WT and ΔcvS and ΔcvR strains and ** denotes a statistically significant difference between the ΔcvR and $\Delta cvRc$ strains with a p-value < 0.01 determined using Student's two-tailed T-test.

CvsSR is associated with growth and virulence of *Pto* in multiple hosts. In addition, since reduced virulence was observed upon dip inoculation (a natural mode of entry via stomates) and vacuum infiltration (which bypasses natural entry), we conclude that CvsSR is necessary for full virulence of *Pto* during growth in the apoplast.

Calcium induces expression of *cvsSR*. The TCS orthologous to CvsSR in *P. aeruginosa* is induced by Ca^{2+} (108). To test for induction of *cvsS* and *cvsR* by Ca^{2+} , we designed a luciferase promoter gene construct that included 400 bps upstream of PSPTO_3383 (P_{cvsSR}) that included a previously mapped transcriptional start site for PSPTO_3383 and introduced it into WT, $\Delta cvsS$, and $\Delta cvsR$ strains of *Pto* (109).

Expression of this construct should reflect expression of the promoter for *cvsS* and *cvsR* as we found that *cvsS*, *cvsR*, PSPTO_3382, and PSPTO_3383 formed an operon using reverse transcriptase-PCR (RT-PCR) (Fig. 2.2). The addition of Ca^{2+} to mannitol glutamate (MG) medium resulted in a significant increase in P_{cvsSR} after 6 h of growth as compared to the basal level of expression in MG medium (Fig. 2.3A). To test whether the chelation of Ca^{2+} would inhibit Ca^{2+} induced expression of P_{cvsSR} , we added the Ca^{2+} chelator EGTA to MG medium supplemented with Ca^{2+} . No increase in expression of P_{cvsSR} was observed when *Pto* was grown in MG medium supplemented with Ca^{2+} and EGTA as compared to *Pto* grown in MG medium (Fig. 2.3A). From these data, we conclude that expression of P_{cvsSR} is induced by Ca^{2+} .

TCSs, including the orthologous TCS to CvsSR in *P. aeruginosa*, commonly autoregulate (110). We compared the expression of P_{cvsSR} in the $\Delta cvsS$ and $\Delta cvsR$ strains to WT when grown in MG medium supplemented with Ca^{2+} . Expression of

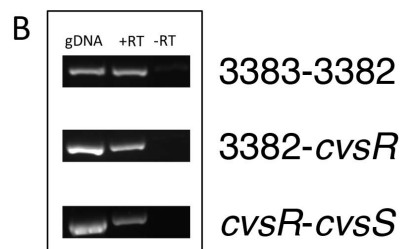
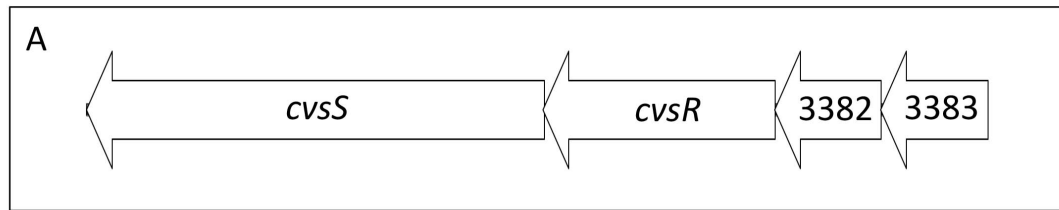


Figure 2.2: (A) Genomic arrangement of operon where *cvsS* and *cvsR* are located. (B) Bands produced by PCR of primers overlapping the junction between 3383 and 3382, 3382 and *cvsR*, and *cvsR* and *cvsS* using either *Pto* genomic DNA (gDNA), cDNA produced by reverse transcription with random hexamers of RNA (+RT), or a no reverse transcriptase control reaction (-RT). RNA was extracted from *Pto* grown for 18 hours on NB supplemented with CaCl₂ and sodium succinate.

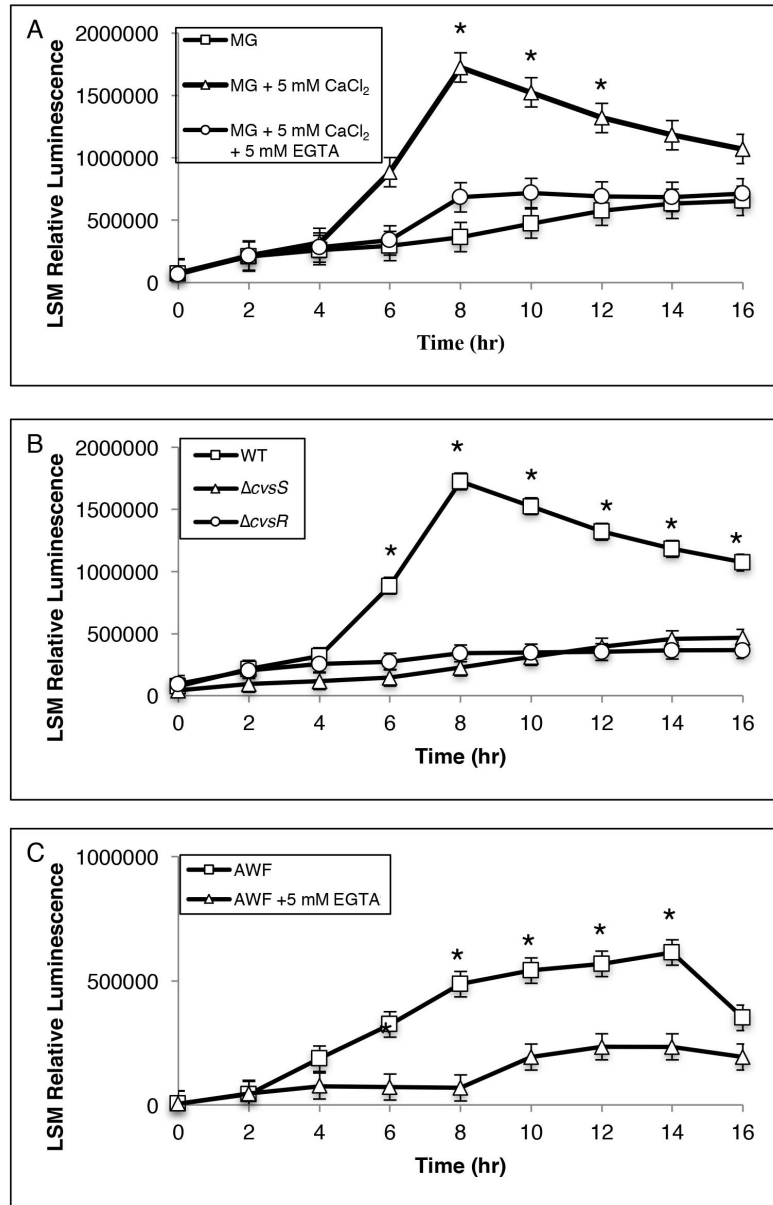


Figure 2.3: Luminescence assays to assess activity of P_{cvsSR} (A) in WT grown in MG, MG with 5 mM $CaCl_2$, and MG with 5 mM $CaCl_2$ and 5 mM EGTA over the course of 16 hours, (B) between WT, $\Delta cvsS$, and $\Delta cvsR$ strains grown in MG with 5 mM $CaCl_2$, and (C) in WT grown in AWF and AWF with 5 mM EGTA. The relative luminescence was calculated by using the total luminescence relative to OD_{600} . Experiments were performed three times. The three experiments were compiled using a least squares mean regression. The error bars represent standard deviation generated by the differences observed between samples. * denotes statistically significant differences determined using a Tukey HSD test with a p-value < 0.01 in (A) between MG with 5 mM $CaCl_2$ and the two other conditions, in (B) between WT and $\Delta cvsS$ and $\Delta cvsR$, and in (C) between AWF and AWF with 5 mM EGTA.

P_{cvsSR} was significantly reduced in the $\Delta cvsS$ and $\Delta cvsR$ strains as compared to WT (Figure 2.3B). These data showed that CvsSR positively autoregulates.

The leaf apoplast contains anywhere from 10 μ M to 10 mM free Ca^{2+} (41). Based on these data, we hypothesized that Ca^{2+} could induce expression of *cvsSR* during growth *in planta*. Apoplastic washing fluid (AWF) was extracted from tomato leaves and elemental analysis was then performed using inductively coupled plasma-mass spectroscopy (ICP-MS). Based on data from three samples, the concentration of calcium in the tomato leaf apoplast was an average of 9.7 mM with a standard deviation of 0.1 mM (Table 2.1). Therefore, we concluded that the concentration of Ca^{2+} was likely high enough to induce expression of P_{cvsSR} in AWF. We grew *Pto* in AWF and found that P_{cvsSR} increased over time (Figure 2.3C). Addition of EGTA to AWF reduced expression of P_{cvsSR} , suggesting that Ca^{2+} likely induced *cvsSR* in AWF and also *in planta* (Figure 2.3C).

Identification of direct targets for CvsR in *Pto*. ChIP-seq was employed in order to determine regions of the genome bound by the predicted DNA-binding response regulator CvsR. The $\Delta cvsR$ *Pto* strain was complemented with pBS46::*cvsR*-FLAG ($\Delta cvsR$ *cvsR*-FLAG). To determine if the FLAG tagged protein was active, expression of pBS59:: P_{cvsSR} was evaluated in the $\Delta cvsR$ *cvsR*-FLAG strain. When $\Delta cvsR$ *cvsR*-FLAG was grown in MG supplemented with Ca^{2+} , expression of P_{cvsSR} was induced (Figure 2.4). This suggested that CvsR-FLAG was active. The $\Delta cvsR$ *cvsR*-FLAG strain was then grown for 18 hours on Nutrient Broth (NB) agar plates supplemented with Ca^{2+} and succinate before cells were collected for ChIP. Prior to sequencing, the genomic region upstream of PSPTO_3383 and *gyrA* were used as positive and

Table 2.1: Concentration of Elements in AWF

- a. Concentration of element given in parts per million
- b. Concentration of element given in molarity

Element	Conc. (ppm)^a	Std Dev. (ppm)	Conc. (M)^b	Std Dev. (M)
Ca	389.1	44.9	9.7 mM	1.1 mM
K	1250.7	210.5	32 mM	5.4 mM
Mg	107.8	7.5	4.4 mM	0.3 mM
Na	25.7	6.1	1.1 mM	0.3 mM
P	36.9	10.4	1.2 mM	0.3 mM
S	247.3	82.8	7.7 mM	2.6 mM
B	2.8	0.9	258.5 μ M	80.4 μ M
Fe	0.12	0.02	2.16 μ M	0.4 μ M
Mn	2.6	0.2	47.5 μ M	3.1 μ M
Zn	0.44	0.03	6.7 μ M	0.5 μ M
Cd	0.008	0.001	66.7 nM	12.4 nM

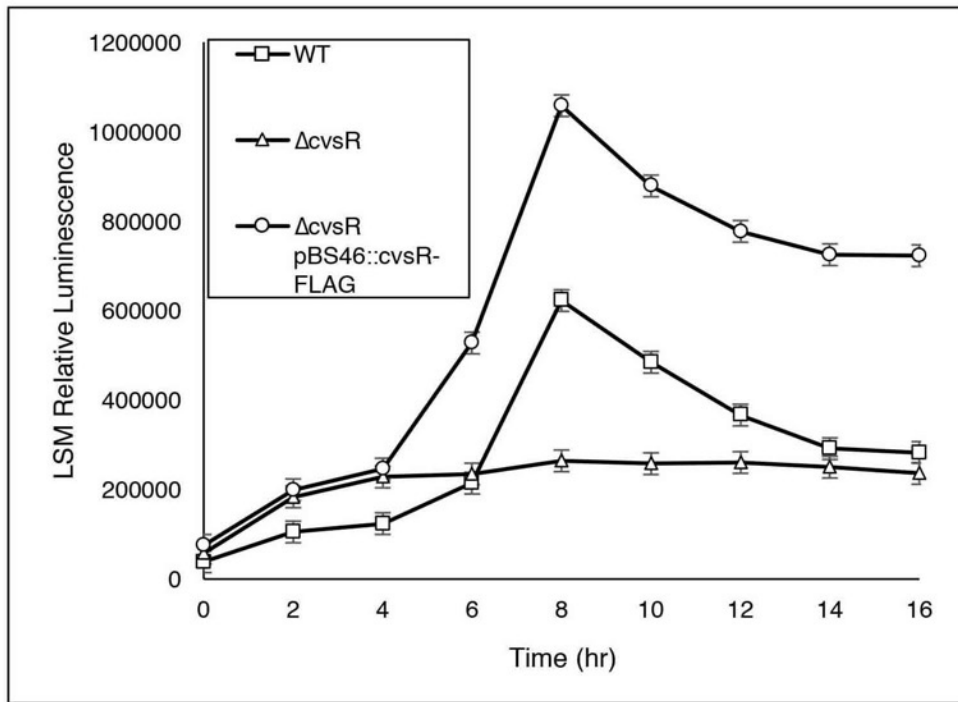


Fig. 2.4: Luminescence assay to assess transcription of P_{cvsSR} WT, $\Delta cvsR$, and $\Delta cvsR$ pBS46::cvsR-FLAG when grown in MG supplemented with Ca^{2+} . The relative luminescence was calculated using the total luminescence relative to the OD_{600} . This experiment was repeated with independent replicates three times and the three independent experiments were compiled using a least-squares regression. The error bars represent standard error generated by the differences observed between samples.

negative controls, respectively, to determine enrichment of the immunoprecipitation (IP) fraction as compared to the input fraction. The genomic region upstream of PSPTO_3383 was chosen as a positive control because CvsSR positively autoregulates and likely binds to an area near the previously mapped transcriptional start site for the operon that includes PSPTO_3383 (109). The gene *gyrA* had been used as a negative control in a previous ChIP-seq experiment on *Pto* (107). It was determined that the region upstream of PSPTO_3383 was enriched 6.4-fold in the IP fraction as compared to the input fraction, while no enrichment was observed for *gyrA* in the IP fraction as compared to the input fraction. Sequencing was performed on libraries made from the IP and input samples. Overall, 5,609,692 reads were sequenced from the IP sample and 1,366,470 reads were sequenced from the input sample. In both cases, 97% of the reads aligned to the *Pto* genome. Using MACS2, 199 peaks were identified using an FDR cutoff less than 0.05 (Table 2.2)². Enriched peaks were found upstream of the gene PSPTO_5255, which codes for a carbonic anhydrase, and within the gene PSPTO_4969, which codes for an RHS-repeat protein (Figure 2.5A). Of note, two peaks were found upstream of the global virulence regulator *hrpR* (Figure 2.5A). This would make CvsR the second described direct transcriptional regulator of *hrpR* (94). The first peak was found 749 bps upstream of the translational start site for *hrpR* (peak #1) and the second peak was found 63 bp upstream of the translational start site for *hrpR* (peak #2). No peak was called in the area upstream of PSPTO_3383. This was due to the fact that the area was disregarded

² Table 2.2 is over 200 lines long and is not shown here. For reference please refer to the published work associated with this study.

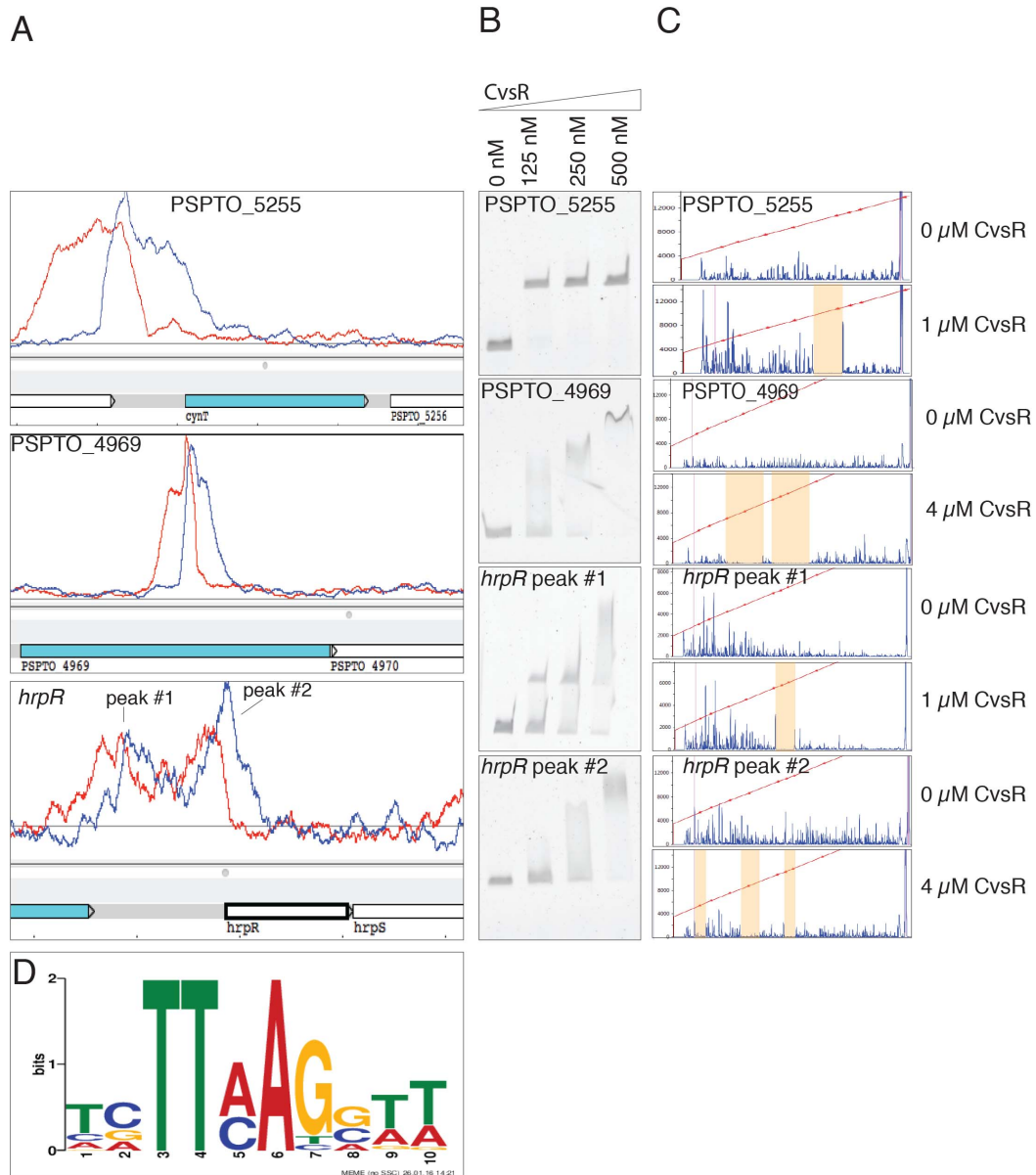


Figure 2.5: Visualization of ChIP-seq data, CvsR DNA binding assays, and a putative CvsR binding motif. (A) A screenshot of the Artemis genome browser depicting areas of enrichment (peaks) in the ChIP-seq data upstream of PSPTO_5255, within PSPTO_4969, and upstream of *hrpR*. The red line represents the forward strand of DNA while the blue line represents the reverse strand of DNA. ChIP-seq peaks occur where enriched areas for each strand overlap. (B) EMSA with concentrations of CvsR increasing from left to right for probes that code for genomic locations found within the ChIP-seq peaks for PSPTO_5255, PSPTO_4969, and *hrpR*. A shift in the migration of the probe with increasing concentrations of CvsR signifies binding of

CvsR to that probe. (C) Fluorescent, non-radioactive DNase footprinting assays showing binding of CvsSR. The red line is a line of best fit that estimates the bp size of each fragment made using a LIZ500 ladder. The blue peaks are fluorescent signal and represent the size of fragmented DNA. The areas that are highlighted in orange are regions with little fluorescence when CvsR is added at 1 μ M or 4 μ M to the reaction as compared to when no CvsR is added. These regions signify areas in the probes that were bound by CvsR. (D) The predicted binding motif for CvsR that was compiled by MEME using the areas 50 bp upstream and 50 bp downstream of the center of the ChIP-seq peak.

during the peak calling using MACS because there was a large peak in *cvsR* due to the over expression of this gene.

Ten areas of the genome that showed enrichment in the ChIP-seq data, were selected for further evaluation by electrophoretic mobility shift assays (EMSA) and DNase footprinting to confirm binding by CvsR. The ten areas investigated included the genomic regions upstream of PSPTO_5255, PSPTO_0203, *katB*, *oprF*, *hrpR*, *gidA*, *t-RNA cys-1*, *spf*, and within the gene PSPTO_4969 (Figures 2.5B, 2.5C, 2.6, 2.7, 2.8). The area upstream of the gene PSPTO_0786 was used as a negative control for CvsR binding (Figures 2.6, 2.7). All showed a binding site using DNase footprinting and all of these areas, except for the area upstream of *oprF* showed a clear shift by EMSA. It is possible that CvsR did not have a high affinity for the area of the genome upstream of *oprF* and that this was reflected in the undefined gel shift. It should be noted that according to the EMSA, CvsR showed a higher binding affinity for the peak 749 bps upstream of the translational start site for *hrpR* compared to the second peak 63 bp upstream of the translational start site for *hrpR*.

We also checked for binding of CvsR upstream of PSPTO_3383 since CvsSR autoregulates and the operon that includes *cvsS* and *cvsR*. The probe we created upstream of PSPTO_3383 included the putative transcriptional start site for the operon (109). We found that CvsR bound upstream of PSPTO_3383 (Figures 2.6, 2.7). These data provided additional support that CvsR autoregulates.

Using the 199 peaks we identified above, one 10-nt long binding motif for CvsR was determined (Figure 2.5D). This type of motif is common for RRs in the OmpR family and suggests that only a single motif is required for CvsR to bind DNA

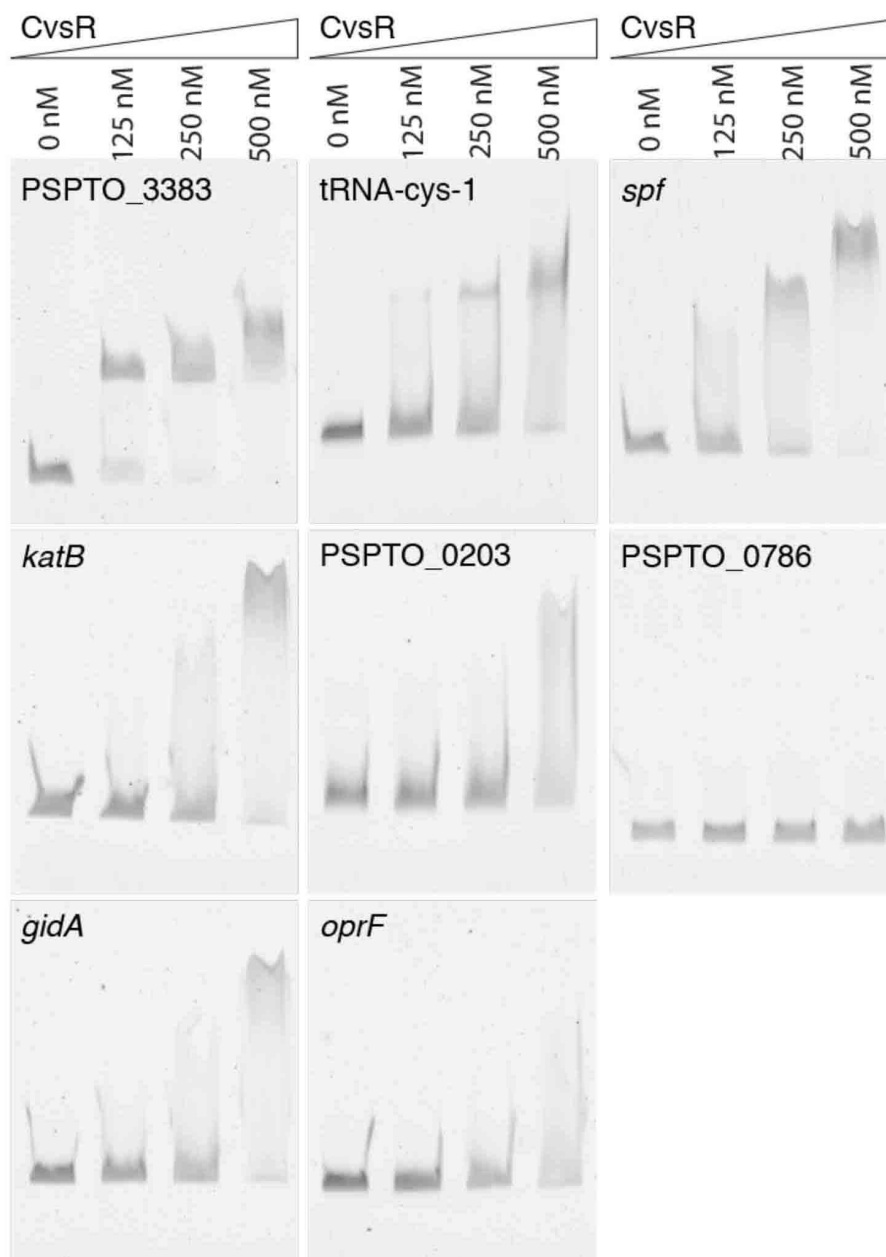


Figure 2.6: EMSA with concentrations of CvsR increasing from left to right as written. Probes were chosen based on the location of ChIP-seq peaks, except for PSPTO_3383 and PSPTO_0786. No peak was found near either of those areas in the chromosome. CvsR was predicted to bind upstream of PSPTO_3383 since CvsSR autoregulates. The probe for PSPTO_0786 is used as a negative control. Probes show a shift with an increased concentration of CvsR due to reduced mobility of the probes upon binding of CvsR. This is not seen for the probe for PSPTO_0786.

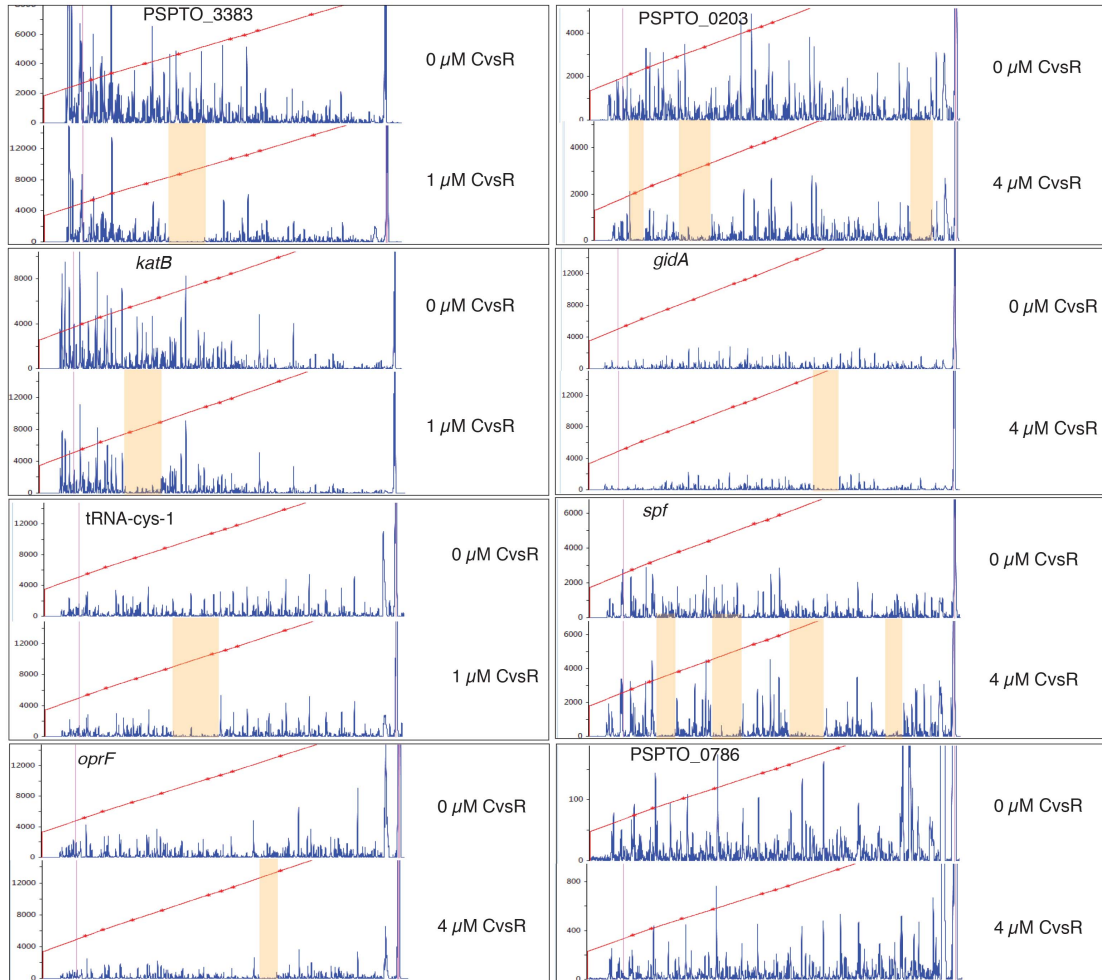


Figure 2.7: Fluorescent, non-radioactive DNase footprinting assays showing binding of CvsSR. The red line is a line of best fit that estimates the bp size of each fragment made using a LIZ500 ladder. The blue peaks are fluorescent signal and represent the size of fragmented DNA. The areas that are highlighted in orange are regions with little fluorescence when CvsR is added at 1 μM or 4 μM to the reaction as compared to when no CvsR is added. These regions signify areas in the probes that were bound by CvsR. A probe for the region PSPTO_0786 was used as a negative control. There were not any regions that CvsR bound to in this probe.

(111). DNase footprinting data were consistent with this prediction, since binding sites mapped for *hrpR* peak #2 and PSPTO_0203 were approximately 11-14 bps and covered a single predicted binding motif (Figure 2.8). Other areas from the DNase footprinting, like those mapped for PSPTO_5255 and *hrpR* peak #1, spanned around 26 bp and covered two direct repeats similar to the predicted binding motif (Figure 2.8). A predicted binding motif was also produced using all the sites CvsR identified using the DNase footprinting probes (Figure 2.9). The resulting motif was similar to the one determined from the ChIP-seq data.

Mapping the transcriptional landscape of CvsR. RNA-seq was used to complement the ChIP-seq data and more thoroughly determine the CvsR regulon. The same condition used to grow cells for the ChIP-seq analysis was also used for extracting RNA for RNA-seq analysis. On average, 50,421,230 reads were generated from the Δ *cvsR* strain cDNA libraries and 35,215,281 reads were generated for the WT cDNA libraries. Of those reads, 97% aligned to the *Pto* genome. From these data sets, 292 genes were differentially regulated between WT and the Δ *cvsR* strain by two-fold or more using an FDR cutoff less than 0.05. Of these genes, 181 genes were upregulated and 111 genes were downregulated in the Δ *cvsR* strain as compared to WT (Table 2.3)³. A subset of these genes is listed in Table 2.4. Changes in expression of a subset of differentially expressed genes were confirmed using qRT-PCR (Table 2.5). Within the RNA-seq dataset, ChIP-seq peaks were found within or upstream of 19 genes that were also differentially expressed in the Δ *cvsR* strain. These genes are listed in Table

³ Table 2.3 is over 290 lines long and is not shown here. For reference please refer to the published work associated with this study.

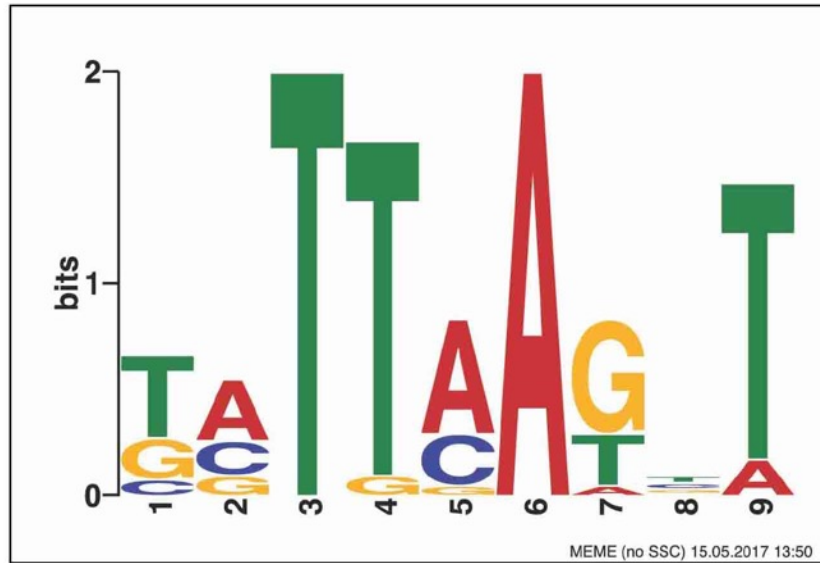


Figure 2.9: The predicted binding motif for CvsR discovered using MEME from the compiled Dnase footprinting data.

Table 2.4: Selected genes differentially expressed between WT and $\Delta cvsR$ strains.

- a. Locus number of differentially expressed gene.
- b. Gene name of differentially expressed gene (if applicable).
- c. Putative functional description of gene as listed on the Uniprot database (112).
- d. Differential expression of gene between $\Delta cvsR$ strain and WT according to RNA-seq data.

Category	Locus Number ^a	Gene ^b	Description ^c	Fold-change ^d
Motility	PSPTO_0911	<i>cheW</i>	Chemotaxis protein	-2.24
	PSPTO_0915	<i>cheY</i>	Chemotaxis protein	-2.73
	PSPTO_1933	<i>flgB</i>	Flagellar basal body rod protein	-2.55
	PSPTO_1936	<i>flgE</i>	Flagellar hook protein	-2.55
	PSPTO_1949	<i>fliC</i>	Flagellin	-4.51
	PSPTO_1952	<i>fliS</i>	Flagellar protein	-2.20
	PSPTO_1953	<i>flgD</i>	Basal-body rod modification protein	-2.35
	PSPTO_4156	<i>motY</i>	Sodium-type flagellar protein	-2.13
Alginate Biosynthesis and Regulation	PSPTO_1232	<i>algA</i>	Alginate biosynthesis protein	2.81
	PSPTO_1233	<i>algF</i>	Alginate biosynthesis protein	3.01
	PSPTO_1234	<i>algJ</i>	Probable alginate O-acetylase	3.21
	PSPTO_1235	<i>algI</i>	Probable alginate O-acetylase	2.42
	PSPTO_1236	<i>algL</i>	Alginate lyase	2.68
	PSPTO_1237	<i>algX</i>	Alginate biosynthesis protein	2.86
	PSPTO_1238	<i>algG</i>	Poly(beta-D-mannuronate) C5 epimerase	3.27
	PSPTO_1239	<i>algE</i>	Alginate production protein	3.29
	PSPTO_1240	<i>algK</i>	Alginate biosynthesis protein	3.60

Table 2.4 (Continued)

	PSPTO_1241	<i>alg44</i>	Alginate biosynthesis protein	3.15
	PSPTO_1243	<i>algD</i>	GDP-mannose 6-dehydrogenase	2.56
	PSPTO_4222	<i>algU</i>	RNA polymerase sigma factor	2.64
	PSPTO_4222	<i>mucB</i>	Sigma factor <i>algU</i> regulatory protein	2.46
	PSPTO_4223	<i>mucA</i>	Sigma factor <i>algU</i> negative regulatory protein	2.19
<i>rsm</i> sRNA	PSPTO_5647	<i>rsmY</i>	sRNA	-3.12
	PSPTO_5671	<i>rsmX</i>	sRNA	-2.23
	PSPTO_5673	<i>rsmX</i> - 3	sRNA	-8.02
	PSPTO_5674	<i>rsmX</i> - 4	sRNA	-3.54
Sulfur uptake and regeneration	PSPTO_0203		Cysteine synthase	-2.04
	PSPTO_0308	<i>sbp</i>	Sulfate-binding protein	8.20
	PSPTO_0309	<i>cysT</i>	Sulfate ABC transporter	2.73
	PSPTO_0310		Sulfate ABC transporter	3.13
	PSPTO_0311	<i>cysA</i>	Sulfate/thiosulfate import ATP-binding protein	3.21
	PSPTO_1793		Uncharacterized protein	2.83

Table 2.4 (Continued)

PSPTO_1795		Alkanesulfonate monooxygenase	2.41
PSPTO_1796		Sulfonate ABC transporter	2.43
PSPTO_1797		Aliphatic sulfonates import ATP-binding protein	2.27
PSPTO_2614		Dioxygenase, TauD/TfdA family	2.31
PSPTO_3438	<i>iscS-3</i>	Cysteine desulfurase	3.53
PSPTO_3451	<i>ssuE</i>	FMN reductase, NADH- dependent	34.00
PSPTO_3466	<i>ssuD</i>	Alkanesulfonate monooxygenase	15.76
PSPTO_4161		Glutaredoxin	-2.04
PSPTO_5187	<i>metQ-1</i>	D-methionine-binding lipoprotein	12.99
PSPTO_5188	<i>metN-1</i>	Methionine import ATP- binding protein	7.68
PSPTO_5189	<i>metI-1</i>	D-methionine ABC transporter	5.76
PSPTO_5198		Dioxygenase, TauD/TfdA family	11.10

Table 2.4 (Continued)				
	PSPTO_5312	<i>tauC</i>	Taurine ABC transporter	3.29
	PSPTO_5314		Aliphatic sulfonates import ATP-binding protein	17.20
	PSPTO_5315	<i>ssuC</i>	Aliphatic sulfonates ABC transporter	18.16
	PSPTO_5316		Sulfonate ABC transporter	16.76
	PSPTO_5319	<i>tauA</i>	Taurine ABC transporter	3.74
	PSPTO_5320	<i>tauB</i>	Taurine import ATP-binding protein	3.02
Quorum Sensing	PSPTO_2048		Transcriptional regulator, LuxR family	-4.12
	PSPTO_2590		Bacterial luciferase family protein	-4.12
	PSPTO_5548		DNA-binding response regulator, LuxR family	-11.62

Table 2.5: qRT-PCR data between WT and the Δ *cvrR* strain for select genes that displayed differential expression in the RNA-seq data.

^aRefer to the Pst DC3000 genome sequence (NC_004578.1).

^bRefers to the gene name.

^cRefers to the ratio of gene expression between WT and Δ *cvrR* strains using the $\Delta\Delta$ Ct method with *gyrA* expression for normalization.

^dIndicates the standard deviation between three replicates.

Locus Number ^a	Gene ^b	Fold Change ^c	Standard Deviation ^d
PSPTO_5647	<i>rsmY</i>	-9.36	0.02
PSPTO_5673	<i>rsmX-3</i>	-5.18	0.09
PSPTO_1243	<i>algD</i>	8.34	3.66
PSPTO_1949	<i>fliC</i>	-3.75	0.02
PSPTO_3292	<i>hopAH2-1</i>	-2.70	0.04

Table 2.6: Genes in CvsR primary regulon.

- a. Nearest gene ID downstream of a ChIP-seq peak.
- b. Refers to the gene name (if applicable)
- c. Putative functional description of gene as listed on the Uniprot database (112).
- d. Differential expression of gene between $\Delta cvsR$ strain and WT according to RNA-seq data.

Nearest Gene ID ^a	Gene Name ^b	Description ^c	Fold-change ^d
PSPTO_0203		Cysteine synthase	-2.04
PSPTO_0279		Uncharacterized protein	-2.62
PSPTO_1062		Uncharacterized protein	-2.52
PSPTO_1304		Uncharacterized protein	-6.23
PSPTO_1609		Uncharacterized protein	-3.10
PSPTO_1626		Uncharacterized protein	2.11
PSPTO_2809		Uncharacterized protein	2.10
PSPTO_3086		Transcriptional regulator	11.29
PSPTO_3288		Uncharacterized protein	6.13
PSPTO_3289		Uncharacterized protein	3.83
PSPTO_3318		Beta-glucosidase	2.53
PSPTO_3582	<i>katB</i>	Catalase	2.86

PSPTO_4631		Sensory box/GGDEF domain/EAL domain protein	-3.07
PSPTO_5255	<i>cynT</i>	Carbonic anhydrase	-23.64
PSPTO_5256		Sulfate transporter family protein	-9.02
PSPTO_5312		Conserved domain protein	3.78
PSPTO_5316		Sulfonate ABC transporter	16.76
PSPTO_5319	<i>tauA</i>	Taurine ABC transporter	3.74
PSPTO_5466		Uncharacterized protein	-2.71
PSPTO_t37	<i>tRNA-Cys-1</i>	tRNA-Cys-1	-2.21

2.6.

CvsSR regulates expression of *algU*. RNA-seq results showed a greater than 2-fold increase in expression of *algU*, *mucA*, and *mucB* in the $\Delta cvsR$ strain. In addition, 94 genes previously reported to be part of the AlgU regulon are shared with the CvsR regulon (95). Of these 94 genes, 77 have the same expression profile in an *algU* overexpressing strain as they do in the $\Delta cvsR$ strain when compared to WT. Notably, genes involved in alginate production, including *algD*, showed an increase in expression in the $\Delta cvsR$ strain as compared to WT. $\Delta cvsS$ and $\Delta cvsR$ strains grown on NB agar supplemented with Ca^{2+} showed a significant increase in alginate production after 12 hours of growth as compared to WT but not when grown on NB agar (Figures 2.10A, 2.11). This provides additional confirmation that CvsSR regulates expression of genes involved in alginate production and that AlgU is active in the $\Delta cvsS$ and $\Delta cvsR$ strains. Since deletion of *cvsR* resulted in increased *algU* expression as compared to WT and CvsS and CvsR regulate alginate production, we conclude that CvsSR indirectly regulates expression of *algU* in *Pto*.

CvsSR regulates bacterial cell attachment and motility. Expression of genes involved in flagellar motility decreased in the $\Delta cvsR$ strain compared to WT and several genes involved in quorum sensing were also differentially expressed in the $\Delta cvsR$ strain as compared to WT (Table 2.4). In *Pseudomonas*, biofilm formation and swarming motility can be impacted by changes in alginate production, flagellar biosynthesis, and quorum sensing genes (113-115). Biofilm assays were performed in MG medium supplemented with Ca^{2+} . The $\Delta cvsR$ strain, but not the $\Delta cvsS$ strain showed a significant increase in attachment compared to WT (Figure 2.10B).

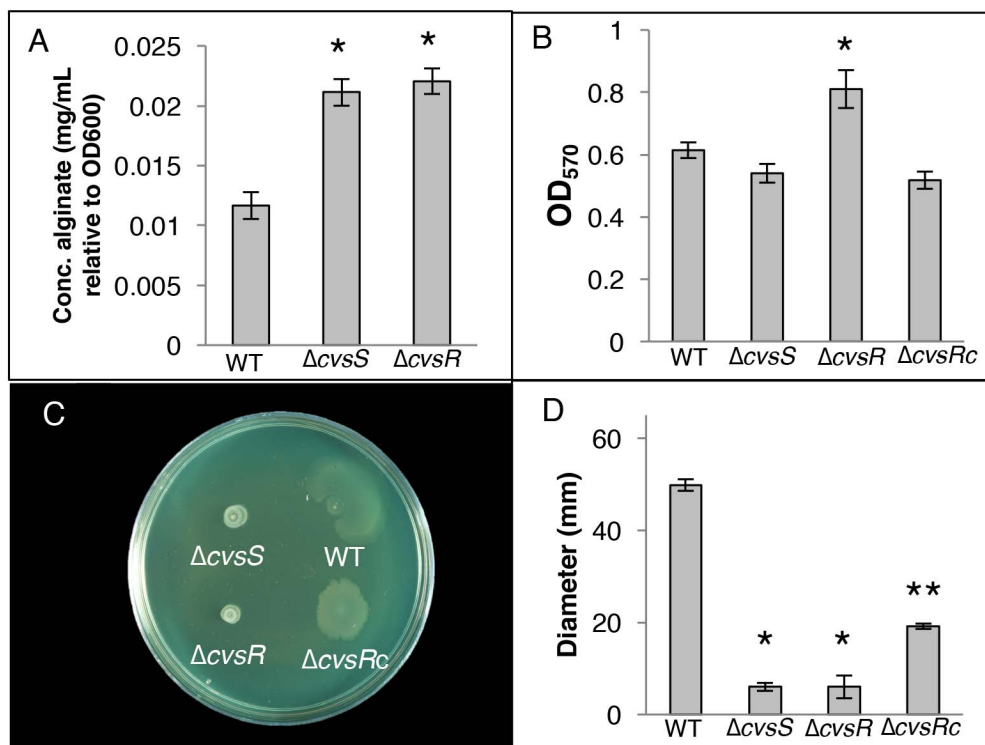


Figure 2.10: Assays assessing phenotypic changes in the $\Delta cvsS$ and $\Delta cvsR$ strains as compared to WT. (A) Amount of alginate present in WT, $\Delta cvsS$, and $\Delta cvsR$ strains of *Pto* when grown on NB agar supplemented with 5 mM $CaCl_2$ for 12 hours. This assay was performed three times and the * denotes a statistically significant difference with a p-value < 0.01 between WT and the $\Delta cvsS$ and $\Delta cvsR$ strains that was determined using a Students, two-tailed T-test. (B) Biofilm formation of WT, $\Delta cvsS$, $\Delta cvsR$, and $\Delta cvsRc$ strains grown in MG pH 7.0 with 2 mM $CaCl_2$ visualized using absorbance of crystal violet at OD₅₇₀. The error bars represent the standard deviation between the replicates. This assay was repeated three times and the * denotes a statistically significant difference with a p-value < 0.05 between WT and the $\Delta cvsR$ strain that was determining using Students two-tailed T-test. (C) Swarming assays of WT, $\Delta cvsS$, $\Delta cvsR$, and $\Delta cvsRc$ strains grown on media with 5 mM $CaCl_2$. Pictures of swarming assays taken a day after spotting. (D) Diameter of swarming colonies measured 24 hours after spotting on NB with 5 mM $CaCl_2$. The experiment was performed three times with three replicates per experiment. Diameter of colonies was measured across two locations and averaged. Error bars represent standard deviation between replicates. The * denote a statistically significant difference with a p-value < 0.01 in swarming diameter between WT and the $\Delta cvsS$ and $\Delta cvsR$ strains that was determined using a Students, two-tailed T-test. The ** denotes a statistically significant difference with a p-value < 0.01 in swarming diameter between the $\Delta cvsR$ and $\Delta cvsRc$ strains.

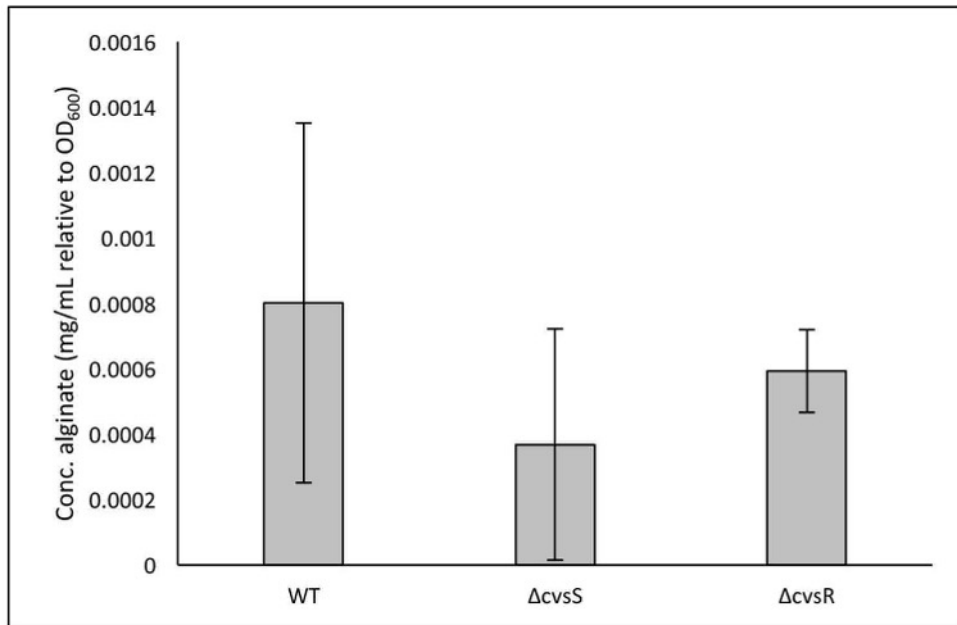


Figure 2.11: Concentration of alginate produced by WT, $\Delta cvsS$, and $\Delta cvsR$ after one day of growth on NB agar plates. The experiment was repeated using four independent biological replicates. Error bars represent standard deviation between replicates.

Swarming motility of the $\Delta cvsS$ and $\Delta cvsR$ strains was reduced compared to WT when Ca^{2+} was added to swarming medium, but not on swarming medium not supplemented with Ca^{2+} (Figures 2.10C, 2.10D, 2.12). This phenotype was partially complemented in the $\Delta cvsRc$ strain (Figures 2.10C, 2.10D). It should be noted that the $\Delta cvsRc$ strain was unable to swarm as well as WT on swarming medium and on swarming medium supplemented with Ca^{2+} (Figures 2.10D, 2.12). Swimming assays were performed to determine whether the $\Delta cvsS$ and $\Delta cvsR$ strains had decreased flagellar motility as compared to WT and whether decreased flagellar motility explained the decreased swarming in the $\Delta cvsS$ and $\Delta cvsR$ strains. No difference in swimming motility was found between the $\Delta cvsS$ and $\Delta cvsR$ strains and WT, suggesting that the decreased swarming motility exhibited by the $\Delta cvsS$ and $\Delta cvsR$ strain was likely not due to decreased flagellar motility (Figure 2.13). To see if decreased swarming was due to overproduction of alginate, we compared swarming from a $\Delta algD$ *Pto* strain with $\Delta cvsS \Delta algD$ and $\Delta cvsR \Delta algD$ *Pto* strains. Swarming was significantly reduced in the $\Delta cvsS \Delta algD$ and $\Delta cvsR \Delta algD$ *Pto* strains as compared to the $\Delta algD$ strain when grown on swarming media supplemented with Ca^{2+} (Figure 2.14). This suggests that CvsSR regulates swarming motility and possibly biofilm formation when Ca^{2+} is present through a mechanism other than flagellar motility and alginate production.

CvsSR regulates cellulose production in *Pto*. *Pto* has the capability of producing the EPSs Psl, cellulose, and levan along with alginate (60). Psl and cellulose can inhibit swarming in *P. syringae* (116, 117). The genes PSPTO_3529-PSPTO_3539, which code for proteins that produce Psl, were not differentially expressed between WT and

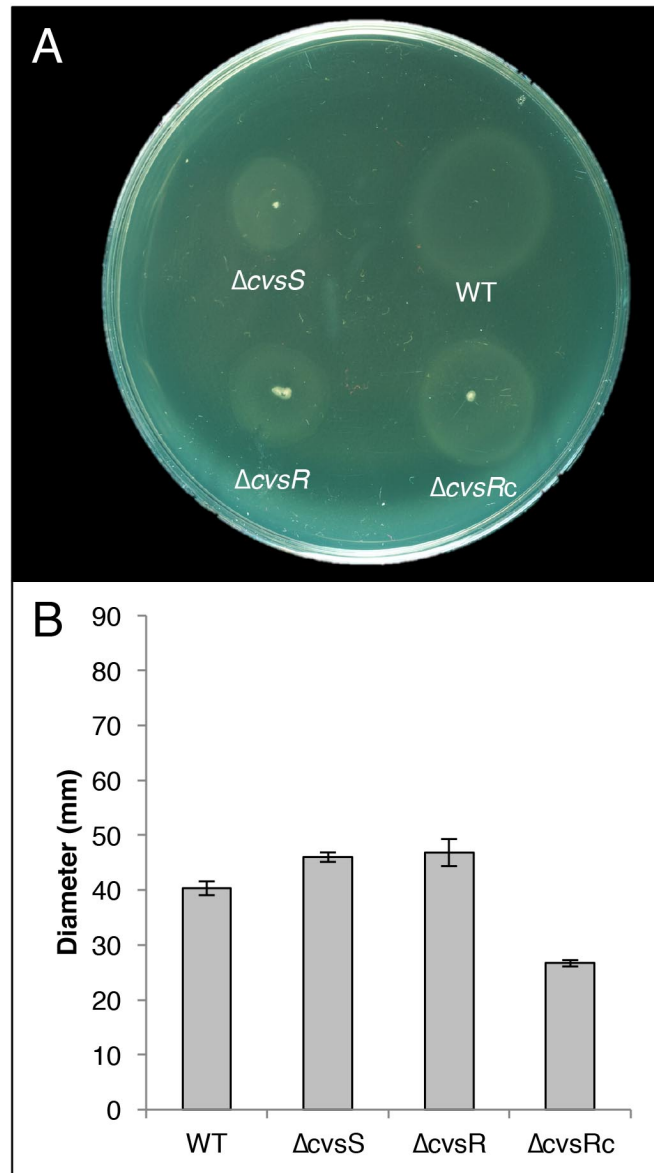


Figure 2.12: (A) Swarming assays of WT, $\Delta cvsS$, $\Delta cvsR$, and $\Delta cvsRc$ strains grown on NB medium. Pictures of swarming assays taken a day after spotting. (B) Diameters of swarming colonies measured 24 hours after spotting on NB with 5 mM $CaCl_2$. The experiment was performed three times with three replicates per experiment. Diameter of colonies was measured across two locations and averaged. Error bars represent standard deviation between replicates.

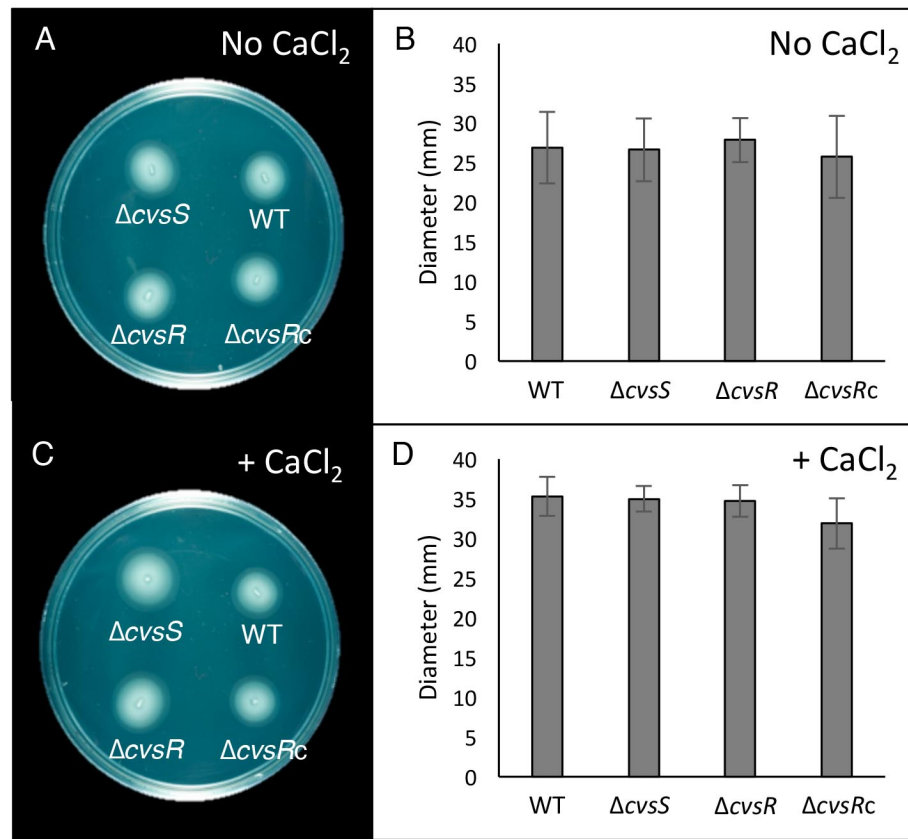


Figure 2.13: Swimming assays of WT, $\Delta cvsS$, $\Delta cvsR$, and $\Delta cvsRc$ strains grown on swimming media. (A) Picture of strains taken two days after the start of a swimming assay without $CaCl_2$. (B) Diameter of swimming by strains in swimming media taken two days after the start of the assay. (C) Picture of strains taken two days after the start of a swimming assay with $CaCl_2$. (D) Diameter of swimming by strains in swimming media with $CaCl_2$ taken two days after the start of the assay. Pictures of the plates are representative of swimming assays that were performed three times. The diameters are averaged from three biological replicates. The error bars represent standard deviation across from the three biological replicates.

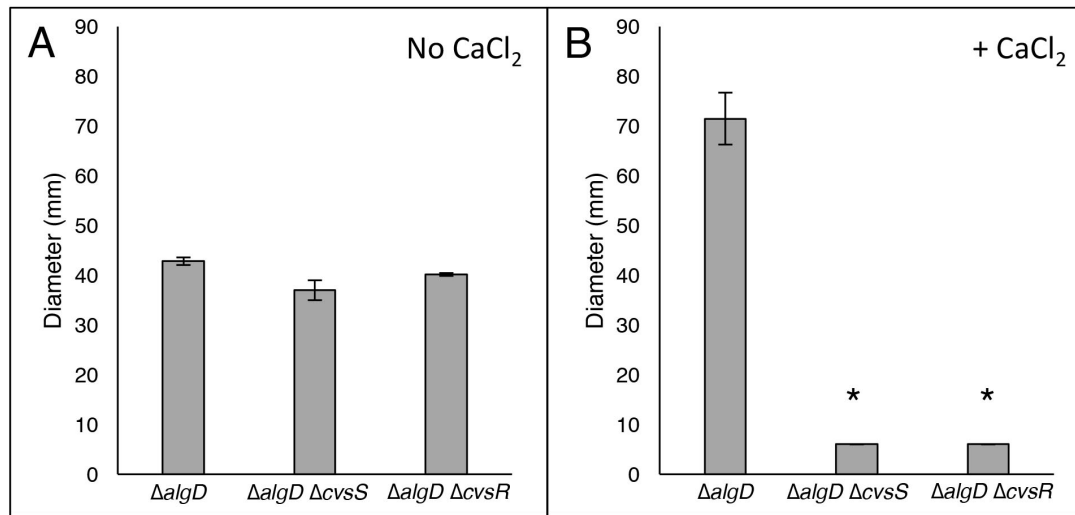


Figure 2.14: Diameters of swarming colonies for $\Delta algD$, $\Delta algD \Delta cvsS$, and $\Delta algD \Delta cvsR$ strains measured 24 hours after spotting on (A) NB or (B) NB supplemented with $CaCl_2$. Diameter of colonies was measured across two locations and averaged. The experiment was performed three times with three replicates per experiment. The graph is from a single experiment and is representative of trends observed in each experiment. Error bars represent standard deviation between replicates. The * denote a statistically significant difference with a p-value < 0.01 in swarming diameter between $\Delta algD$, $\Delta algD \Delta cvsS$, and $\Delta algD \Delta cvsR$ strains.

the $\Delta cvrR$ strain, nor was there a ChIP-seq peak near these genes. In addition, no difference was found in the amount of Psl between WT and the $\Delta cvrS$ and $\Delta cvrR$ strains through the use of a Psl specific antibody (data not shown) (118), suggesting that the $\Delta cvrR$ strain and the $\Delta cvrS$ strain produce the same amount of Psl as WT. Like Psl, none of the genes that code for the cellulose biosynthetic genes cluster showed differential expression between the $\Delta cvrR$ strain and WT in the RNA-Seq data. However, changes in cellulose production can occur even if gene expression for cellulose biosynthesis genes do not show differential expression between two strains since cellulose is post-transcriptionally regulated in *Pto* (119). In order to test for changes in cellulose production, WT, $\Delta cvrS$, $\Delta cvrR$, and $\Delta cvrRc$ were grown on NB medium supplemented with Ca^{2+} and calcofluor white (CW). CW is a dye that fluoresces when it binds beta-1,4 glycosyl linkages and it is commonly used to visualize cellulose production in microbes (119). After three days of growth on NB medium supplemented with Ca^{2+} and CW the $\Delta cvrS$ and $\Delta cvrR$ strains fluoresced, but WT and the $\Delta cvrRc$ strain did not (Figure 2.15). In contrast, WT, $\Delta cvrS$, $\Delta cvrR$, and $\Delta cvrRc$ did not fluoresce on NB medium supplemented only with CW after three days of growth (Figure 2.16). From this we conclude that the CvsSR regulates cellulose production in *Pto* when Ca^{2+} is present in the medium.

CvsSR regulates expression of several T3SS-related genes. ChIP-seq data showed that *hrpR*, and the effectors *hopAT1*, *hopAD1*, *hopAO1*, *avrPtoB*, *hopG1*, *hopD1*, and *hopAA1* had a CvsR binding site upstream of the gene or within the gene itself, suggesting CvsSR regulates expression of several T3SS genes. A binding site for CvsR was also found upstream PSPTO_4966, a recently identified member of the

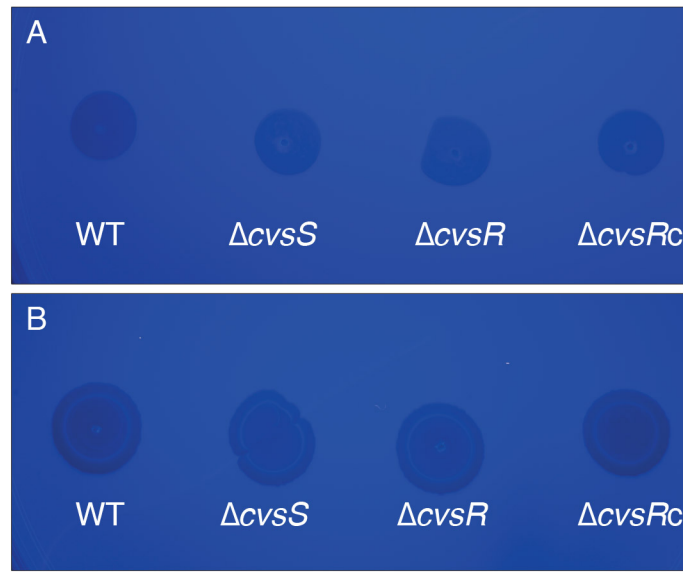


Figure 2.16: Growth of WT, $\Delta cvsS$, $\Delta cvsR$, and $\Delta cvsRc$ on NB supplemented with CW after 16 hours (A) and 3 days (B) of growth. Fluorescence of the bacterial strains under ultra-violet light indicated production of cellulose. Bacterial strains were grown to stationary phase in KB media were resuspended at an OD_{600} of 0.3 in NB media and then five μL of each culture were spotted onto the appropriate media. The plate is representative of assays that were performed three times.

HrpL-regulon (90). Two recently discovered HrpL-regulated genes, PSPTO_2129 and PSPTO_2130, were the only HrpL-regulated genes differentially expressed between the $\Delta cvsR$ strain and the WT strain at a fold-change cut-off of 2-fold (90, 91). If the fold change cutoff for differentially expression genes is lowered to 1.7-fold or more, *hopG1* showed increased expression and the pseudogene *hopAT1* showed decreased expression in the $\Delta cvsR$ strain compared to WT. Both genes are part of the HrpL-regulon. We also observed decreased expression of *hopAH2-1* in the $\Delta cvsR$ strain as compared to WT. HopAH2-1 is thought to be secreted through the T3SS, but is not regulated by HrpL (120). From these data, we conclude that CvsR binds near several T3Es and directly regulates at least two T3Es.

Although differential expression of *hrpRS* was not observed in the RNA-seq data, we investigated if we could detect differences in expression of *hrpRS* between the $\Delta cvsS$, $\Delta cvsR$ and WT strains using a reporter gene construct that contained 800 bp upstream of *hrpR* (P_{hrpRS}). This reporter gene construct included both CvsR binding sites and should report expression of both *hrpR* and *hrpS* (28). P_{hrpRS} showed a significant decrease in expression in both the $\Delta cvsS$ and $\Delta cvsR$ strains as compared to WT when grown in MG medium supplemented with Ca^{2+} , but not when grown in MG medium (Figures 2.17A, 2.18A). Since *hrpRS* regulates expression of *hrpL*, it was possible that there was also a difference in *hrpL* expression in the $\Delta cvsS$ and $\Delta cvsR$ strains as compared to WT. Therefore, we transformed WT, $\Delta cvsS$, and $\Delta cvsR$ strains with the vector pBS63, which includes a promoter fusion previously used to measure expression of P_{hrpL} (121). A significant difference in expression of P_{hrpL} in WT as compared to the $\Delta cvsS$ and $\Delta cvsR$ strains was seen when strains were grown in MG

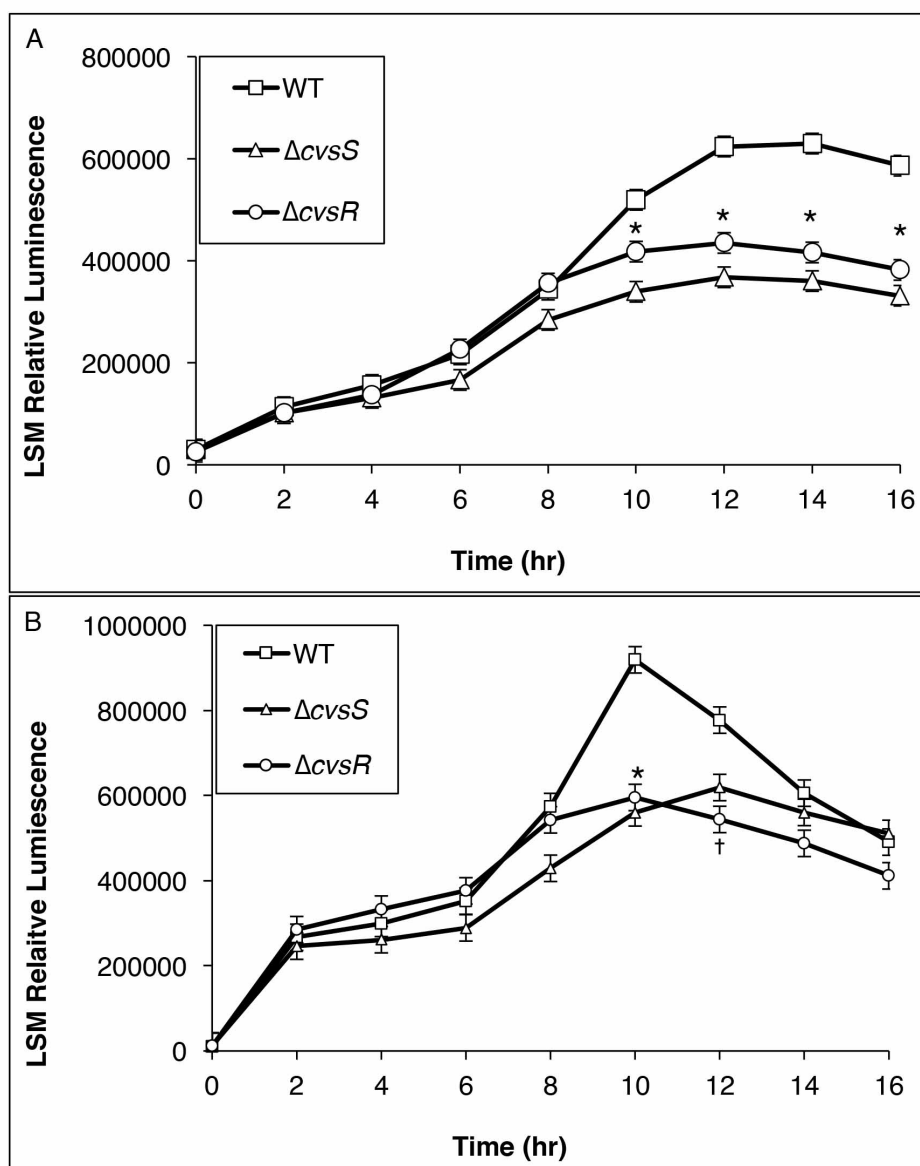


Figure 2.17: Luminescence assay to assess activity of (A) P_{hrpRS} and (B) P_{hrpL} in WT, the $\Delta cvrS$, and the $\Delta cvrR$ when grown in MG supplemented with 5 mM $CaCl_2$. The relative luminescence was calculated using the total luminescence relative to OD_{600} . For P_{hrpRS} the experiment was performed three times with three independent replicates per experiment and for P_{hrpL} the experiment was performed seven times with three independent replicates per experiment. The experiments for each reporter gene construct were compiled using a least squares mean regression. The error bars represent standard error generated by the differences observed between samples. The * denotes statistically significant differences determined using a Tukey HSD test with a p-value < 0.01 between relative luminescence of WT, $\Delta cvrS$, and $\Delta cvrR$. The † denotes statistically significant differences determined using a Tukey HSD test with a p-value < 0.01 between the relative luminescence of WT and $\Delta cvrR$.

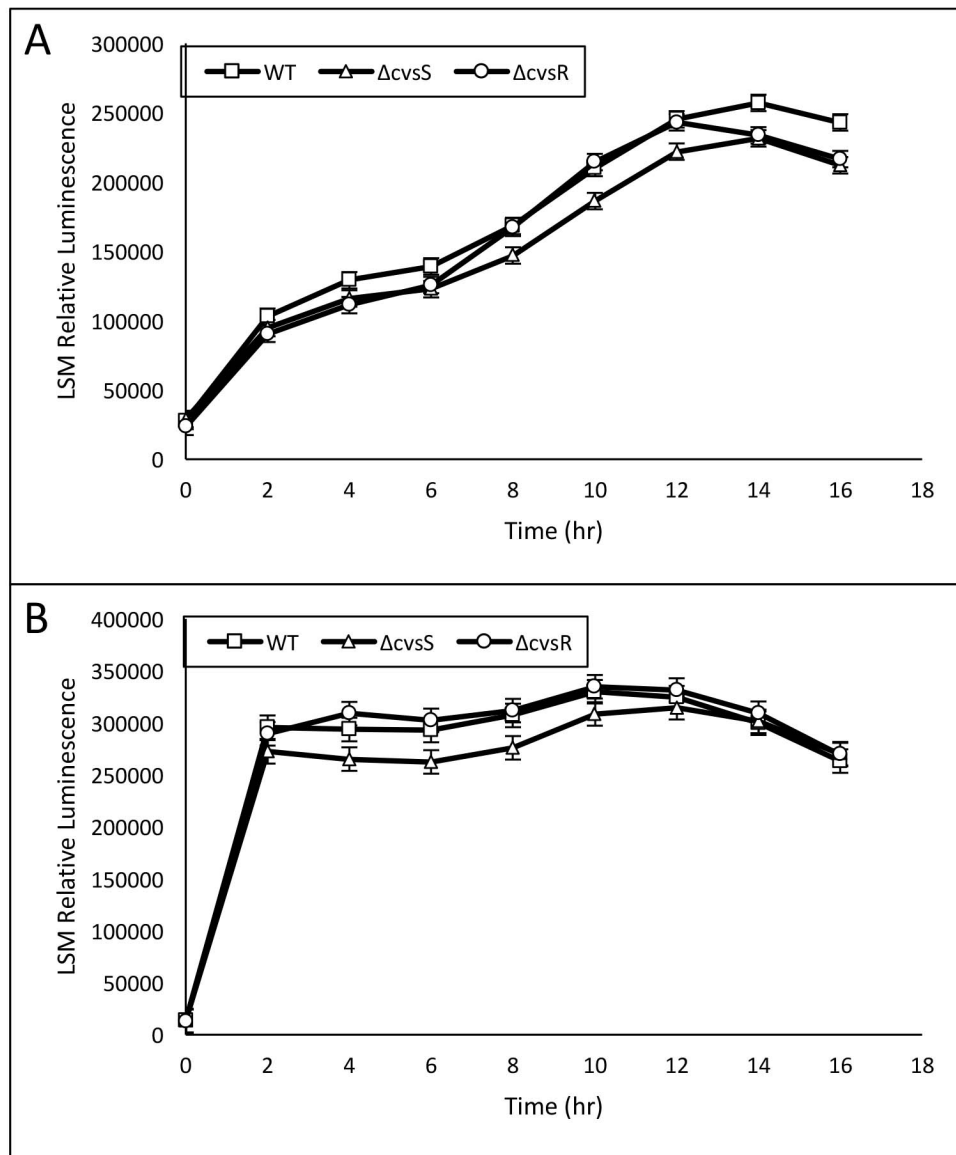


Fig. 2.18: Luminescence assay to assess transcription of (A) P_{hrpRS} and (B) P_{hrpL} in WT, the ΔcvS , and the ΔcvR when grown in MG. The relative luminescence was calculated using the total luminescence relative to OD_{600} . This experiment was independently replicated three times. The three independent experiments were compiled using a least squares regression. The error bars represent standard error generated by the differences observed between samples.

medium supplemented with Ca^{2+} , but not MG medium (Fig. 2.17B, 2.18B). Since decreased expression of *hrpRS* and *hrpL* could reduce production of the T3SS and deployment of T3Es, we then tested the hypersensitive response (HR) in *Nicotiana tabacum* and *N. benthamiana* to see if the ΔcvsS and ΔcvsR strains would elicit the HR at the same level as WT. We found no difference in the HR for *N. tabacum* or *N. benthamiana* when infiltrated with the ΔcvsS or ΔcvsR strain as compared to WT (Figure 2.19). Even though CvsSR regulates *hrpRS* and *hrpL*, these data suggest that CvsSR does not affect production of the T3SS or overall deployment of the T3Es during growth *in planta*.

Ca^{2+} does not influence growth of the ΔcvsS and ΔcvsR strains *in planta*.

The ΔcvsR strain demonstrated increased expression of catalase and genes related to methionine uptake as well as decreased expression of some thiol biosynthesis related genes (Table 2.4). Similar gene expression patterns were seen in *E. coli* during treatment with toxic levels of homocysteine and in *E. coli* treated with antimicrobial peptidoglycan recognition proteins (122, 123). This suggested that the bacteria are under distress when grown in a Ca^{2+} supplemented medium. In fact, growth of the ΔcvsS and ΔcvsR strains was reduced during stationary phase growth when Ca^{2+} was added to medium (Figure 2.20). This concurs with the RNA-seq data and suggests the ΔcvsR strain is under duress when Ca^{2+} is present in media *in vitro*. Since the leaf apoplast is abundant in Ca^{2+} , it is possible that the decreased virulence and growth of the ΔcvsS and ΔcvsR strains in planta is a result of the concentration of Ca^{2+} in the apoplast. Deleting the T3SS in addition to *cvsS* or *cvsR* should result in an additive loss of growth in tomato leaves if the concentration of Ca^{2+} in the apoplast was the

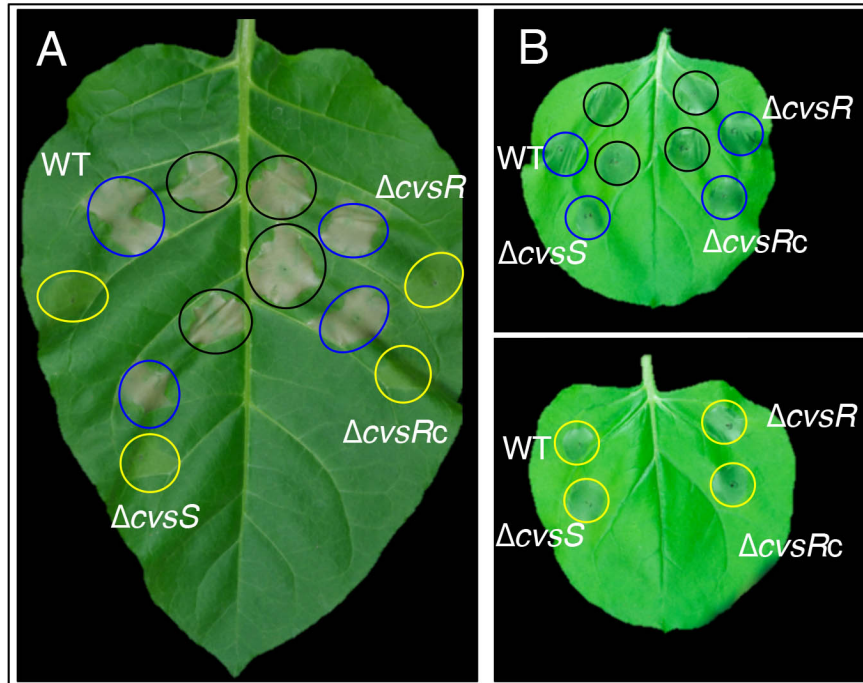


Figure 2.19: (A) HR in *N. tabacum* to WT, $\Delta cvsS$, $\Delta cvsR$, and $\Delta cvsRc$ from *Pto* strains at 2×10^8 (black), 2×10^7 (blue), and 2×10^6 (yellow) cfu/mL. (B) HR in *N. benthamiana* with the same *Pto* strains using the same amount of inocula as in *N. tabacum*. Bacterial strains that were inoculated at the same level of inoculum are circled with the same color. The images shown were photographed 2 days after inoculation for *N. tabacum* and 1 day after inoculation for *N. benthamiana*. The experiment was repeated three times.

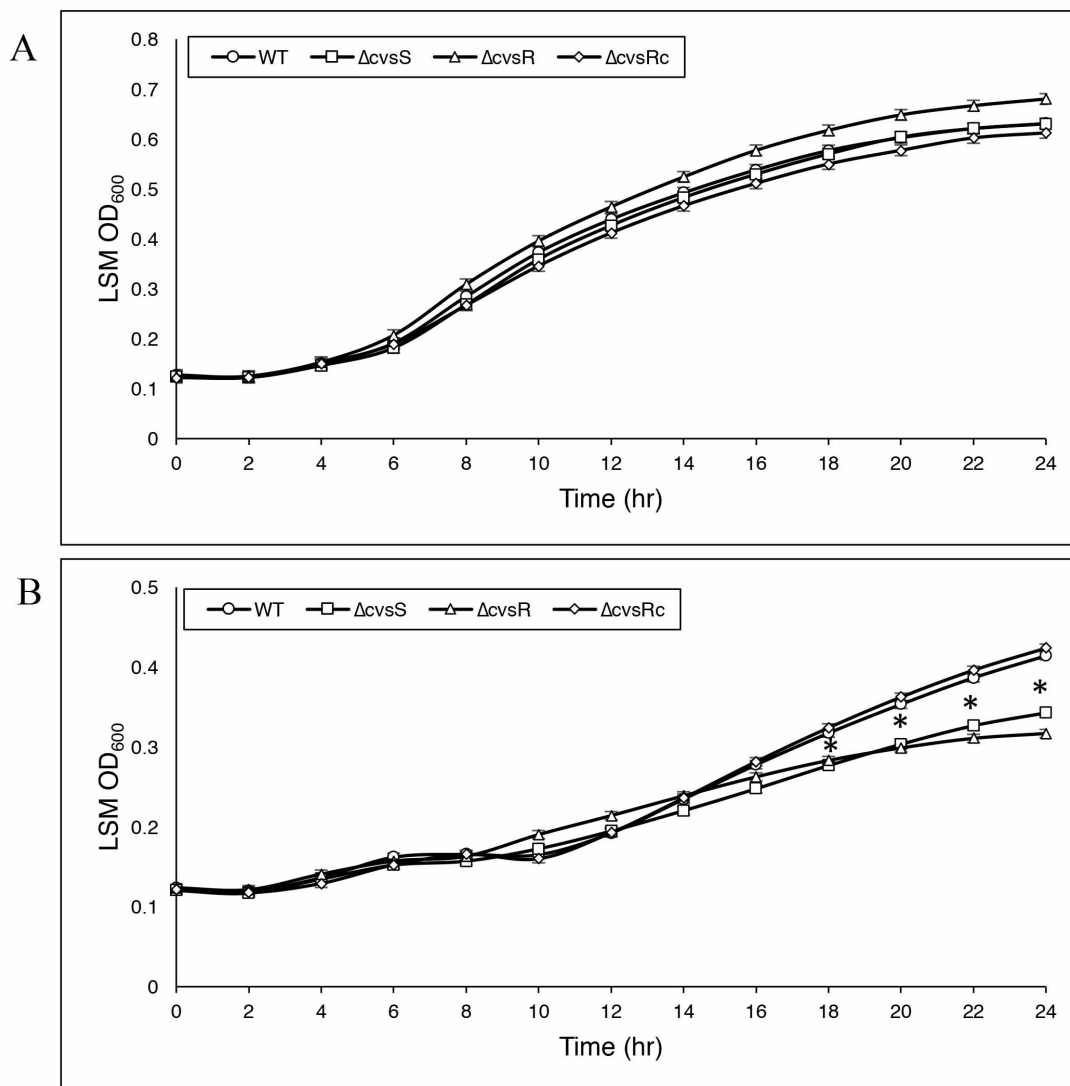


Figure 2.20: The least-squares mean of three separate growth curves of WT, $\Delta cvsS$, $\Delta cvsR$, and $\Delta cvsRc$ grown in (A) MG or (B) MG supplemented with Ca^{2+} . The * denotes statistically significant differences determined using a Tukey HSD test with a p-value < 0.01 between OD_{600} of WT, $\Delta cvsS$, and $\Delta cvsR$.

primary cause for the reduced growth of the $\Delta cvtS$ and $\Delta cvtR$ strains when inoculated in plants. (124). The $\Delta hrcQb-U Pto$ strain no longer produces a T3SS and has been used to look at *Pto*-host interactions when it can no longer deliver effectors (125). *Pto* $\Delta hrcQb-U$, $\Delta hrcQb-U \Delta cvtS$, and $\Delta hrcQb-U \Delta cvtR$ were syringe infiltrated into tomato leaves. Growth of all of the strains was similar at 4 DPI and 6 DPI (Figure 2.21). This suggests that the concentration of Ca^{2+} in the apoplast does not adversely affect growth of the $\Delta cvtS$ and $\Delta cvtR$ strains.

Discussion

The results here identify and characterize *CvsSR* as a virulence-associated TCS that is induced by Ca^{2+} *in vitro* and *in planta*. Through the use of ChIP-seq and RNA-seq we discovered that *CvsSR* impacts expression of two main regulators of pathogenicity, *algU* and *hrpRS*. Our results highlight and emphasize the importance of Ca^{2+} as a signal used by *Pto* during pathogenesis and show that the TCS, *CvsSR*, is a key player in the regulation of genes important for full virulence of *Pto* (Figure 2.22).

Mechanisms by which *Pto* senses and responds to Ca^{2+} were previously unknown. Several TCSs that either sense or are induced by Ca^{2+} have previously been characterized in other bacteria. The histidine kinase PhoQ in *Salmonella enterica* serovar Typhimurium binds to Ca^{2+} , Mg^{2+} , and Mn^{2+} and regulates several virulence factors (126). *CarSR* in *Vibrio cholerae* is induced by Ca^{2+} and negatively regulates biofilm formation and exopolysaccharide production (104). In *P. aeruginosa* PAO1, the orthologous TCS to *CvsSR*, *BqsSR*, is also induced by Ca^{2+} and regulates cytosolic Ca^{2+} concentration (108). However, to our knowledge, *CvsSR* is the first Ca^{2+} induced TCS characterized in a hemibiotrophic plant pathogenic bacteria. Thus,

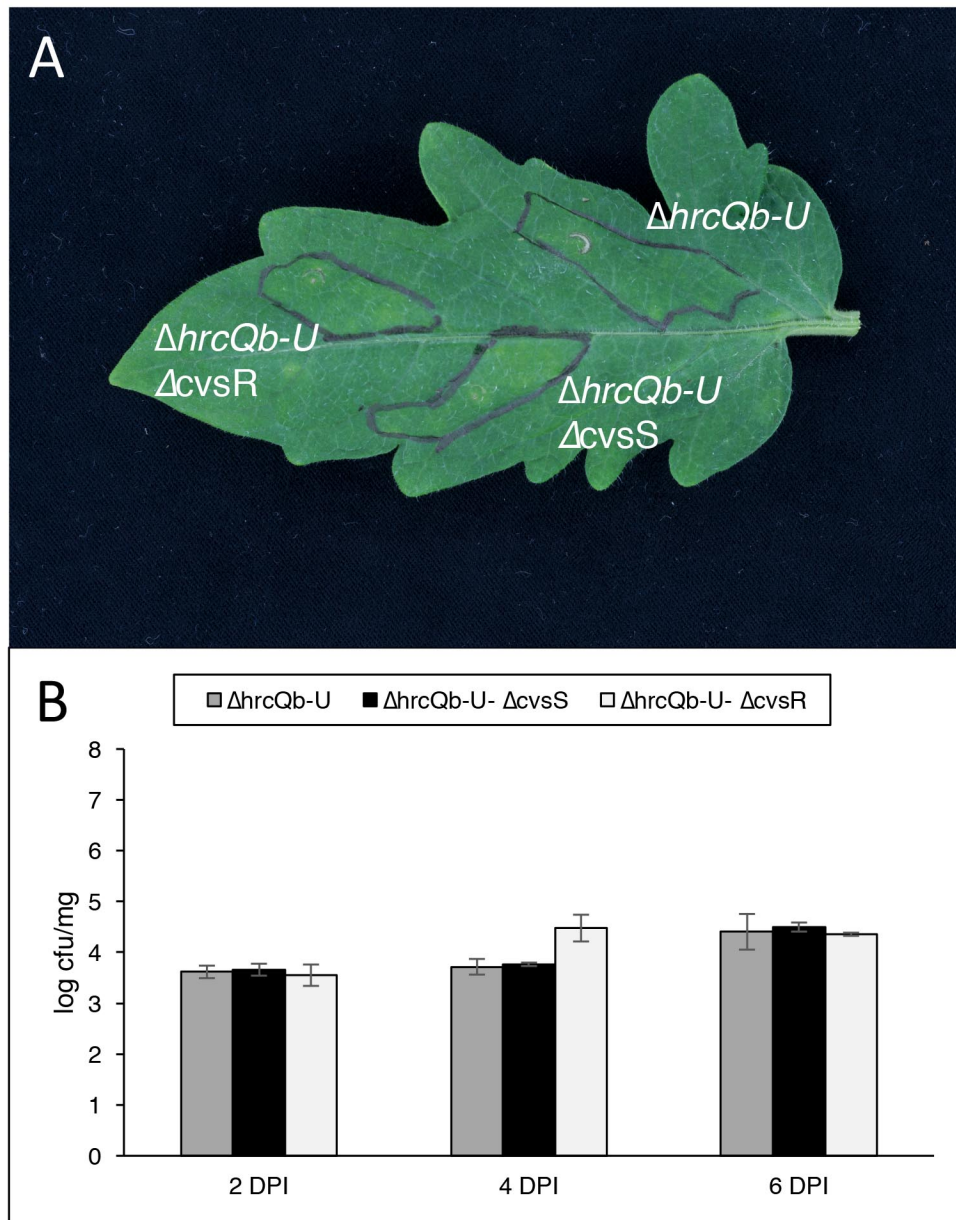


Figure 2.21: (A) Picture of syringe infiltrated leaf of tomato at 6 DPI. Areas infected with $\Delta hrcQb-U$, $\Delta hrcQb-U \Delta cvsS$, and $\Delta hrcQb-U \Delta cvsR$ are labeled as such (B) Growth curves over time in log cfu/mg are shown for $\Delta hrcQb-U$, $\Delta hrcQb-U \Delta cvsS$, and $\Delta hrcQb-U \Delta cvsR$ infecting tomato at 4 DPI and 6 DPI. The strains were inoculated at 1×10^6 cfu/mL using a blunt syringae. Average bacterial growth in three plants was used with the error bars representing the standard error between the three replicates.

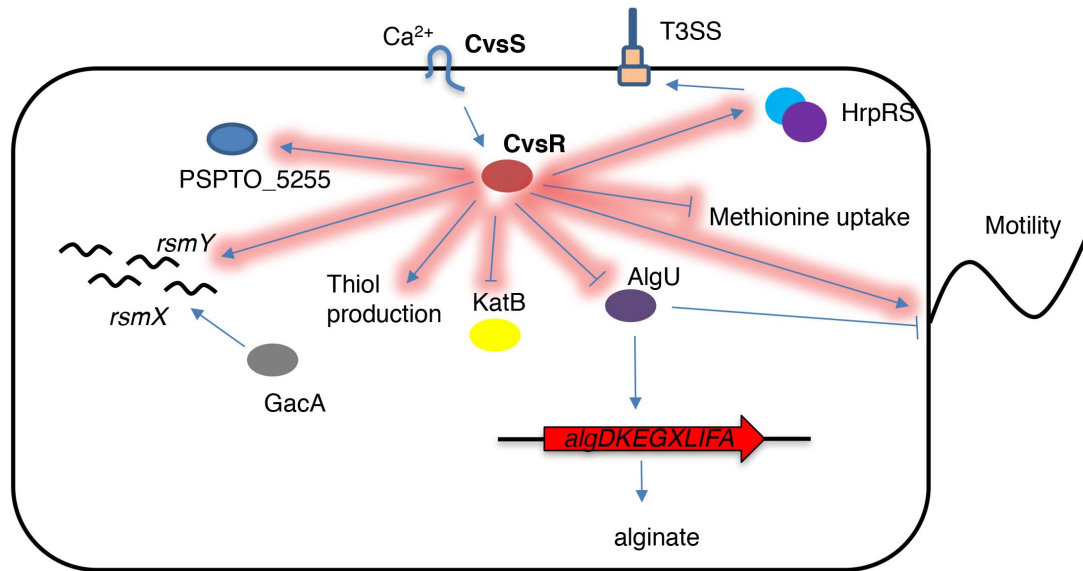


Figure 2.22: Model of a partial regulon of CvsR in *Pto*. Arrows highlighted in red are part of the CvsR regulon.

Ca²⁺ can now be added to the list of environmental cues that *Pto* uses during pathogenesis.

According to ChIP-seq and RNA-seq data, CvsR directly promotes expression of several genes, including PSPTO_5255, PSPTO_1304, and PSPTO_1609 and directly represses expression of several genes including *katB* and *tauA* (Table 2.6). Response regulators within the OmpR family can act as both transcriptional promoters or repressors. OmpR in *E. coli* reciprocally regulates *ompF* and *ompC* depending on the osmotic conditions of the environment (127). CpxR in *E. coli* promotes expression of *marR* and represses expression of *ung* (128, 129). CvsR appears to be similar in its ability to promote and repress expression of different genes.

CvsR regulates transcription of *algU* and the regulons of CvsR and AlgU have noticeable overlap (95). It is currently unclear how CvsR transcriptionally regulates *algU* in *Pto*. Most characterized negative regulation of *algU* in *Pseudomonas* occurs post-transcriptionally through RsmA or post-translationally through MucA and MucB (130, 131). Indirect repression of *algU* by CvsR would add another layer of regulatory control over *algU* that was previously unknown. Even with decreased expression of several *rsm* sRNAs and increased expression of *mucA* and *mucB* in the Δ *cvsR* strain as compared to WT, AlgU was still active in the Δ *cvsR* strain (Table 2.4). One explanation for this phenomenon is that activity of RsmA, MucA, and MucB can be repressed post-translationally through various mechanisms. Post-translational repression would not be captured through ChIP-seq or RNA-seq. This could result in reduced activity of these proteins even if there was increased transcription. In the case of MucA, AlgW degrades MucA in *P. aeruginosa* and something similar could be

occurring in the $\Delta cvsR$ strain (131). For RsmA, *rsmZ* and the *rsmX* paralogs not regulated by CvsR could sequester RsmA in the $\Delta cvsR$ strain even when the other *rsm* sRNAs are not abundant. Further characterization of CvsR-based *algU* regulation is necessary to discern the exact mechanism.

AlgU regulates expression of genes involved in osmoadaptation, ROS detoxification, alginate biosynthesis, and pathogenicity in *Pto* (95). Interestingly, and somewhat contradictory to reported results that show overexpression of *algU* increases virulence of *Pto*, the $\Delta cvsR$ strain was less virulent than WT on tomato plants even though it showed an increase in expression of *algU* compared to WT. Overexpression of *algU* in *Pto* resulted in increased expression of *cvsS* and *cvsR* (95). Both *cvsS* and *cvsR* are directly regulated by CvsR. Even though we observed up-regulation of *algU* in the $\Delta cvsR$ strain as compared to WT, we did not observe an accompanied up-regulation of *cvsS* and *cvsR* in the $\Delta cvsR$ strain as compared to WT. It is possible that up-regulation of *cvsS* and *cvsR* is critically involved in AlgU-related virulence. One might speculate that upon deletion of *cvsR*, *algU* overexpression may no longer positively regulate virulence because up-regulation of *cvsSR* no longer occurs.

Biofilm formation and swarming motility are typically antagonistic with only rare examples of these lifestyles being sympathetic (132). In our study, CvsR appears to regulate biofilm formation and swarming motility in the typical antagonistic way. However, this was not the case with CvsS. The orthologous TCS, BqsSR, in *P. aeruginosa* PAO1 positively regulates biofilm dispersal when *P. aeruginosa* PAO1 was grown in LB (133). However, when grown on BM2 agar supplemented with 10 mM CaCl₂, swarming motility was not reduced upon deletion of *bqsSR* (108). As

such, while each assay was performed under different conditions it appears that BqsSR regulates biofilm lifestyle and swarming motility in a sympathetic way in *P. aeruginosa* PAO1. While BqsSR and CvsSR are considered to be orthologous TCSs, they may not function in entirely the same way and regulation of swarming motility may be an area where these TCSs differ.

Increased EPS production, decreased flagellar motility, and decreased biosurfactant production all result in decreasing swarming motility in *P. syringae* (116, 134). It should be noted that, we did not investigate whether changes in biosurfactant production occur in *Pto* upon deletion of *cvsS* or *cvsR*. However, we did investigate whether changes in EPS production or flagellar motility reduced swarming in the $\Delta cvsS$ and $\Delta cvsR$ strains. We ruled out overproduction of alginate as a possible explanation for decreased swarming motility in the $\Delta cvsS$ and $\Delta cvsR$ strains (Figure 2.14) and there is no clear evidence that the $\Delta cvsS$ and $\Delta cvsR$ strains overproduce Psl EPS. It has been reported that increased cellulose production affects swarming motility in *Pto* (135). We feel this cannot fully explain the reduced swarming observed in the $\Delta cvsS$ and $\Delta cvsR$ strains since it takes a substantial amount of time to observe noticeable differences in cellulose production in the $\Delta cvsS$ and $\Delta cvsR$ strains compared to WT. Cellulose production commonly correlates with increased c-di-GMP in *Pto* (116, 136). Increases in c-di-GMP decrease swarming motility in *Pseudomonas* (137). Although outside the scope of this work, c-di-GMP concentrations between the $\Delta cvsR$ strain and WT may differ. Current evidence also suggests that decreased swarming motility is not due to decreased flagellar motility since swimming is not compromised in the $\Delta cvsR$ strain. However, the ability to swim is not always reflective

of proper flagellar function as several chemotaxis proteins and flagellar motors are necessary for swarming, but not swimming in *P. aeruginosa* (138, 139). Genes that code for six putative chemotaxis proteins and the rotary flagellar motor protein, *motY*, are down-regulated in the $\Delta cvsR$ strain as compared to WT (Table 2.4). Therefore, it is possible that down-regulation of these genes could reduce swarming without reducing swimming. Further investigation into the role CvsSR plays in swarming is currently being pursued.

CvsR is, to our knowledge, the first direct transcriptional activator of *hrpRS* identified in *Pto*. The conservation of orthologous TCSs to CvsSR in other *P. syringae* pathovars opens the possibility of a conserved *hrpRS* transcriptional activator across pathovars (27). Disruption in *hrpRS* expression in *Pto* through either deletion of *hrpRS* or deletion of an *hrpRS* indirect regulator, like GacA, resulted in loss of the HR (28). One curiosity about CvsSR is that deletion of *cvsS* or *cvsR* does not disrupt the HR. Baseline expression of *hrpR* and *hrpS* still occurs when *cvsS* or *cvsR* is deleted. From these data, it is likely that CvsSR tunes expression of *hrpRS*. It is not uncommon for TCSs to tune expression of genes. For example, in *Salmonella enterica* PhoPQ tunes expression of the effector *steA* during osmotic stress and PhoBR tunes expression of itself in *E. coli* according to environmental phosphate concentrations (140, 141). If CvsSR tunes expression of *hrpRS* then it is conceivable that deletion of *cvsS* or *cvsR* may only cause subtle changes T3SS and T3E deployment that does not affect the HR, but could still influence pathogenesis.

The exact mechanism by which CvsSR is involved in virulence remains elusive. The growth assay of the $\Delta hrcQb-U$, $\Delta hrcQb-U \Delta cvsS$, and $\Delta hrcQb-U \Delta cvsR$

strains in tomato brought us to believe that the concentration of Ca^{2+} in the apoplast did not adversely affect growth of the ΔcvsS and ΔcvsR strains *in planta*. Decreased growth accompanied with decreased virulence of *Pto*, as seen in the ΔcvsS and ΔcvsR strains when assayed for virulence on tomato plants and *A. thaliana*, could be indicative of increased susceptibility of these strains to the plant immune response or a defect in phytotoxin or T3E deployment in these strains. Decreased spread of chlorotic symptoms by *Pto* commonly occur as a result of changes in T3Es or coronatine production (142-144). While we have not investigated whether CvsSR regulates coronatine production in *Pto*, CvsR does bind upstream of several T3Es within the *Pto* genome. It is possible that regulation of these T3Es by CvsSR *in planta* plays a role in the reduced chlorosis and loss of necrotic specks observed in the plants inoculated with the ΔcvsS or the ΔcvsR strains. HopAA1-1 is directly regulated by CvsR and is necessary for chlorosis and production of necrotic specks in tomato plants (142). HopG1 is also directly regulated by CvsR and is another T3E that is necessary for chlorosis (145). CvsR also positively regulates expression of the gene *fliC*, which codes for flagellin. Flagellin is a major pathogen associated molecular pattern (PAMP) that triggers a defense response called PAMP triggered immunity (PTI) in plants (7). This means that deletion of CvsSR could result in less production of a major PAMP by *Pto*. Decreased expression of PAMPs can recover growth of certain effector depleted *Pto* mutants (146). With the regulon of CvsR including *hrpRS*, several T3Es, and *fliC*, CvsR regulates multiple components involved in virulence of *Pto*. Characterization of the CvsSR regulon *in planta* could provide a clearer picture by

which CvsSR regulates each of these factors during endophytic growth and how they synergistically affect virulence of *Pto*.

MATERIALS AND METHODS

Bacterial Strains and Growth Conditions. The primers and bacterial strains and plasmids used in this study can be found in Supplementary Tables 2.7 and 2.8, respectively. *Escherichia coli* DH5 α and *E. coli* TOP10 (ThermoFisher Scientific, Waltham) were used for cloning. *E. coli* BL21 (DE3) was used for expressing proteins. *E. coli* was grown in Luria-Bertani (LB) medium or Terrific Broth (TB) medium supplemented with the appropriate antibiotics when necessary. *Pto* was routinely cultured on King's B (KB) agar (147). For select assays, strains were grown in MG medium (10g Mannitol, 2.5 g L-glutamate, 0.2 g MgSO₄ 7H₂O, 0.5 g KH₂PO₄, and 0.2 g NaCl per liter) at the specified pH (16).

Creation of *Pto* mutants. Unmarked deletion strains were constructed using pK18mobsacB plasmid (148). DNA fragments of approximately 1.1 kb upstream and 1.0 kb downstream of *cvsS* (PSPTO_3380) and *cvsR* (PSPTO_3381) were amplified by PCR, gel-purified and then joined by splicing by overlap extension PCR. These products were then gel-purified using Qiagen Gel Extraction Miniprep Kit (Qiagen, Valencia, CA), digested with the appropriate restriction enzymes and cloned into pK18mobsacB using EcoRI (New England Biolabs, Ipswich, MA) and BamHI (NEB). The pK18mobsacB deletion constructs were confirmed by sequencing at the Biotechnology Resource Center of Cornell University before introduction into WT, Δ *hrcQb-U*, or Δ *algD* *Pto* via electroporation. Integration events were selected on

Table 2.7: Primers used in this study

Primer	Sequence (5'-3')	Description
oSWC01445	ATGCTTCCGGCTCGT ATGTTGTGT	Forward M13 primer
oSWC01446	GGCGATTAAGTTGGG TAACGCCAG	Reverse M13 primer
oSWC01662	TCGTTGATCGCGGTC GCCACC	Downstream forward <i>cvsS</i> KO
oSWC01663	CACATGGAATTCTTT CCGAGCGTTGCGCCT GC	Downstream forward nested <i>cvsS</i> KO with EcoRI site
oSWC01664	ATTGACCTGCCGGAA CGTACC	Downstream reverse <i>cvsS</i> KO
oSWC01665	GGTACGTTCCGGCAG GTCAATCAACCGCCT TTGTATGGACTTC	Upstream forward <i>cvsS</i> KO with overlap
oSWC01666	TGATGCGCAGGATAT TGAGTGG	Upstream reverse <i>cvsS</i> KO
oSWC01667	CACATGGGATCCAGC GTCTCTGTGCCATCCT TGG	Upstream nested reverse <i>cvsS</i> KO with BamHI site
oSWC01668	TCGTCGTCAATCAAC AGGC	Downstream forward <i>cvsR</i> KO
oSWC01669	CACATGGAATTCAAA CGCACCTCGCTATCG GC	Downstream forward nested <i>cvsR</i> KO with EcoRI site
oSWC01670	TATCTTTACGGTGGA GCCGGGG	Downstream reverse <i>cvsR</i> KO
oSWC01671	CGGCTCCACCGTAAA GATATTCAACCAGTA ACAGGCGCATC	Upstream forward <i>cvsR</i> KO with overlap
oSWC01672	TGTCTGTCAGTGCCA CCAG	Upstream reverse <i>cvsR</i> KO
oSWC01673	CACATGGGATCCTTC GCTTAGGCAGGGAAG G	Upstream nested reverse <i>cvsR</i> KO with BamHI site
oSWC01700	TTGGGCACAGGTTTCG GTCTTG	Downstream forward PCR screen <i>cvsS</i> KO
oSWC01701	AAGCACCAGTCCTGA TGGC	Downstream reverse PCR screen <i>cvsS</i> KO
oSWC01702	TTGAGTCCGGCAGAC TCCAGC	Upstream forward PCR screen <i>cvsS</i> KO
oSWC01703	TAAGGGTCTGGCGAC ACCG	Upstream reverse PCR screen <i>cvsS</i> KO

Table 2.7 (Continued)

oSWC01704	AGCAAGTGGTTGATC TGGG	Downstream forward PCR screen <i>cvsR</i> KO and used in RT-PCR for <i>cvsR-cvsS</i>
oSWC01705	ATCACGGTGCAGG GCGCTTC	Downstream reverse PCR screen <i>cvsR</i> KO
oSWC01706	TGATTCCTGTAGACC TGGC	Upstream forward PCR screen <i>cvsR</i> KO
oSWC01707	ATGCCAAAGCACTGA GCAAG	Upstream reverse PCR screen <i>cvsR</i> KO
oMRF0150	GCCTTGCGGGTCAA CAA	Reverse for RT-PCR for PSPTO_3383-PSPTO_3382
oSWC05046	GACAAGCGTCTCTGT GCCATCCT	Forward primer for RT-PCR for PSPTO_3382- <i>cvsR</i>
oMRF0145	GGCCAGGTCTACAGG AATCATC	Forward primer for RT-PCR for PSPTO_3383-PSPTO_3382
oMRF0148	GGTGTCCGACACCC TTACC	Reverse primer for RT-PCR for PSPTO_3382- <i>cvsR</i>
oMRF0535	GGCGTGCAGGATCG AG	Reverse primer for RT-PCR for <i>cvsR-cvsS</i>
oMRF0010	CACCGTTTTATTGTT AGGAGGGTCCATAG	reverse promoter fusion without PSPTO_3383 gene, begins at end of PSPTO_3383
oMRF0011	TGTCGTAATGCTGTG TCTGTCAGTG	forward promoter fusion 400bp upstream of PSPTO_3383
oMRF0016	GCGGCTTAACAAG CGTTAGA	forward primer for pBS59
oMRF0017	TCCTGAGGTAGCCAT TCATCCA	reverse primer for pBS59
oMRF0050	TCACTTGTCATCGTC GTCCTTGTAGTCACC CCCGGCTCCACCG	C-terminal FLAG-tag gateway overexpression C-terminus of <i>cvsR</i>
oMRF0051	CACCATGCGCCTGTT ACTGGTTGAAG	C-terminal FLAG-tag gateway overexpression N-terminus of <i>cvsR</i>
oMRF0233	CAAGCGTCTCTGTGC CATC	<i>algD</i> qPCR sense
oMRF0234	CGAGCGGAAGAATG ACACC	<i>algD</i> qPCR antisense
oSWC02061	TTTCTGCAGCAACCG CCTTTGTATGG	<i>cvsR</i> complement forward primer
oSWC02063	TTTAAGCTTTTGGCAT GTTTTGATGG	<i>cvsR</i> complement reverse primer

Table 2.7 (Continued)

oMRF0355	CGGCGGCCGCCGCCT TTGTATGGACTTCAA CC	Reverse primer for <i>cvsR</i> insertion into pET21 with NotI site
oMRF0357	CGGGATCCATGCGCC TGTTACTGGTTGAA	Forward primer for <i>cvsR</i> insertion into pET21 with BamHI site
oMRF0375	CTGTAAGCGCTTGTT CGCATT	<i>hrpR</i> peak #2 ChIP-seq peak 5'-FAM tag for EMSA and DNase footprinting
oMRF0376	AGAAACGCGCTATTC ATTGCA	<i>hrpR</i> peak #2 ChIP-seq peak 3' for EMSA and DNase footprinting
oMRF0377	TGCGGAGTAAATCGC AGGC	<i>spf</i> ChIP-seq peak 5'-FAM tag for EMSA and DNase footprinting
oMRF0378	GCAGTGCCGCTGCTG GT	<i>spf</i> ChIP-seq peak 3' for EMSA and DNase footprinting
oMRF0381	TGCAGGCGTCGAGTC TAACA	PSPTO_3383 ChIP-seq peak 5'-FAM tag for EMSA and DNase footprinting
oMRF0382	TGCGGATCGATGCCA CG	PSPTO_3383 ChIP-seq peak 3' for EMSA and DNase footprinting
oMRF0385	GCAAGTGTCAATATT GAGTTGACTCAAC	PSPTO_0203 ChIP-seq peak 5' for EMSA and DNase footprinting
oMRF0386	CCTTGATGCTTCCAC CAGGA	PSPTO_0203 ChIP-seq peak 3' with 5'FAM for EMSA and DNase footprinting
oMRF0387	TGGCCGTTATTTAAC GCATTG	<i>katB</i> ChIP-seq peak 5'-FAM for EMSA and DNase footprinting
oMRF0388	GCGCGACGTTAAGAG TGCA	<i>katB</i> ChIP-seq peak 3' for EMSA and DNase footprinting
oMRF0389	CCTTACGCAGCCCGT GAG	tRNA-cys-1 ChIP-seq peak 5'-FAM for EMSA and DNase footprinting
oMRF0390	GCCGAGGTCGGAATC GAA	tRNA-cys-1 ChIP-seq peak 3' for EMSA and DNase footprinting
oMRF0391	GGCATCGACCTTGTC AGATCC	PSPTO_4969 ChIP-seq peak 5' for EMSA and DNase footprinting
oMRF0392	TATGGTTTCCCGGTC AAGGA	PSPTO_4969 ChIP-seq peak 3' w/ 5'FAM tag for EMSA and DNase footprinting
oMRF0393	CACGAAAATCTTCAT CGAGTGGA	<i>gidA</i> ChIP-seq peak 5' for EMSA and DNase footprinting
oMRF0394	AGCTGTGGAAAATC GCGAA	<i>gidA</i> ChIP-seq peak 3' with 5' FAM tag for EMSA and DNase footprinting
oMRF0395	CGGACTTGATCGCTG GCTT	<i>oprF</i> ChIP-seq peak 5'-FAM for EMSA and DNase footprinting

Table 2.7 (Continued)

oMRF0396	TCATCCGTTAAATCC CCATCTG	<i>oprF</i> ChIP-seq peak 3' for EMSA and DNase footprinting
oKMD0123	GCGCTAGCGCTCAAG GGA	PSPTO_5255 3' FAM-tag for EMSA and DNase footprinting
oMRF0062	TGTCACTCTTGTAAC GAACTTG	PSPTO_5255 5' for EMSA and DNase footprinting
oKMD0137	GCCATCACCTAGAAT GT	<i>hrpR</i> peak #1 3' FAM-tag for EMSA and DNase footprinting
oSWC06572	CGAACAACACAGAG GCTTGGATAC	<i>hrpR</i> peak #1 5' for EMSA and DNase footprinting
oMRF0191	CGCTCAAAGTACCAA TC	<i>fliC</i> qPCR sense
oMRF0192	GCTCAAAGTCAGAGA GA	<i>fliC</i> qPCR antisense
oMRF0231	GGATAACAAGGCGT AAA	<i>hopAH2-1</i> qPCR sense
oMRF0232	GCCTGATTCAACTTG TC	<i>hopAH2-1</i> qPCR antisense
oSWC06118	GTGCCAACGGACAGG CACA	<i>rsmZ</i> qPCR sense
oSWC06119	CCCTTGTCATCGTCCT GATGAA	<i>rsmZ</i> qPCR antisense
oSWC06338	GCAGGAAGCGCAAC AAGACAT	<i>rsmY</i> qPCR sense
oSWC06339	GCTTCCAGACTGTTT CCCTGAT	<i>rsmY</i> qPCR antisense
oSWC06348	GGTGAACAAGGAGTT CACCAGGA	<i>rsmX-3</i> qPCR sense
oSWC06349	CCAAGACCATTCCAA CTCCCTGT	<i>rsmX-3</i> qPCR antisense

Table 2.8: Strains and plasmids used in this study

Strain name	Genotype	Reference
<i>Pseudomonas syringae</i> pv. <i>tomato</i> DC3000 strains		
<i>Pto</i> (WT)	<i>Pseudomonas syringae</i> pv. <i>tomato</i> DC3000 wild type, Rif ^R	(60)
BBPS33	<i>Pto</i> Δ <i>cvsS</i>	(107)
BBPS34	<i>Pto</i> Δ <i>cvsR</i>	(107)
BBPS35	BBPS34 <i>attTn7::Tn7</i> -PSPTO 3383- <i>cvsR</i>	(107)
MFPS03	<i>Pto</i> pBS59:: <i>P_{cvsSR}</i>	This study
MFPS04	<i>Pto</i> Δ <i>cvsS</i> pBS59:: <i>P_{cvsSR}</i>	This study
MFPS04	<i>Pto</i> Δ <i>cvsR</i> pBS59:: <i>P_{cvsSR}</i>	This study
BMS2	<i>Pto</i> pBS44	(149)
PS392	<i>Pto</i> Δ <i>algD</i>	(95)
MFPS10	<i>Pto</i> Δ <i>algD</i> Δ <i>cvsS</i>	This study
MFPS11	<i>Pto</i> Δ <i>algD</i> Δ <i>cvsR</i>	This Study
CUCPB5113	<i>Pto</i> Δ <i>hrcQb-U</i> , Sp ^R	(125)
MFPS05	<i>Pto</i> Δ <i>hrcQb-U</i> Δ <i>cvsS</i> , Sp ^R	This study
MFPS06	<i>Pto</i> Δ <i>hrcQb-U</i> Δ <i>cvsS</i> , Sp ^R	This study
MFPS09	<i>Pto</i> Δ <i>cvsR</i> pBS46:: <i>cvsR</i> -FLAG	This study
MFPS20	<i>Pto</i> pBS58:: <i>P_{hrpRS}</i>	This study
MFPS21	<i>Pto</i> Δ <i>cvsS</i> pBS58:: <i>P_{hrpRS}</i>	This study
MFPS22	<i>Pto</i> Δ <i>cvsR</i> pBS58:: <i>P_{hrpRS}</i>	This study
MFPS24	<i>Pto</i> pBS63	This study
MFPS25	<i>Pto</i> Δ <i>cvsS</i> pBS63	This study
MFPS26	<i>Pto</i> Δ <i>cvsR</i> pBS63	This study
<i>Escherichia coli</i> strains		
DH5 α	<i>huA2 lac(del)U169 phoA glnV44 Φ80' lacZ(del)M15 gyrA96 recA1 relA1 endA1 thi-1 hsdR17</i>	ThermoFisher Scientific
TOP10	F- <i>mcrA</i> Δ (<i>mrr-hsdRMS-mcrBC</i>) Φ 80 <i>lacZ</i> Δ M15 Δ <i>lacX74 recA1 araD139</i> Δ (<i>ara leu</i>) 7697 <i>galU galK</i> rpsL (StrR) <i>endA1 nupG</i>	ThermoFisher Scientific
BL21 (DE3)	<i>fhuA2 [lon] ompT gal (λ DE3) [dcm] Δ<i>hsdS</i> λ DE3 = λ <i>sBamHI</i>o Δ<i>EcoRI</i>-B <i>int::(lacI::PlacUV5::T7 gene1) i21</i> Δ<i>nin5</i></i>	ThermoFisher Scientific

Table 2.8 (Continued)

Plasmids		
Name	Description	Reference
pK18mobSacB	pMB1 <i>mob sacB</i> , sucrose ^S , Km ^R	(148)
pZB20	pK18mobSacB with regions flanking PSPTO_3380 cloned into it using the EcoRI-BamHI site	(107)
pZB21	pK18mobSacB with regions flanking PSPTO_3381 cloned into it using the EcoRI-BamHI site	(107)
pENTR/D/TOPO	Directional cloning vector for entry to the Gateway System	ThermoFisher Scientific
pENTR/SD/TOPO	Directional cloning vector with ribosome binding site for entry to the Gateway System	ThermoFisher Scientific
pMRF2	pENTR/D/TOPO::P _{cvsSR}	This study
pBS58	luxCDABE destination vector	(149)
pBS59	luxCDABE destination vector	(149)
pMRF11	pBS59::P _{cvsSR}	This study
pBS44	luxCDABE destination vector control without insertion	(149)
pUC18miniTn7	mini-Tn7 mobilizable transposon with multicloning site, Gm ^R	(150)
pNTS2	mini-Tn7 helper plasmid	(150)

Table 2.8 (Continued)

pJZ1	pUC18miniTn7::PSPTO_3383- <i>cvsR</i>	This study
pBS46	<i>nptII</i> destination vector	(151)
pMRF14	pENTR/SD/TOPO:: <i>cvsR</i> -FLAG	
pMRF15	pBS46:: <i>cvsR</i> -FLAG	This study
pET21	Bacterial expression vector with T7 lac promoter, N-terminal T7 epitope tag, and C-terminal His tag, Ap ^R	Novagen
pMRF21	pET21:: <i>cvsR</i>	This study
pMRF22	pBS58::P _{<i>hrpRS</i>}	This Study
pBS63	pBS58::P _{<i>hrpL</i>}	(121)

KB medium containing 50 µg/ml kanamycin. Colonies were transferred to KB containing 10% sucrose to select for crossover events that resulted in the loss of the *sacB* gene. Sucrose-resistant colonies were screened by PCR, and clones containing the appropriate deletion(s) were confirmed by sequencing.

Complementation of Δ *cvsR* strain. The Δ *cvsR* complement was made using a pUC18 mini-Tn7 vector (150). Briefly a genomic fragment containing *cvsR*, PSPTO_3382, and PSPTO_3383 was amplified via PCR. The products were gel-purified using the Qiagen Gel Extraction Mini-Prep Kit (Qiagen), digested with HindIII (NEB) and PstI (NEB), and cloned into a pUC18miniTn7 plasmid which had been digested with HindIII and PstI. The resulting ligation was transformed into DH5 α *E. coli* cells. Δ *cvsR Pto* strain was transformed through electroporation with pUC18miniTn7::*cvsR*-3383 and the helper plasmid pTNS2. Colonies were selected by plating on KB supplemented with 10 µg/mL gentamicin. Positive clones were confirmed through sequencing.

Creation of CvsR-FLAG tagged strain. The CvsR-FLAG tagged strain was made using pBS46 (151). Briefly, the sequence for a FLAG tag was added to the 3' end of *cvsR* (*cvsR*-FLAG) using PCR amplification. The PCR product was gel extracted using the Zymoclean Gel Extraction Kit (Zymo, Irvine, CA) and then cloned into a pENTR/SD/TOPO vector (ThermoFisher Scientific) and transformed into Top10 *E. coli* (ThermoFisher Scientific). Positive clones for pENTR/SD/TOPO::*cvsR*-FLAG were selected by plating on LB supplemented with 50 µg/mL kanamycin agar plates and confirmed through sequencing. *cvsR*-FLAG was moved to from the pENTR/SD/TOPO entry vector to a vector containing a *nptII* promoter, pBS46, using

the LR reaction (ThermoFisher Scientific) and transformed into TOP10 *E. coli* (ThermoFisher Scientific). Positive clones were selected on LB supplemented with 10 µg/mL gentamicin agar plates and confirmed through sequencing. $\Delta cvsR$ *Pto* was then transformed with pBS46::*cvsR*-FLAG and selected on KB agar plates supplemented with 10 µg/mL gentamicin.

Luciferase reporter assays. 400 bp upstream of PSPTO_3383 (P_{cvsSR}) and 850 bp upstream of *hrpR* (P_{hrpRS}) were PCR amplified. PCR products were purified using Qiagen PCR purification kit, (Qiagen) cloned into pENTR/D/TOPO vectors (ThermoFisher Scientific) and transformed into TOP10 *E. coli* (ThermoFisher Scientific). Positive clones and constructs for pENTR/D/TOPO:: P_{cvsSR} and pENTR/D/TOPO:: P_{hrpRS} were generated, selected, and transformed into appropriate strains of *Pto* as previously described (149).

Pto strains were grown on KB plates and transferred to MG medium pH 6.0 or apoplastic washing fluid (AWF) at an OD₆₀₀ of 0.1. 5 mM CaCl₂ or 5 mM EGTA were added to the cultures when appropriate. Strains were grown in 96-well plates (Nunc) at 28°C with shaking in a Biotek Synergy II microplate reader (Winooski, VT). OD₆₀₀ and luminescence measurements were taken every two hours. Relative luminescence measurements were normalized to OD₆₀₀. The assays were repeated three times and sampling was conducted in triplicate. Averages and standard deviation were generated from each experiment. Statistical significance was determined by performing a least squares mean regression on the combined biological replicates.

Extraction of apoplastic washing fluid. A procedure used to extract apoplastic washing fluid (AWF) from bean plants was used to extract AWF on three to four-

week-old *Solanum lycopersicum* cv. Moneymaker plants (152). After extracting AWF, samples were analyzed for cellular contamination by testing for glucose-6-phosphate dehydrogenase and maltose dehydrogenase activity using a glucose-6-phosphate dehydrogenase activity assay kit (Sigma) and a maltose dehydrogenase activity assay kit (Sigma). AWF was then lyophilized and resuspended to an equivalent undiluted state.

Inductively coupled plasma mass spectrometry (ICP-MS). AWF was diluted four-fold and eighty-fold in double deionized water (ddH₂O) depending on the element being examined and analyzed on an iCap Q ICP-MS (ThermoFisher Scientific). Standards for calcium, potassium, zinc, sulfur, iron, cadmium, magnesium, and phosphorous (ThermoFisher Scientific) were included for each sample tested.

Tomato virulence assays. Three to four-week old *Solanum lycopersicum* cv. Moneymaker were inoculated with WT, $\Delta cvsS$, $\Delta cvsR$, $\Delta cvsRc$, *Pto* strains at 2×10^7 colony forming units (cfu)/mL through dip inoculation as was previously described (153). To assay $\Delta hrcQb-U$, $\Delta hrcQb-U \Delta cvsS$, and $\Delta hrcQb-U \Delta cvsR$, three to four-week old *Solanum lycopersicum* cv. Moneymaker were inoculated with *Pto* strains at 1×10^6 cfu/mL using a blunt-tipped syringe. Timepoints for growth of the bacteria (in cfu/mg) were taken at 4 and 6 days post-inoculation (DPI). The experiment was repeated three times, and three technical replicates were performed for each experiment. Averages and standard deviations were generated for growth of bacteria for each experiment. Student's two-tailed t-test was used to determine statistical significance between growth of different strains.

***A. thaliana* virulence assays.** *A. thaliana* was grown and inoculated as previously described (4). Plants were dipped in a bacterial suspension at 3×10^4 cfu/mL and vacuum-infiltrated at 20 mm Hg. Symptoms were observed at 4 and 6 DPI and growth of the bacteria (cfu/mg) was measured at 4 and 6 DPI. The experiment was repeated three times, and three replicates were used during each experiment. Averages and standard deviations were generated for growth of bacteria for each experiment.

Hypersensitive response (HR) assays. Three to four-week-old *N. tabacum* cv. *xanthi* or *N. benthamiana* plants were syringe-infiltrated with *Pto* strains resuspended in 10mM MgCl₂ at 2×10^6 , 2×10^7 , and 2×10^8 cfu/mL (154). HR was observed 1 and 2 DPI. Pictures were taken at 2 DPI. This experiment was repeated three times with three technical replicates for each biological replicate.

Chromatin immunoprecipitation (ChIP) and preparation of DNA for ChIP-seq.

Δ *cvsR* *Pto* complemented with pBS46::*cvsR*-FLAG was grown overnight in KB medium to stationary phase and 200 μ L of the culture was plated on NB (Becton Dickinson, Franklin Lake, NJ) medium supplemented with 5 mM CaCl₂ and 0.5% (w/v) sodium succinate hexahydrate (Sigma). After 18 hours of growth at 28°C the cells were scraped from the plates using a sterile slide and resuspended in NB medium with 1% formaldehyde and then processed as described previously (107).

qPCR. qPCR was performed on DNA from input and IP fractions on a Bio-rad CFX Connect (Bio-rad, Hercules, CA) using Sso Advanced SYBR Green Supermix (Bio-rad). Primers upstream of PSPTO_3383 were used to determine enrichment for predicted targets of CvsR in the IP fraction. Enrichment of these areas was determined relative to regions in the gene *gyrA* (107).

Analysis of ChIP-seq data. Sequenced reads from three separate MiSeq runs were first compiled and then analyzed. Sequencing reads were trimmed using the FASTX toolkit (version 0.0.14) and the UTILS toolkit (release tag 822) (155). Bowtie2 2.2.6 was used to align sequencing reads to the *Pto* genome (156). Ambiguous reads were removed using a custom script as previously described (157). MACS version 2.1.0.20140616 was used to identify regions of enrichment in the *Pto* genome from the IP sample using the following parameters:

```
macs2 callpeak -t CHIP_FILE -c CONTROL_FILE
--seed 1 -g 6.1e6 --fix-bimodal \
--keep-dup all -q 0.0.5
```

Several peaks were called within *cvsR*. Since these were likely an artifact due to overexpression of *cvsR* during the ChIP-seq experiment they were disregarded.

CvsR binding motif generation. Regions 50 bps up and downstream of called peaks were identified. Any regions that overlapped were merged. These regions were then compiled and motif discovery was performed using MEME version 4.10.0 patchlevel 1 with the following parameters (158):

```
-revcomp -nmotifs 3 -minw 6 -maxw 50 \
-minsites 2 -maxsites NUMBER_OF_INPUT_SEQUENCES
-mod zoops
```

RNA Extraction and RNA-seq cDNA library preparation. *Pto* strains were grown overnight in KB media to stationary phase and 200 μ L of these cultures were plated and spread on NB with 5 mM CaCl₂ supplemented with 0.5% (w/v) sodium succinate hexahydrate. The cultures were allowed to grow for 18 hours at 28 °C then RNA was

extracted using the Zymo Direct-zol kit (Zymo). Ribosomal RNA (rRNA) was then extracted using Ribo-zero for Gram negative bacteria (Illumina, Madison, WI) as previously described (157). cDNA libraries were made using Scriptseq V.2 according to the manufacturer's instructions. The cDNA libraries were sequenced on a HiSeq 2000 at the Cornell Core Facility.

Analysis of RNA-seq data. Sequenced reads were first trimmed using fastq-mcf (release tag 1.04.807) and then aligned to the *Pto* genome using Bowtie2 2.2.6 (156). Ambiguous reads were removed as previously described (157). Next a list of regions to be considered for differential analysis was constructed as previously described (95).

qRT-PCR. Extracted RNA was reverse transcribed into cDNA using the qScript cDNA Supermix (Quanta, Gaithersburg, MD). qRT-PCR was performed on a Bio-Rad CFX Connect using Sso Advanced SYBR Green Supermix. The reference gene *gyrA* was used to normalize expression between samples (159). Experiments were performed three times. Averages and standard deviations from each biological replicate were generated from the experiments.

RT-PCR. Extracted RNA was reverse transcribed into cDNA using the iScript cDNA Supermix (Bio-Rad). In addition, a no reverse transcriptase control was made using extracted RNA as well. RT-PCR was performed on *Pto* gDNA, cDNA, and a no reverse transcriptase RNA control on a Bio-Rad T100 thermocycler using Onetaq (NEB). PCR products were then run on an agar gel and visualized using a Bio-Rad Chemidoc transilluminator (Bio-Rad). RT-PCR experiments were performed using three times on three biological replicates.

Overproduction and purification of CvsR. The *cvsR* gene was amplified with Phusion (ThermoFisher Scientific) using primers oMRF0355 and oMRF0356 and *Pto* genomic DNA as a template. Amplified *cvsR* was cloned into pET21 using NotI and SpeI (NEB) to make pET21::*cvsR* (pMRF21). pMRF21 was transformed into BL21 (*DE3*) *E. coli* cells (ThermoFisher Scientific). Transformed cells were grown at 37°C in 4 liters of LB medium supplemented with 100 µg/mL ampicillin to an OD₆₀₀ of 0.8 before 0.5 mM IPTG (Sigma) was added to the culture to induce expression. Cells were allowed to grow for another 4 hours at 37°C then pelleted and frozen at -80°C. Thawed cells were resuspended in wash buffer (20 mM Tris [pH 8], 500 mM KCl, 20 mM imidazole, and 10% glycerol) and lysed through sonication. Insoluble material removed through centrifugation and supernatant was applied to Ni-NTA Superflow Agarose (Qiagen) using gravity column chromatography. CvsR was eluted off the agarose using elution buffer (20 mM Tris [pH 8], 500 mM KCl, 100 mM imidazole, and 10% glycerol), dialyzed overnight into storage buffer (40.1 K₂HPO₄, 9.9 mM KH₂PO₄ [pH 7.4], 300 mM KCl, 50% glycerol), and stored at -80°C.

Electrophoretic mobility shift assay. 6-carboxyfluorescein (6-FAM) labelled probes were generated through PCR with Onetaq (NEB) using *Pto* genomic DNA as a template. Probes were gel purified using Zymoclean Gel DNA Recovery Kit (Zymo). Electrophoretic mobility shift assays (EMSA) were performed with increasing concentrations of CvsR (0 nM to 500 nM). Labelled probes were incubated with CvsR in 20 µL of binding buffer (40.1 mM K₂HPO₄, 9.9 mM KH₂PO₄ [pH 7.4], 15 mM KCl, 1 mM MgSO₄, 10% glycerol, and 40 ng/µL poly dI-dC DNA [Thermofisher Scientific]) for 20 minutes at room temperature. Reaction mixtures were then added to

6% polyacrylamide gels (0.5X TBE, 29:1 acrylamide:bis-acrylamide [Bio-Rad], 30% glycerol) and run at 215V for 3 hours on ice. Gels were visualized on a Typhoon 9400 image system (GE Healthcare, Pittsburgh, PA).

Non-radioactive DNase footprinting. 6-FAM labelled probes were generated and purified in the same manner as for EMSA. DNase footprinting assays were performed with 1 to 4 μ M CvsR. Labelled probes were incubated with CvsR in 20 μ L of DNase footprinting buffer (15 mM Tris-HCl [pH 7.4], 10 mM KCl, 6 mM MgSO₄, 1 mM CaCl₂, 10% glycerol, 2.5 ng/ μ L salmon sperm DNA [Sigma], 100 μ g/mL Bovine serum albumin [NEB]) for 20 minutes at room temperature. 0.001 U of DNase (NEB) was then added to reaction mixtures and allowed to incubate for 2 minutes before an equal volume to the reaction mixture of DNase stop solution (20 mM EDTA [pH 8.0], 1% SDS, 200 mM NaCl) was added. Digested probes were purified using the Oligo Clean and Concentrator (Zymo). Results were analyzed as previously described (107). The location of regions protected by CvsR were estimated by mapping the position of the binding site back to the genomic location of the probe using a LIZ500 ladder (ThermoFisher Scientific). The genomic locations of regions protected by CvsR were compiled and motif discovery was performed on MEME version 4.11.3 (158) with the following parameters (158):

-revcomp -nmotifs 3 -minw 4 -maxw 50 -mod zoops \

Quantification of alginate. *Pto* strains were grown overnight in KB medium to stationary phase and 200 μ L of these cultures were plated and spread on NB agar or NB agar supplemented with 5 mM CaCl₂ plates. The cultures were grown at 28 °C before being scraped off the plate and resuspended in 0.9% NaCl. Resuspended cells

were pelleted by centrifugation, supernatant was removed and alginate production determined using the carbazole-borate method with sodium alginate (Sigma Aldrich) used as a standard (160).

Motility assays. Swarming assays were performed using NB plates containing 0.5% (w/v) agar supplemented with 5 mM CaCl₂ when appropriate. *Pto* strains were grown overnight in KB medium and 5 µL of each culture was spotted on a swarming plate (161). Swarming zones were measured after plates were incubated for 24 hours at room temperature. A student's two-tailed t-test was used to determine statistical significance.

Swimming assays were performed using swimming plates (10 g Tryptone, 5 g NaCl per liter) with 0.3% (w/v) agar and supplemented with 5 mM CaCl₂ when appropriate (162). *Pto* strains were grown overnight in KB medium. Toothpicks were dipped into the overnight cultures grown to stationary phase in KB medium and inserted into the center of the swimming plates (163). Diameter of bacterial zones were measured after plates were incubated for 48 hours. Pictures of swimming zones were taken after 24 hours of growth at room temperature.

Biofilm assays. Biofilm assays were modified from a previously described protocol (164). *Pto* strains were grown overnight at 28 °C in KB medium, washed twice with MG medium, then sub-inoculated into MG pH 7.0 medium with 2 mM CaCl₂ at an OD₆₀₀ of 0.02. 100 µL of each bacterial suspension was grown in clear flat-bottom 96-well plates in a BioTek Synergy 2 microplate reader for 24 hours at 28 °C with shaking. Cultures were removed from the wells using a pipette and then the wells were washed with double distilled H₂O (ddH₂O). Following washing, wells were stained

with 0.1% crystal violet for 10 minutes and washed twice with ddH₂O. Stained biofilms were dissolved with 100 μ L of 30% acetic acid and the OD₅₇₀ was recorded using a Biotek Synergy 2 microplate reader. Experiments were repeated three times. Four technical replicates of each strain were used during each experiment. A students two-tailed t-test was used to determine statistical significance.

Statistical analysis. All statistical analysis was performed using JMP Pro 12.

Acknowledgements

We would like to thank Kent Loeffler and Claire Smith for pictures used in this manuscript. We would like to thank Eric Craft and Shree K. Giri for running samples for ICP-MS. We would like to thank Alan Collmer for reviewing this manuscript and providing helpful comments. The U.S. Department of Agriculture (USDA) is an equal opportunity provider and employer. Mention of trade names or commercial products in this publication is solely for the purposes of providing specific information and does not imply recommendation or endorsement by the USDA. The authors declare no conflicts of interest.

CHAPTER 3

CVSSR REGULATES PREVENTION OF SURFACE-ASSOCIATED CALCIUM PRECIPITATION IN *PSEUDOMONAS SYRINGAE* PV. TOMATO DC3000⁴

ABSTRACT

The two-component system (TCS) CvsSR is a Ca²⁺-induced TCS in the plant pathogen *Pseudomonas syringae* pv. tomato DC3000 (*Pto*). In addition to CvsSR being induced by Ca²⁺, it is also induced by Fe³⁺, Zn²⁺, and Cd²⁺. CvsSR regulated swarming motility in *Pto* in a Ca²⁺-dependent manner, but swarming behavior was not regulated by Fe³⁺, Zn²⁺, or Cd²⁺. We hypothesized that this was likely due precipitation of calcium phosphate on the surface of Δ cvsS and Δ cvsR strains grown on agar medium supplemented with Ca²⁺. Swarming of the Δ cvsS and Δ cvsR strains was restored by reducing the initial pH of the medium. Alternatively, swarming motility could also be restored in the Δ cvsS and Δ cvsR strains by adding glucose to medium supplemented with Ca²⁺. Under these conditions, the Δ cvsS and Δ cvsR strains no longer precipitated calcium phosphate on the surface of cells. *Pto* secretes gluconic acid and acidifies the medium when grown in medium supplemented with Ca²⁺ and glucose. Lastly, constitutive expression a CvsSR regulated carbonic anhydrase and a CvsSR regulated putative sulfate major facilitator superfamily transporter in the Δ cvsS and Δ cvsR strains revert the Δ cvsS and Δ cvsR strains back to a wild-type phenotype

⁴ Maxwell R. Fishman and Melanie J. Filiatrault. CvsSR regulates prevention of surface-associated calcium precipitation in *Pseudomonas syringae* pv. tomato DC3000. In prep.

where they no longer precipitate calcium phosphate on the surface of cells. This indicates that *Pto* may secrete protons and bicarbonate to suppress calcium precipitation on the surface of cells.

INTRODUCTION

Two-component systems (TCSs) are one mechanism through which bacteria sense and adapt to environmental changes. They are commonly composed of a transmembrane histidine kinase and a cytoplasmic response regulator (19). Often, upon activation, TCSs regulate genes that are appropriate for the given environment. The genome of the plant pathogenic bacteria *Pseudomonas syringae* pv. tomato DC3000 (*Pto*) encodes 69 histidine kinases and 95 response regulators (27). Among the TCSs within *Pto*, is a virulence associated TCS that is induced by Ca^{2+} *in planta* called CvsSR (165).

TCSs may be activated or induced by multiple substrates. PhoPQ is activated in *Salmonella enterica* by cationic antimicrobial peptides, Mg^{2+} , Ca^{2+} , and decreases intracellular pH and PmrAB in *S. enterica* is induced by both Mg^{2+} and Fe^{3+} (22, 166, 167). CvsSR has been shown to be induced by Ca^{2+} but could be induced by other metal cations as well. Transcription of *cvsS* and *cvsR* was previously found to be up-regulated in the presence of Fe (III) citrate (16). CvsSR autoregulates, which suggests that Fe (III) citrate may be an inducer of CvsSR. The orthologous TCS to CvsSR in *Pseudomonas aeruginosa*, called BqsSR, is directly activated by Fe^{2+} and the orthologous TCS in *Haemophilus influenzae*, FirSR, is directly activated by Fe^{2+} and

Zn²⁺ (110, 168, 169). Given the similarities between CvsSR, BqsSR, and FirSR, it suggests that metal cations other than Ca²⁺ may induce or activate CvsSR.

CvsSR regulates swarming motility in a Ca²⁺-dependent manner. Both Δ cvsS and Δ cvsR strains are unable to swarm when medium is supplemented with Ca²⁺. Bacterial swarming motility is negatively impacted by increased exopolysaccharide (EPS) production and decreased flagellar motility (170). CvsSR regulates flagellar biosynthesis genes and also alginate biosynthesis genes, however flagellar motility and overproduction of the EPS alginate were not responsible for inhibiting swarming in the Δ cvsS and Δ cvsR strains (165). In the presence of extracellular Ca²⁺, many bacteria may also precipitate calcium carbonate or calcium phosphate through microbially induced calcium precipitation (MICP) (61). *Pseudomonas* can precipitate calcium carbonate or calcium phosphate around colonies or on colonies depending on the strains and growth conditions (171, 172). Bacterial cells and secreted exopolysaccharides (EPSs), like alginate, can act as nucleation points for calcium carbonate or calcium phosphate during MICP (173, 174). MICP has been shown to phenotypically change, but not reduce, swarming motility in *Bacillus* sp. JH7 (175).

Opposite to MICP is calcium dissolution or, as it is also called in the case of calcium phosphate and apatite, phosphate solubilization (69, 74, 75). Phosphate solubilization by bacteria is thought to occur through two possible mechanisms. The first mechanism being when bacteria lower the pH of the external environment through the production of organic acids, including malic acid, acetic acid, and gluconic acid in the periplasm and the second mechanism being when organic anions chelate Ca²⁺ (69, 176). Gluconic acid, in particular, is prominent among phosphate

solubilizing bacteria and is commonly produced through direct oxidation of glucose by periplasmic glucose dehydrogenase (GCD) (177). Several *Pseudomonas* species perform phosphate solubilization through the secretion of gluconic acid (71, 73). On occasion, inorganic acids have been implicated in calcium dissolution, one such inorganic acid is carbonic acid (75). Carbonic acid is one possible product produced by carbonic anhydrases during the hydration of CO₂. Carbonic anhydrases in fungi and *Bacillus mucilaginosus* are involved in microbial calcium dissolution (74, 77). In addition, *Brevibacterium linens* BS258 up-regulates transcription of genes that code for carbonic anhydrases during calcium dissolution (76). CvsSR directly regulates expression of the beta-carbonic anhydrase PSPTO_5255 and a major facilitator superfamily (MFS) transporter, PSPTO_5256, that are found within the same putative operon (Figure 3.1). MFS transporters found in the same operon with a carbonic anhydrase could potentially function as bicarbonate or carbonic acid transporters (178).

In this manuscript, we show that *cvsS* and *cvsR* are induced by several metal cations other than Ca²⁺. We also show that swarming motility is not impacted by the addition of these metal cations to medium. We then show that surface-associated MICP occurs in the Δ *cvsS* and Δ *cvsR* strains. Surface-associated MICP is also likely involved in disrupting swarming motility in the Δ *cvsS* and Δ *cvsR* strains of *Pto* when Ca²⁺ is added to medium. Lastly, we show that the carbonic anhydrase PSPTO_5255 and the MFS transporter PSPTO_5256 are involved in CvsSR suppression of surface-associated MICP in *Pto*.

MATERIALS AND METHODS

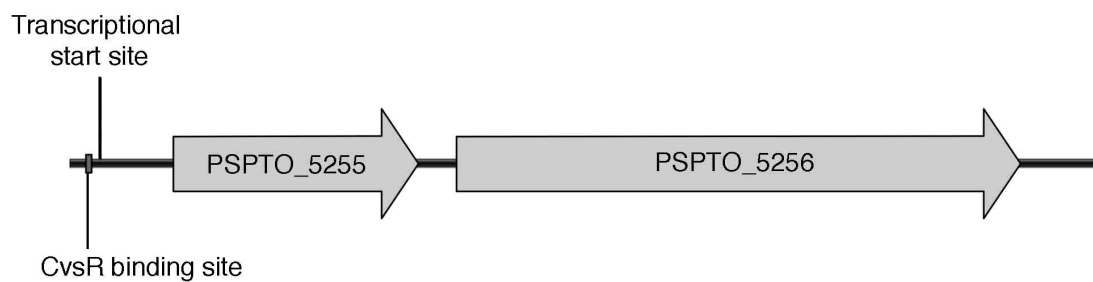


Figure 3.1: Illustration of the arrangement of the putative operon that includes PSPTO_5255 and PSPTO_5256. The illustration includes the CvsR binding site and a precisely mapped transcriptional start site.

Bacterial Strains and Growth Conditions. The bacterial strains and primers used in this study can be found in Tables 3.1 and 3.2, respectively. *Pto* was routinely cultured on King's B (KB) agar (147). Experiments were performed in nutrient broth (NB) medium (Becton Dickinson, Franklin Lake, NJ) or Mannitol Glutamate (MG) medium (16). *Escherichia coli* was routinely cultured on Lysogeny Broth medium.

Motility Assays. Swarming assays were performed using 0.5% agar NB plates that were measured to be at a pH of 6.5, 6.2, 5.8, or 5.3 with the following reagents added when appropriate: 5 mM CaCl₂, 50 μM Fe (III) citrate, 50 μM ZnCl₂, 10 μM CdCl₂, 0.5% (w/v) D-glucose, or 0.5% (w/v) of the glucose analog D-alpha-methyl-glucopyranoside (DAP) (Sigma-Aldrich). *Pto* strains were grown overnight in KB medium to stationary phase and 5 μL of each culture was spotted on a swarming plate. Swarming zones were measured after plates were incubated for 18-20 hours at room temperature. A Student's two-tailed t-test was used to determine statistical significance. Photos of swarming plates were taken after plates were incubated for 18-20 hours at room temperature.

Alizarin red S staining. *Pto* strains were grown overnight in KB media, washed twice in NB and then resuspended in NB at an optical density measured at 600 nm (OD₆₀₀) of 0.3. Five μL of each culture was spotted onto NB agar plates with 5mM CaCl₂ plates. Plates were stained with 1% w/v Alizarin Red S (Sigma Aldrich) pH 4.1 for five minutes and then rinsed with water to assay for areas of high calcium concentration after one day of growth on NB agar or NB swarming agar supplemented with 5 mM CaCl₂. This experiment was repeated three times.

Table 3.1: Bacterial Strains and plasmids used in this study

<i>Pseudomonas syringae</i> pv. tomato DC3000 strains		
Strain Name	Genotype	Reference
<i>Pto</i> (WT)	<i>Pseudomonas syringae</i> pv. tomato DC3000 wild type, Rif ^R	(60)
BBPS33	<i>Pto</i> Δ <i>cvsS</i>	(107)
BBPS34	<i>Pto</i> Δ <i>cvsR</i>	(107)
BBPS35	BBPS34 <i>attTn7::Tn7</i> -PSPTO_3383- <i>cvsR</i>	(107)
MFPS03	<i>Pto</i> pBS59:: <i>P_{cvsSR}</i>	(165)
MFPS05	<i>Pto</i> Δ PSPTO_5255	This study
MFPS15	<i>Pto</i> Δ PSPTO_5255 pBS46:PSPTO_5255	This study
MFPS16	<i>Pto</i> Δ <i>cvsS</i> pBS46:PSPTO_5255	This study
MFPS17	<i>Pto</i> Δ <i>cvsR</i> pBS46:PSPTO_5255	This study
MFPS18	<i>Pto</i> Δ <i>cvsS</i> pBS46:PSPTO_5255/5256	This study
MFPS19	<i>Pto</i> Δ <i>cvsR</i> pBS46:PSPTO_5255/5256	This study
<i>Escherichia coli</i> strains		
TOP10	F- <i>mcrA</i> Δ (<i>mrr</i> - <i>hsdRMS</i> - <i>mcrBC</i>) ϕ 80lacZ Δ M15 Δ lacX74 <i>nupG</i> <i>recA1</i> <i>araD139</i> Δ (<i>ara-leu</i>)7697 <i>galE15</i> <i>galK16</i> <i>rpsL</i> (StrR) <i>endA1</i> λ -	ThermoFisher Scientific
Plasmids	Description	Reference
pK18mobsacB	Small mobilizable suicide vector with Km ^R and sucrose-sensitivity (<i>sacB</i>)	(148)
pENTR/SD/D/TOPO	Gateway entry vector with ribosome binding site and Km ^R	ThermoFisher Scientific
pBS46	Gateway destination vector with <i>nptII</i> promoter and Gm ^R	(151)
pMRF16	pK18mobsacB: Δ PSPTO_5255	This study
pMRF35	pENTR/SD/D:: <i>PSPTO_5255</i>	This study
pMRF36	pBS46:: <i>PSPTO_5255</i>	This study

Table 3.2: Primers used in this study

Primer name	Sequence (5' – 3')	Description
oMRF0080	GCTCTAGAGCTTGAGGTATTG CTGCGCT	PSPTO_5255 KO upstream forward with XbaI site
oMRF0081	CGTCTAGAAGTCATCGGCAACGCA CC	PSPTO_5255 KO downstream reverse with XbaI site
oMRF0136	GCTCTTCCTGCTGAGGGAAGA	PSPTO_5255 KO reverse upstream
oMRF0137	TCTTCCCTCAGCAGGAAGAGCTGA CACCTTCGTGCCGCT	PSPTO_5255 KO downstream forward with overlap
oMRF0554	CACCATGAAGAATCGACATCAATC CGTC	PSPTO_5255 forward gateway
oMRF0555	GCCGTCAGTAGTGACTGATATCA	PSPTO_5255 reverse gateway
oMRF0568	CGACCCCGGGCTCTGTGTTGCGAC GATCAGG	PSPTO_5255/5256 reverse gateway

X-ray diffraction. *Pto* strains were grown overnight in KB to stationary phase. 200 μ L of each culture was plated on NB agar plates supplemented with 5 mM CaCl_2 . The strains were grown for one day then desiccated with a vacuum concentrator. The desiccated cultures were ground into a powder and analyzed on the Scintag Theta-Theta X-ray diffractometer (ThermoFisher Scientific, Waltham, MA, USA) at the Cornell Center for Materials Research, Cornell University.

Raman Spectroscopy. *Pto* strains were grown overnight in KB media, washed twice in NB and then resuspended in NB at an OD_{600} of 0.3. 5 μ L of each culture was spotted onto NB agar plates supplemented with 5mM CaCl_2 plates. After one day of growth, Raman spectroscopy was performed on cells growing on NB supplemented with 5 mM CaCl_2 agar plates using a 735 nm laser on a Renishaw InVia Confocal Raman microscope (Renishaw Inc., Hoffman Estates, IL, USA).

pH measurements. *Pto* was grown overnight in KB medium and then washed twice in NB before being resuspended in NB at an OD_{600} of 0.1. Cultures were then aliquoted into 14 mL culture tubes in 3 mL aliquots. The following reagents were added to the cultures when appropriate at the final concentration of: 5 mM CaCl_2 , 0.5% (w/v) D-glucose, or 0.5% (w/v) DAP. Cultures were grown overnight, centrifuged, and then the culture supernatant was sterilized using a 0.2 μ m filter. Following sterilization, the culture supernatant pH was measured using a pH probe. The experiment was performed three independent times.

pH measurements on agar plates. *Pto* strains were grown in a 3 mL KB culture overnight and then washed twice in NB before being diluted to an OD_{600} of 0.3. 5 μ L of cultures were then spotted on NB agar plates with 0.01% (w/v) bromothymol that

were supplemented with 5 mM CaCl₂, 5 mM CaCl₂ and 0.5% (w/v) glucose, or 5 mM CaCl₂ and 0.5% (w/v) DAP plates. Pictures of plates were taken after one day of growth.

Gluconic acid concentration assays. *Pto* was grown overnight in KB medium and then washed two times in NB medium before being resuspended in 3 mL of NB, NB supplemented with 5 mM CaCl₂, NB supplemented with 0.5% (w/v) glucose, NB supplemented with 5 mM CaCl₂ and 0.5% (w/v) glucose, or NB supplemented with 5 mM CaCl₂ and 0.5% (w/v) DAP. Cultures were allowed to grow for 24 hours before 1 mL of each culture was collected and centrifuged. The amount of gluconate/gluconic acid in each culture supernatant was determined using the D-Gluconate (D-Gluconic Acid) Assay Kit (Colorimetric) (Sigma) according to the manufacturer's directions. This assay was repeated using with three biological replicates that were collected during three independent experiments.

Luciferase assays. *Pto* pBS59::P_{cvsSR} was grown overnight in KB medium and then washed 2X in MG medium at a pH 6.0 before being resuspended in MG pH 6.0 at an OD₆₀₀ of 0.1. Luminescence of *Pto* pBS59::P_{cvsSR} cultures grown in MG pH 6.0 supplemented with 50 μM Fe (III) citrate, 50 μM ZnCl₂, or 10 μM CdCl₂ was then measured on Biotek Synergy II plate reader (Winooski, VT). Relative luminescence was measured as previously described and used as a proxy for expression of *cvsSR* (165). These assays were repeated three times independently and compiled using a least squares mean regression.

Creation of PSPTO_5255 mutant. A *Pto* strain with a clean deletion of PSPTO_5255 was generated using pK18mobsacB (148). DNA fragments

approximately 0.9 kb and 1.0 kb upstream and downstream of PSPTO_5255 that included the beginning and end of the gene were PCR amplified. The PCR products were gel purified using the Zymoclean Gel Extraction Kit (Zymo, Irvine, CA). These fragments were then joined using splicing by overlap extension and the PCR products were gel purified using the Zymoclean Gel Extraction Kit. After gel extraction, the PCR product was restriction enzyme digested with XbaI (New England Biolabs, Ipswich, MA) and then ligated into pK18mobsacB that had been previously digested with XbaI. The ligated product was transformed into TOP10 *E. coli* cells (ThermoFisher Scientific, Waltham, MA). Transformed *E. coli* cells were plated on LB agar plates with 50 µg/mL kanamycin added. Positive colonies were determined through PCR and plasmids were isolated from them using the Qiagen Mini-prep kit (Qiagen, Valencia, CA). Plasmids with the correct insert were determined through sequencing at the Cornell Biotechnology Resource Center. Plasmids were then transformed into *Pto* via electroporation. Colonies with a deletion were determined through PCR and then sequenced in order to confirm that the insertion product was correct.

Production of constitutively expressing PSPTO_5255 and

PSPTO_5255/PSPTO_5256 strains. PSPTO_5255 or PSPTO_5255 and

PSPTO_5256 were PCR amplified using the Q5 DNA polymerase (NEB) and the PCR products were purified using Zymo DNA clean and concentrator – 5 (Zymo). These PCR products were inserted into a pENTR/SD/D/TOPO vector (ThermoFisher Scientific) and transformed into TOP10 *E. coli* cells. Transformed *E. coli* cells were then plated on LB agar plates with 50 µg/mL kanamycin added. Positive clones were

selected and verified by PCR prior to purification of the plasmid using a Qiagen Mini-prep kit. Plasmids were sequenced at the Cornell Biotechnology Resource Center to confirm that the insertion sequence was correct. The insertion was then transferred to pBS46 using the LR clonase II enzyme mix (ThermoFisher Scientific) and transformed into TOP10 *E. coli* cells. Transformed *E. coli* was plated on LB agar with 10 µg/mL gentamicin added. Positive clones were selected and verified by PCR prior to purification of the plasmid using a Qiagen Mini-prep kit. These plasmids were also sequenced at the Cornell Biotechnology Resource Center to confirm that the insertion sequence was correct. pBS46::PSPTO_5255 and pBS46::PSPTO_5256 were then transformed into $\Delta cvsS$, $\Delta cvsR$, and $\Delta PSPTO_5255$ *Pto* strains through electroporation. Transformants were selected using KB agar plates with 10 µg/mL gentamicin added.

Statistical analysis. Jmp Pro 12 was used to perform statistical analyses.

RESULTS

***cvsS* and *cvsR* expression is induced by multiple metal cations.** The orthologous TCS to CvsSR in *P. aeruginosa* is activated by Fe²⁺ and we had found previously that *cvsSR* transcription was elevated in medium with Fe (III) citrate added as compared to iron-free medium (16, 110). CvsSR positively autoregulates and we had previously used a P_{*cvsSR*} luciferase reporter gene construct to show that *cvsSR* was induced by Ca²⁺ (165). We found that Fe (III) citrate induced transcription of *cvsSR* (Figure 3.2A). In addition, we found that transcription of *cvsSR* was induced by Zn²⁺ and Cd²⁺ (Figure 3.2B, C). It appeared that *cvsSR* could be induced by multiple metal cations.

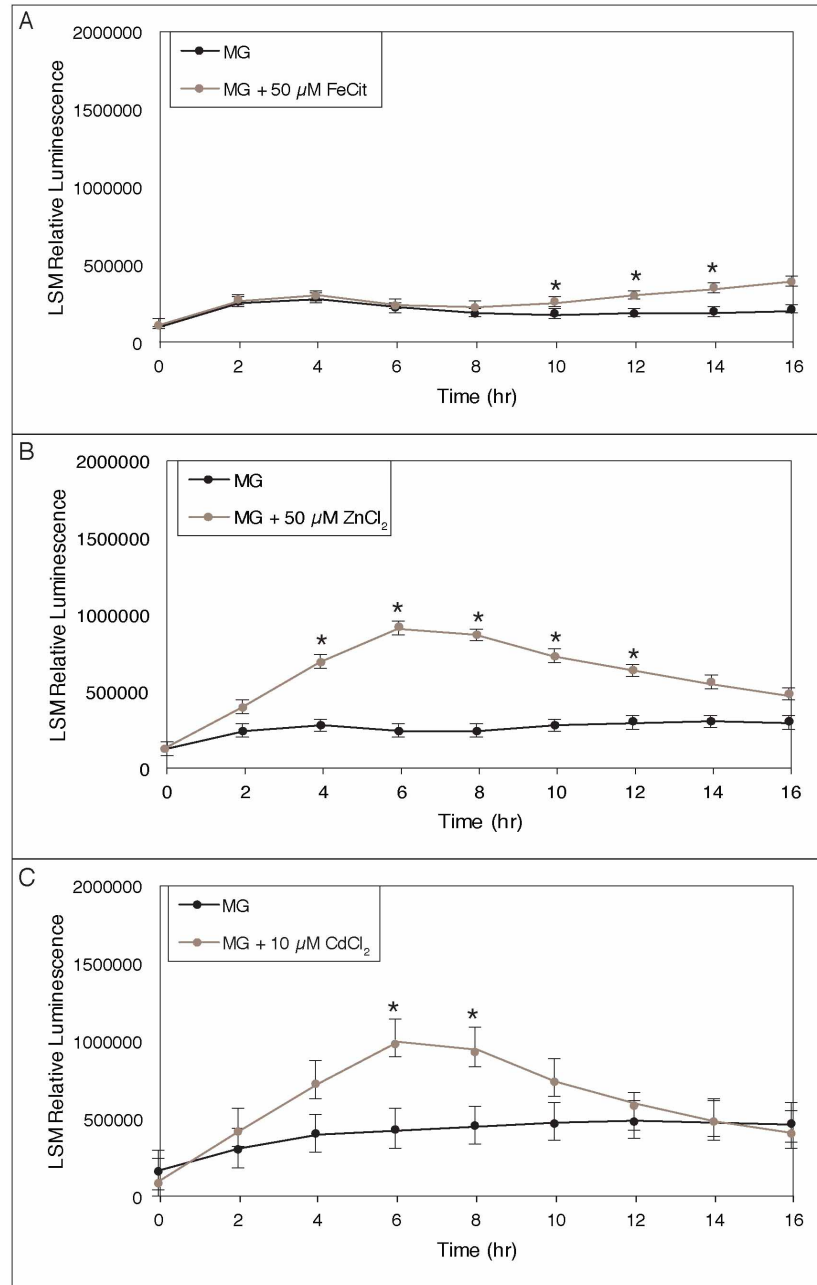


Figure 3.2: Luminescence assays to assess activity of P_{cvsSR} in WT grown in MG as compared to (A) MG supplemented with 50 μ M Fe (III) citrate, (B) MG supplemented with 50 μ M ZnCl₂, or (C) MG supplemented with 10 μ M CdCl₂. The relative luminescence was calculated by using the total luminescence relative to OD₆₀₀. Experiments were performed three times. The three experiments were compiled using a least squares mean regression. The error bars represent standard deviation generated by the differences observed between samples. The * denotes statistically significant differences determined using a Tukey HSD test with a p-value < 0.01.

Other metal cations do not inhibit swarming motility in the $\Delta cvsS$ and $\Delta cvsR$ strains. One of the prominent phenotypes we previously observed in the $\Delta cvsS$ and $\Delta cvsR$ strains was that they did not swarm on NB swarming agar supplemented with Ca^{2+} (165). To determine whether the $\Delta cvsS$ and $\Delta cvsR$ strains could swarm on other *cvsSR* inducing conditions we tested swarming motility of the $\Delta cvsS$ and $\Delta cvsR$ strains as compared to WT on NB swarming agar supplemented with Fe (III) citrate, Zn^{2+} , or Cd^{2+} . We found that swarming motility was similar between WT and the $\Delta cvsS$ and $\Delta cvsR$ strains under these conditions (Figure 3.3). From these data, we concluded that swarming motility is inhibited only when additional Ca^{2+} is present.

$\Delta cvsS$ and $\Delta cvsR$ are rugose and opaque on calcium supplemented media. In previous swarming assays performed with WT and the $\Delta cvsS$ and $\Delta cvsR$ strains on NB supplemented with Ca^{2+} the $\Delta cvsS$ and $\Delta cvsR$ strains appeared much more opaque than WT (165). This opaque phenotype was also visible on the $\Delta cvsS$ and $\Delta cvsR$ strains when they were grown on NB agar supplemented with Ca^{2+} , while WT and the $\Delta cvsRc$ strain formed a clear, smooth colony (Figure 3.4A). The $\Delta cvsS$ and $\Delta cvsR$ strains did not form opaque colonies on NB or NB supplemented with Fe (III) citrate, Zn^{2+} , or Cd^{2+} (Figure 3.5). The opaque nature of the $\Delta cvsS$ and $\Delta cvsR$ strains when grown on NB agar supplemented with Ca^{2+} was similar in appearance to *Pseudomonas* strains that precipitated calcium on the surface of colonies when grown under the same conditions (Fishman et al., submitted). In order to test for calcium precipitate, we stained WT, $\Delta cvsS$, $\Delta cvsR$, and $\Delta cvsRc$ strains grown on NB agar supplemented with Ca^{2+} with Alizarin Red S (ARS) (Figure 3.4A). ARS is a dye that stains calcium rich areas and has previously been used to stain areas of calcium precipitate on or

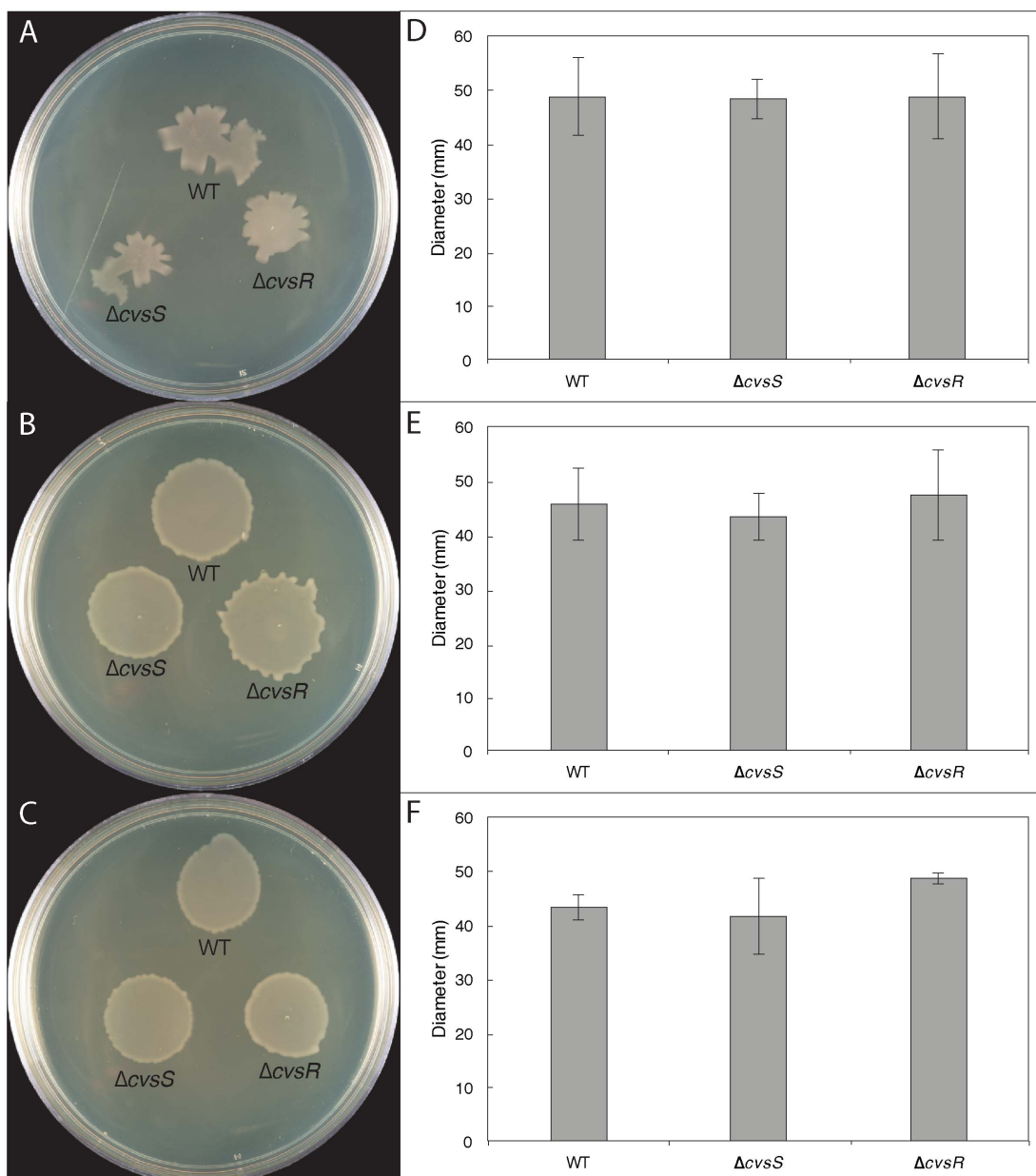


Figure 3.3: Pictures of swarming colonies WT, ΔcvS , and ΔcvR on NB swarming agar supplemented with (A) 50 μ M Fe (III) citrate, (B) 50 μ M ZnCl₂, or (C) 10 μ M CdCl₂. These pictures are representative of swarming colonies of these strains on the given medium. Diameters of swarming colonies of WT, ΔcvS , and ΔcvR were measured after 16-20 hours of growth on NB swarming agar supplemented with (D) 50 μ M Fe (III) citrate, (E) 50 μ M ZnCl₂, or (F) 10 μ M CdCl₂. The error bars represent standard error. This experiment was performed three times. Pictures of swarming colonies were taken after 16 hours of growth and are representative of experiments that were repeated three times.

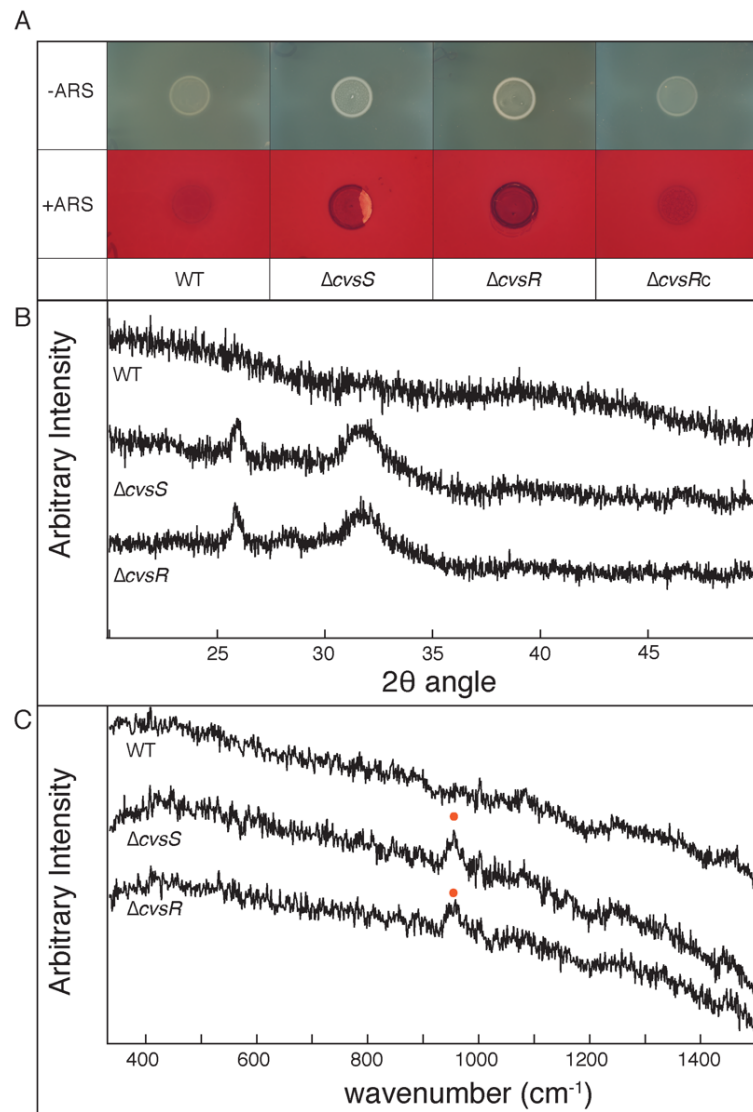


Figure 3.4: WT, $\Delta cvsS$, $\Delta cvsR$, and $\Delta cvsRc$ grown on NB agar supplemented with 5mM CaCl₂ after one day of growth without Alizarin red S staining and with Alizarin red S staining. These pictures are representative of experiments that were repeated three times. (B) X-ray diffraction patterns from WT, $\Delta cvsS$, and $\Delta cvsR$ cultures grown on NB supplemented with 5 mM CaCl₂ for one day. The y-axis is in arbitrary intensity units and the x-axis is the 2θ angle from 20° to 50°. Peaks in the spectra for the $\Delta cvsS$ and $\Delta cvsR$ strains are for amorphous apatite. (C) Raman spectroscopy patterns from WT, $\Delta cvsS$, and $\Delta cvsR$, cultures grown on NB supplemented with 5 mM CaCl₂ for one day. The peak centered at 955 cm⁻¹ is expected when amorphous calcium phosphate is present. This peak is indicated in the $\Delta cvsS$ and $\Delta cvsR$ strain spectra with an orange dot. The y-axis is in arbitrary intensity units and the x-axis is in wavenumber (cm⁻¹).

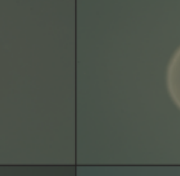
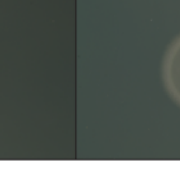
	WT	$\Delta cvsS$	$\Delta cvsR$
NB			
NB + FeCit			
NB + ZnCl ₂			
NB + CdCl ₂			

Figure 3.5: Photos taken of WT, $\Delta cvsS$, and $\Delta cvsR$ strains grown for one day on NB, NB supplemented with Fe³⁺, NB supplemented with Zn²⁺, or NB supplemented with Cd²⁺. This experiment was repeated three times and these photos are representative of those experiments.

around *Pseudomonas* colonies (M. Fishman submitted). The $\Delta cvsS$ and $\Delta cvsR$ strains were both stained by ARS within a day of growth, in contrast to the WT and $\Delta cvsRc$ which did not stain. This suggests that the $\Delta cvsS$ and $\Delta cvsR$ strains concentrate calcium on the surface of colonies.

$\Delta cvsS$ and $\Delta cvsR$ precipitate amorphous calcium phosphate on the cell surface.

ARS stains calcium rich areas which could represent calcium precipitates or areas of abundant chelated calcium. In order to determine whether the surface of the $\Delta cvsS$ and $\Delta cvsR$ colonies contained calcium precipitates and what was the form of that precipitate, we analyzed the colonies using both X-ray diffraction (XRD) and *in vivo* Raman spectroscopy. XRD of dried WT, $\Delta cvsS$, and $\Delta cvsR$ colonies that had been grown on NB agar supplemented with Ca^{2+} showed that amorphous apatite was present in the $\Delta cvsS$ and $\Delta cvsR$ colonies, but not in the WT colony (Figure 3.4B). *In vivo* Raman spectroscopy from one day old colonies grown on NB agar supplemented with calcium showed that the surface of live $\Delta cvsS$ and $\Delta cvsR$ colonies produced amorphous calcium phosphate, but WT colonies did not (Figure 3.4C). Therefore, we concluded that the $\Delta cvsS$ and $\Delta cvsR$ strains precipitated amorphous calcium phosphate on the surface of cells.

Ca^{2+} -specific swarming inhibition in the $\Delta cvsS$ and $\Delta cvsR$ strains is pH

dependent. Similar to when grown on NB agar supplemented with Ca^{2+} , the $\Delta cvsS$ and $\Delta cvsR$ strains were opaque on NB swarming agar supplemented with Ca^{2+} and were stained by ARS, while WT and the $\Delta cvsRc$ strain were not stained by ARS when grown under the same conditions (Figure 3.6). This suggested that calcium phosphate

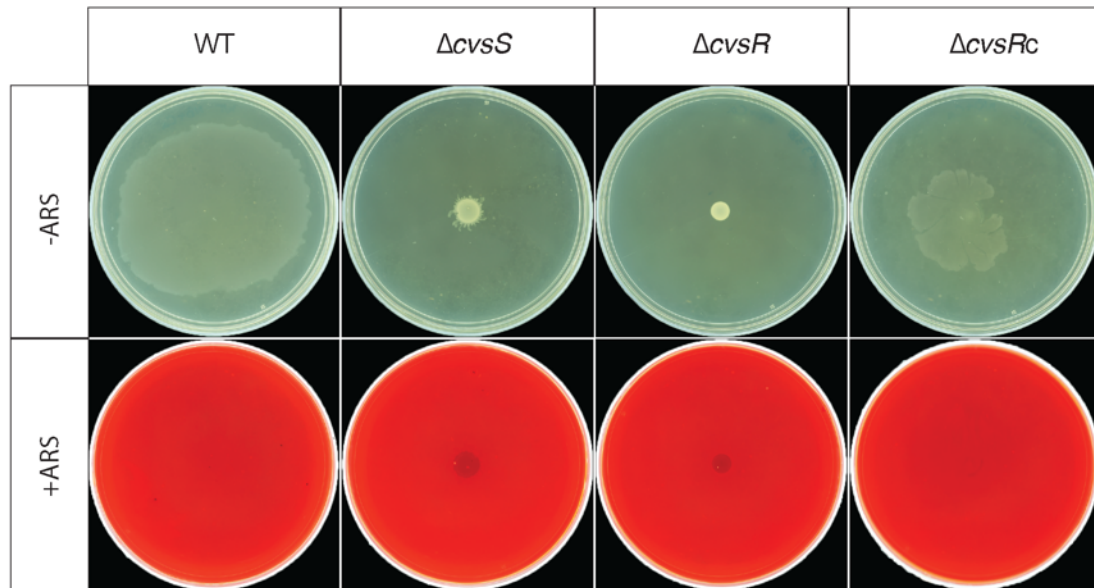


Figure 3.6: Photos of WT, $\Delta cv s S$, $\Delta cv s R$, and $\Delta cv s R c$ swarming colonies on NB swarming agar supplemented with Ca^{2+} before and after ARS staining. ARS can be seen staining the $\Delta cv s S$ and $\Delta cv s R$ strains, but not WT and $\Delta cv s R c$. This experiment was repeated three times and these photos are representative of phenotypes observed during each experiment.

was precipitated on the surface of $\Delta cvsS$ and $\Delta cvsR$ strains grown on NB swarming agar supplemented with Ca^{2+} .

In vitro, calcium phosphate can readily precipitate at a pH of 8.0 or above and lowering the pH will either inhibit or slow the spontaneous precipitation of calcium phosphate (179). *Pto* raises the pH of surrounding medium over time and this may facilitate the precipitation of calcium phosphate by *Pto* (Figure 3.7). Therefore, we hypothesized that lowering the initial pH of the medium could influence the time it takes for *Pto* to precipitate calcium phosphate in the surrounding medium. This same concept could hold true for the $\Delta cvsS$ and $\Delta cvsR$ strains. Therefore, lowering the initial pH of the medium may delay the precipitation calcium phosphate on the surface of the $\Delta cvsS$ and $\Delta cvsR$ strains. A lag phase occurs before swarming after bacteria are spotted on swarming agar from a liquid culture (170). If surface associated calcium phosphate precipitation is involved in inhibiting swarming in the $\Delta cvsS$ and $\Delta cvsR$ strains when grown on NB supplemented with Ca^{2+} , then delaying calcium precipitation by lowering the initial pH of the medium may partially restore swarming in the $\Delta cvsS$ and $\Delta cvsR$ strains on NB supplemented with Ca^{2+} . NB swarming agar supplemented with Ca^{2+} was measured to be at an initial pH of 6.5 to 6.7. NB swarming agar plates supplemented with Ca^{2+} were made at a pH of 6.5, 6.2, 5.8, or 5.3. Swarming ability in the $\Delta cvsS$ and $\Delta cvsR$ strains started to recover at a pH of 5.8 and was fully recovered at a pH of 5.3 (Figure 3.8). The $\Delta cvsS$ and $\Delta cvsR$ strains swarmed as well or better than WT at all the pH's assayed on NB swarming agar without additional Ca^{2+} (Figure 3.9). The opaque, calcium phosphate-rich area in the center of the swarming colonies for $\Delta cvsS$ and $\Delta cvsR$ decreased in size as the initial

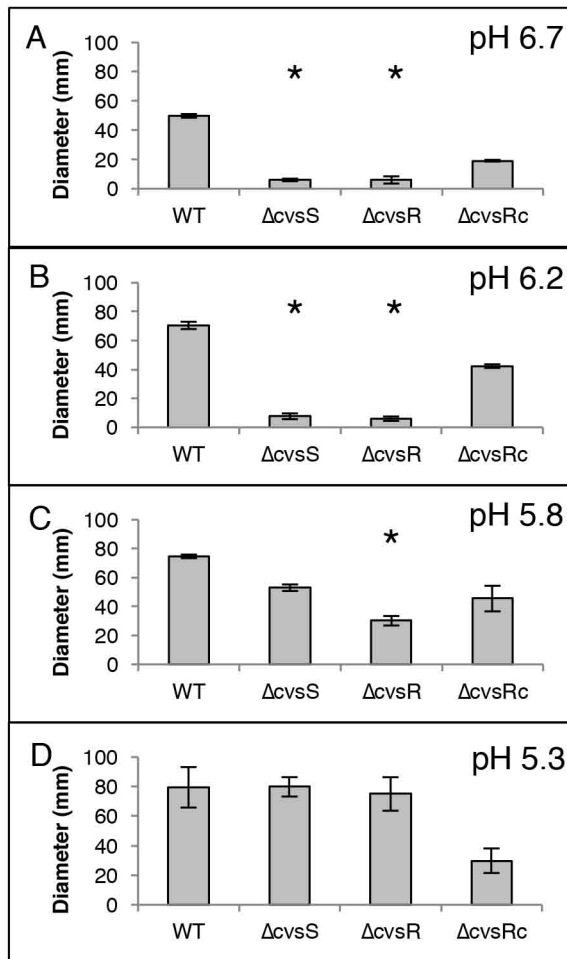


Figure 3.8: Diameters of WT, $\Delta cvsS$, $\Delta cvsR$, and $\Delta cvsRc$ colonies when grown on NB swarming agar supplemented with 5 mM $CaCl_2$ at a pH of (A) 6.7, (B) 6.2, (C) 5.8, and (D) 5.3 measured after 18 to 20 hours of growth. Swarming assays were performed three separate times. Recorded measurements from each experiment were compiled and average. The * signifies when there is a significant difference with a p-value < 0.1 between the measured diameter of the $\Delta cvsS$ and $\Delta cvsR$ strains and WT according to a one-way ANOVA. Raman spectra taken from the edge of WT, $\Delta cvsS$, or $\Delta cvsR$ colonies grown on NB swarming agar supplemented with 5 mM $CaCl_2$ at a pH of (E) 6.7, (F) 6.2, (G) 5.8, and (H) 5.3 taken after 18 to 20 hours of growth.

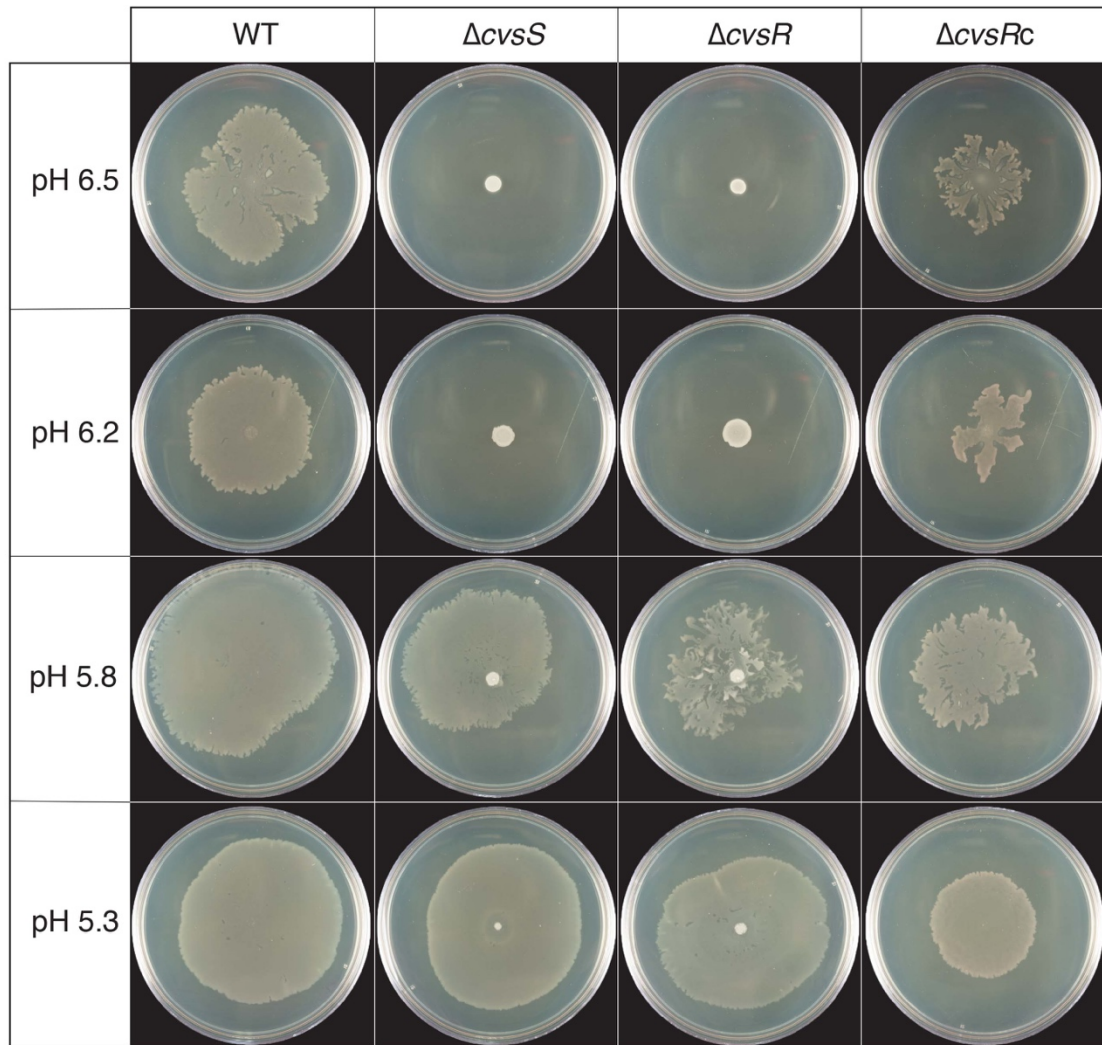


Figure 3.9: Photos of swarming colonies of WT, $\Delta cv s S$, $\Delta cv s R$, and $\Delta cv s R c$ taken on NB swarming agar supplemented with Ca^{2+} at the listed pH for each row of pictures. This experiment was repeated three times and these photos are representative of the phenotypes observed during those experiments.

pH of the agar decreases (Figure 3.9). This suggests that lowering the initial pH of the medium inhibited or delayed calcium phosphate precipitation on the surface of $\Delta cvsS$ and $\Delta cvsR$ strains allowing them to swarm.

Calcium phosphate precipitation in the $\Delta cvsS$ and $\Delta cvsR$ strains is inhibited by the addition of glucose to medium. Even though lowering the pH of NB swarming agar supplemented with Ca^{2+} recovered swarming in the $\Delta cvsS$ and $\Delta cvsR$ strain, we found that calcium phosphate still precipitated on the surface of the $\Delta cvsS$ and $\Delta cvsR$ strains even with the initial pH of NB supplemented with Ca^{2+} was lowered to a pH of 5.3 (data not shown). One condition where microbes may lower or prevent an increase in the pH of the surrounding medium is during phosphate solubilizing conditions. During phosphate solubilization, microbes may secrete organic acids produced by microbes that lower the pH of the surrounding environment (69). One such organic acid that microbes use to solubilize phosphate is gluconic acid made through the oxidation of glucose (70). The genome of *Pto* includes a gene that codes for glucose dehydrogenase (*gdh*) so it should be able to oxidize glucose to gluconic acid (60). It would be expected that the pH of medium would become acidic if gluconic acid was being produced by *Pto*. *Pto* raises the pH of NB medium supplemented with Ca^{2+} to a pH of 8.52 +/- 0.12 after one day of growth, however *Pto* lowers the pH of NB medium supplemented with Ca^{2+} and glucose to a pH of 4.14 +/- 0.06 after one day of growth. An acidic pH suggests that *Pto* produced a weak acid when glucose was present in the medium. In comparison, *Pto* raised the pH of NB medium supplemented with Ca^{2+} and the glucose analog DAP to a pH of 8.46 +/- 0.03 after one day of growth. DAP cannot be metabolized by *Pto* and suggests gluconic acid is not

produced. Similarly, by using the pH indicator dye bromothymol blue it can be seen that *Pto* raises the pH of the environment when grown on NB agar plates supplemented with Ca^{2+} or NB agar plates supplemented with Ca^{2+} and DAP and lowers the pH of the environment when grown on NB agar plates supplemented with Ca^{2+} and glucose (Figure 3.7). Indeed, when *Pto* was grown in NB supplemented with Ca^{2+} and glucose there was a tremendous increase in gluconate production as compared to NB supplemented with Ca^{2+} or NB supplemented with Ca^{2+} and DAP (Table 3.3). *Pto* produced over 10-fold more gluconate when grown in NB supplemented with glucose and Ca^{2+} as compared with NB supplemented with only and glucose, suggesting that the addition of Ca^{2+} was essential for the increased production of gluconate. Similar to WT, the ΔcvsS and ΔcvsR strains also produced millimolar concentrations of gluconic acid when grown in NB medium supplemented with Ca^{2+} and glucose (Table 3.3). Since the production of gluconic acid can dissolve calcium phosphate, it may prevent calcium phosphate precipitation on the surface of the ΔcvsS and ΔcvsR strains. We grew WT, ΔcvsS , ΔcvsR , and ΔcvsRc on NB agar supplemented with Ca^{2+} and glucose. When grown under these conditions, the ΔcvsS and ΔcvsR strains looked similar to WT and were not stained by ARS (Figure 3.10A). In comparison, ΔcvsS and ΔcvsR strains grown on NB agar supplemented with Ca^{2+} and DAP were rugose and opaque and were stained by ARS (Figure 3.10B). From this we conclude that addition of glucose to NB agar supplemented with Ca^{2+} did not allow for calcium precipitation on the surface of the ΔcvsS and ΔcvsR strains to form. This was likely due to phosphate solubilization conditions caused by the oxidation of glucose to gluconic acid by *Pto*.

Table 3.3: Concentration of gluconate/gluconic acid in *Pto* spent medium

- a. Concentration of gluconate/gluconic acid was determined by averaging three independent biological replicates.
- b. Standard deviation was generated from using the concentration generated in three biological replicates sampled.

Condition	WT		$\Delta cvsS$		$\Delta cvsR$	
	[Gluconate] (mM) ^a	Standard deviation (mM) ^b	[Gluconate] (mM) ^a	Standard deviation (mM) ^b	[Gluconate] (mM) ^a	Standard deviation (mM) ^b
NB	2.2	1.4	12.8	1.0	16.5	4.2
NB + CaCl ₂	4.4	2.2	14.3	7.1	7.6	1.5
NB + Glucose	66.6	7.9	87.5	86.7	130.2	75.8
NB + CaCl ₂ + Glucose	1672.8	87.4	2190.9	22.5	2001.8	85.0
NB + CaCl ₂ + DAP	7.2	4.5	9.7	2.9	7.4	0.7

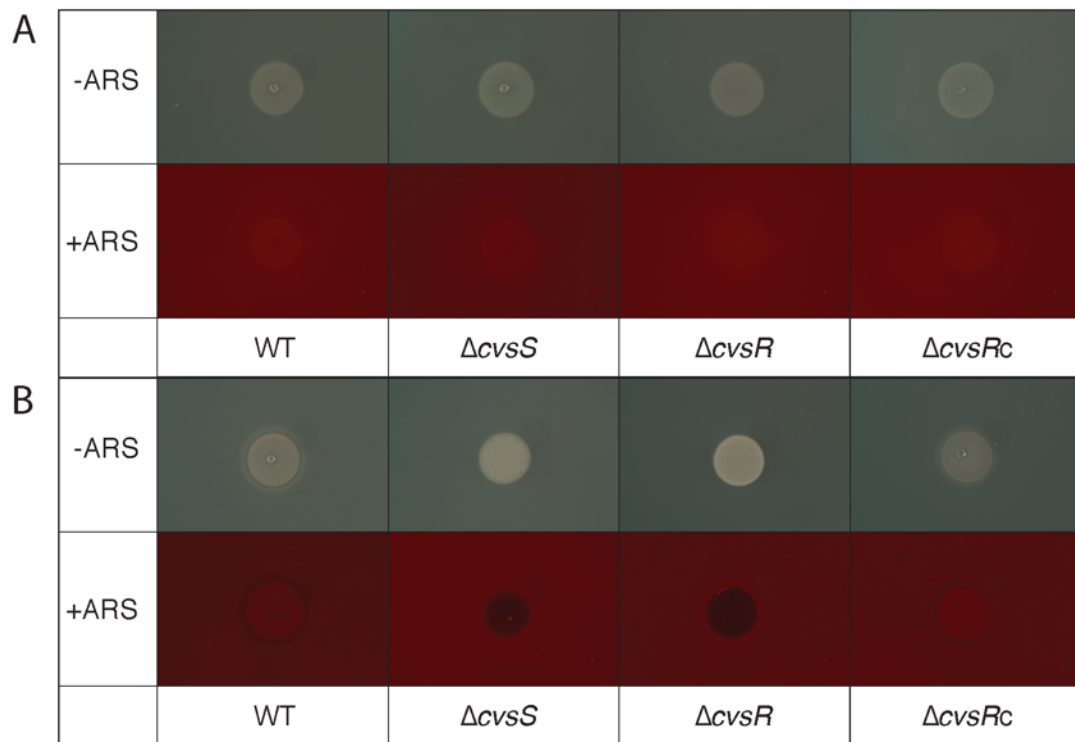


Figure 3.10: WT, $\Delta cvsS$, $\Delta cvsR$, and $\Delta cvsRc$ grown on (A) NB agar supplemented with 5 mM CaCl_2 and 0.5% (w/v) glucose or (B) NB agar supplemented with 5 mM CaCl_2 and 0.5% (w/v) DAP after one day of growth without ARS staining and with ARS staining. These pictures are representative of experiments that were repeated three times.

Calcium precipitation inhibits swarming motility in the $\Delta cvsS$ and $\Delta cvsR$ strains.

Since the $\Delta cvsS$ and $\Delta cvsR$ strains no longer precipitate calcium phosphate on the surface of colonies when grown on NB agar supplemented with Ca^{2+} and glucose, we added glucose to NB swarming agar supplemented with Ca^{2+} and found that the $\Delta cvsS$ and $\Delta cvsR$ strains swarmed similarly to WT (Figure 3.11A, B). In comparison, when adding DAP to NB swarming agar supplemented with Ca^{2+} , swarming was still inhibited in the $\Delta cvsS$ and $\Delta cvsR$ strains (Figure 3.11C, D). Taken together, these results suggest that surface-associated calcium precipitation in the $\Delta cvsS$ and $\Delta cvsR$ strains was correlated with reduced swarming motility in these strains.

CvsSR regulates a carbonic anhydrase and putative sulfate transporter involved in inhibiting calcium precipitation in *Pto*.

We established that the TCS CvsSR prevents the formation of calcium phosphate on the cell surface of the bacterium. Given that CvsSR is a global regulator in *Pto*, we wanted to determine the genes regulated by CvsSR that might play a role in calcium phosphate precipitation or dissolution. Microbes can dissolve calcium minerals through the use of carbonic acid made by carbonic anhydrases (74). CvsSR regulates the carbonic anhydrase PSPTO_5255 (5255) that is found in a putative operon with a putative sulfate permease PSPTO_5256 (5256) (165). In order to test whether this carbonic anhydrase was involved in preventing the formation of surface associated calcium precipitation in *Pto*, we grew WT, $\Delta 5255$, and a $\Delta 5255$ complement that constitutively expressed 5255 ($\Delta 5255c$) on NB agar supplemented with Ca^{2+} . We stained colonies with ARS at one and two days after spotting on NB agar supplemented with Ca^{2+} . Unexpectedly, calcium precipitation did not occur on the surface of the $\Delta 5255$ colony like it did with

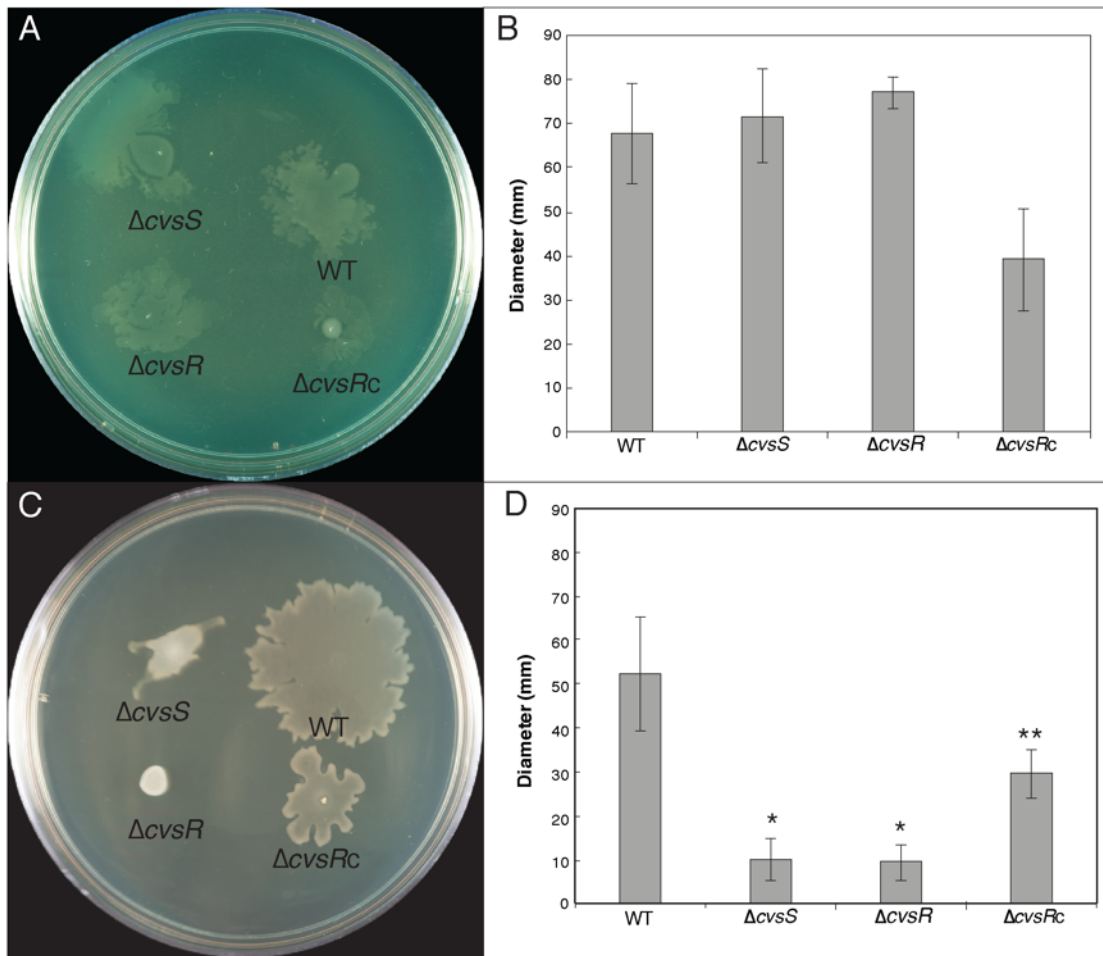


Figure 3.11: Photos and measured diameters of WT, $\Delta cvsS$, $\Delta cvsR$, and $\Delta cvsRc$ strains swarming on (A, B) NB supplemented with CaCl₂ and glucose or (C, D) NB supplemented with CaCl₂ and DAP. Diameters of the strains were measured after 18 to 20 hours of growth on swarming plates. Error bars are representative of standard error between three separate experiments. The * denotes a significant difference in diameter between WT and the given strain with a p-value < 0.01 as determined using Student's two-tailed T-test. The ** denotes a significant difference in diameter between the $\Delta cvsR$ and $\Delta cvsRc$ strain in diameter. These experiments were repeated three times and averaged when measuring the diameter.

the $\Delta cvsS$ and $\Delta cvsR$ strains (Figure 3.12). This suggested that 5255 was not involved in preventing calcium phosphate from accumulating on the surface of *Pto* colonies. However, the $\Delta 5255c$ strain had a prominent zone of clearing between the colony and the white halo around the colony and the beginning of a brown halo after two days of growth, while WT and the $\Delta 5255$ strain did not have a zone of clearing (Figure 3.12). The white halo has previously been shown to be composed of amorphous calcium phosphate that would later be replaced by a brown halo of amorphous apatite (M. Fishman, submitted). This zone of clearing and the subsequent formation of amorphous apatite could be a form of calcium dissolution by *Pto*. The appearance of calcium dissolution in the $\Delta 5255c$ strain before WT could be because of constitutive expression of 5255. If this was the case, 5255 may play a role in calcium dissolution in *Pto*.

Even though a $\Delta 5255$ strain did not have the same phenotype as a $\Delta cvsS$ or $\Delta cvsR$ strain, constitutive expression of 5255 in a $\Delta cvsS$ or $\Delta cvsR$ may prevent calcium phosphate from accumulating on the surface of colonies. $\Delta cvsS$ pBS46::5255 and $\Delta cvsR$ pBS46::5255 strains were spotted on NB agar supplemented with Ca^{2+} . $\Delta cvsS$ pBS46::5255 and $\Delta cvsR$ pBS46::5255 strains precipitated calcium phosphate on the surface of cells after one day of growth on NB agar supplemented with Ca^{2+} and looked similar to the $\Delta cvsS$ and $\Delta cvsR$ strains (Figure 3.13). However, after two days of growth, the $\Delta cvsS$ pBS46::5255 strain became less opaque and did not produce as prominent a white halo around the colony as compared to the $\Delta cvsS$ strain (Figure 3.13). This likely indicated that some or all of the calcium phosphate had been dissolved in the $\Delta cvsS$ pBS46::5255 strain. This was not the case with the $\Delta cvsR$

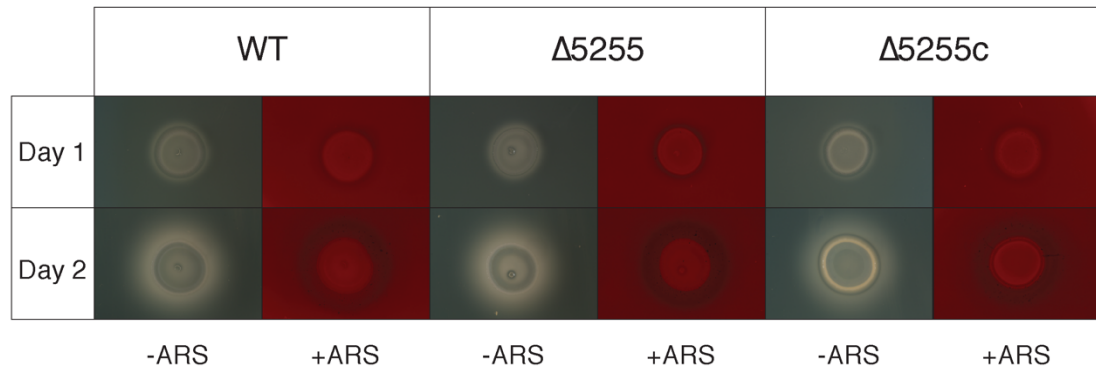


Figure 3.12. Photos of WT, $\Delta 5255$, and $\Delta 5255c$ strains after one day and two days of growth on NB supplemented with Ca^{2+} . A brown ring and a zone of clearing can be seen after two days of growth around the $\Delta 5255c$ that is not present in either the WT or $\Delta 5255$ strain.

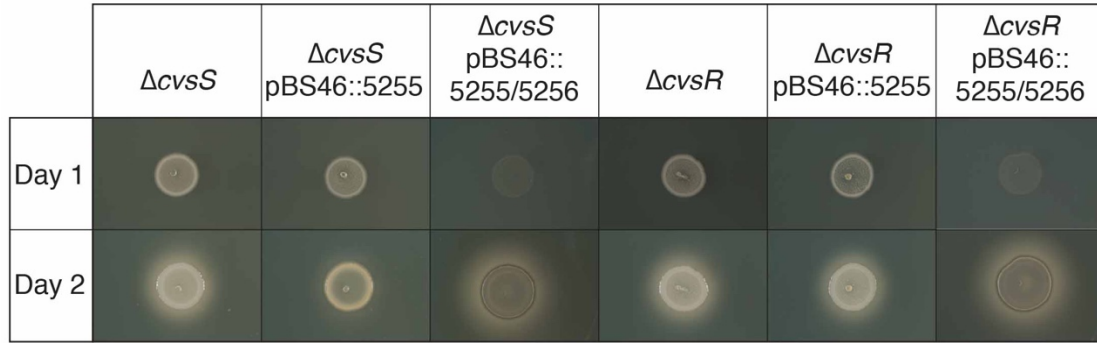


Figure 3.13: Photos taken of $\Delta cvtS$, $\Delta cvtR$, $\Delta cvtS$ pBS46::5255, $\Delta cvtR$ pBS46::5255, $\Delta cvtS$ pBS46::5255/5256, and $\Delta cvtR$ pBS46::5255/5256 strains after one and two days of growth on NB supplemented with Ca^{2+} . It can be seen that after two days of growth the $\Delta cvtS$ pBS46::5255 strain is less opaque and does not form as strong of a white halo compared to the $\Delta cvtS$ strain, while the $\Delta cvtR$ pBS46:5255 strain was still opaque and precipitated calcium phosphate. The $\Delta cvtS$ pBS46:5255/5256 and $\Delta cvtR$ pBS46:5255/5256 strains were not opaque. Loss of opaqueness suggests that calcium phosphate has been dissolved or did not precipitate.

pBS46:5255 strain as after two days of growth it was still opaque and looked similar to the $\Delta cvsR$ strain (Figure 3.13). This suggests that *cvsR* is essential for 5255 to dissolve calcium phosphate precipitated by *Pto*. Since 5255 is part of a putative operon with the permease 5256, it was possible that 5256 could be involved in preventing accumulation of calcium phosphate on the surface of *Pto* cells. (165). Indeed, constitutive expression of 5255 and 5256 in the $\Delta cvsS$ and $\Delta cvsR$ strains prevented surface-associated calcium precipitation (Figure 3.13). This suggests that 5255 and 5256 or possibly solely 5256 can prevent calcium phosphate from accumulating on the surface of *Pto* colonies.

Discussion

Here we show that the deletion of *cvsS* or *cvsR* in *Pto* causes calcium phosphate to precipitate on the surface of bacterial colonies when grown on medium supplemented with Ca^{2+} . This phenotype is unique to when $\Delta cvsS$ and $\Delta cvsR$ strains are grown on medium supplemented with Ca^{2+} as a similar phenotype does not occur when with strain was grown on medium supplemented with other metal cations that induce *cvsSR*. This surface-associated calcium phosphate precipitation in the $\Delta cvsS$ and $\Delta cvsR$ strains is likely involved in dramatically reducing swarming motility in the $\Delta cvsS$ and $\Delta cvsR$ strains.

Expression of *cvsSR* is induced by Fe^{3+} , Zn^{2+} , Cd^{2+} , and Ca^{2+} (165). It is not unusual for TCSs to be induced by multiple signals. PhoPQ responds to cationic antimicrobial peptides, Mg^{2+} , Ca^{2+} , and acidic conditions (22). ColSR responds to Fe^{3+} , Zn^{2+} , Mn^{2+} , and Cd^{2+} through a conserved EXXE motif on ColS (23). BqsSR in *P. aeruginosa* responds to Fe^{2+} through an REXXE motif on BqsS (169). A NXXE

motif can be found on CvsS in the sensor domain rather than an REXXE motif. NXXE motifs in ribokinases are reported to bind various metal cations including, Ca^{2+} and Zn^{2+} (180, 181). While *cvsSR* has only been shown to be induced by Fe^{3+} , Zn^{2+} , Cd^{2+} , and Ca^{2+} , it is possible that CvsS binds to these metal cations through those residues in a similar fashion to the way BqsS binds to Fe^{2+} using an REXXE motif. More research into the signaling domain of CvsS would need to be done to confirm this hypothesis, but if the NXXE motif does bind metal cations then it could explain why *cvsSR* is induced by so many different signals. Even with so many different inducers for CvsSR, the one thing that is certain is that only the addition of Ca^{2+} results in surface-associated calcium precipitation and a reduction of swarming in the ΔcvsS and ΔcvsR strains.

The mechanism behind microbially induced calcium precipitation (MICP), like that seen on the ΔcvsS and ΔcvsR strains, is believed to a passive process that occurs due to the nucleation of Ca^{2+} on the surface of bacterial cells or around bacterial cells due to metabolic behavior. Negatively charged exopolysaccharides, like alginate, are thought to be associated with MICP (173, 182). ΔcvsS and ΔcvsR *Pto* strains produce more alginate than WT, however we found that surface associated MICP occurred even in ΔcvsS ΔalgD and ΔcvsR ΔalgD strains (Figure 3.14) (74). When grown on NB agar supplemented with Ca^{2+} , calcium phosphate will normally precipitate in the region surrounding *Pto* colonies, but not on the surface of colonies (M. F submitted). Based off of this data, it may be more appropriate to say that surface-associated MICP in the ΔcvsS and ΔcvsR strains could be a loss of mineral phosphate solubilization instead of a gain of surface-associated MICP. During mineral phosphate solubilization

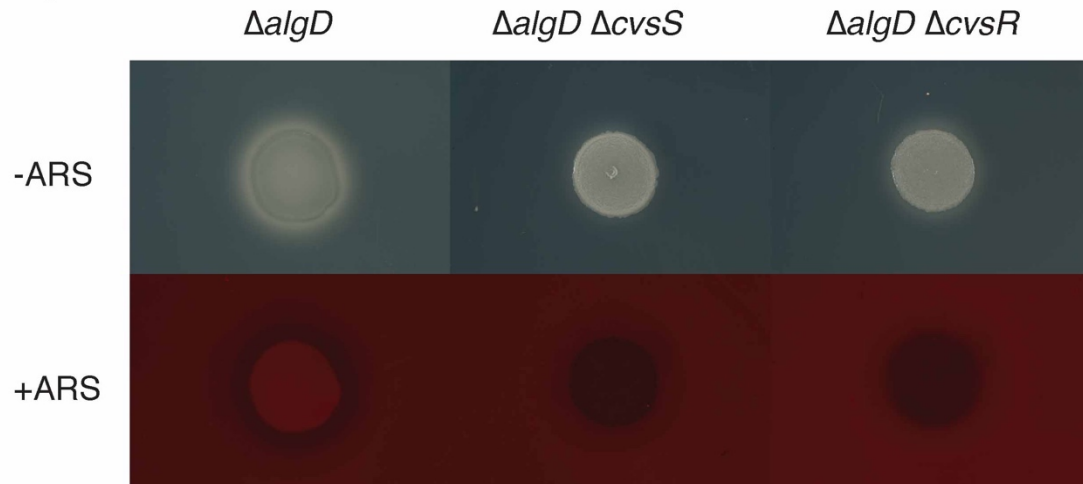


Figure 3.14: Photos of *ΔalgD*, *ΔalgD ΔcvsS*, and *ΔalgD ΔcvsR* before and after ARS staining after one day of growth on NB supplemented with Ca^{2+} . The *ΔalgD ΔcvsS*, and *ΔalgD ΔcvsR* strains were stained by ARS, while the *ΔalgD* strain was not stained by ARS. This assay was repeated three separate times. These photos are representative of *ΔalgD*, *ΔalgD ΔcvsS*, and *ΔalgD ΔcvsR* strains when grown on NB supplemented with Ca^{2+} . These photos are representative of an experiment that was repeated three times.

microbes secrete organic acids, such as gluconic acid, that dissolve calcium phosphate (70). The acidic pH that *Pto* produced when grown on NB supplemented with calcium and glucose was caused by *Pto* converting glucose into gluconic acid. Since the $\Delta cv s S$ and $\Delta cv s R$ strains did not have calcium phosphate on the surface of cells when grown on NB supplemented with calcium and glucose, it suggests that a weak acid may be utilized in a CvsSR dependent manner by *Pto* to dissolve or prevent calcium phosphate from accumulating on the surface of cells when grown on NB supplemented with Ca^{2+} .

CvsSR regulates the carbonic anhydrase, 5255, and the SulP MFS transporter, 5256 (165). Constitutive expression of both genes in a $\Delta cv s S$ or a $\Delta cv s R$ strain prevented calcium phosphate precipitation and restored the WT phenotype. Carbonic anhydrases hydrate CO_2 to H^+ and HCO_3^- and these products are capable of dissolving calcium mineral (74). SulP MFS transporters that are found in an operon with a carbonic anhydrase are commonly able to transport bicarbonate (178). Given that calcium phosphate precipitation was prevented in the $\Delta cv s S$ and $\Delta cv s R$ strains only when 5255 and 5256 were constitutively expressed, it would suggest that 5256 is essential for preventing calcium phosphate precipitation in the $\Delta cv s S$ and $\Delta cv s R$ strains and may transport H^+ and HCO_3^- . This promotes the idea that one mechanism through which *Pto* prevents surface-associated calcium precipitation is through the secretion of H^+ and HCO_3^- . *Bacillus mucilaginosus* and *Brevibacterium linens* BS258 upregulate expression of carbonic anhydrases during calcium dissolution (76, 77). Bicarbonate increases the solubility of apatite and it is possible that a common mechanism by which bacteria dissolve calcium precipitate is through the production of

H⁺ and HCO₃⁻ by carbonic anhydrases followed by secretion of H⁺ and HCO₃⁻ (183). Characterization of $\Delta cv s S$ and $\Delta cv s R$ strain constitutively expressing only 5256 would show whether 5256 by itself is capable of preventing calcium phosphate accumulation in these strains. Further investigation into the activity of 5255 and 5256 in *Pto* would provide greater insight into their role in calcium phosphate precipitation or calcium dissolution in *Pto*.

The reduced swarming phenotype in the $\Delta cv s S$ and $\Delta cv s R$ strains only occurred when additional Ca²⁺ was added to medium but not when other inducers of CvsSR were added to the medium. Similarly, surface associated calcium precipitation only occurred on the colonies of the $\Delta cv s S$ and $\Delta cv s R$ strains when additional Ca²⁺ was added to the medium. Swarming was recovered under conditions where calcium precipitation was likely delayed or did not occur in the $\Delta cv s S$ and $\Delta cv s R$ strains, correlating calcium precipitation with the reduced swarming phenotype. Swarming motility in bacteria is dependent on bacteria reducing the surface tension of the liquid around them. It is for this reason that bacteria produce biosurfactants that lower the surface tension of water during swarming motility (184). Calcium precipitation on the surface of cells may inhibit swarming by creating a physical barrier that prevents motility. The link between surface-associated calcium precipitation and motility of *Pto* implies that preventing the accumulation of surface-associated calcium phosphate precipitation may be important for *Pto* in Ca²⁺-rich surroundings.

Ca²⁺ is abundant in the leaf apoplast, with concentrations around 10 mM (165, 185). This concentration is not static during biotic stress as studies in *Phaseolus vulgaris* infected with *P. syringae* pv. *phaseolicola* RJ3 suggest that apoplastic Ca²⁺

concentrations actually increase during a compatible interaction (185). Given the high concentration of Ca^{2+} in the apoplast, it is possible that *P. syringae* precipitates calcium at some point during growth *in planta* and also dissolves calcium precipitate. Ca^{2+} is an important signaling molecule during pattern triggered immunity (PTI) (186). Other bacterial plant pathogens use EPSs to chelate Ca^{2+} as a way to reduce PTI (187). Given the fact that CvsSR is involved in virulence, MICP and calcium dissolution could be employed by *Pto* during growth *in planta* as a way to evade or dampen PTI. Follow-up studies on the role of CvsSR during *Pto* growth *in planta* could help identify whether *Pto* performs MICP and/or calcium dissolution during endophytic growth.

Acknowledgements

We would like to thank Jenny Russ Kunitake for helping perform pilot experiments on the Raman confocal microscope. The U.S. Department of Agriculture (USDA) is an equal opportunity provider and employer. Mention of trade names or commercial products in this publication is solely for the purposes of providing specific information and does not imply recommendation or endorsement by the USDA. This work made use of the Cornell Center for Materials Research Facilities supported by the National Science Foundation under Award Number DMR-1719875. The authors declare no conflicts of interest.

CHAPTER 4

PSPTO_5255 IS A NOVEL VIRULENCE ASSOCIATED GENE IN *PSEUDOMONAS SYRINGAE* PV. TOMATO DC3000⁵

Abstract

Pseudomonas syringae pv. tomato DC3000 (*Pto*) is a hemibiotrophic plant pathogen. During entry into the plant and growth in the apoplast, *Pto* utilizes two-component systems (TCSs) and extra cytoplasmic function sigma factors to sense and responds to changes in the apoplast. The TCS CvsSR is a Ca²⁺-induced TCS that regulates virulence in *Pto*. Among the genes CvsSR positively regulates is the carbonic anhydrase PSPTO_5255 (5255). Along with being regulated by CvsSR, 5255 is regulated by RpoF. Transcription of 5255 can result in truncated transcripts that do not include the entirety of 5255. Carbonic anhydrases are enzymes found in all biological life. 5255 is not essential for growth of *Pto* but is involved in virulence on tomato. *Nicotiana benthamiana* plants infiltrated with the Δ 5255 strain show a delay in the hypersensitive response as compared to WT suggesting 5255 is involved in virulence of *Pto* through regulation of the type III secretion system. Deletion of 5255 in *Pto* results in *Pto* producing more cellulose and killing fewer foreign bacteria when additional Ca²⁺ is present in medium. The identification and characterization of 5255 provides an example of a unique role by a bacterial carbonic anhydrase that affects multiple stages of the *Pto* lifecycle.

⁵ Maxwell R. Fishman, Alexa Cohen, and Melanie J. Filiatrault. PSPTO_5255 is a novel virulence associated gene in *Pseudomonas syringae* pv. tomato DC3000. in prep.

Introduction

Carbonic anhydrases function to catalyze the hydration of CO₂ to bicarbonate or dehydrate bicarbonate to CO₂ (44, 188). They are found in all biological organisms and are essential for life. Carbonic anhydrases also provide bicarbonate that is used during the TCA cycle and the production of fatty acids (189, 190). In plants, carbonic anhydrases play an essential role during photosynthesis and dehydrate HCO₃⁻ to CO₂ during fixation of carbon (191). In bacteria, carbonic anhydrases are essential in *Escherichia coli*, *Pseudomonas aeruginosa*, and *Streptococcus pneumoniae* during growth at atmospheric (48, 52, 53). The essential nature of carbonic anhydrases in bacteria have made them a potential drug target in animal pathogens but have yet to be fully investigated in plant pathogens.

Pseudomonas syringae pv. *tomato* DC3000 (*Pto*) is a hemibiotrophic plant pathogenic bacteria that infects tomato plants, *Arabidopsis thaliana*, and collard (192). The loci PSPTO_0993, PSPTO_1340, and PSPTO_5255 code for carbonic anhydrases in the genome of *Pto* (60). Multiple copies of genes with similar functions commonly signify redundancy among genes. The *P. aeruginosa* genome has at least three genes that code for carbonic anhydrases and there is some functional redundancy (52). The carbonic anhydrase orthologous to PSPTO_5255 (5255) in *P. aeruginosa* is the most highly expressed and deletion of that gene leads to a growth defect under atmospheric conditions (52). Several plant pathogens produce carbonic anhydrases that are thought to be secreted and could be virulence factors. *Pectobacterium carotovorum* has an α -carbonic anhydrase that is a candidate virulence factor (58). *Phytophthora infestans*

produces several carbonic anhydrases that are thought to be secreted by the pathogen (59).

CvsSR is a two-component in *Pto* that is induced by Ca^{2+} and regulates *hrpRS* and *hrpL* (165). 5255 is directly regulated by CvsSR in *Pto* and is down-regulated 22-fold in a ΔcvsR mutant as compared to wild-type (WT). Deletion of *cvsS* or *cvsR* results in decreased virulence of *Pto* on tomato and *Arabidopsis thaliana*. CvsSR also regulates swarming motility and cellulose biosynthesis in a Ca^{2+} -dependent manner.

Cellulose biosynthesis in *Pto* is commonly reflective of high intracellular cyclic-di-GMP concentrations (cdG) (116). CdG is a secondary messenger in bacteria that regulates several lifestyle switches (116, 135, 137, 193, 194). Among the most well characterized lifestyle switches that cdG regulates are the switch from sessile to motile and also the switch from expressing the type III secretion system (T3SS) to expressing the type VI secretion system (T6SS) (116, 137, 193, 195). The T3SS is utilized by pathogens during host infection, *Pto* relies on the T3SS during infection to secrete type III effectors (T3Es) that suppress the plant immune response (3). While T3Es are meant to help *Pto* overcome the plant immune response, they can also cause effector triggered immunity (ETI) during an incompatible interaction that results in plant cell death localized to the cells that received T3Es (5). This type of plant cell death is called the hyper sensitive response (HR). On the other hand, the T6SS is typically utilized by bacteria to kill foreign bacteria that are nearby (196). *Pto* has a T6SS and utilizes it during bacterial competition (197).

In this section of this thesis 5255 is identified as a virulence-associated gene in *Pto* when it infects tomato. The transcriptional regulation of 5255 is then characterized

and putative transcriptional attenuation of this gene is identified. Lastly, it is shown that deletion of 5255 in *Pto* delays the HR and also reduces *Pto*'s ability to kill foreign bacterial cells.

Materials and Methods

Bacterial strains and growth conditions. The primers and plasmids and bacterial strains used in this study can be found in Supplementary Table 4.1 and 4.2, respectively. *Escherichia coli* TOP10 cells (ThermoFisher Scientific, Waltham, MA) were used for cloning. *E. coli* was grown in Lysogeny Broth (LB) medium supplemented with the appropriate antibiotics when necessary. *Pto* was routinely cultured on King's B (KB) agar (147). For select assays, strains were grown in mannitol glutamate (MG) medium (10g Mannitol, 2.5 g L-glutamate, 0.2 g MgSO₄ 7H₂O, 0.5 g KH₂PO₄, and 0.2 g NaCl per liter) at the specified pH (16).

Creation of *Pto* mutants. Unmarked mutant strains were constructed using the pK18mobsacB plasmid (148). DNA fragments of approximately 0.9 kb upstream and 1.0 kb downstream of PSPTO_5256, and *fliA* were amplified by PCR, gel-purified using Qiagen Gel Extraction Miniprep Kit (Qiagen, Valencia, CA) and then joined by splicing by overlap extension PCR. These final PCR products were then gel-purified, digested with XbaI (New England Biolabs, Ipswich, MA), and cloned into pK18mobsacB. The pK18mobsacB constructs were confirmed by sequencing at the Biotechnology Resource Center of Cornell University before being introduced into WT *Pto* via electroporation. Integration events were selected for on KB medium containing 50 µg/ml kanamycin. Colonies were transferred to KB containing 8% sucrose to select for crossover events that resulted in the loss of the *sacB* gene.

Table 4.1: Strains and plasmids used in this study.

<i>Pseudomonas syringae</i> pv. tomato DC3000 strains		
Strain Name	Genotype	Reference
<i>Pto</i> (WT)	<i>Pseudomonas syringae</i> pv. tomato DC3000 wild type, Rif ^R	(60)
MFPS05	<i>Pto</i> ΔPSPTO_5255	Chapter 3 of thesis
MFPS14	MFPS05 attTn7::Tn7-PSPTO_5255	This study
MFPS15	MFPS05 pBS46:PSPTO_5255	Chapter 3 of thesis
MFPS06	<i>Pto</i> ΔPSPTO_5256	This study
MFPS07	<i>Pto</i> ΔPSPTO_5255/5256	This study
MFPS18	<i>Pto</i> ΔPSPTO_5255s	This study
MFPS19	<i>Pto</i> PSPTO_5255 H98A C101A	This study
	<i>Pto</i> Δhcp-2	This study
<i>Escherichia coli</i> strains		
TOP10	F- mcrA Δ(mrr-hsdRMS-mcrBC) φ80lacZΔM15 ΔlacX74 nupG recA1 araD139 Δ(ara-leu)7697 galE15 galK16 rpsL(StrR) endA1 λ ⁻	ThermoFisher Scientific
DB3.1 λpir	F- gyrA462 endA1 glnV44 Δ(sr1-recA) mcrB mrr hsdS20(rB -, mB -) ara14 galK2 lacY1 proA2 rpsL20(SmR) xyl5 Δleu mtl1 λpir-lysogen	(198)
Plasmids		
pK18mobsacB	Small mobilizable suicide vector with Km ^R and sucrose-sensitivity (sacB)	(148)
pMRF17	pK18mobsacB::ΔPSPTO_5256	This study
pMRF18	pK18mobsacB::ΔPSPTO_5255/5256	This study
pMRF33	pK18mobsacB::ΔPSPTO_5255s	This study
pMRF34	pK18mobsacB::PSPTO_5255 H98A C101A	This study
pUC18R6KT-mini-Tn7Ttc	Mini-Tn7 with tetracycline resistance	(150)
pTNS2	Tn7 helper plasmid	(150)
pMRF20	pUC18R6KT-mini-Tn7Ttc::PSPTO_5255	This study

Table 4.2: Primers used in this study

Primer name	Sequence (5' – 3')	Description
oMRF0080	GCTCTAGAGCTTGAGGTATT GCTGCGCT	PSPTO_5255s KO and PSPTO_5255 H98A C101A and PSPTO_5255/5256 upstream forward with XbaI site
oMRF0081	CGTCTAGAAGTCATCGGCAA CGCACC	PSPTO_5255s KO and PSPTO_5255 H98A C101A downstream reverse with XbaI site
oMRF0509	TCCAGGTGAAGACTGAGTGA TCAATTCGGGCACGA	PSPTO_5255s KO upstream reverse with overlap
oMRF0510	TCAGTCTTCACCTGGAGATTT GTTC	PSPTO_5255s KO downstream forward
oMRF0536	GCCTGCGTCGGATGCCCCGC AAACAATGATGTGC	PSPTO_5255 H98A C101A upstream reverse
oMRF0537	GCATCCGACGCAGGCGCAAT GCGTGCC	PSPTO_5255 H98A C101A downstream forward
oMRF0085	CGTCTAGACGTGATGCCCGT TACAGGTG	PSPTO_5256 KO upstream forward with XbaI site
oMRF0084	CGTCTAGAAACAAGGTGCTC GGCGC	PSPTO_5256 and PSPTO_5255/5256 KO downstream reverse with XbaI site
oMRF0086	GGAGAAGCGCCATGGGTATT TCGTGCAACACAGAGTAAT TGA	PSPTO_5256 KO downstream forward with overlap
oMRF0085	CGTCTAGACGTGATGCCCGT TACAGGTG	PSPTO_5256 KO upstream forward
oMRF0136	GCTCTTCCTGCTGAGGGAAG A	PSPTO_5255/5256 KO upstream reverse
oMRF0138	TCTTCCCTCAGCAGGAAGAG CCGCAACCTGATCGTCGCA	PSPTO_5255/5256 KO downstream forward with overlap
oMRF0408	CGGAATTCCGAACTTGGTAC TATCGTGCAAAC	PSPTO_5255 Tn7 complement forward with EcoRI site
oMRF0411	CGGGATCCCATCATGCGTAG CCGCCA	PSPTO_5255 Tn7 complement reverse with BamHI site

Sucrose-resistant colonies were screened by PCR and clones containing the appropriate deletion(s) were confirmed by sequencing.

Creation of PSPTO_5255 complement. A 5255 complement was created using pCPP6351 (143). 5255 and its native promoter were PCR amplified using Phusion (ThermoFisher Scientific). The amplified PCR product was gel extracted using the Zymoclean Gel Recovery kit (Zymo) and then restriction digested with BamHI and EcoRI (NEB). This digested PCR product was then ligated into pCPP6351 that had been restriction digested with BamHI and EcoRI using T4 DNA ligase (NEB). The ligation product was transformed into DH5alpha lambda pir *E. coli* cells and plated on LB with 10 µg/mL tetracycline. Positive colonies were checked for the plasmid through PCR. Plasmids were then isolated using a Qiagen spin miniprep kit (Qiagen) and verified through sequencing at the Biotechnology Resource Center at Cornell. Verified plasmids were transformed into a Δ5255 strain of *Pto* through electroporation. Positive colonies of Δ5255 were selected for on KB with 10 µg/mL tetracycline and confirmed through sequencing.

Tomato virulence assays. Three to four-week-old tomato plants were inoculated with *Pto* strains through either dip inoculation or syringe infiltration as described previously (165). Briefly, for dip inoculation *Pto* strains were resuspended in 10 mM MgCl₂ with 0.2% (w/v) Silwet at 2 x 10⁷ cfu/mL. Tomato plants were dipped in inocula for 30 seconds and then allowed to dry before being stored in a room set at 28C, with 70% relative humidity and 16-hour day length. Growth of bacteria was assessed at four days post inoculation (DPI) and 6 DPI. Pictures of diseased tomato leaves were taken at 4, 5, and 6 DPI. For syringe infiltration, tomato plants were

infiltrated with *Pto* strains resuspended in 10 mM MgCl₂ at 5 x 10⁴ cfu/mL using a blunt tip syringe. Following infiltration, infiltrated areas of plants were allowed to dry before being stored in a room set to the same conditions as described above. Growth of bacteria was assessed at 2, 4, and 6 DPI. Photos of infected leaves were taken at 6 DPI. These experiments were repeated three separate times. Three separate tomato plants were infiltrated for each experiment. A Student's two-tailed t-test was used to determine statistical significance when analyzing growth of mutant *Pto* strains.

3' rapid amplification of cDNA ends (3'-RACE). RNA was extracted from *Pto* grown on Nutrient Broth (NB) (Becton Dickinson, Franklin Lakes, NJ) agar plates supplemented with 5 mM CaCl₂ and 0.5% (w/v) sodium succinate hexahydrate using Zymo Direct-zol RNA miniprep kit (Zymo Research, Irvine, CA) according to the manufacturer's directions. Extracted RNA was then treated with DNase (ThermoFisher) and then purified using the Zymo RNA clean and concentrator – 5. Following purification, first strand cDNA synthesis was performed using qScript cDNA synthesis kit (Quantabio, Beverly, MA) with 1 µg of RNA. cDNA was then amplified using a primer specific to the 5' UTR upstream of 5255 and a primer designed to randomly bind throughout the genome of *Pto* using OneTaq (NEB). PCR products were purified using a Zymo DNA clean and concentrator – 5 prior to Topo-TA cloning (ThermoFisher). Cloned vectors were sequenced at the Biotechnology Resource Center of Cornell University in order to determine the DNA sequence of the insert.

Growth curves. *Pto* strains were grown overnight in KB medium. Cultures were then washed twice in MG medium set at a pH of 6.0 before being resuspended at an OD₆₀₀

of 0.1. OD_{600} was used to measure growth of bacteria in MG pH 6.0 and MG pH 6.0 supplemented with 5 mM $CaCl_2$ for 24 hours in a Synergy 2 plate reader (BioTek, Winooski, VT). This experiment was repeated three times. Statistical significance was determined by performing a least squares mean regression on the combined experiments.

Construction of luciferase reporter vectors. 250 bp upstream of 5255 (P_{5255}) was PCR amplified. PCR products were gel-extracted using a Zymoclean Gel DNA recovery kit (Zymo), cloned into pENTR/D/TOPO (ThermoFisher) and transformed into TOP10 *E. coli* cells (ThermoFisher Scientific). Clones of pENTR/D/TOPO:: P_{5255} were selected and sequenced at the Biotechnology Resource Center of Cornell University. A positive clone of pENTR/D/TOPO:: P_{5255} was then mixed with pBS58 in the presence of the LR clonase II mix (ThermoFisher) to transfer P_{5255} to pBS58. This mixture was then transformed into TOP10 *E. coli* cells (ThermoFisher) and clones of pBS58:: P_{5255} were selected and sequenced at the Biotechnology Resource Center of Cornell University. A positive clone of pBS58:: P_{5255} was then transformed into the appropriate *Pto* strains through electroporation.

Luciferase reporter assays. Luciferase reporter assays were performed as precisely described (165). Briefly, *Pto* strains grown on KB plates with 50 $\mu\text{g}/\text{mL}$ kanamycin and 10 $\mu\text{g}/\text{mL}$ tetracycline were scraped off the plates and then resuspended in MG pH 6.0. Cultures were then diluted to an OD_{600} of 0.1 in MG pH 6.0 and MG pH 6.0 supplemented with 5 mM $CaCl_2$. Luminescence and OD_{600} were measured over the course of 16 hours. Relative luminescence measurements were normalized to OD_{600} .

Three independent replicates of these experiments were performed. A least squares mean regression was used to determine statistical significance.

Calcofluor white assays. Calcofluor white (CW) assays were performed as previously described (165). Briefly, *Pto* strains were grown overnight in KB medium and then washed twice in NB medium. Cultures were then diluted to an OD₆₀₀ of 0.3. 5 µL of each culture was spotted on NB supplemented with 5 mM CaCl₂ and 0.02% (w/v) CW. CW binding colonies were determined by illuminating colonies with UV light. Pictures were taken at one, two, and three days after spotting. This experiment was repeated three independent times.

Hypersensitive response (HR) assays. HR assays were performed as previously described (165). Briefly, *Nicotiana benthamiana* was infiltrated with 1×10^8 , 1×10^7 , or 1×10^6 cfu/mL of the appropriate *Pto* strain suspended in 10 mM MgCl₂ using a blunt tip syringe. *N. benthamiana* plants were then observed over the course of three day for cell collapse. Pictures of infiltrated leaves were taken over the course of three days. This experiment was repeated three independent times.

Bacterial killing assays. *Pto* strains were grown in KB medium overnight and *E. coli* DH5alpha pAR::007 was grown in LB medium overnight. Three OD units of each bacterial culture were transferred to a microfuge tube and then washed twice with NB medium. Cultures were then resuspended in 300 µL of NB. *Pto* strains and *E. coli* cultures were then mixed at a ratio of 10:1. 5 µL of mixed cultures were spotted on sterile 0.2 µm nitrocellulose membrane that we placed on NB agar plates supplemented with 5 mM CaCl₂ and 0.5% (w/v) sodium succinate hexahydrate when appropriate. Cells were allowed to grow at 28C for six hours before being

resuspended in 100 μ L sterile ddH₂O and spotted on KB with 50 μ g/mL rifampicin or LB with 50 μ g/mL kanamycin using serial dilutions in order to determine the number of *Pto* and *E. coli* cells present in the cultures, respectively. This experiment was performed three independent times. A Student's two-tailed T-test was used to determine statistical significance.

Statistical Analysis. Jmp Pro 12 was used for statistical analysis throughout this manuscript.

Results

PSPTO_5255 is a virulence factor in *Pto*. PSPTO_5255 (5255) is in a putative operon with PSPTO_5256 (5256). Both 5255 and 5256 are regulated by CvsSR (165). Because CvsSR regulates virulence of *Pto*, it was possible that 5255 or 5256 were involved in virulence. To determine whether 5255 or 5256 was involved in virulence of *Pto* deletion strains for 5255 (Δ 5255), 5256 (Δ 5256) as well as a double deletion strain of 5255 and 5256 (Δ 5255/5256) were constructed and dip assays were performed. A reduction in symptom development was observed in the Δ 5255 and the Δ 5255/5256 strains starting at 4 DPI, but not the Δ 5256 strain. A significant reduction in growth in tomatoes inoculated with Δ 5255 and Δ 5255/5256 strains as compared to WT was also observed (Figure 4.1). Based on these data, we conclude that 5255, a gene regulated by CvsSR, plays a role in virulence of *Pto*.

The 5' region of 5255 produces several truncated transcripts. The previously mapped transcriptional start site for 5255 appeared to be 200 bp upstream of the translational start site for 5255 (109). RNA-seq data of *Pto* grown on NB

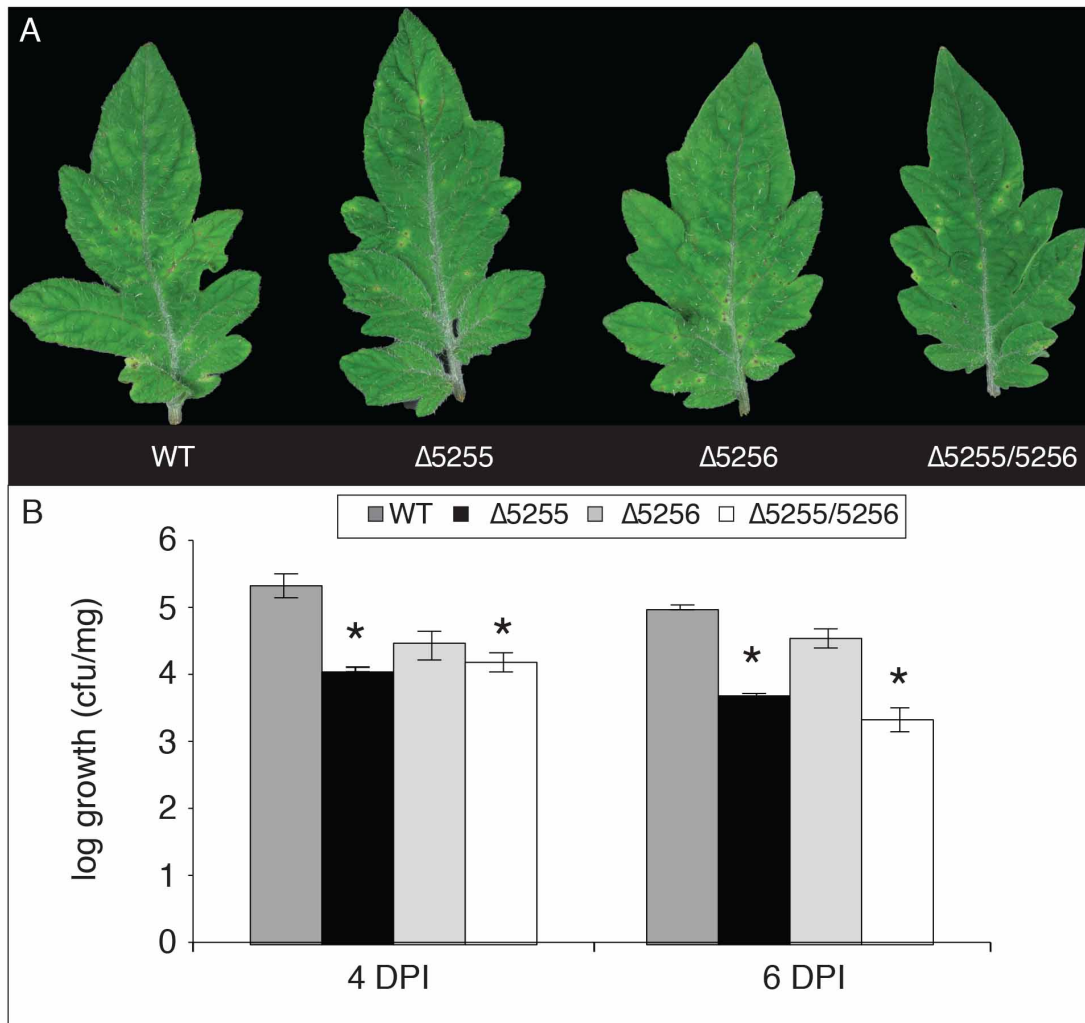


Figure 4.1: (A) Pictures of tomato leaves dip inoculated with WT, $\Delta 5255$, $\Delta 5256$, and $\Delta 5255/5256$ strains at 6 DPI. Tomato leaves inoculated with the $\Delta 5255$ and $\Delta 5255/5256$ strains show less chlorosis than WT and the $\Delta 5256$ strain. These photos are representative of symptom development in tomatoes after 6 DPI. (B) Growth of WT, $\Delta 5255$, $\Delta 5256$, and $\Delta 5255/5256$ strains at 4 DPI and 6 DPI. The y-axis displays growth of the bacteria in log cfu/mg tissue. Error bars signify standard error between three biological replicates. Asterisks above bars are representative of a significant difference between growth of that particular strain as compared to WT, with a p-value < 0.01 . This experiment was independently replicated three times and the growth of the designated strains portrayed here are representative of what was repeatedly observed.

supplemented with Ca²⁺ and succinate showed that the 5' UTR upstream of 5255 had more mapped reads than the gene itself (Figure 4.2). Previous research also suggested that there was a putative rho-independent terminator 369 bp downstream of the transcriptional start site and 170 bp downstream of the translational start site of 5255 (personal communication with Paul Stodghill). The location of this putative rho-independent terminator is in the area where transcript levels appear to decrease in our RNA-seq data. We performed 3' RACE in order to determine if transcription terminated at the predicted location of the rho-independent terminator. We found transcripts that began at the transcriptional start site for 5255 but were only 112-130 bps and 294-386 bps long (Figure 4.3). The longer of the two transcripts extended into the 5'-end of the translational start site for 5255. The expected size of the 5255 transcript is predicted to be 866 bp long. Therefore, these data suggest that truncated transcripts that include the 5' UTR or the 5' UTR and the initial coding region of 5255 are transcribed.

The original Δ 5255 strain included deletion of a portion of the truncated transcript and may have disrupted production of these transcripts along with 5255. In order to determine whether the function of the truncated transcripts was involved in virulence, a silent mutation that made changes to the nucleotides so as to not change the amino acid when the mRNA was translated but removed the putative rho-independent terminator was made within 5255 (5255s). This should not reduce the transcribed amount of mRNA transcribed but could reduce the number of truncated transcripts made when 5255 is transcribed. Along with the silent mutation that was

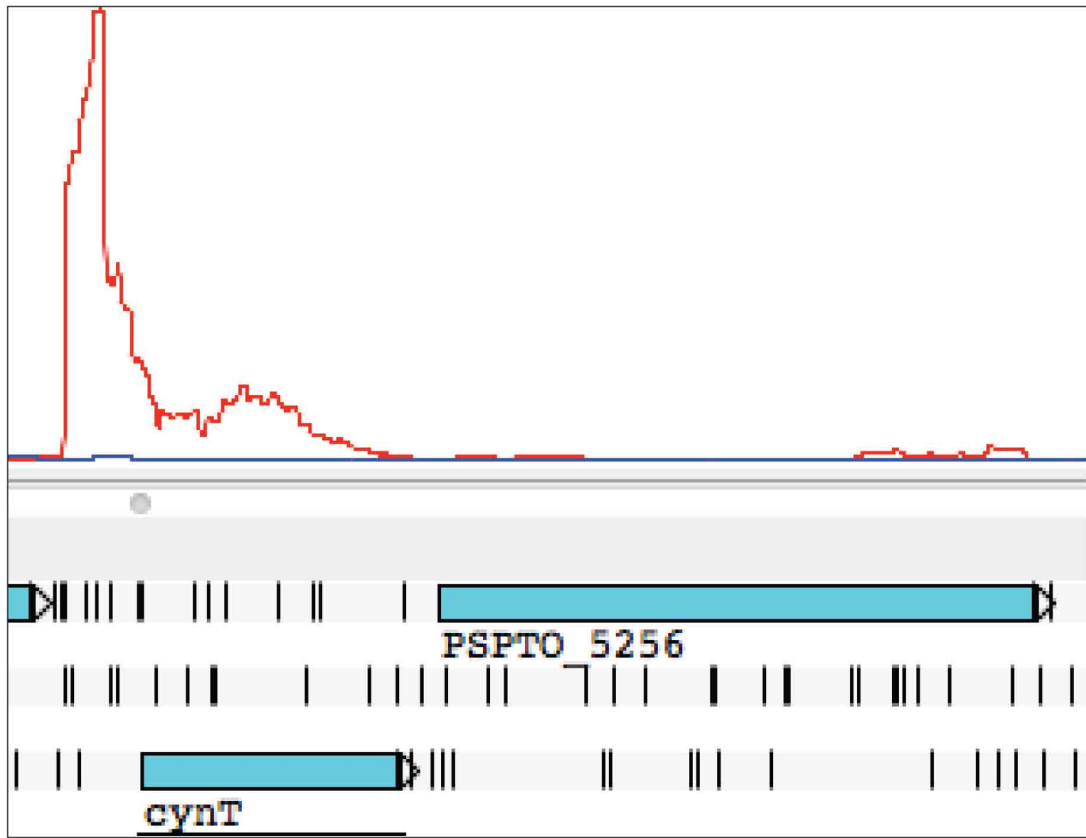


Figure 4.2: An Artemis genome browser screenshot of RNA-seq reads from the area upstream of 5255 (*cynT*) to the end of 5256 of *Pto* when grown on NB supplemented with Ca^{2+} and succinate. The red line represents transcription in the direction of 5255 and 5256. The height of the red line represents relative abundance of that transcript.

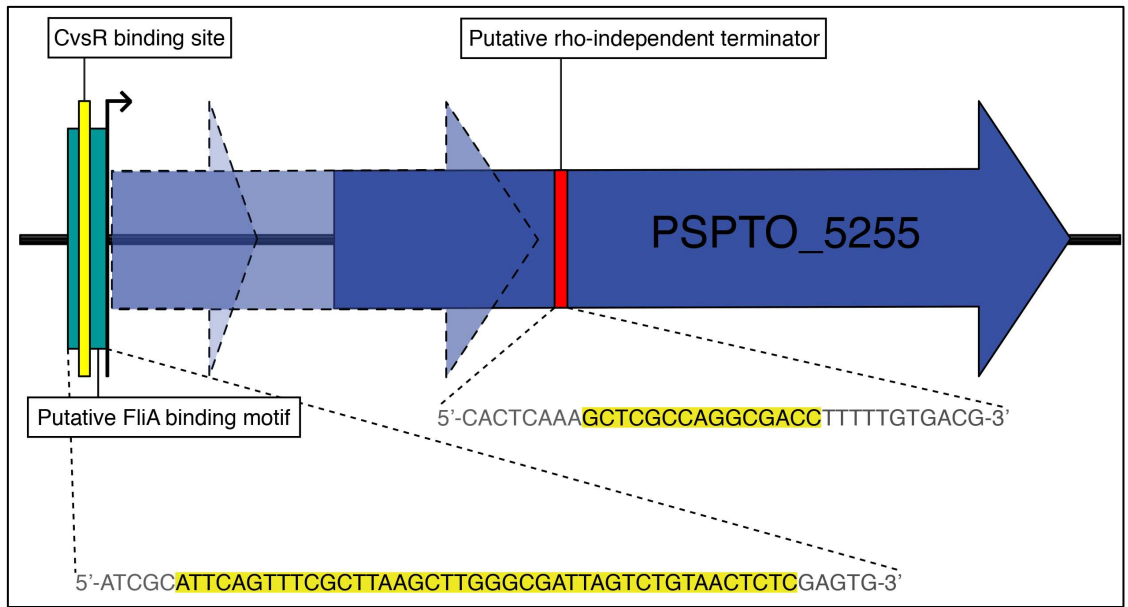


Figure 4.3: An illustration of the transcriptional landscape upstream and within 5255. The cyan bar is where the putative FliA binding motif is found and the yellow bar represents the CvsR binding site upstream of 5255. The black arrow represents that transcriptional start site for 5255. The two lighter arrows outlined with dashed lines represent the two truncated transcripts and the darker arrow outlined with a solid line is the annotation for 5255. The red bar represents the area where a putative rho-independent terminator can be found within 5255. Insets of the associated nucleotide sequence for the putative FliA binding motif and the putative rho-independent terminator are displayed. The black, hi-lighted nucleotides signify the FliA binding motif and the rho-independent terminator.

made, we made a 5255 H98A C101A mutant in order to disrupt the active site of 5255. The coding regions for H98 and C101 in 5255 are downstream of the 3'-end for the longer of the two truncated transcripts and should not interfere with production of these transcripts. WT, Δ 5255, a Δ 5255 complement (Δ 5255c), 5255s, and 5255 H98A C101A were infiltrated into tomato using a blunt tip syringe. Tomato syringe infiltration assays showed that the 5255 H98A C101A strain had reduced symptoms and growth in tomato leaves in much the same way as the Δ 5255 strain, while the 5255s strain was similar to WT in virulence and growth (Figure 4.4). This suggests that 5255, and not the truncated transcripts, is the virulence factor in *Pto*.

Deletion of 5255 in *Pto* does not disrupt growth under normal atmospheric conditions. Deletion of the orthologous carbonic anhydrase to 5255 in *P. aeruginosa* resulted in the mutant strain having a growth defect under atmospheric conditions (52). It was possible that the Δ 5255 strain had a similar growth defect and that this could have contributed to the virulence defect in tomato. However, growth of the Δ 5255 strain was comparable to WT when grown in MG medium under atmospheric conditions (Figure 4.5). This suggests that under normal atmospheric conditions *Pto* grows fine without 5255 and that 5255 affects virulence of *Pto* through another mechanism.

PSPTO_5255 is regulated by FliA but does not affect swarming motility. The promoter for 5255 was inspected for previously predicted sigma-factor binding motifs (109). A FliA binding site is predicted upstream of the 5255 transcriptional start site (Figure 4.3). To determine whether 5255 is regulated by FliA in *Pto*, we transformed WT and a Δ *fliA* mutant with a luciferase reporter gene construct that included the

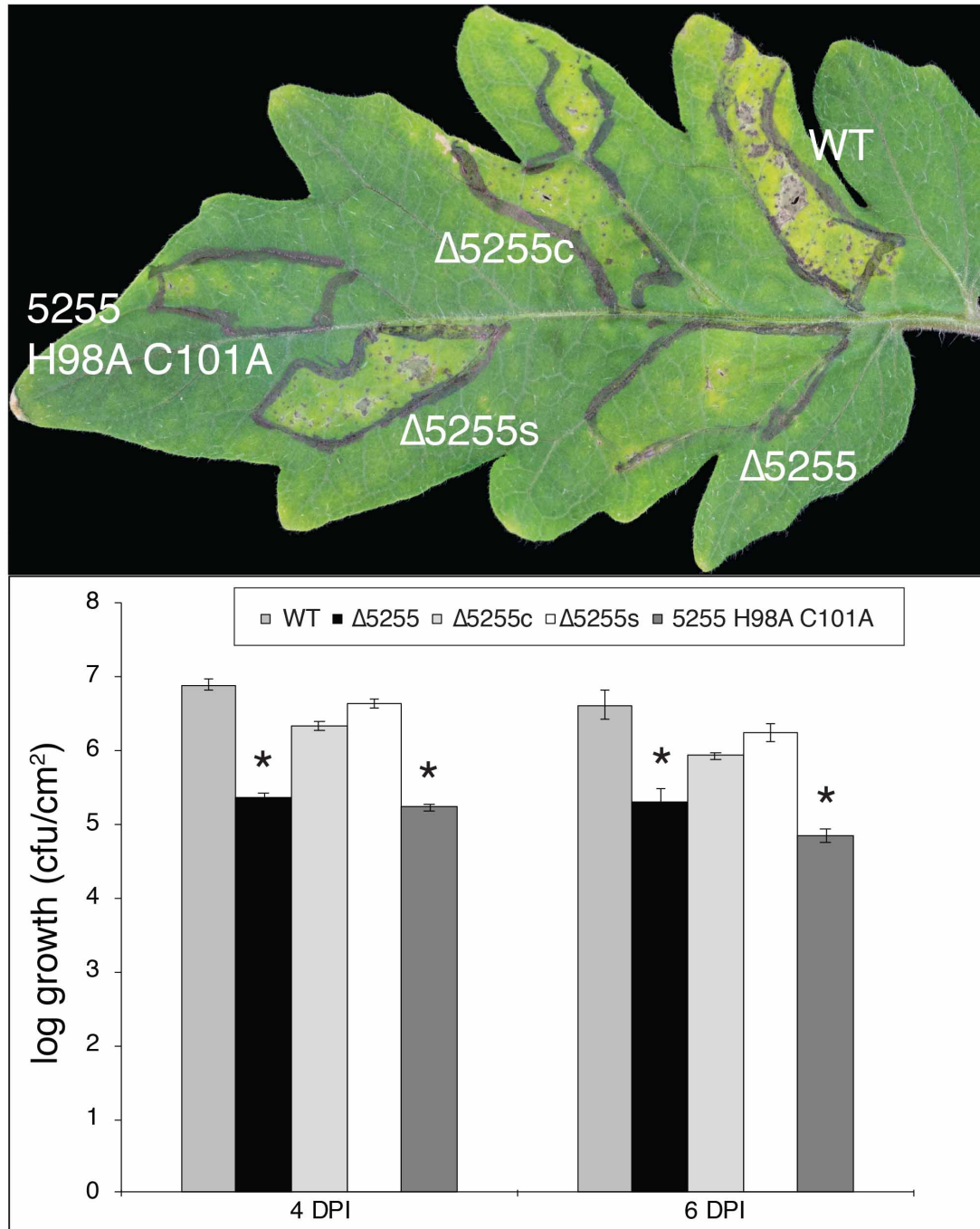


Figure 4.4: (A) Picture at 6 DPI of a tomato leaf that had been syringe inoculated with WT, $\Delta 5255$, $\Delta 5255c$, $\Delta 5255s$, and $\Delta 5255$ H98A C101A. A clear decrease in symptom development can be observed in the $\Delta 5255$ and 5255 H98A C101A strains as compared to WT. (B) Growth of WT, $\Delta 5255$, $\Delta 5255c$, $\Delta 5255s$, and 5255 H98A C101A at 4 DPI and 6 DPI measured using log cfu/cm² of plant tissue. Errors bars signify standard error between three biological replicates. An asterisk designated a significant difference in growth between that strain and WT with a p-value <0.01.

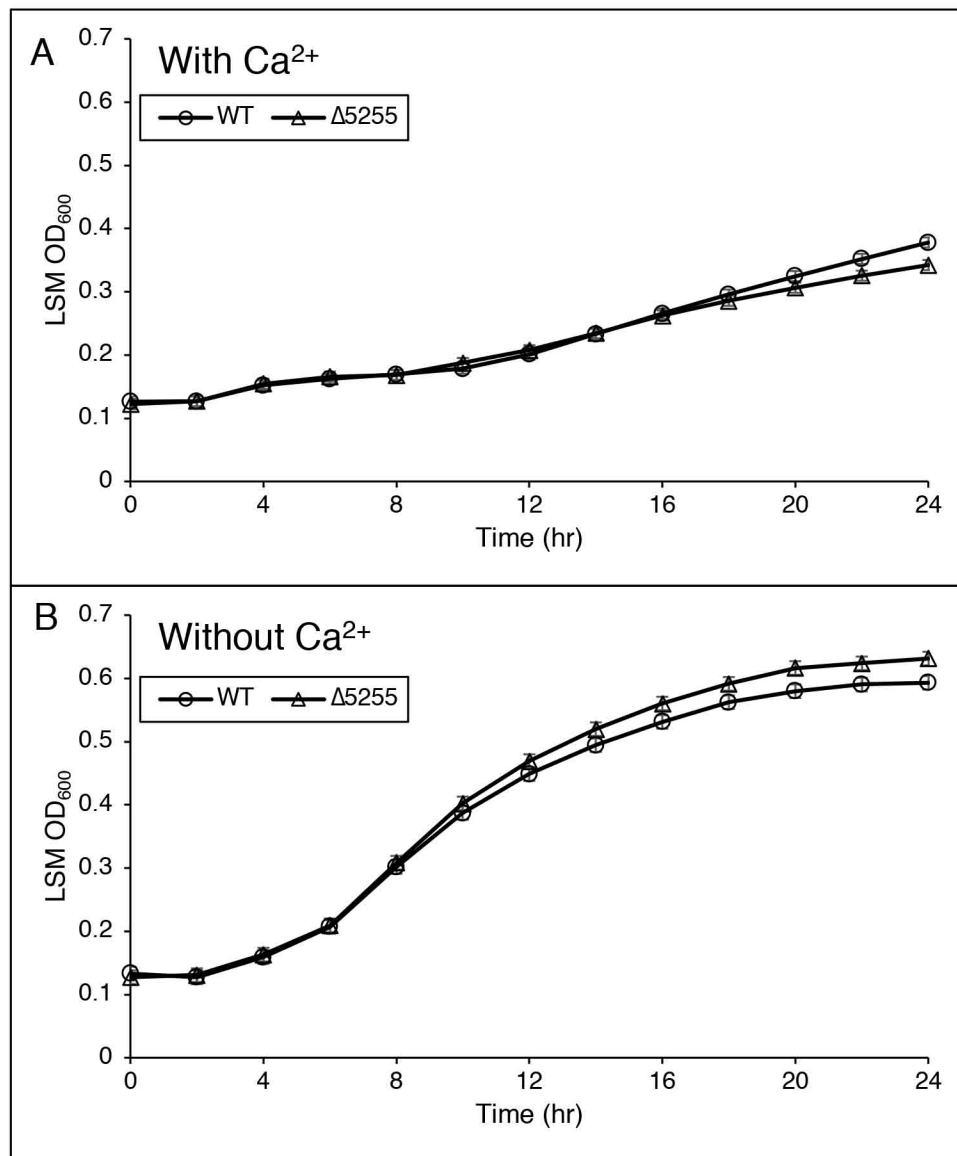


Figure 4.5: Growth curves of WT and the $\Delta 5255$ strain over the course of 24 hours when grown in (A) MG media supplemented with Ca^{2+} or (B) MG media. The y-axis shows growth of the bacteria in OD_{600} . The x-axis shows the time after inoculation in hours. This experiment was repeated three independent times and values from those experiments were combined and averaged using a least squares mean regression. The error bars represent standard error between replicates.

promoter region for 5255 (pBS58::P₅₂₅₅). We then compared expression of 5255 in the Δ *fliA* pBS58::P₅₂₅₅ strain to WT pBS58::P₅₂₅₅ in MG medium and MG medium supplemented with Ca²⁺. We found a significant decrease in expression of 5255 in the Δ *fliA* strain as compared to WT under both conditions (Fig. 4.6). From this we concluded that 5255 is regulated by FliA.

FliA commonly regulates genes involved in flagellar production and motility. We previously found that CvsSR regulates swarming motility under relatively high Ca²⁺ conditions. Since 5255 is regulated by both FliA and CvsSR, we predicted that 5255 regulates motility in *Pto*. We tested swarming motility between WT and the Δ 5255 strain on NB medium and NB medium supplemented with Ca²⁺. Deletion of 5255 slightly reduced the diameter of the swarming zone in both conditions tested (Fig. 4.7). However, this difference was not statistically significant. Thus, even though 5255 is regulated by FliA, it is not clear whether it is involved in swarming motility of *Pto*.

PSPTO_5255 is involved in cellulose production in *Pto*. FliA has also been implicated in regulating genes involved in cyclic-di-GMP (cdG) production and turnover in *P. aeruginosa* (195). In a previous study, we found that CvsSR regulates cellulose production of *Pto* when it is grown on NB agar supplemented with Ca²⁺ (165). Cellulose production is commonly correlated with increased cdG concentration in *Pseudomonas syringae* cells (116). Given that 5255 is regulated by both FliA and CvsSR, it was possible that down-regulation of 5255 was involved in cellulose over-production in the Δ *cvsS* and Δ *cvsR* strains. We grew WT, Δ 5255, and Δ 5255c on NB agar supplemented with Ca²⁺ and calcofluor white (CW). The Δ 5255 strain was

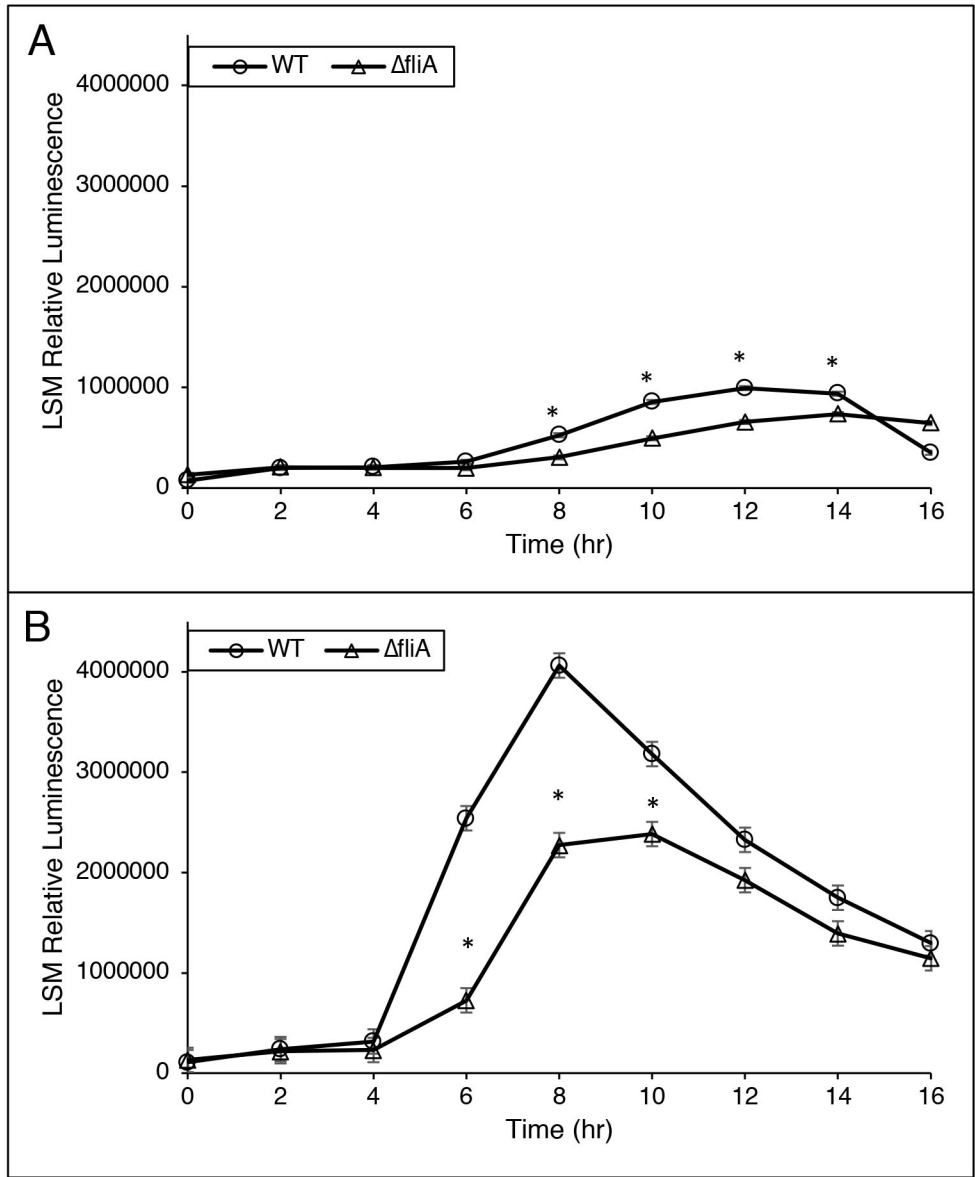


Figure 4.6: Expression of p5255 as measured through relative luminescence of WT and a $\Delta fliA$ strain in (A) MG and (B) MG supplemented with 5 mM CaCl₂. Asterisks indicate timepoints where there was a significant difference in expression between WT and the $\Delta fliA$ strain with a p-value < 0.01. Data from two independent experiments was compiled using a least squares mean regression. Error bars signify standard error between replicates.

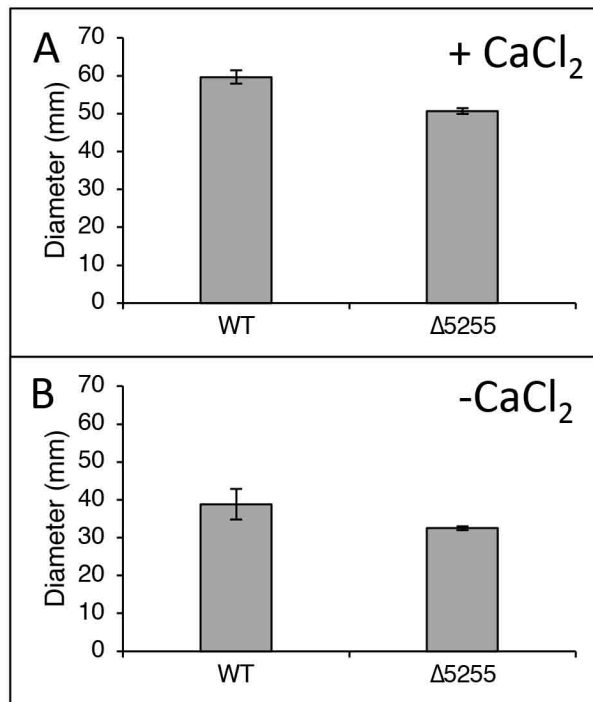


Figure 4.7: Swarming motility of WT and the $\Delta 5255$ strain on (A) NB supplemented with Ca^{2+} and (B) NB. Diameters of the swarming strains were measured 16-20 hours after spotting and measured in mm. Error bars represent the standard deviation between samples. This assay was repeated three independent times and the graphs above are representative of the swarming distance observed by each strain during those experiments.

stained by CW within one day of spotting on NB agar, while WT was not (Figure 4.8).

This phenotype could be restored by complementation with 5255 *in cis* (5255oe).

Interestingly enough, this phenotype was dependent on Ca²⁺ being present in the medium as the Δ 5255 strain did not produce excess cellulose when grown on NB agar without supplemented Ca²⁺ (Figure 4.8). From this we conclude that 5255 regulates cellulose production in *Pto* when *Pto* is grown on medium supplemented with Ca²⁺.

5255 involved in causing the HR in *Nicotiana benthamiana*. CdG production and turnover regulate the T3SS in *P. aeruginosa*, with high cdG concentrations repressing production of the T3SS (193). A similar mechanism may be true in *Pto*. 5255 regulates cellulose production in *Pto*, which could be reflective of increased cdG concentrations in the Δ 5255 strain as compared to WT. The HR is a defense response by plants during an incompatible interaction due to the secretion of T3Es by the T3SS and has been used as a proxy for proper T3SS production and T3E secretion (17). We found that *N. benthamiana* infiltrated with the Δ 5255 strain showed a delay in the HR as compared to WT (Figure 4.9). This suggests that 5255 is involved in regulating the T3SS and T3E delivery or somehow modulates ETI during *Pto* infection.

Deletion of 5255 in *Pto* is detrimental to bacterial competition. In addition to regulating the T3SS in *P. aeruginosa*, cdG also regulates the T6SS (193). Given that the 5255 may impact cdG concentrations in *Pto*, it was possible that the Δ 5255 strain would show differences in bacterial competition as compared to WT. We performed bacterial competition of WT, Δ 5255, and a Δ *hcp-2* strain that has been previously shown to lack the ability to kill foreign bacteria as well as WT using *E. coli* as the prey (197). Strains were plated with *E. coli* on NB supplemented with succinate and NB

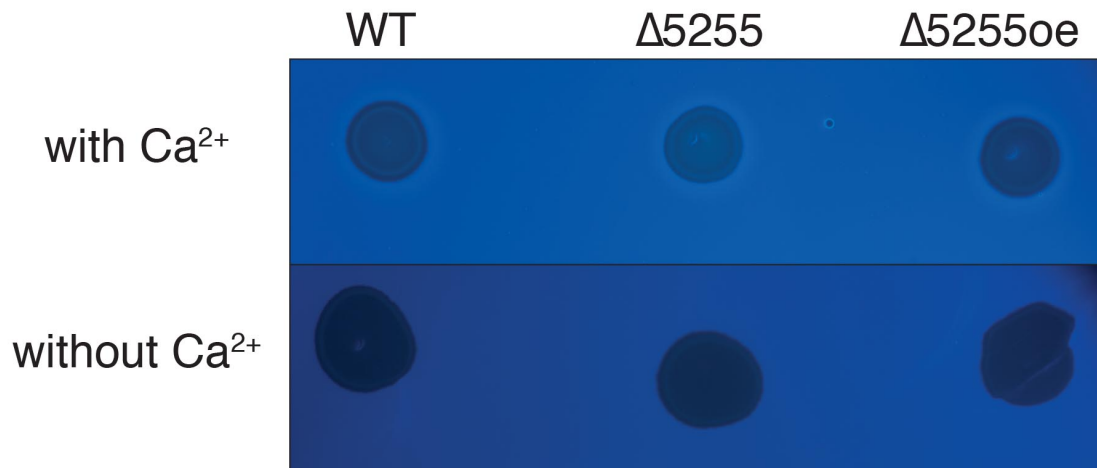


Figure 4.8: Pictures of WT, $\Delta 5255$, and $\Delta 5255oe$ illuminated with UV light after one day of growth on NB supplemented with Ca^{2+} and 0.01% (w/v) CW or NB with 0.01% (w/v) CW. Increased luminescence can be observed in the $\Delta 5255$ strain as compared to WT and the $\Delta 5255oe$ strain when grown on NB supplemented with Ca^{2+} and 0.01% (w/v) CW, but not on NB with 0.01% (w/v) CW. This signifies increased production of cellulose in the $\Delta 5255$ strain under conditions with increased concentrations of Ca^{2+} . Three independent replicates of this experiment were repeated. This picture is representative of observed phenotypes present in each of those experiments.

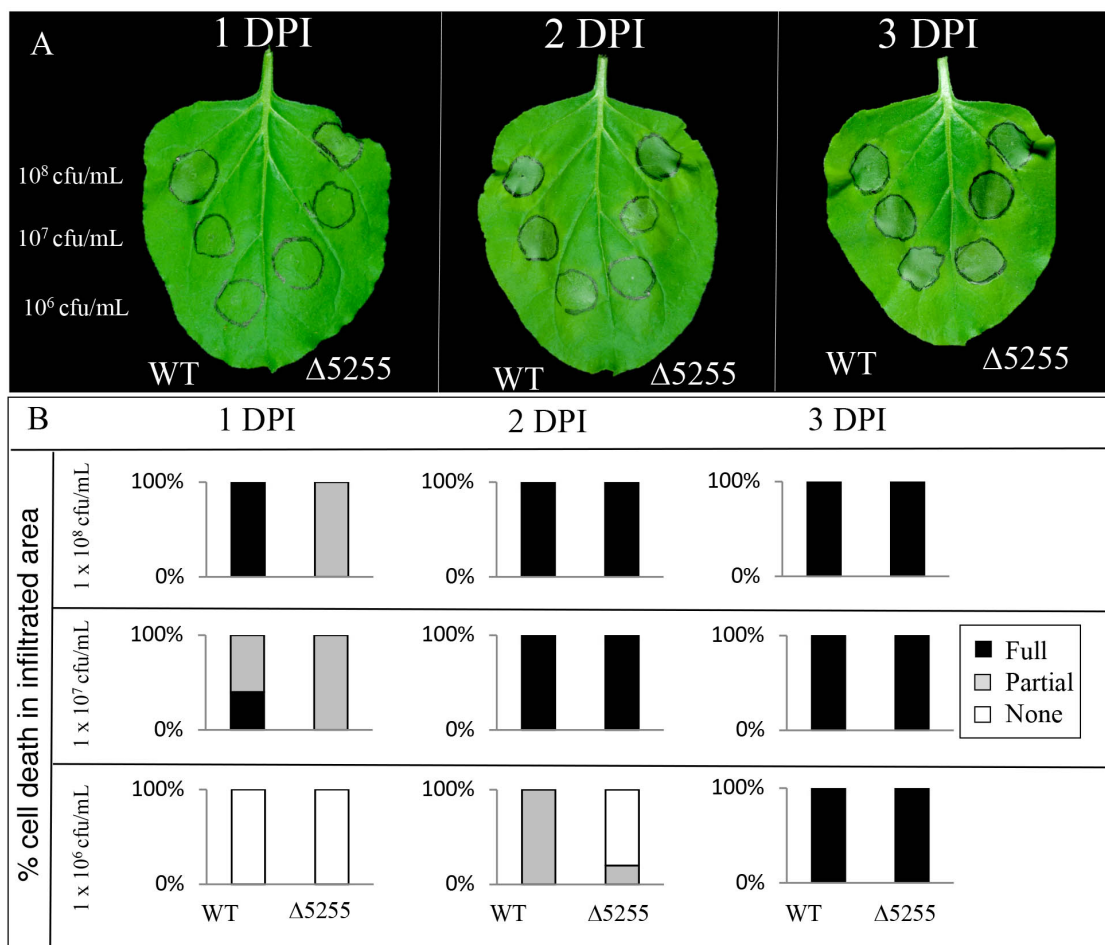


Figure 4.9: (A) Photos of *N. benthamiana* plants at 1 DPI, 2 DPI, and 3 DPI that had been syringe infiltrated with 1×10^8 , 1×10^7 , and 1×10^6 cfu/mL of WT and $\Delta 5255$ strains. Darkening of the infiltrated areas are indicative of the HR. This experiment was independently replicated three times and these photos are representative of the timing of the HR observed in *N. benthamiana* infiltrated with these strains. (B) Quantitation of the percent cell in infiltrated areas of nine independent biological replicates of *N. benthamiana* at different titers over the course of three days. A delay in the HR can be observed in the $\Delta 5255$ strain as compared to WT. This was most easily observed when inoculant was at 1×10^6 cfu/mL.

supplemented with Ca^{2+} and succinate. We found that the $\Delta 5255$ strain killed fewer *E. coli* than WT only when grown on NB supplemented with Ca^{2+} and succinate (Figure 4.10). The amount of *E. coli* that the $\Delta 5255$ strain killed when grown on NB supplemented with Ca^{2+} and succinate was similar to that of the $\Delta hcp-2$ strain. From this we concluded the 5255 is involved in competition of *Pto* with other bacteria when Ca^{2+} is present in the environment.

Discussion

In this chapter of this thesis, we show that the CvsSR regulated beta-carbonic anhydrase, 5255, is also regulated by FliA and is a novel virulence gene in *Pto*. The CvsSR regulon includes *hrpR*, *hrpS*, *hrpL*, and several effector genes and CvsSR regulation of those genes may cumulatively affect virulence (165). However, it also appears that 5255 plays a significant role in virulence of *Pto* and likely adds to the decreased virulence observed in the $\Delta cvsS$ and $\Delta cvsR$ strains. The exact way that 5255 is involved in virulence is still a mystery, but it seems to involve regulating or signaling the T3SS and possibly the T6SS.

Carbonic anhydrases are involved in the tricarboxylic acid cycle, and are implicated in fatty acid biosynthesis, amino acid biosynthesis, and nucleic acid biosynthesis (199). They are typically essential for growth of bacteria when grown under atmospheric conditions. Beta-carbonic anhydrases have been found to be involved in the growth of *Escherichia coli*, *Streptococcus pneumoniae*, and *Ralstonia eutropha* under normal atmospheric conditions (48, 49, 53). In addition, the orthologous beta-carbonic anhydrase in *P. aeruginosa* PAO1 was found to be necessary for full growth of *P. aeruginosa* PAO1 under normal atmospheric

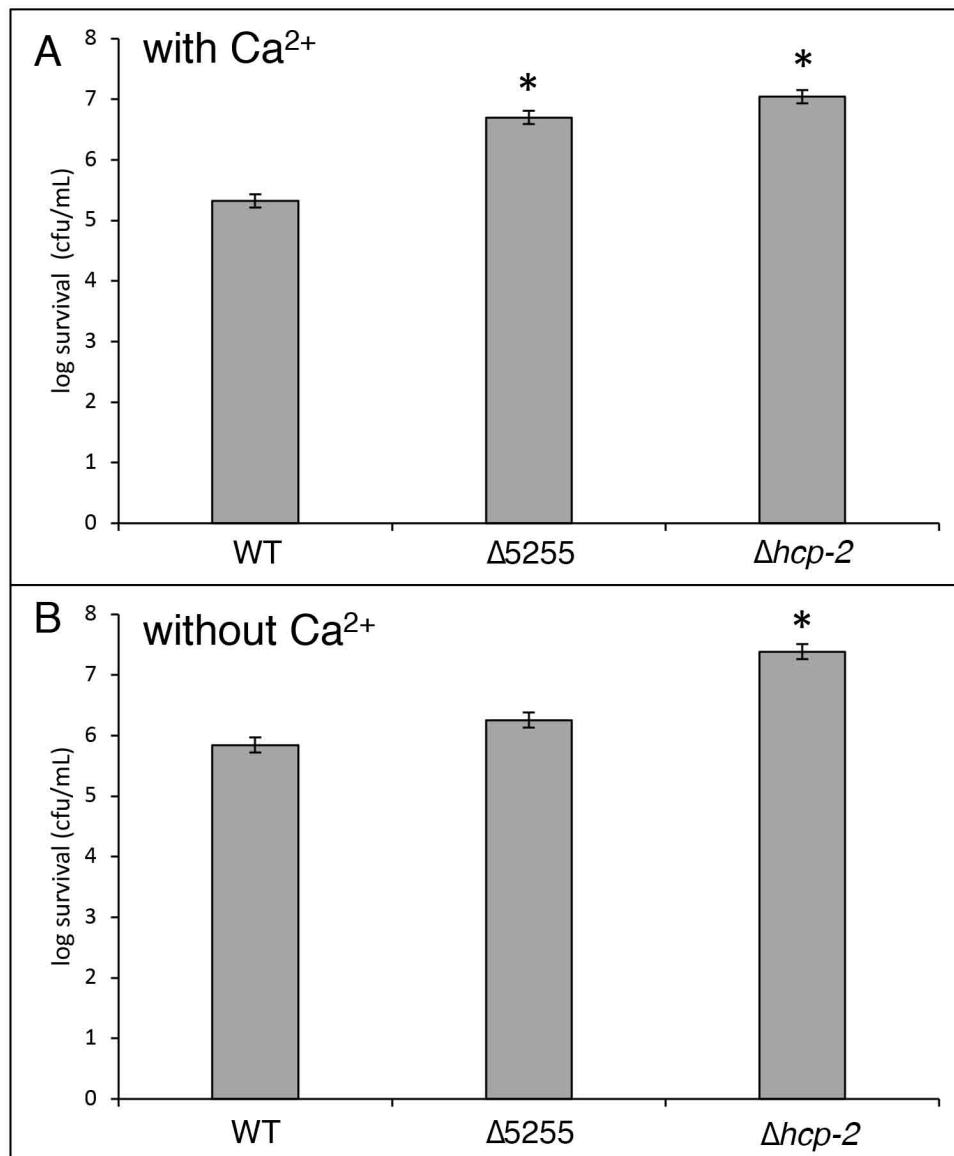


Figure 4.10: Amount of *E. coli* present after being incubated for six hours with WT, $\Delta 5255$, or $\Delta hcp-2$ strains on (A) NB supplemented with Ca^{2+} and succinate or (B) NB supplemented with succinate. The y-axis represents the log survival of *E. coli* as measured in cfu/mL. This experiment was repeated three independent times and the average of those experiments is displayed. The error bars represent standard deviation between replicates. Asterisks represents a significant difference with a p-value < 0.01 between WT and the mutant strain.

under atmospheric conditions. PSPTO_1340 and PSPTO_0994 are two other genes in *Pto* that code for carbonic anhydrases and may be able to compensate for the deletion of 5255 when *Pto* is grown under atmospheric conditions (60). PSPTO_1340 is up-regulated in the $\Delta cvsR$ strain as compared to WT, which could mean that *Pto* uses PSPTO_1340 to compensate for deletion or down-regulation of 5255 (165). Given that deletion of 5255 does not affect growth in *Pto* under atmospheric conditions, 5255 affects virulence of *Pto* through another mechanism.

Carbonic anhydrases effect CO₂ concentration and pH balance in cells by hydrating CO₂ to H⁺ and HCO₃⁻ (44). Bicarbonate has been found to be an environmental signal for certain bacteria. In *Vibrio cholera* bicarbonate abolishes induction of intracellular increases in cdG production from bile (200). In *Mycobacterium avium*, *M. abscessus*, and *M. chelonae* bicarbonate induced export of eDNA independent of pH due to the activity of carbonic anhydrases (201). Thus, bicarbonate is a signaling molecule in certain bacteria. It is less clear-cut whether bicarbonate is a signaling molecule in *Pseudomonas*. Addition of bicarbonate to media does induce dispersal of *P. aeruginosa*, but this dispersal is not thought to be due to signaling mechanisms (202). Given that 5255 is involved in virulence in *Pto* and one of its main roles in the cell is hydrating CO₂ to bicarbonate, it is possible that bicarbonate is an environmental or intracellular signal *Pto* senses. Several of the observed phenotypes in the $\Delta 5255$ strain would suggest that 5255 is producing a signaling molecule for *Pto*.

The $\Delta 5255$ strain produced more cellulose than WT when grown on NB supplemented with Ca²⁺. Increased cellulose production in *Pto* commonly correlates

with increased levels of cdG (116). Increased intracellular cdG concentrations have been implicated in reducing virulence of *Pto* when it infects hosts through natural entry, but not when it is artificially inoculated inside the host using syringe infiltration (203). 5255 shows reduced virulence when it infected the host through natural entry and when it was inoculated via syringe infiltration. The fact that 5255 is involved in virulence no matter the inoculation procedure implicates additional mechanisms other than putative regulation of cdG through which 5255 could be involved in virulence.

5255 follows similar transcriptional expression to *hrpL* transcription in *Pto* when grown in Fe³⁺ replete conditions (16). There is a delay in the HR in *N. benthamiana* infiltrated with the Δ 5255 strain as compared to WT and this suggests that 5255 is necessary for proper production of the T3SS and deployment of T3Es in *Pto*. Strangely enough, Δ *cvsS* and Δ *cvsR* strains do not affect the HR in *N. benthamiana* even though *CvsSR* regulates 5255. Basal levels of 5255 transcription are observed in the Δ *cvsR* strain and it is possible these basal levels of expression of 5255 in the Δ *cvsR* strain are enough to enable the HR to occur at the same rate as WT *Pto* (165). Bicarbonate is an environmental signal for the production of the T3SS in *Yersinia pestis* and is a signal for the locus for enterocyte effacement (LEE) in *E. coli* O157:H7 (204-206). It has also been postulated that increases in internal CO₂ concentration induce virulence factor production in enterohemorrhagic *E. coli* by increasing the internal stores of bicarbonate (207). Bicarbonate also induces expression of the T3SS in *P. aeruginosa* through the bicarbonate sensitive adenylyl cyclase *CyaB* (208, 209). While not through the same mechanism in *P. aeruginosa*, *Y. pestis*, or *E. coli* O157:H7, bicarbonate could induce T3SS production in *Pto*. If so,

this could explain why there is a delay in the HR in the $\Delta 5255$ strain as compared to WT.

Bacterial competition is commonly facilitated through the T6SS during adherent growth but can also be mediated through secretion of a bacteriocin or an antibiotic. *Pto* has the capability to make seven bacteriocins, but bacteriocins are species specific and are unlikely to kill a distantly related bacteria (210). It also does not have genes that code for known antibiotics that are made by other *P. syringae* pathovars, like syringomycin (60). There are several genes that code for uncharacterized non-ribosomal peptide synthetases in the genome of *Pto* that could code for unknown antibiotics that kill *E. coli* (60). It is known that the T6SS is involved in bacterial competition and killing by *Pto* (197). The T6SS is commonly reciprocally regulated to the T3SS in pathogenic bacteria like *P. aeruginosa* by the GacSA TCS (211). Previous studies on regulation of the T6SS by *P. syringae* would suggest that *P. syringae* regulates the T6SS by derepression of the GacSA system in a similar fashion to *P. aeruginosa* (117). GacA is also a positive regulator of the T3SS in *Pto*, while GacA is a negative regulator of the T3SS in *P. aeruginosa* (28, 212). This opens up the possibility that *Pto* may not reciprocally regulate the T3SS and T6SS like other bacterial strains and that 5255 may play a role in this when Ca^{2+} is present in the environment. Further study into the mechanism through which 5255 affects virulence and bacterial competition is necessary to unravel how 5255 is related to the T3SS and the T6SS.

Acknowledgements

We would like to thank Andrew Read for letting us use pAR007 during bacterial competition assays. The U.S. Department of Agriculture (USDA) is an equal opportunity provider and employer. Mention of trade names or commercial products in this publication is solely for the purposes of providing specific information and does not imply recommendation or endorsement by the USDA.

CHAPTER 5

CALCIUM PRECIPITATION IN *PSEUDOMONAS*: DIFFERENCES, COMMONALITIES, AND THE GENES INVOLVED⁶

Abstract

Microbial biomineralization is a widespread phenomenon. The ability to induce calcium precipitation around bacterial cells has been reported in several *Pseudomonas* species but has not been thoroughly tested. We assayed 14 *Pseudomonas* strains representing five different species for the ability to precipitate calcium. Calcium phosphate precipitated adjacent to the colonies of all the *Pseudomonas* strains tested and also precipitated on the surface of colonies for several of the *Pseudomonas* strains assayed. The precipitate was commonly precipitated as amorphous calcium phosphate, however seven of the 14 *Pseudomonas* strains tested precipitated amorphous apatite in agar adjacent to the colonies. Out of the seven *Pseudomonas* strains that precipitated amorphous apatite, six are plant pathogenic. The formation of amorphous apatite was commonly observed in the area of the agar where amorphous calcium phosphate had previously formed. A transposon mutagenesis screen in *Pseudomonas syringae* pv. tomato DC3000 revealed genes involved in general metabolism, lipopolysaccharide and cell wall biogenesis, and in regulation of virulence play a role in calcium precipitation. These results shed light on the common ability of *Pseudomonas* species to perform calcium precipitation and the underlying genetic regulation involved in biomineralization.

⁶ Maxwell R. Fishman, Krista Giglio, David Fay, and Melanie J. Filiatrault. Calcium precipitation in *Pseudomonas*: Differences, commonalities, and the genes involved. Submitted.

Introduction

Biom mineralization is the precipitation of inorganic minerals by biological organisms. In particular, bacteria readily perform biom mineralization and the precipitation of calcium based minerals by bacteria are thought to be among the most common observed in nature (171). Apatite is a calcium phosphate based mineral that is precipitated by a large number of bacteria including *Escherichia coli*, *Corynebacterium matruchotii*, *Ramlibacter tatouinensis*, *Streptococcus mutans*, *Pseudomonas aeruginosa*, *Pseudomonas fluorescens*, *Serratia marcescens*, *Streptococcus mutans* and *Streptococcus sanguis* (213-217). Microbial apatite biom mineralization occurs both extracellularly and intracellularly and is classified as either an active or passive process. The active process is called microbially controlled calcium precipitation (MCCP) and involves specific proteins or peptides and relies on a microbially produced matrix (218). The passive process is thought to be a byproduct of bacterial metabolism and is referred to as microbially induced calcium precipitation (MICP) (61). MICP is an extracellular process commonly initiated by a high concentration of calcium at a nucleation point on the cell surface (171). Bacterial membranes and exopolysaccharides are major nucleation points for MICP (182, 214, 219). An alkaline microenvironment occurs during MICP as a result of metabolic behavior of bacteria (171). The end result of MICP is particles of different sizes with no set morphology (61). In contrast to MICP, MCCP produces crystals of a common size and shape and is most commonly an intracellular process (218). There are few examples of MCCP in bacteria, one being in the case of intracellular MCCP by *R. tatouinensis* (216).

Pseudomonas species live in diverse environments and many are associated with higher organisms. The species *Pseudomonas putida*, *Pseudomonas fluorescens*, *Pseudomonas syringae*, *Pseudomonas savastanoi*, and *Pseudomonas viridiflava* commonly associate with plants. *P. putida* and *P. fluorescens* are rhizosphere-associated microbes that are considered plant-beneficial microorganisms (220, 221). In contrast, *P. syringae*, *P. savastanoi*, and *P. viridiflava* are foliar plant pathogens (222-224). *Pseudomonas* is one of the many bacterial genera that is able to precipitate calcium. This has been observed as the precipitation of calcium carbonate in several ureolytic *Pseudomonas* species and in certain *P. aeruginosa* strains. In phosphate-sequestering *Pseudomonas* species, certain *P. aeruginosa* strains, and *P. fluorescens* strains, the precipitation of calcium results in apatite formation (65, 217, 225-228). Calcium is abundant in and around plants. Inorganic calcium phosphate is found in the rhizosphere of plants and up to millimolar concentrations of calcium are found in the plant apoplast (41, 229). Calcium concentration increases in the apoplast of bean leaves during *P. syringae* pv. *phaseolicola* 1448a infection and in the xylem of tobacco plants during *Xyllela fastidiosa* infection (43, 185). It is currently unknown whether plant pathogenic *Pseudomonas* species can precipitate calcium when grown in high calcium environments.

In the current study, we demonstrate calcium precipitation by several plant-beneficial, rhizosphere-associated *Pseudomonas* species and by several plant-pathogenic, epiphytic *Pseudomonas* species. We show that this phenomenon occurs near neutral pH and that the spatial patterning and morphology of the calcium

precipitate differs across species and strains. Lastly, we identify several genes that are involved in apatite biomineralization in *P. syringae* pv. tomato DC3000.

Results

***Pseudomonas* species increase the pH of medium during growth:** An increase in pH is commonly observed and thought to be necessary during MICP. Some *Pseudomonas* are reported to increase the pH of their immediate environment (230). To determine if the 14 *Pseudomonas* species we were assaying could increase the pH of the surrounding environment, bromothymol blue (BB) was used to monitor the change in pH during growth on nutrient broth (NB) agar plates. BB can detect changes in pH from a pH of 6.0 to a pH of 8.0. The initial pH of NB medium was 6.4 after calcium was added so any increase in pH should be detectable using BB. *Pseudomonas* colonies were monitored for two days after spotting on NB supplemented with calcium and 0.1% (w/v) BB. All the *Pseudomonas* species assayed raised the pH of the surrounding medium to varying degrees, as determined by the blue color found adjacent to all of the bacterial colonies (Figure 5.1). Some differences were observed between species as *P. syringae* pathovars, *P. viridiflava* NYS-1, and *P. savastanoi* pv. *savastanoi* 4352 produced a less alkaline environment than *P. putida* KT2440 and all the *P. fluorescens* strains assayed. In addition, the colonies of *P. syringae* pv. *morsprunorum* 5795, *P. syringae* pv. tomato DC3000, *P. spp.* 92, *P. viridiflava* NYS-1, *P. savastanoi* pv. *savastanoi* 4352, *P. syringae* pv. *maculicola* ES4326, and *P. syringae* pv. *syringae* B728a turned yellowish, suggesting the colony is a more acidic environment than the adjacent environment. This yellowish color was

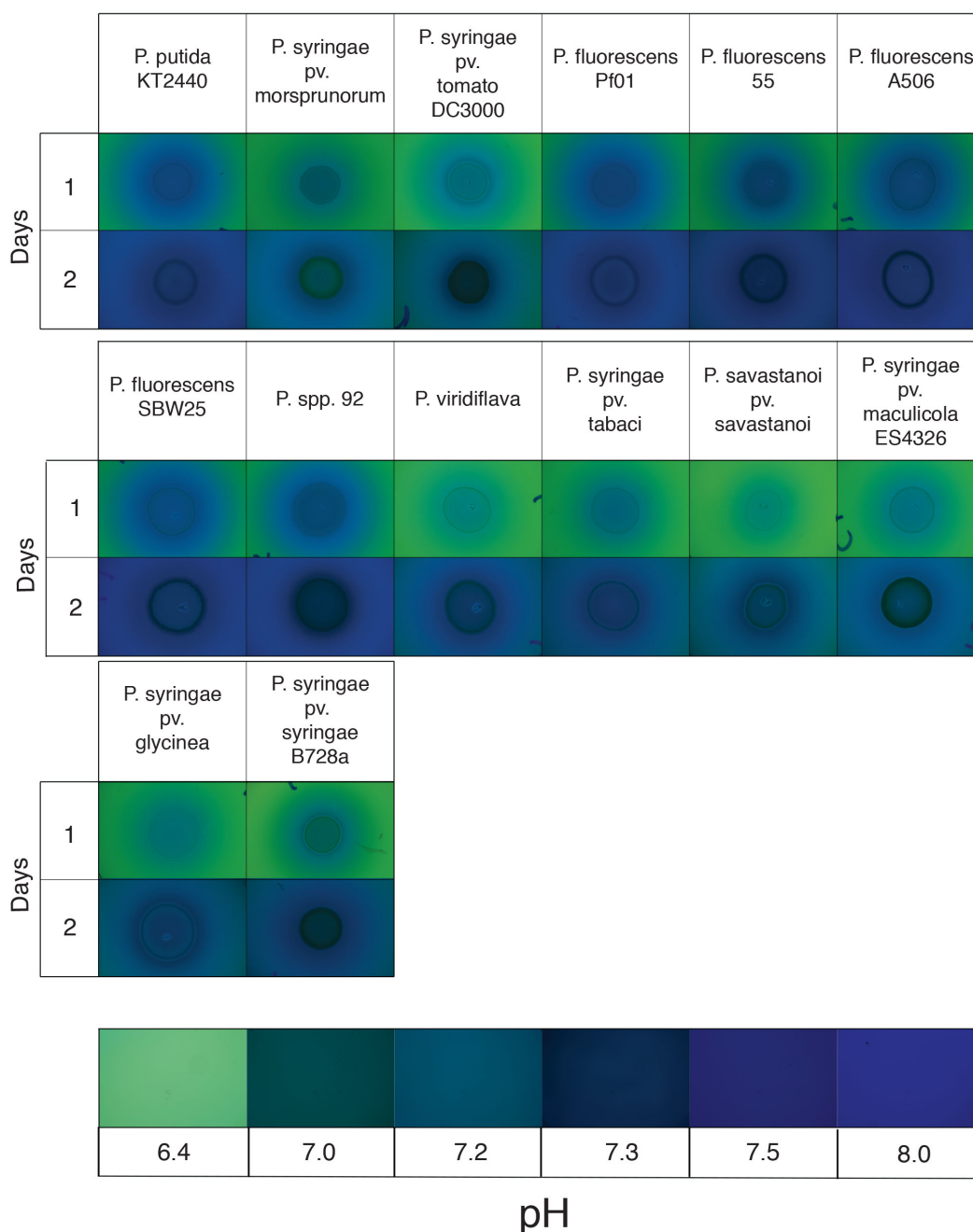
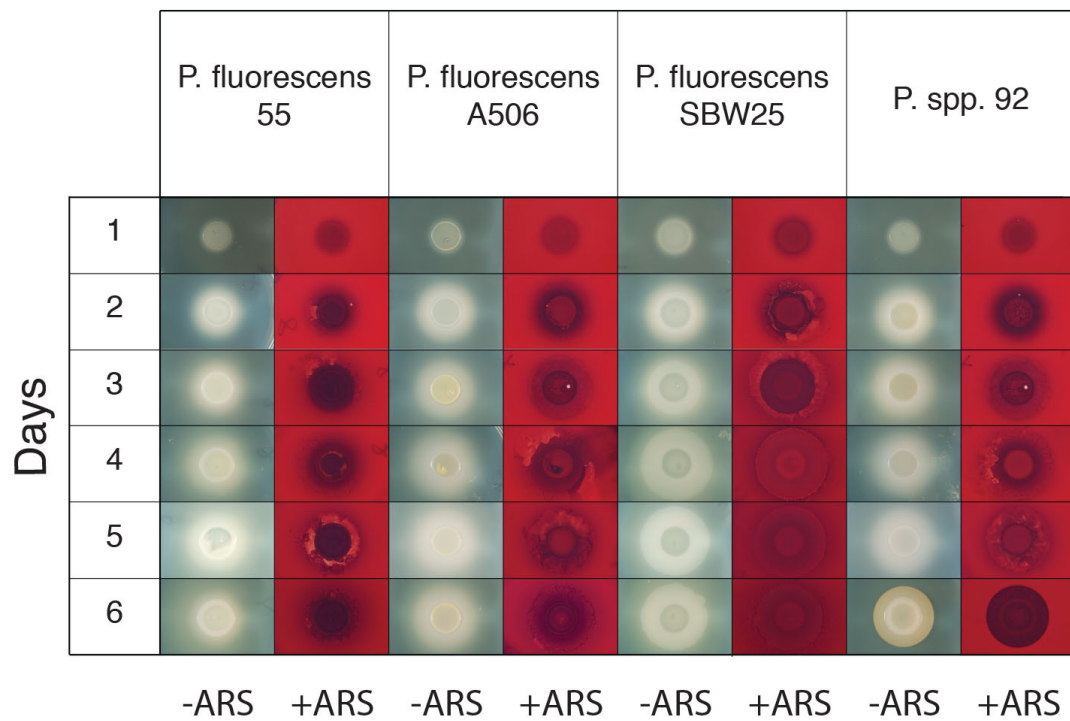
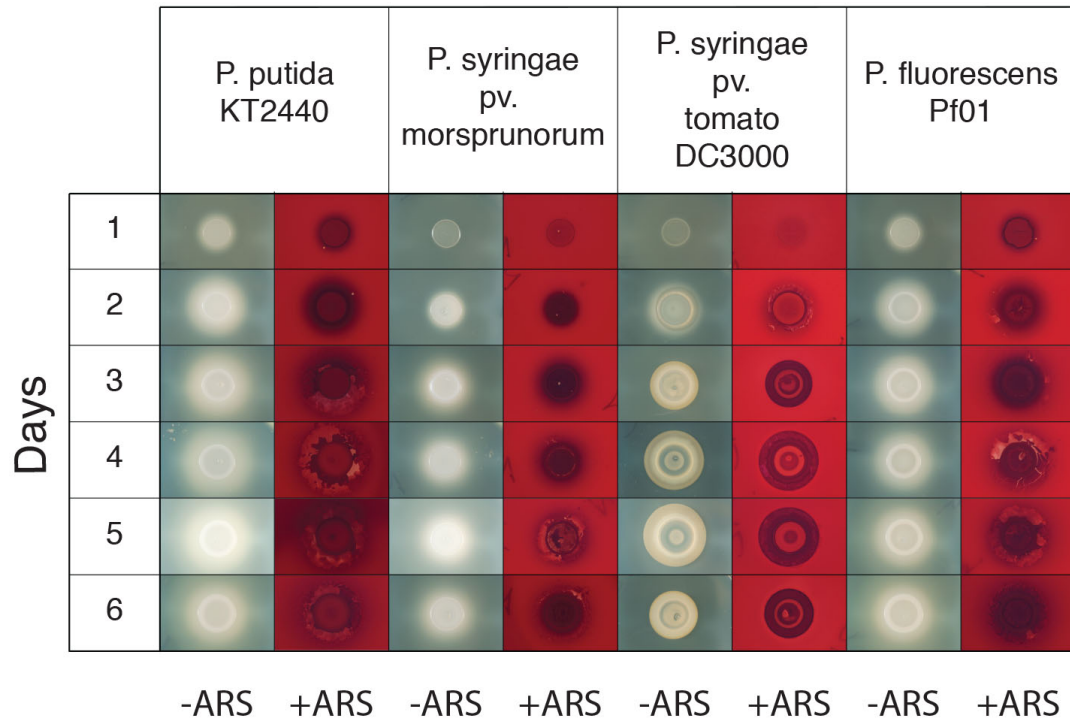


Figure 5.1: Pictures of *Pseudomonas* species grown on NB agar supplemented with calcium and 0.1% (w/v) BB over the course of two days. Pictures are of the same colony on day one and day two. This assay was repeated with three biological replicates. The relative pH of the media can be determined by the change in the color of BB. Pictures of the color change in NB agar supplemented with calcium and 0.1% (w/v) BB from a pH of 6.4 to 8.0 is shown below the pictures of the bacterial colonies. This assay was repeated three separate times and the pictures are representative of those assays.

not observed in the other *Pseudomonas* strains assayed. Overall, since all the *Pseudomonas* species assayed increased the pH of the surrounding environment, they may possess the characteristics needed to precipitate calcium in the surrounding environment as well.

Calcium precipitation among several *Pseudomonas* species: The dye Alizarin Red S (ARS) was employed to quickly screen bacterial colonies for calcium precipitates. Within one day of growth on NB agar plates supplemented with Ca^{2+} , ARS stained the agar around *Pseudomonas* colonies more heavily than other regions of the agar. This staining was visualized as a dark red area surrounding the colonies (Figure 5.2). Prior to staining with ARS, these darkened areas were seen as a white halo in the agar around the bacterial colonies (Figure 5.2). The staining of these white halos by ARS suggested they represented calcium rich areas. White halos did not form around bacterial colonies grown on NB agar plates without additional Ca^{2+} and bacterial colonies and agar on NB agar plates without additional Ca^{2+} added were not stained by ARS (Figure 5.3). A white halo that could be stained by ARS persisted around *P. putida* KT2440 and *P. fluorescens* strains throughout six days, however the ARS-stained areas were occasionally dislodged during rinsing of the plates (Figure 5.2). In contrast to *P. putida* KT2440 and the *P. fluorescens* strains, most of the *P. syringae* strains (except *P. syringae* pv. morsprunorum 5795) and *P. spp.* 92, had a calcium rich white halo form around the colonies that subsequently changed into a brown halo (Figure 5.2). This transition from a white to brown halo occurred in *P. syringae* pv. tomato DC3000 after two days of growth (Figure 5.2). ARS stained the brown halos,



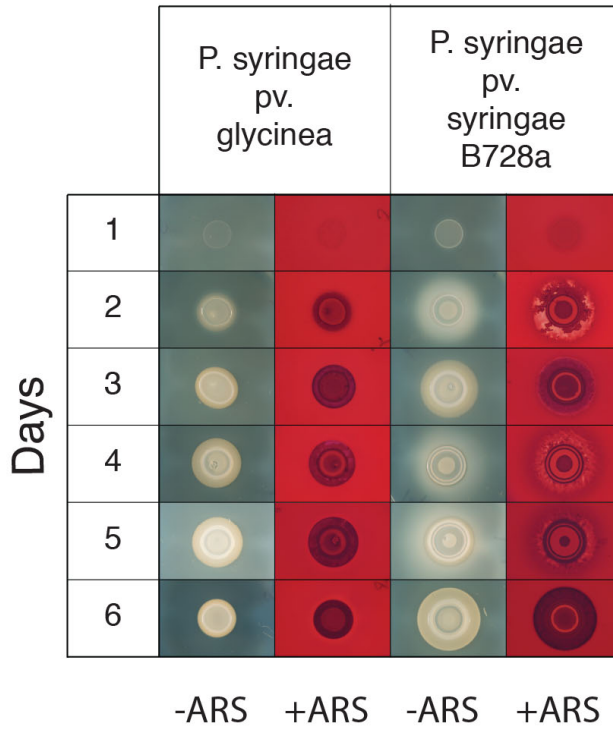
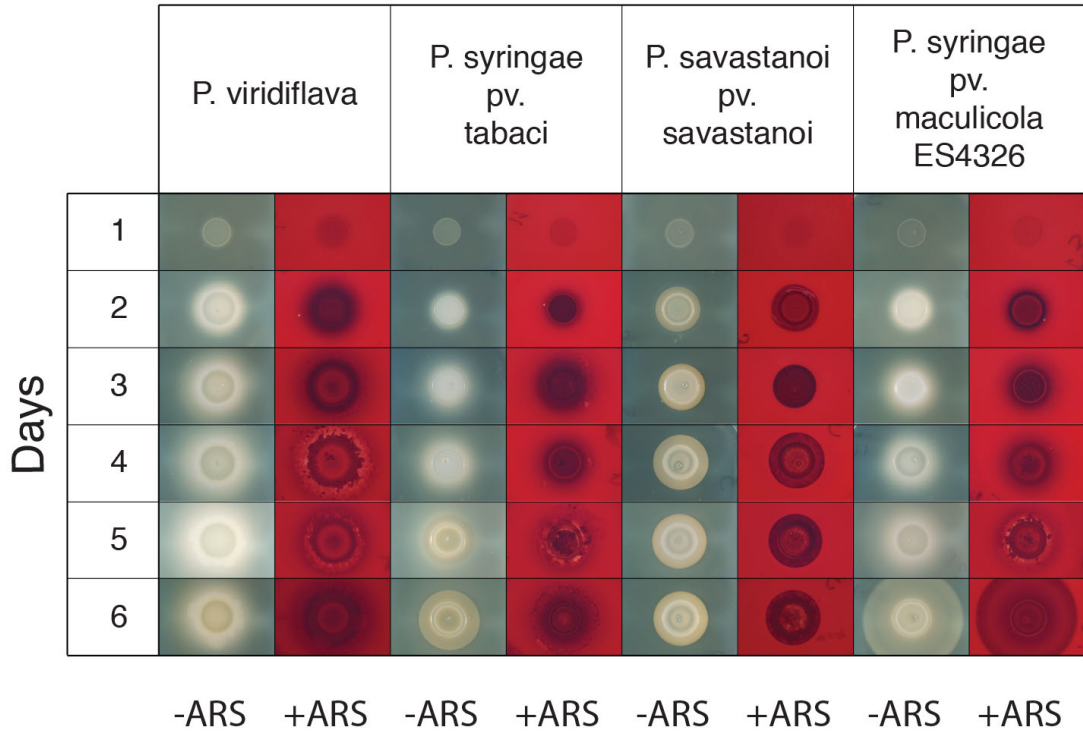
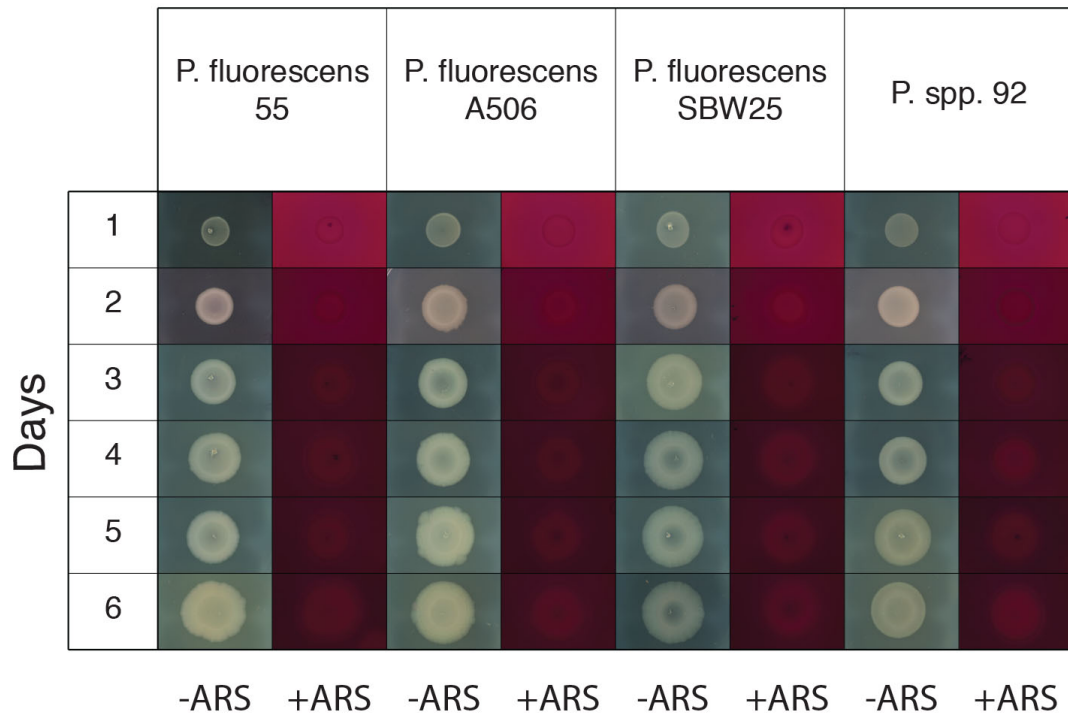
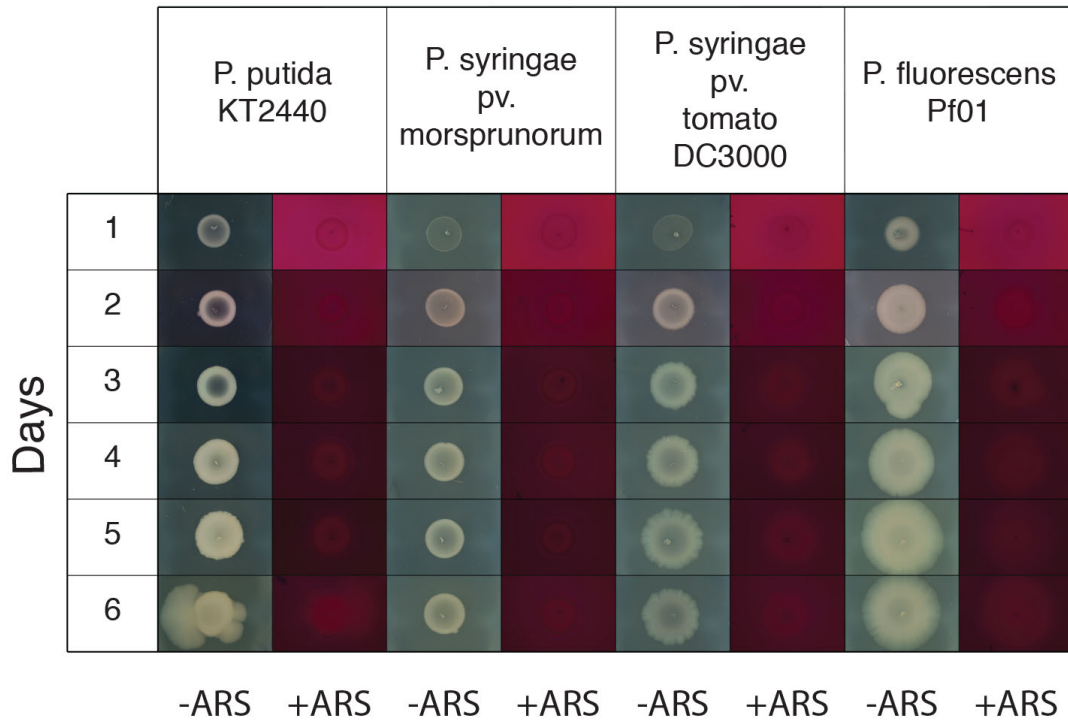


Figure 5.2: Pictures of *Pseudomonas* species grown on NB agar supplemented with calcium over the course of six days. Pictures were taken of the same colony before (-) and after (+) staining of the colonies with 1.0% (w/v) ARS. These pictures are representative of growth for each *Pseudomonas* species on NB agar with calcium. The assay was repeated five separate times and the pictures are representative of those assays.



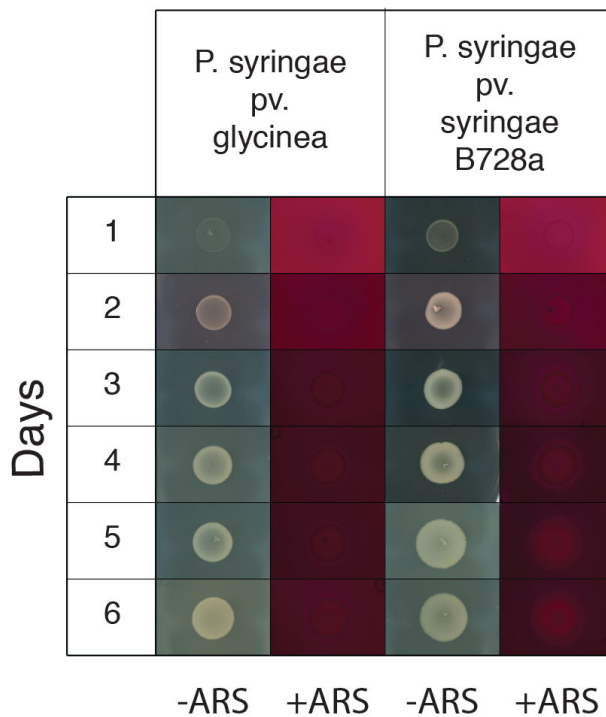
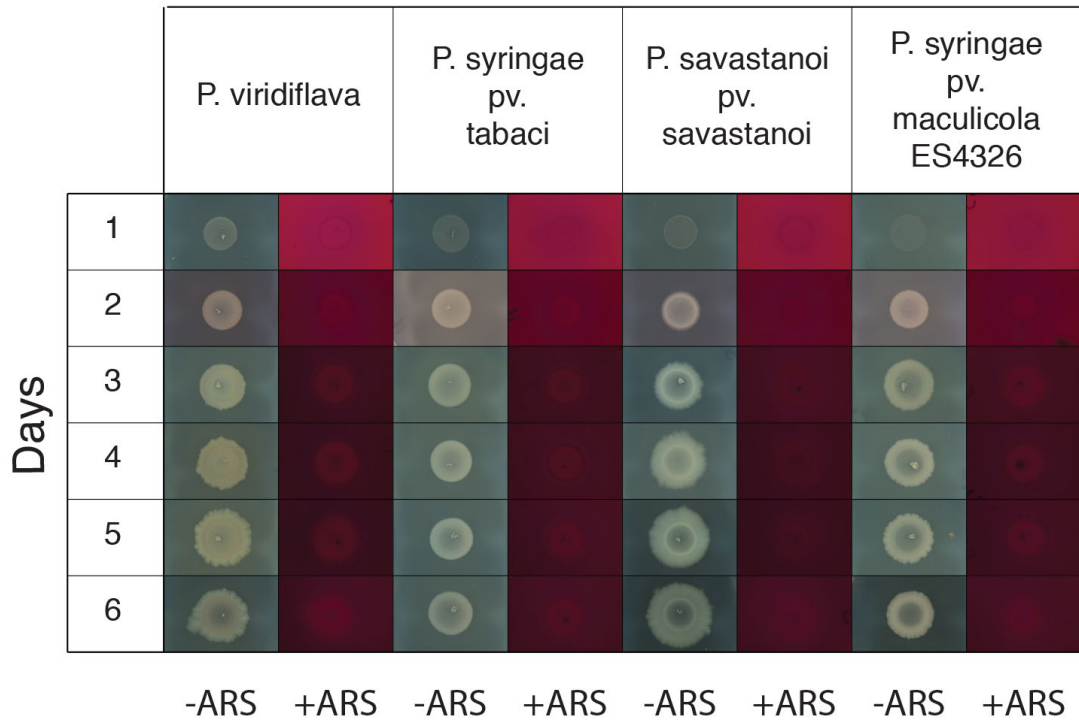


Figure 5.3: Pictures of *Pseudomonas* species grown on NB agar without supplemental Ca^{2+} over the course of six days. Pictures were taken of the same colony before (-) and after (+) staining of the colonies with 1.0% (w/v) ARS. These pictures are representative of growth for each *Pseudomonas* species on NB agar. The assay was repeated with three biological replicates.

suggesting that they represent calcium rich areas as well.

ARS staining on the surface of colonies was prominent on *P. syringae* pv. morsprunorum 5795, *P. fluorescens* Pf0-1, *P. fluorescens* 55, *P. syringae* pv. tabaci ATCC11528, *P. savastanoi* pv. savastanoi 4352, and *P. syringae* pv. maculicola ES4326, suggesting that calcium is enriched on the surface of these *Pseudomonas* strains when grown on NB supplemented with Ca^{2+} (Figure 5.2). ARS staining did not occur when strains were grown on NB agar plates lacking supplemental Ca^{2+} (Figure 5.3). The colonies for *P. syringae* pv. tomato DC3000, *P. syringae* pv. glycinea 2159 Race 1, *P. savastanoi* pv. savastanoi 4325, and *P. syringae* pv. syringae B728a stained with ARS only after the brown halo was present (Figure 5.2).

Characterization of calcium phosphate precipitated by *Pseudomonas* species:

Since ARS could not distinguish if calcium was precipitated or in another form, such as chelated to a substrate, another method was required to further characterize the calcium rich areas. Spectroscopic techniques are able to distinguish whether a calcium precipitate, such as calcium phosphate or calcium carbonate, is present. Raman spectroscopy was employed as a noninvasive and nondestructive method that allowed for the same bacterial colony to be analyzed over the course of several days. After spotting cultures on agar plates supplemented with Ca^{2+} , spectra were obtained from the center of the colonies and from the agar directly adjacent to the colonies (Figures 5.4-5.10). Spectra taken from the colonies of *P. syringae* pv. morsprunorum 5795, *P. fluorescens* Pf0-1, *P. fluorescens* 55, *P. fluorescens* A506, *P. syringae* pv. tabaci ATCC11528, and *P. syringae* pv. maculicola ES4326 exhibited a broad peak centered

Fig. 3

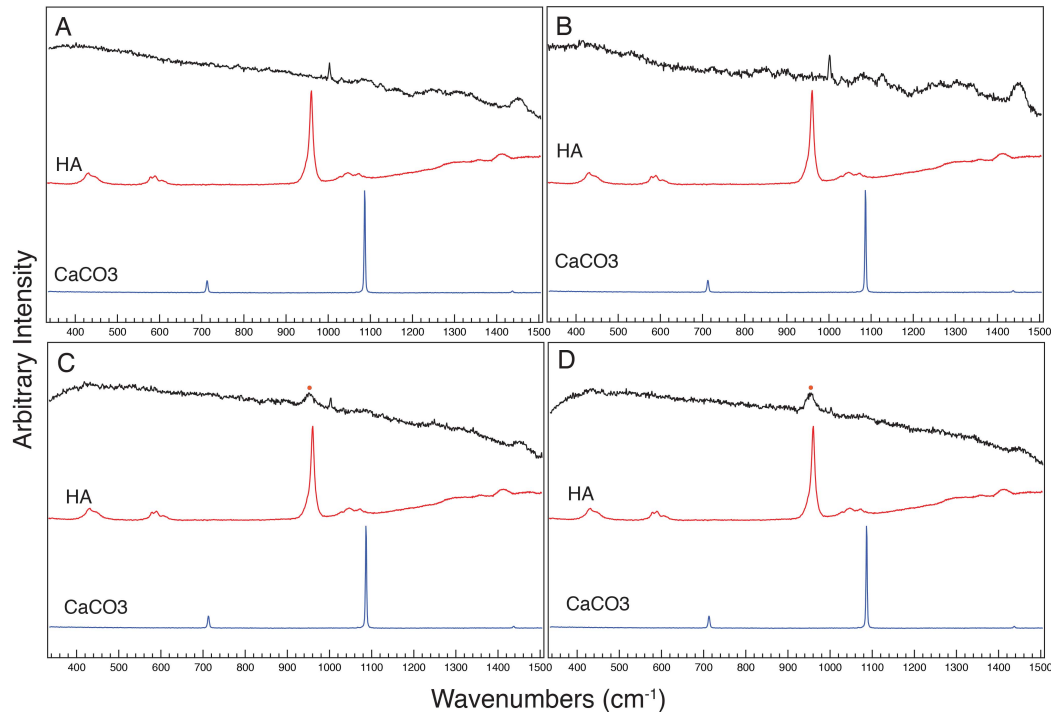


Figure 5.4: Raman spectra taken from the center of the surface of colonies of (A) *P. putida* KT2440, (B) *P. syringae* pv. morsprunorum 5795, (C) *P. syringae* pv. tomato DC3000, and (D) *P. fluorescens* Pf0-1, at six days of growth are colored black in each panel. A control for hydroxyapatite is labelled HA and is colored red and a control for calcium carbonate is labelled CaCO₃ and is colored blue. A broad peak slightly downshifted from 960 cm⁻¹ is labelled with an orange dot and signifies the presence of amorphous calcium phosphate on the surface of cells. Bands commonly associated with biological organisms, including a peak for DNA (782 cm⁻¹) and phenylalanine (1004 cm⁻¹) and broad bands associated with amides (1230-1300 cm⁻¹) and methyl groups (1430-1460 cm⁻¹) can be seen on these spectra as well. This assay was performed three separate times and the spectra are representative of the assays. The y-axis is in arbitrary intensity units and the x-axis is in wavenumbers (cm⁻¹).

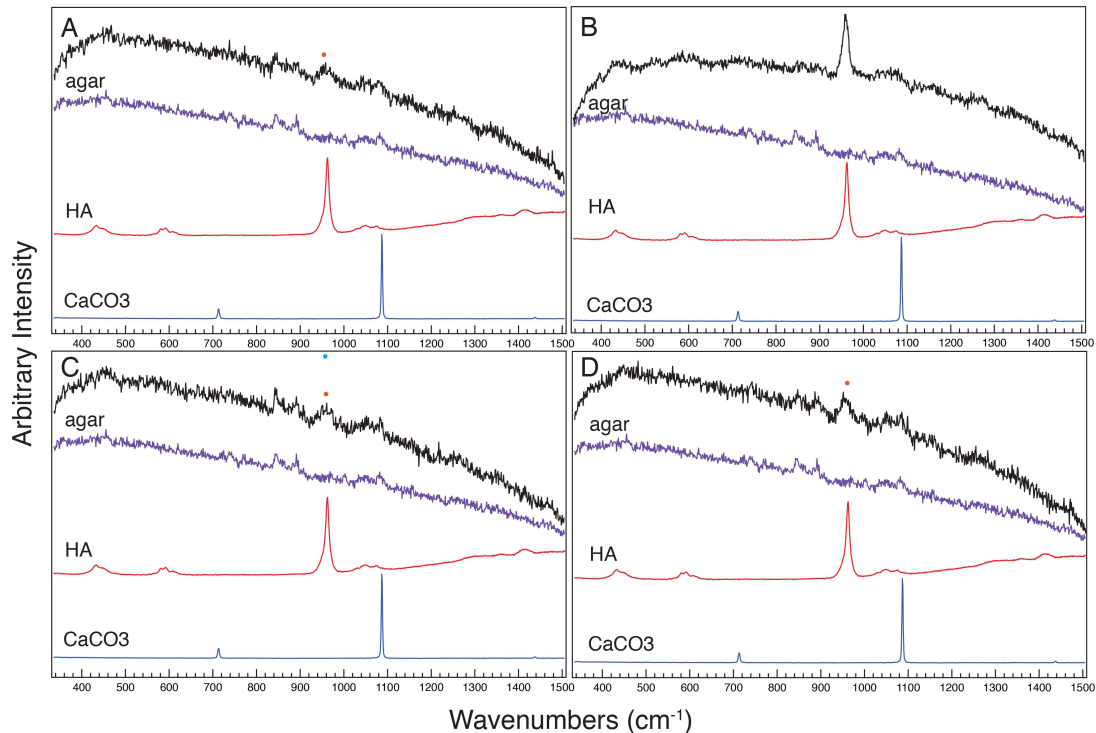


Figure 5.5: Raman spectra taken from the agar directly adjacent to live colonies of (A) *P. putida* KT2440, (B) *P. syringae* pv. morsprunorum 5795, (C) *P. syringae* pv. tomato DC3000, and (D) *P. fluorescens* Pf0-1, at six days of growth are colored black in each panel. A control spectrum for NB agar is labelled agar and colored in purple, a control spectrum for hydroxyapatite is labelled HA and colored in red, and a control spectrum for calcium carbonate is labelled CaCO₃ and is colored in blue. A broad peak centered around 955 cm⁻¹ is labelled with an orange dot in the spectra for *P. putida* KT2440, *P. syringae* pv. morsprunorum 5795, and *P. fluorescens* Pf0-1 and reflects the presence of amorphous calcium phosphate in these samples. A sharper peak centered at 958 cm⁻¹ in *P. syringae* pv. tomato DC3000 is labelled with a light blue dot and reflects the presence of amorphous apatite. The assay was repeated three separate times and the spectra are representative of those assays. The y-axis is in arbitrary intensity units and the x-axis is in wavenumbers (cm⁻¹).

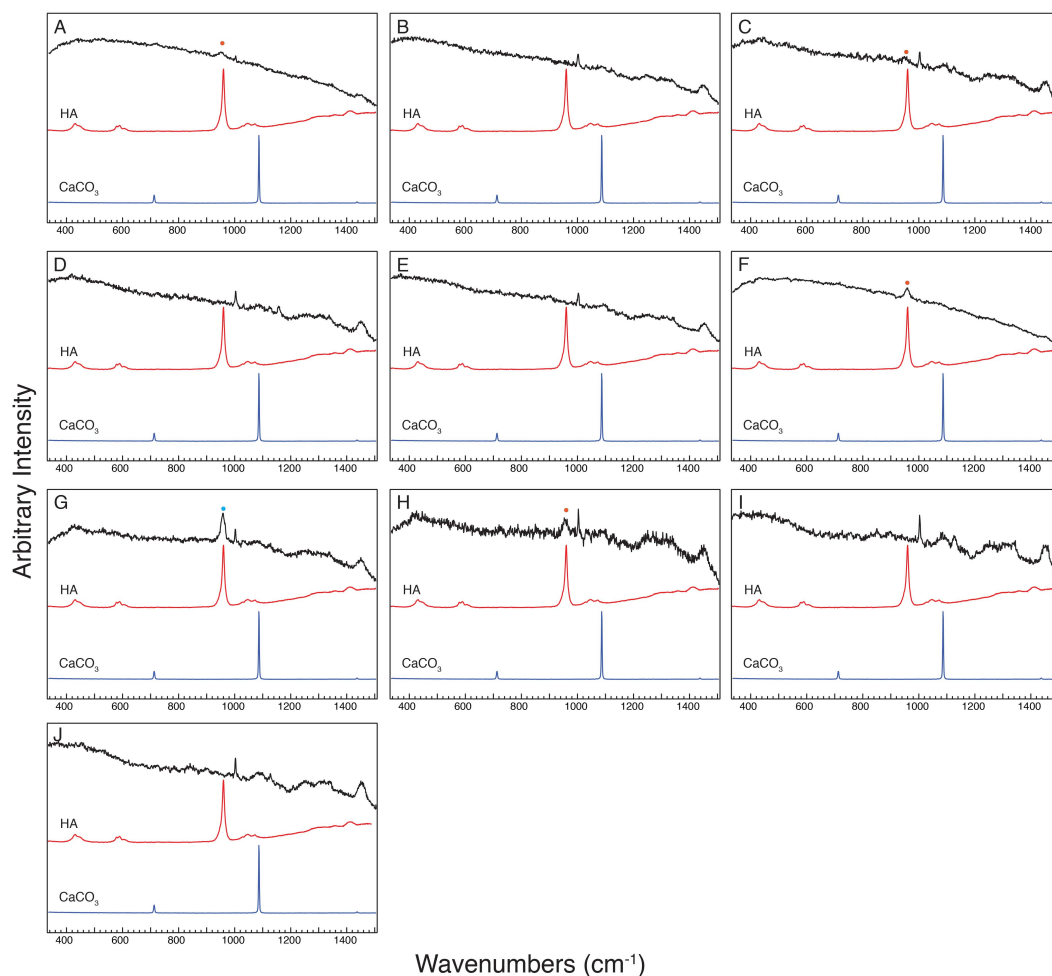
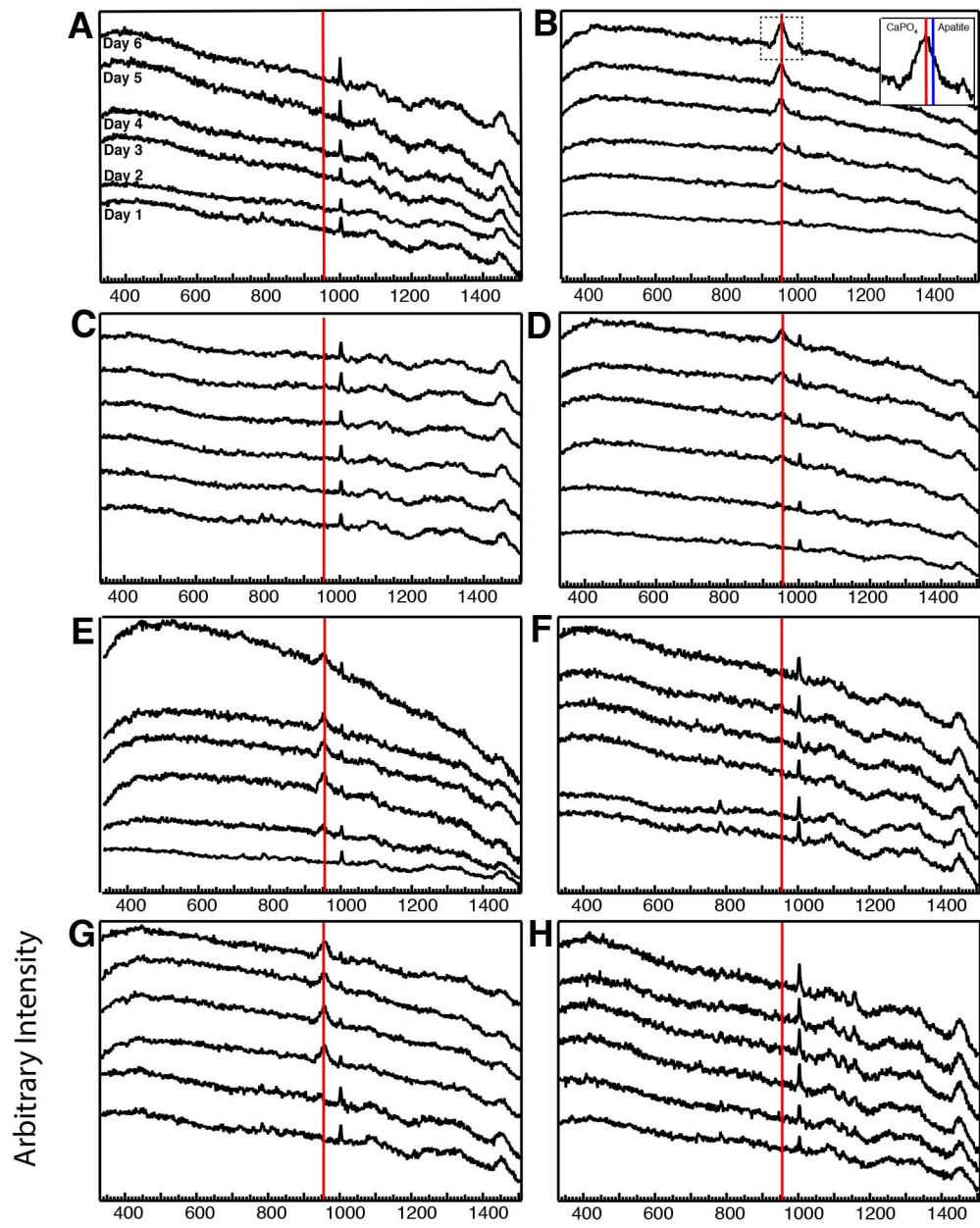


Figure 5.6: Raman spectra of (A) *P. fluorescens* 55, (B) *P. fluorescens* SBW25, (C) *P. fluorescens* A506, (D) *P. viridiflava* NYS-1, (E) *P. spp* 92, (F) *P. syringae* pv. *tabaci* ATCC11528, (G) *P. savastanoi* pv. *savastanoi* 4325, (H) *P. syringae* pv. *maculicola* ES4326, (I) *P. syringae* pv. *glycinea* 2159 Race 1, and (J) *P. syringae* pv. *syringae* B728a colonies taken from 335 cm^{-1} to 1515 cm^{-1} after six days of growth on NB supplemented with Ca^{2+} in black. A hydroxyapatite control spectrum labelled “HA” and colored red and a calcium carbonate control spectrum labelled “CaCO₃” and colored blue is present each panel. A broad band in the bacterial colony spectra centered around 955 cm^{-1} is labelled with an orange dot where present and signifies the presence of amorphous calcium phosphate on the colony surface. A sharp band in the bacterial colony spectra centered at 959 cm^{-1} signifies the presence of amorphous apatite and is labelled with a light blue dot where present. Bands commonly associated with biological organisms, including a peak for DNA (782 cm^{-1}) and phenylalanine (1004 cm^{-1}) and broad bands associated with amides (1230-1300 cm^{-1}) and methyl groups (1430-1460 cm^{-1}) can be seen on these spectra as well. These spectra are representative of spectra taken from three separate biological replicates grown for the amount of time under the same conditions.



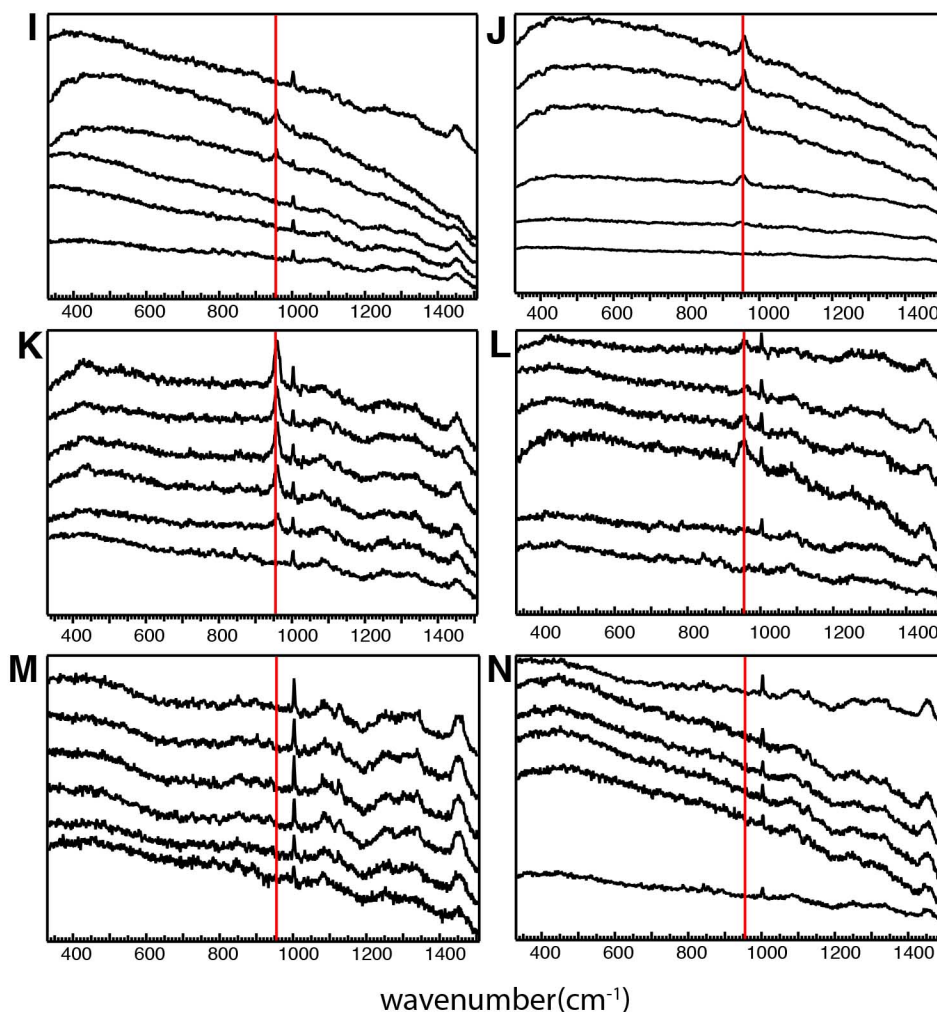


Figure 5.7: Raman spectra taken from the center of the surface of colonies of (A) *P. putida* KT2440, (B) *P. syringae* pv. morsprunorum 5795, (C) *P. syringae* pv. tomato DC3000, (D) *P. fluorescens* Pf0-1, (E) *P. fluorescens* 55, (F) *P. fluorescens* SBW25, (G) *P. fluorescens* A506, (H) *P. viridiflava* NYS-1, (I) *P. spp.* 92, (J) *P. syringae* pv. tabaci ATCC11528 (K) *P. savastanoi* pv. savastanoi 4325 (L) *P. syringae* pv. maculicola ES4326, (M) *P. syringae* pv. glycinea 2159 Race 1, and (N) *P. syringae* pv. syringae B728a at 1, 2, 3, 4, 5, and 6 days of growth as labeled in 2A. The y-axis is in arbitrary intensity units and the x-axis is in wavenumbers (cm^{-1}). The red line at 955 cm^{-1} indicates the center of a peak for amorphous calcium phosphate. The inset in panel 2B shows a close-up of the peak formed due to amorphous calcium phosphate production on the surface of *P. syringae* pv. morsprunorum 5795 colonies at six days of growth. The specific wavenumber where peaks for amorphous calcium phosphate (955 cm^{-1}) and apatite (961 cm^{-1}) occur are labeled in red and blue, respectively.

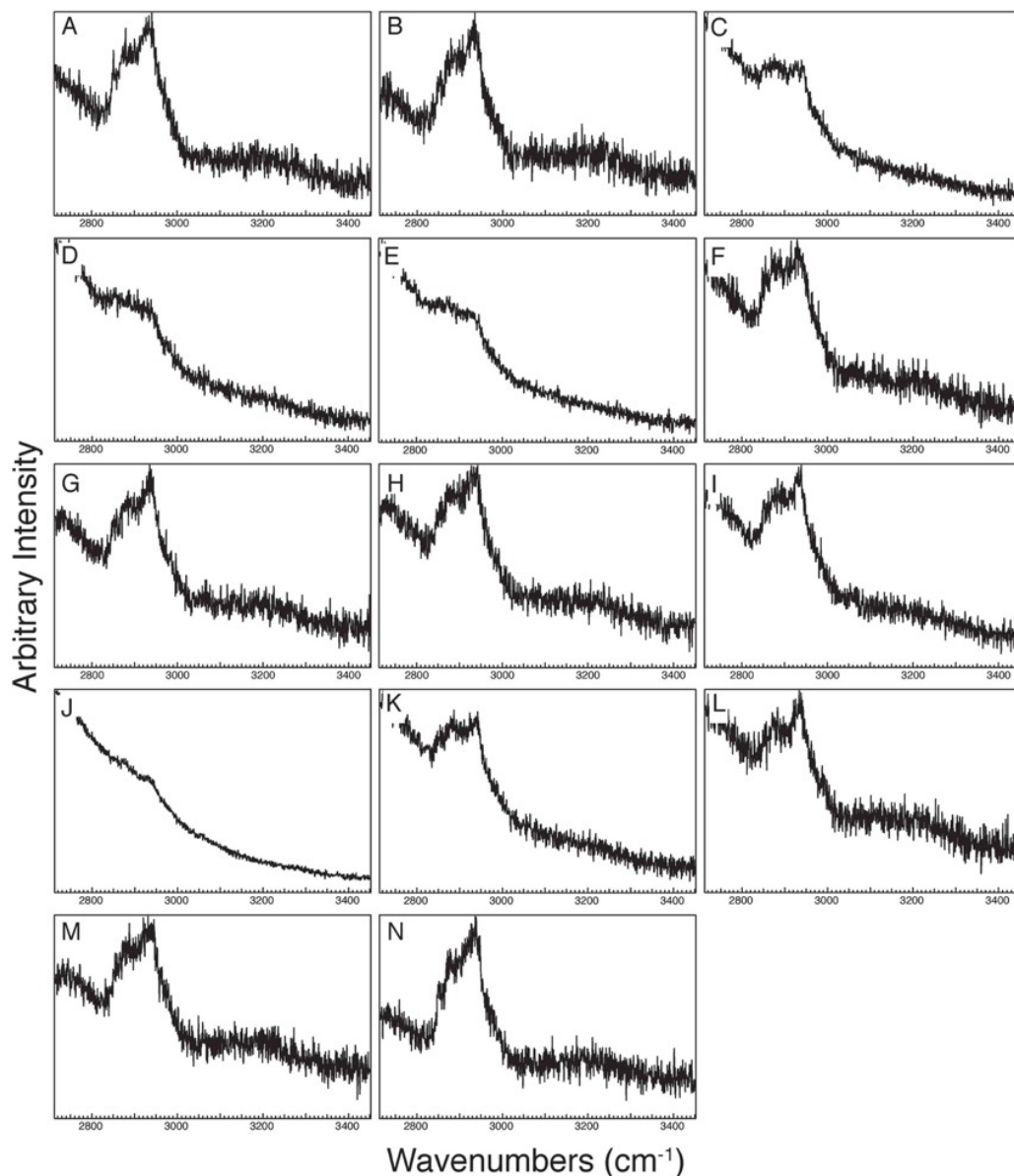


Figure 5.8: Raman spectra of (A) *P. putida* KT2440, (B) *P. syringae* pv. tomato DC3000, (C) *P. fluorescens* Pf0-1, (D) *P. syringae* pv. morsprunorum 5795, (E) *P. fluorescens* 55, (F) *P. fluorescens* SBW25, (G) *P. fluorescens* A506, (H) *P. viridiflava* NYS-1, (I) *P. spp* 92, (J) *P. syringae* pv. tabaci ATCC11528, (K) *P. savastanoi* pv. savastanoi 4325, (L) *P. syringae* pv. maculicola ES4326, (M) *P. syringae* pv. glycinea 2159 Race 1, and (N) *P. syringae* pv. syringae B728a colonies taken from 2715 cm^{-1} to 3450 cm^{-1} after six days of growth on NB supplemented with Ca^{2+} . The peaks found centered at 2880 cm^{-1} and 2930 cm^{-1} reflect that lipids are present on the bacterial cells. This assay was performed three separate times and the spectra are representative of the assays.

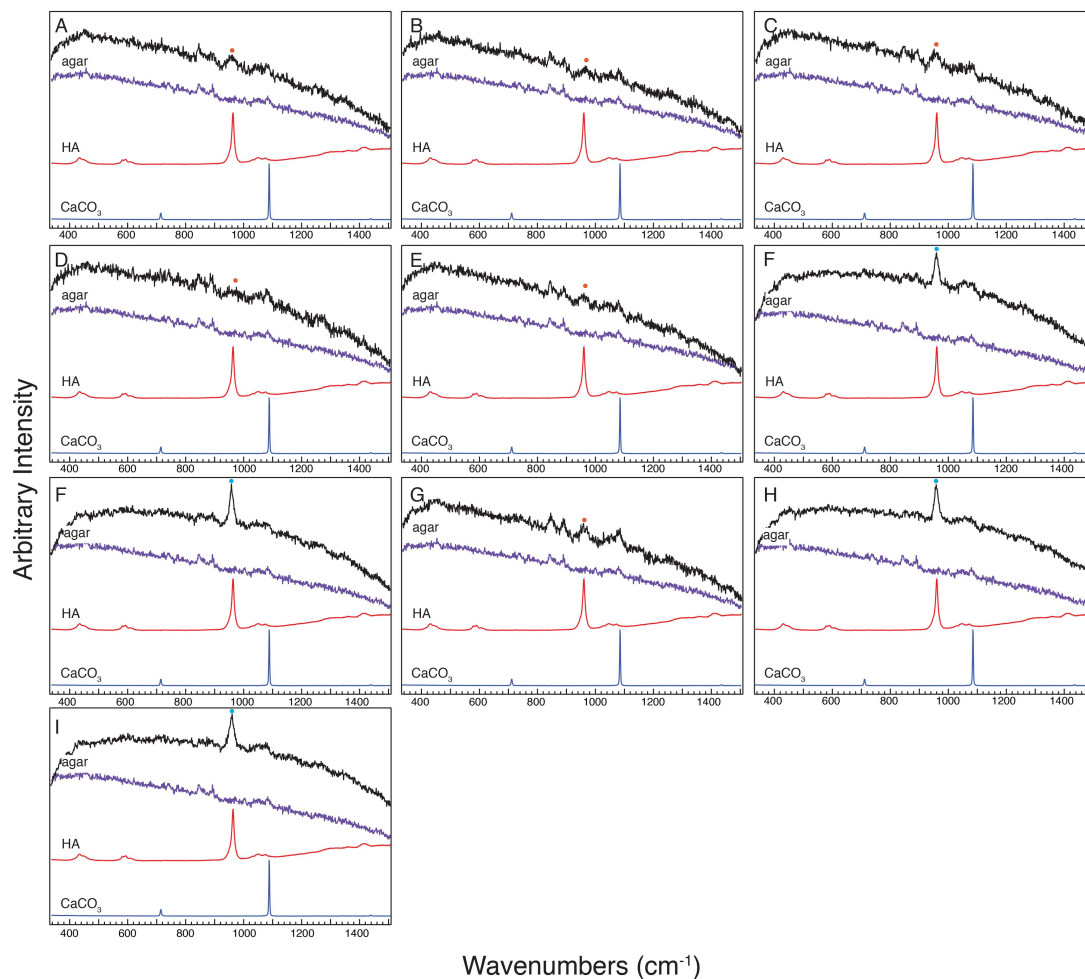
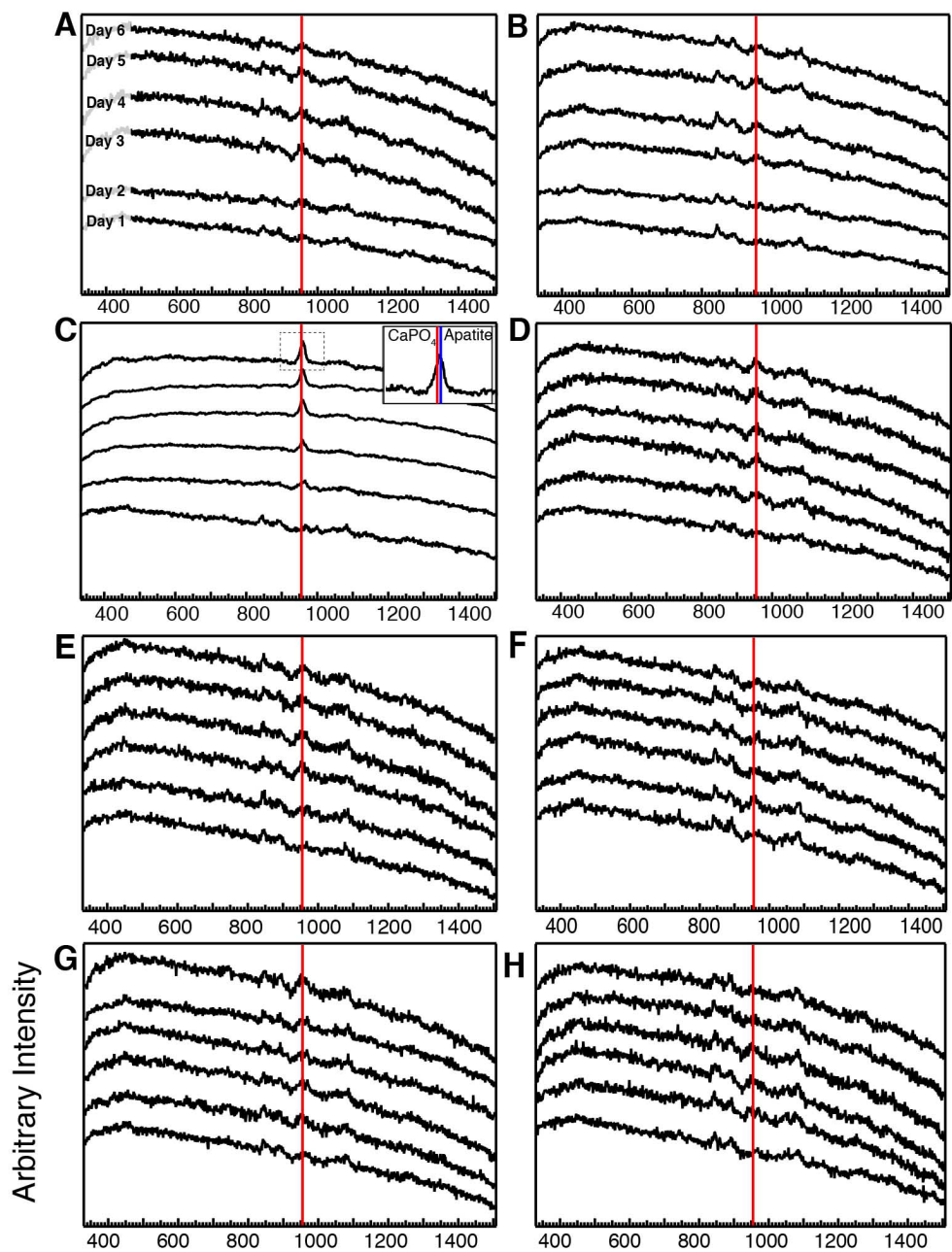


Figure 5.9: Raman spectra of the agar adjacent to (A) *P. fluorescens* 55, (B) *P. fluorescens* SBW25, (C) *P. fluorescens* A506, (D) *P. viridiflava* NYS-1, (E) *P. spp* 92, (F) *P. syringae* pv. tabaci ATCC11528, (G) *P. savastanoi* pv. savastanoi 4325, (H) *P. syringae* pv. maculicola ES4326, (I) *P. syringae* pv. glycinea 2159 Race 1, and (J) *P. syringae* pv. syringae B728a colonies taken from 335 cm^{-1} to 1515 cm^{-1} after six days of growth on NB supplemented with Ca^{2+} in black. An agar control spectrum labeled “agar” and colored purple, a hydroxyapatite control spectrum labeled “HA” and colored red, and a calcium carbonate control spectrum labeled “ CaCO_3 ” and colored blue is present each panel. A broad band in the bacterial colony spectra centered around 955 cm^{-1} is labeled with an orange dot where present and signifies the presence of amorphous calcium phosphate on the colony surface. A sharp band in the bacterial colony spectra centered at 959 cm^{-1} signifies the presence of amorphous apatite and is labelled with a light blue dot where present. This assay was performed three separate times and the spectra are representative of the assays.



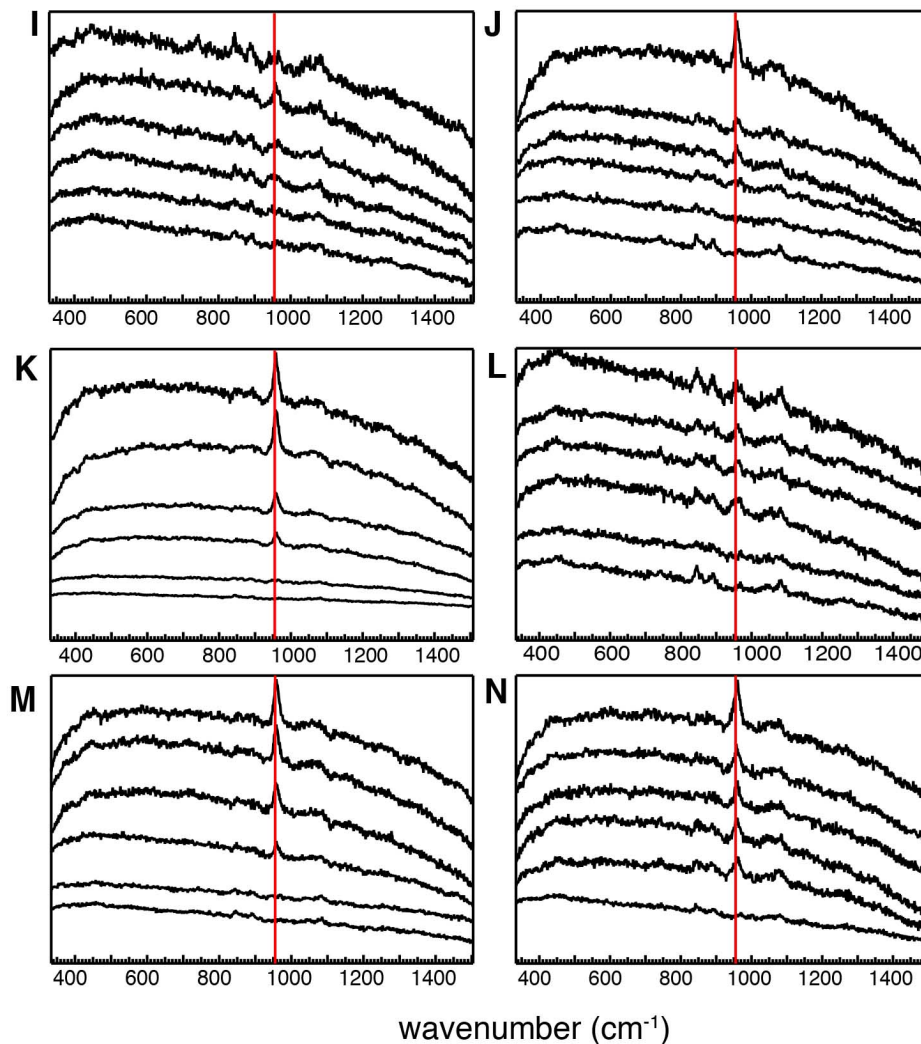


Figure 5.10: Raman spectra taken from the agar directly adjacent to live colonies of (A) *P. putida* KT2440, (B) *P. syringae* pv. morsprunorum 5795, (C) *P. syringae* pv. tomato DC3000, and (D) *P. fluorescens* Pf0-1, (E) *P. fluorescens* 55, (F) *P. fluorescens* SBW25, (G) *P. fluorescens* A506, (H) *P. viridiflava* NYS-1, (I) *P. spp.* 92, (J) *P. syringae* pv. tabaci ATCC11582 (K) *P. savastanoi* pv. savastanoi 4325 (L) *P. syringae* pv. maculicola ES4326, (M) *P. syringae* pv. glycinea 2159 Race 1, and (N) *P. syringae* pv. syringae B728a at 1, 2, 3, 4, 5, and 6 days of growth as labeled in 3A. The y-axis is in arbitrary intensity units and the x-axis is in wavenumbers (cm^{-1}). The red line is at 955 cm^{-1} indicates the center of a peak for amorphous calcium phosphate. The inset in panel 3C shows a close-up of the peak formed due to amorphous apatite production in the agar adjacent to a colony of *P. syringae* pv. tomato DC3000 at six days of growth and the specific wavenumber where a peak for amorphous calcium phosphate (955 cm^{-1}) and apatite (961 cm^{-1}) would occur are labeled in red and blue, respectively. This assay was performed three separate times and the spectra are representative of the assays.

at 955 cm^{-1} within six days of growth (Figures 5.4, 5.6). Relative to the other peaks in the spectra, this peak increased over time for most of the *Pseudomonas* strains where it was detected (Figure 5.7). Raman spectra taken from the surface of *P. savastanoi* pv. *savastanoi* 4352 colonies produced a relatively sharp peak centered at 959 cm^{-1} (Figure 5.6). The sharpness and upshift of this peak suggests that the calcium precipitate on the cell surface of *P. savastanoi* pv. *savastanoi* 4352 is a different composition than the calcium precipitate on the cell surface of the other *Pseudomonas* strains. The broad peaks centered at 955 cm^{-1} and the sharp peak at 959 cm^{-1} are slightly downshifted from the expected peak at 961 cm^{-1} for hydroxyapatite (Figures 5.4, 5.6) (231). A broad peak centered around $950\text{-}960\text{ cm}^{-1}$ is a standard peak associated with calcium phosphate and precipitation of this mineral on the cell surface is likely the cause of this peak in spectra from *P. syringae* pv. *morsprunorum* 5795, *P. fluorescens* Pf0-1, *P. fluorescens* 55, *P. fluorescens* A506, *P. syringae* pv. *tabaci* ATCC11528, and *P. syringae* pv. *maculicola* ES4326 colonies (232). Since the peak from spectra produced by *P. savastanoi* pv. *savastanoi* 4352 was slightly lower than the expected peak for hydroxyapatite, the calcium precipitate on the cell surface of *P. savastanoi* pv. *savastanoi* 4352 likely represents amorphous apatite (231, 232). Overall, the Raman spectra indicate calcium phosphate precipitate occurred on the cell surface of six of the fourteen strains assayed. Surprisingly, no peaks for calcium carbonate were detected on the surface of any colonies (Figures 5.4, 5.6).

Exopolysaccharides (EPSs) produced by bacteria are considered nucleation points during calcium precipitation. *Pseudomonas* species produce the EPSs alginate and cellulose, which can act as nucleation points for calcium precipitation (233, 234).

Raman spectra of alginate had several expected peaks below 1400 cm^{-1} and a broad peak centered at 3400 cm^{-1} , while Raman spectra of cellulose had a sharp peak at 2900 cm^{-1} (235-237). In order to determine whether alginate and cellulose were present on bacterial colonies, Raman spectra from 335 cm^{-1} to 1515 cm^{-1} and from 2715 cm^{-1} to 3450 cm^{-1} were analyzed for peaks characteristic of alginate or cellulose from bacterial colonies grown on NB supplemented with Ca^{2+} . (Figures 5.4, 5.6, 5.8). Within these spectra, none of the peaks associated with alginate or cellulose were detected. In the Raman spectra from 2715 cm^{-1} to 3450 cm^{-1} , the only detected peaks were two broad peaks centered around 2872 cm^{-1} and 2946 cm^{-1} that correspond to the presence of lipids (238). From this we conclude that alginate and cellulose are likely not abundant on the surface of any *Pseudomonas* colonies assayed.

As previously mentioned, on NB plates supplemented with Ca^{2+} , the agar immediately adjacent to some colonies had a white or brown halo that stained with ARS. The spectra obtained from the agar where the white halos were present contained a small, broad peak that was centered at 955 cm^{-1} that likely represents amorphous calcium phosphate (Figures 5.5, 5.9, 5.10). In comparison, the spectra from the agar where the brown halos were present contained a strong peak centered at 959 cm^{-1} and likely represents amorphous apatite (Figures 5.5, 5.9, 5.10). These peaks were not present in the NB agar supplemented with Ca^{2+} control plate (Figures 5.5, 5.9). Peaks associated with biological organisms were absent in the spectra taken from the agar adjacent to the cells, providing evidence that cells were not present in the surrounding halos. It should be noted that, *P. syringae* pv. *maculicola* ES4326 produced a brown halo in the agar on the sixth day of growth. However, the Raman

spectra of the agar after six days of growth only had a small, broad peak with a center slightly upshifted from 955 cm^{-1} rather than a peak centered at 959 cm^{-1} as was seen with the other brown halos. The brown halo produced by *P. syringae* pv. *maculicola* ES4326 was more translucent than the brown halos produced by other strains. The translucent nature of the brown halo may have made it difficult for the Raman confocal microscope to detect a signal for amorphous apatite. Peaks expected for calcium carbonate were not observed in any of the samples (Figures 5.5, 5.9). Overall from these data, we conclude that all of the *Pseudomonas* strains assayed precipitate calcium phosphate in the adjacent environment, but the characteristics of the calcium phosphate differs between strains.

Structure of calcium precipitates on the surface of *Pseudomonas* colonies: *P.*

putida KT2440, *P. syringae* pv. *morsprunorum* 5795, *P. syringae* pv. *tomato* DC3000, and *P. fluorescens* Pf0-1 were analyzed using scanning electron microscopy (SEM) to determine the structure(s) of the calcium phosphate precipitated by these strains.

These strains were chosen to further characterize via SEM because they represented three different *Pseudomonas* species and encompassed the different spatial patterns of calcium precipitation observed in the 14 *Pseudomonas* species tested.

The strains were first observed after 12 hours of growth. By this time, several blebs appeared on the cell surface on all bacterial strains as well as small calcium phosphate particles on the surface of *P. syringae* pv. *morsprunorum* 5795 (Figure 5.11).

Subsequent observations of colonies after six days of growth showed that *P. putida* KT2440 had what appeared to be particles on the cell surface, *P. syringae* pv. *tomato* DC3000 did not appear to have any particles on the surface of cells, and *P. syringae*

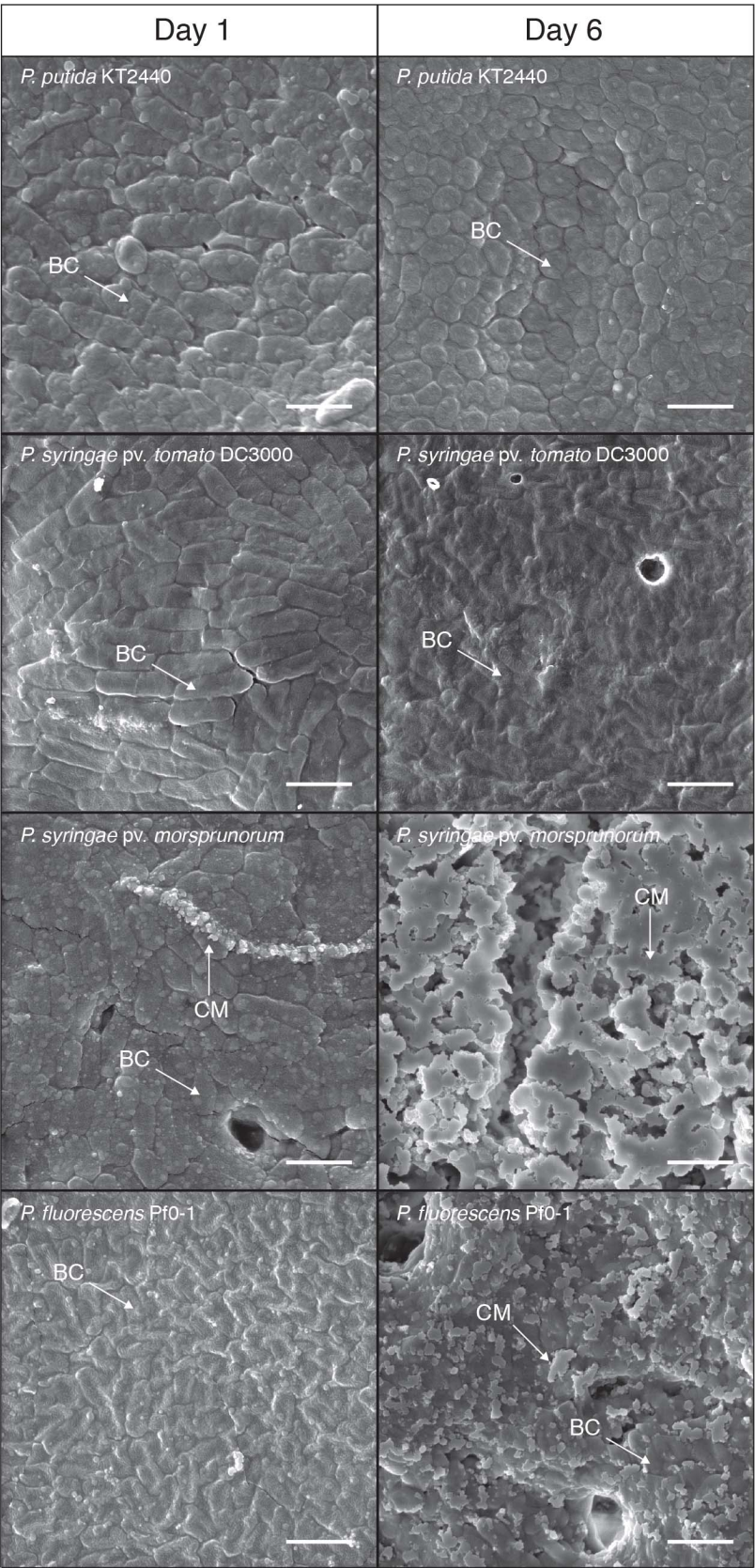


Figure 5.11: SEM images at 18,000x magnification of colony *surface* for *P. putida* KT2440, *P. syringae* pv. morsprunorum 5795, *P. syringae* pv. tomato DC3000, and *P. fluorescens* Pf0-1 at 12 hours of growth and six days of growth. 2 μm scale bars are indicated in the lower right-hand corner of the images. An arrow labelled “CM” points to calcium phosphate on the surface of cells are included on each image where calcium phosphate is thought to be present. An arrow labelled “B” points to bacterial cells in each image. Imaging of cells with SEM was performed three times using separate biological replicates for each image. This image is representative of what was seen on the other replicates.

pv. morsprunorum 5795 and *P. fluorescens* Pf0-1 cell surfaces were partially mineralized (Figure 5.11). The SEM data was consistent with the Raman spectra of the colonies.

Structure of calcium precipitates in the agar adjacent to *Pseudomonas* colonies:

SEM analysis of the agar adjacent to the bacterial colonies showed that calcium phosphate particles formed next to *P. putida* KT2440, *P. fluorescens* Pf0-1, *P. syringae* pv. tomato DC3000, and *P. syringae* pv. morsprunorum 5795 colonies after 12 hours of growth (Figure 5.12). These particles clustered around the bacterial colony and varied in size, shape, and number depending on the *Pseudomonas* strain. Sizes of the particles ranged from 200-400 nm long in the agar adjacent to *P. putida* KT2440 and *P. fluorescens* Pf0-1 cells, 200-600 nm long in the agar adjacent to *P. syringae* pv. tomato DC3000 cells, and 100-400 nm long in the agar adjacent to *P. syringae* pv. morsprunorum 5795 cells. Particles were present in the NB agar supplemented with Ca^{2+} control plate, however these particles were distinct from those that accumulated around bacterial colonies. Particles in the control plate were less numerous, smaller (100-200 nm in length), and diffuse throughout the entire agar plate instead of being heavily concentrated at a particular site (Figure 5.13).

After six days of growth, larger calcium phosphate particles were seen via SEM in the agar adjacent to *P. putida* KT2440, *P. fluorescens* Pf0-1, and *P. syringae* pv. morsprunorum 5795 colonies (Figure 5.12). The calcium phosphate precipitates on the agar adjacent to *P. putida* KT2440 and *P. fluorescens* Pf0-1 were around 2 μm long while calcium phosphate particles surrounding *P. syringae* pv. morsprunorum 5795 were numerous and around 600 nm long. The calcium precipitate that formed in

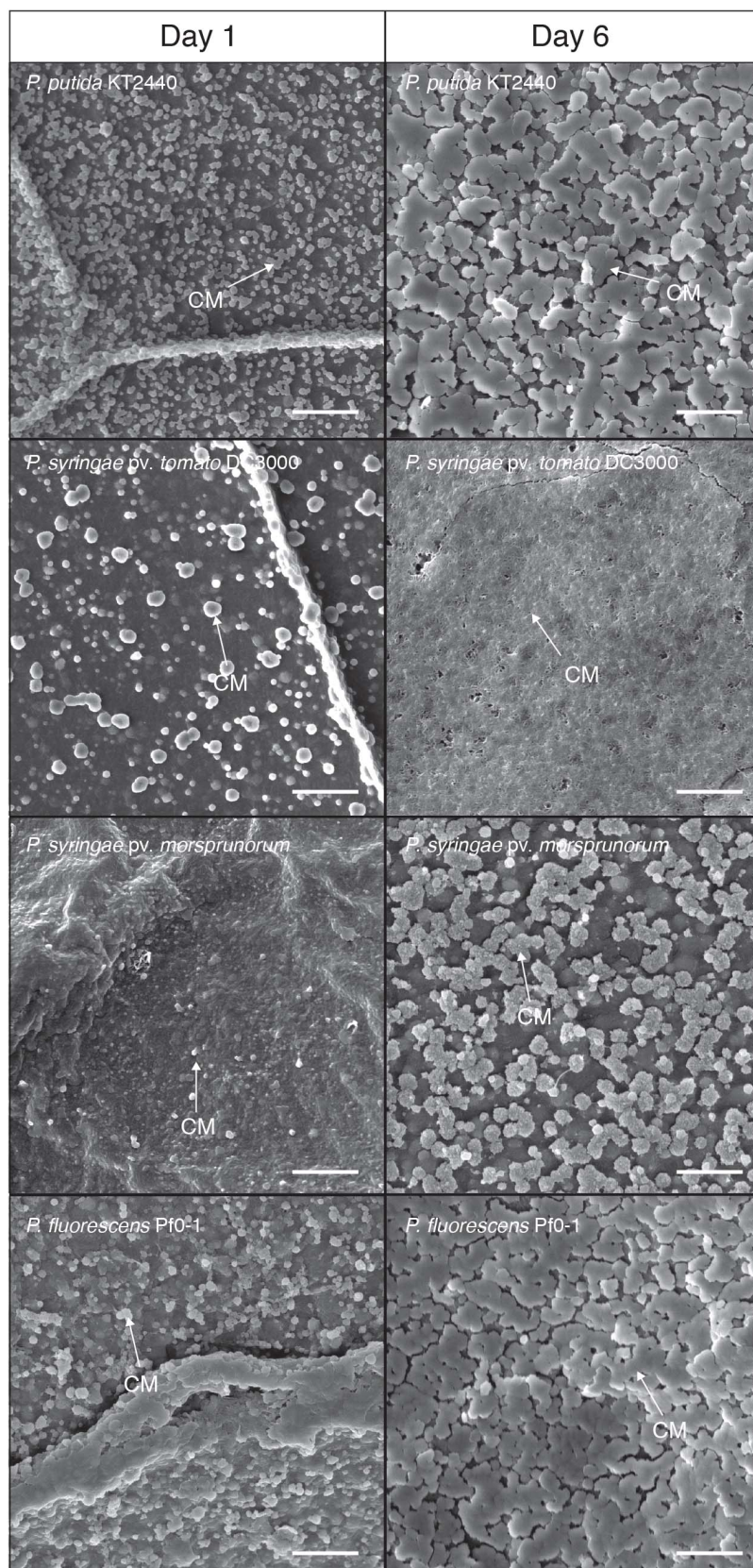


Figure 5.12: SEM images at 18,000x magnification of the agar adjacent to bacterial colonies for *P. putida* KT2440, *P. syringae* pv. morsprunorum 5795, *P. syringae* pv. tomato DC3000, and *P. fluorescens* Pf0-1 after 12 hours and six days of growth. 2 μm scale bars are indicated in the lower right-hand corner of the images. Arrows labelled “CM” points to calcium phosphate has formed on the agar. Imaging of the agar adjacent to colonies was performed three times using three separate biological replicates. This image is representative of what was seen on the other replicates.

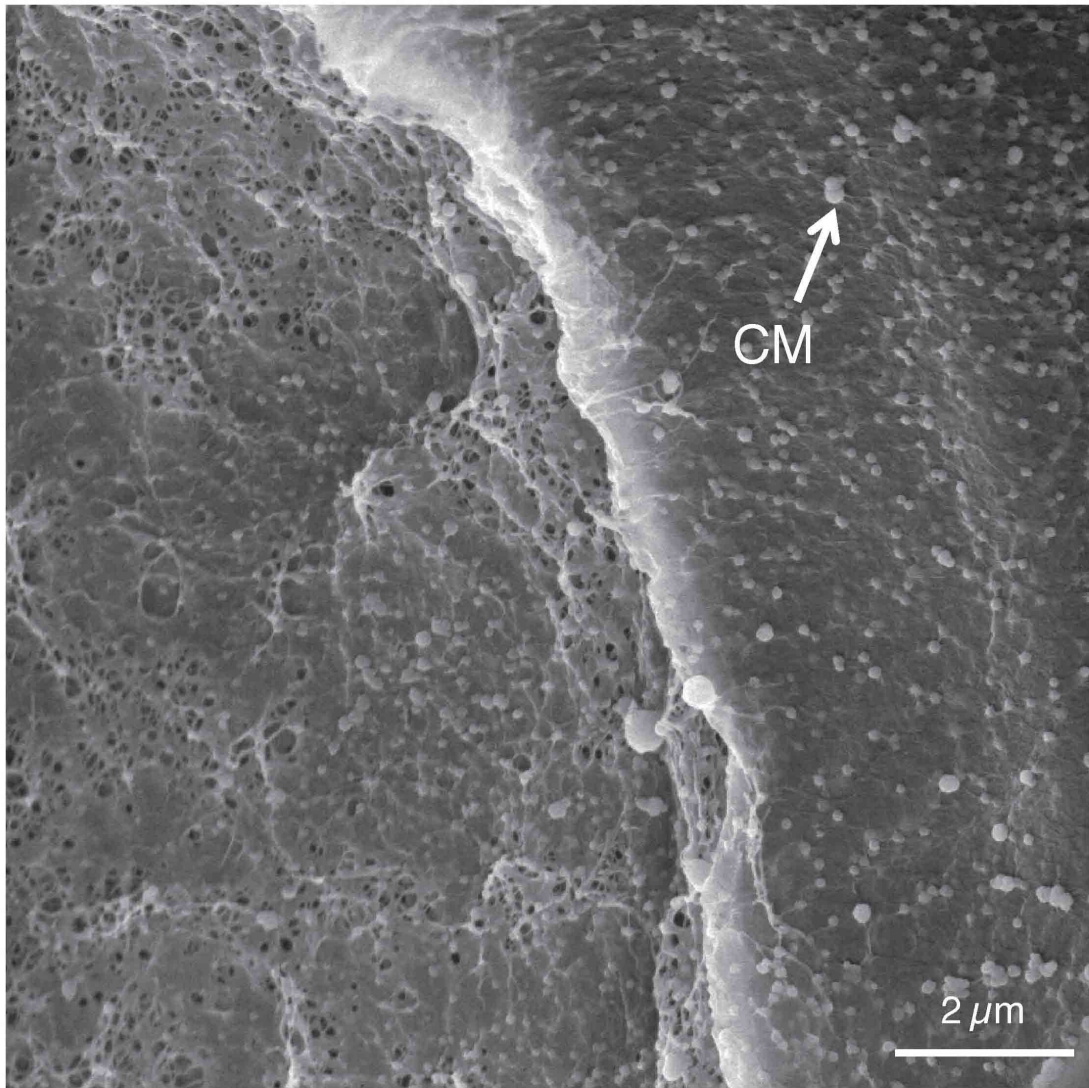


Figure 5.13: SEM images at (A) 18,000x and of NB agar with calcium. The arrow labeled “CM” indicates a calcium phosphate particle. The scale bar is indicated in the lower right-hand corner of the image.

the agar around *P. syringae* pv. tomato DC3000 was quite different in nature. By six days of growth, *P. syringae* pv. tomato DC3000 formed a brown halo of amorphous apatite around the colony (Figure 5.2). This precipitate looked fibrous and porous at high magnification and the morphology was distinctly different from the precipitate formed by *P. putida* KT2440, *P. fluorescens* Pf0-1, or *P. syringae* pv. morsprunorum 5795 (Figures 5.12, 5.14). Overall from these data, we conclude that the calcium precipitates that formed in white and brown halos on the agar adjacent to bacterial colonies are not structured and have considerably different morphologies when compared to each other. This suggests that the precipitates are likely the product of MICP. However, the differing morphologies suggests that they are likely produced through different mechanisms.

Identification of genes important for calcium precipitation of *P. syringae* pv. tomato DC3000.

tomato DC3000. To better understand the genes involved in calcium precipitation in *Pseudomonas* species, we performed a transposon (Tn) mutagenesis screen using *P. syringae* pv. tomato DC3000 (*Pto*). *Pto* was chosen since it has a well annotated genome and produced a brown halo of amorphous apatite around the colonies. Our Tn mutagenesis screen resulted in approximately 55,000 Tn mutants. Of these, we selected 31 colonies that displayed an altered calcium precipitation phenotype. The phenotypes for each of the Tn mutants were re-tested for altered calcium precipitation as described in the methods section. The altered phenotypes included colonies that had: 1) increased amorphous apatite precipitation in the form of a brown halo that was darker or wider than WT, 2) reduced amorphous apatite precipitation that had a lighter

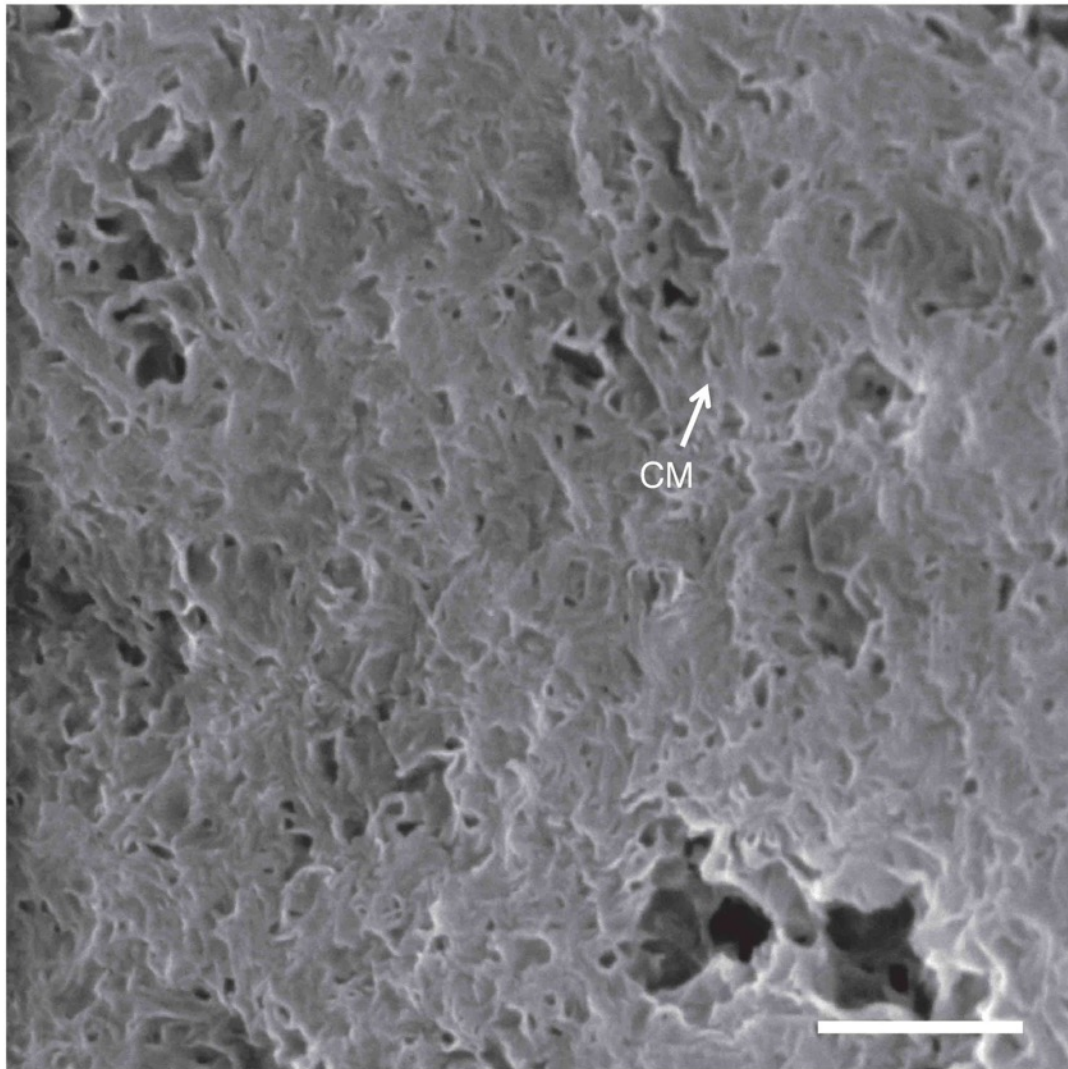


Figure 5.14: SEM image at 80,000x magnification of agar directly adjacent to *P. syringae* pv. tomato DC3000 after six days of growth. The arrow labeled “CM” indicates calcium phosphate precipitation. The scale bar is 500 nm and is indicated in the lower right-hand corner of the image.

brown halo as compared to WT or did not form a brown halo, or 3) altered calcium precipitation on the colony surface with or without a brown halo present in the agar (Figure 5.15). Of the 31 strains that had altered calcium precipitation phenotypes, 14 were identical siblings after sequence determination of the Tn5 insertion site. One clone from each set of identical siblings was considered for further analysis. The site of the Tn insertion and the phenotype of the resultant set of 17 mutant strains that displayed altered calcium precipitation are summarized in Table 5.1. Growth curves were performed on the 17 mutant strains in NB medium and NB medium supplemented with Ca²⁺ (Figure 5.16). It should be noted, several of the strains that had altered calcium precipitation or little to no visible amorphous apatite precipitation did not grow as well in NB whether or not there was Ca²⁺ supplementation. We categorized the 17 genes according to function and found that many genes encode for proteins related to general metabolism, cell wall and lipopolysaccharide homeostasis and transport, and pathogenesis (Table 5.1).

RetS and TvrR regulate calcium phosphate precipitation in *Pto*. Surprisingly, the global regulators TvrR and RetS appeared to be involved in regulating calcium precipitation in *Pto*. Disruption of *tvrR* resulted in altered calcium precipitation, while disruption of *retS* resulted in little to no amorphous apatite precipitation in the form of a brown halo around the colony. Both of these genes are known as global regulators of virulence in *P. syringae* and we therefore further characterized the calcium precipitate defect in *tvrR* and *retS* mutant strains (pΩ::*tvrR* and pΩ::*retS*)(135, 239). The phenotypes of the *tvrR* and *retS* mutant strains were consistent with the Tn mutants

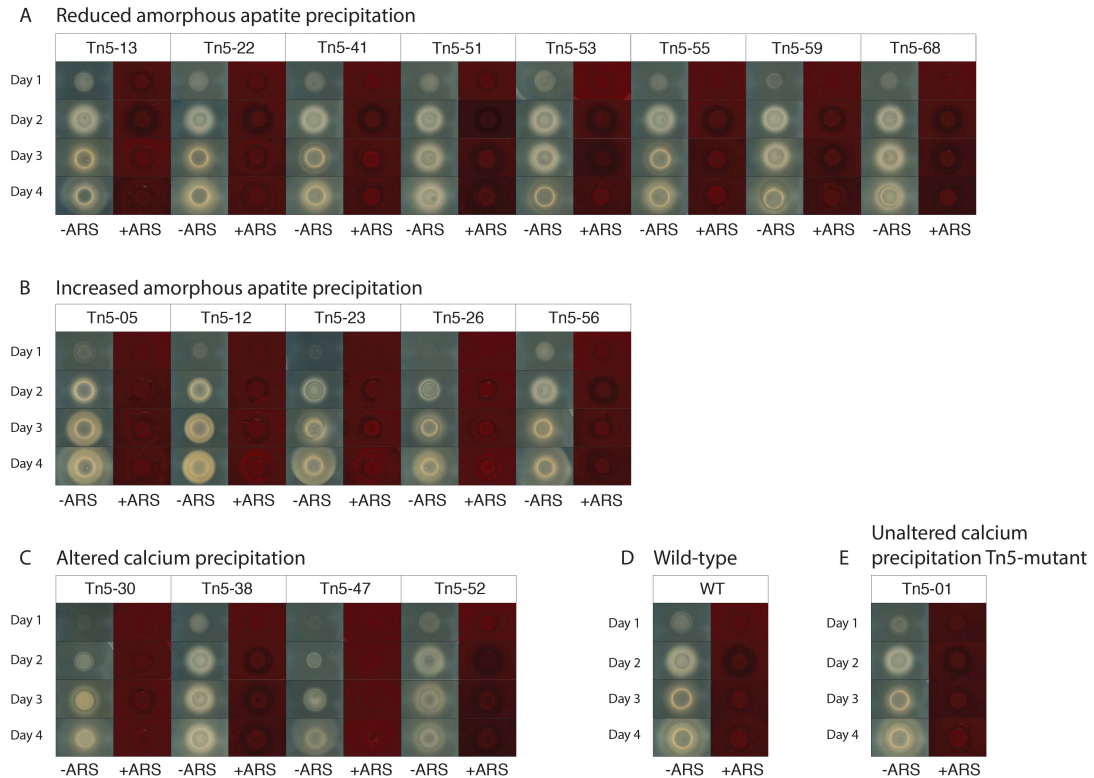


Figure 5.15: Pictures of Tn5 mutants of Pto over the course of four days of growth that displayed differences in calcium precipitation as compared to WT before and after ARS staining. Tn5 mutants are grouped according to phenotype during or after four days of growth. These phenotypes are either (A) reduced amorphous apatite precipitation, (B) increased amorphous apatite precipitation, and (C) altered calcium precipitation. These phenotypes were compared to (D) WT and considered (E) unaltered if they produced similar patterns of calcium precipitation after four days of growth as compared to WT. This assay was performed three separate times and the photos are representative of the assays.

Figure 5.16: Growth curves of Tn-mutants scored with (A) little to no, (B) excessive, or (C) altered calcium precipitation phenotypes as compared to WT when grown in NB medium or NB medium supplemented with 5 mM CaCl₂. The Tn-mutant being compared to WT in each panel can be found in the panel legend. Growth curves were made by compiling three independent experiments into a least-squares mean. Error bars represent standard deviation between experiments.

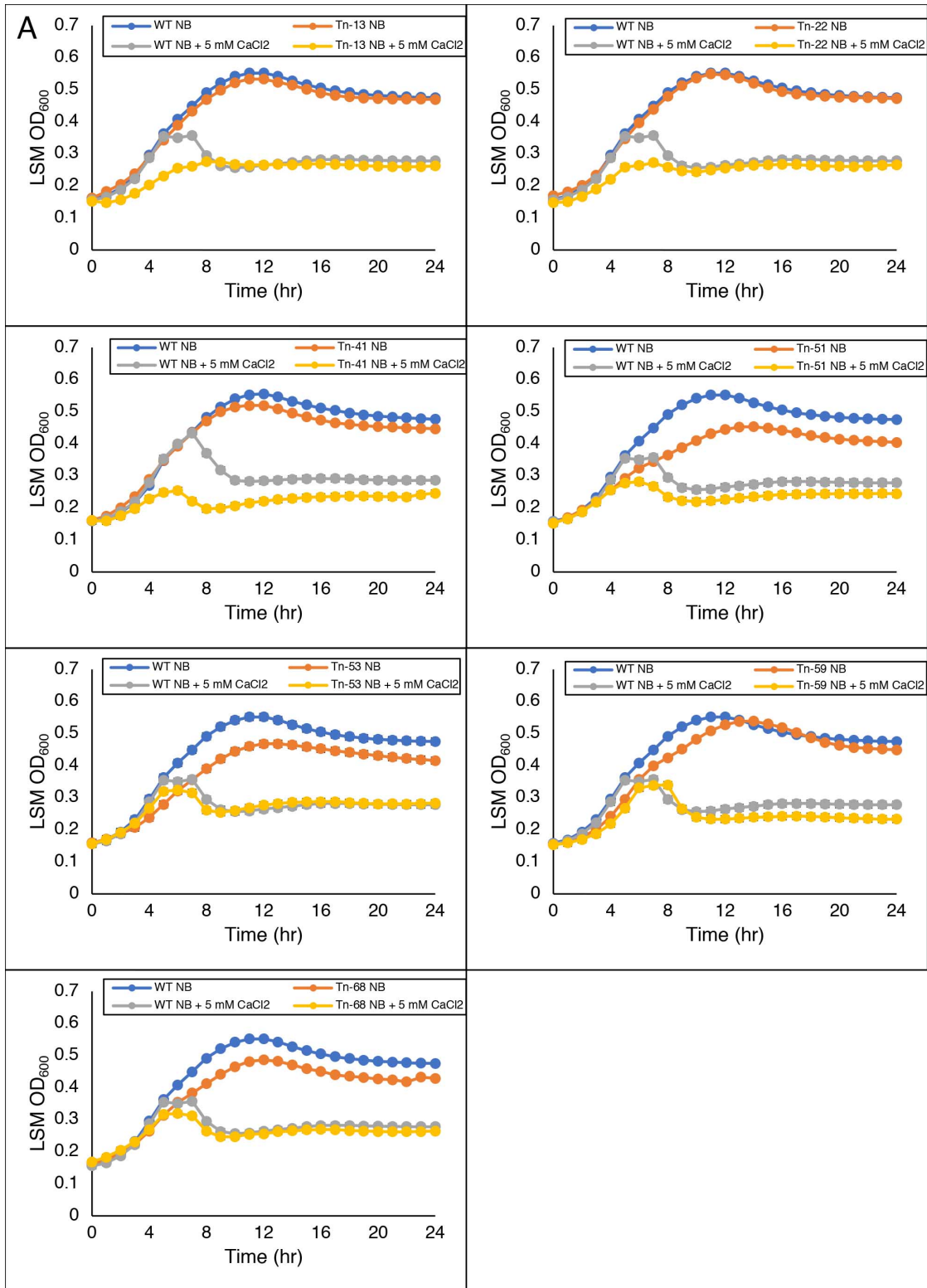


Figure 5.16 (Continued)

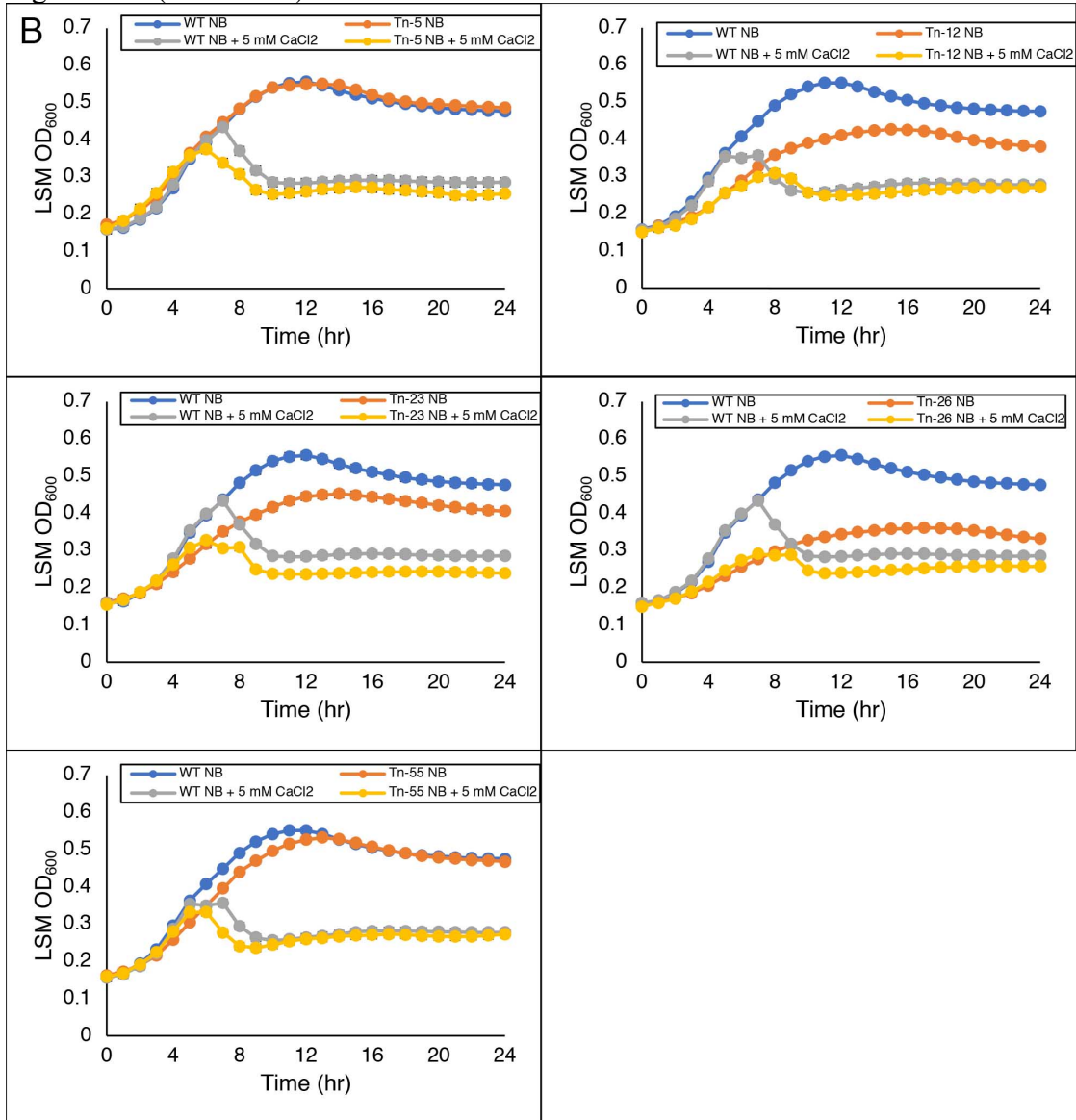


Figure 5.16 (continued)

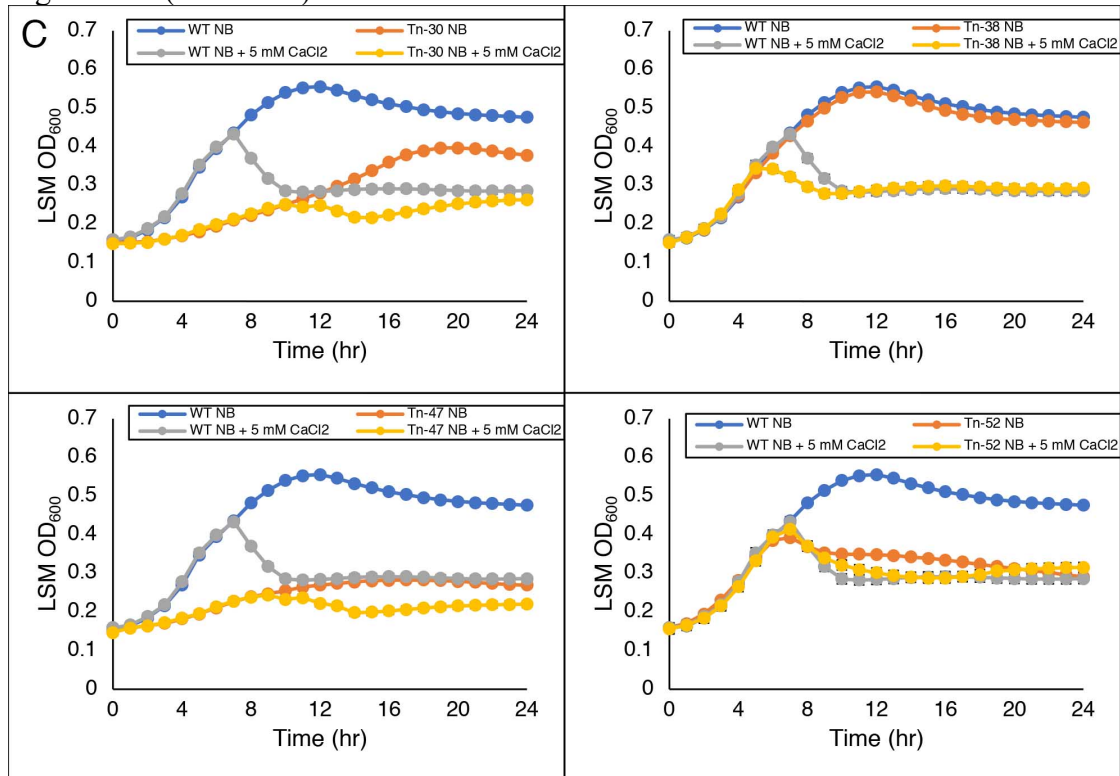


Table 5.1: Transposon mutant strains, observed phenotype, and the description of the disrupted gene

- a. The phenotype observed during the confirmation of calcium precipitation Tn-mutants. The phenotypes are as follows: A – altered calcium precipitation, E – excessive amorphous apatite precipitation, and R – reduced amorphous apatite precipitation
- b. Description of protein coded for by the gene as found using Uniprot (112).
- c. The gene ontology for the protein coded for each gene. This was collected using Uniprot (112).

Transposon Mutant Strain Number	Phenotype^a	Gene Disrupted	Gene name	Protein Description^b	Gene Ontology^c
Tn5-13	R	PSPTO_4986		Membrane protein, putative	
Tn5-22	R	PSPTO_1067		Glycosyl transferase, group 2 family protein	
Tn5-41	R	PSPTO_4991		Glycosyl transferase, group 1 family protein	
Tn5-51	R	PSPTO_2147		Pyoverdine sidechain peptide synthetase I, epsilon-Lys module	metabolic process [GO:0008152]
Tn5-53	R	PSPTO_5516	<i>uvrD</i>	DNA helicase (EC 3.6.4.12)	metabolic process [GO:0008152]
Tn5-55	R	PSPTO_0917	<i>ndh</i>	NADH dehydrogenase	oxidation-reduction process [GO:0055114]
Tn5-59	R	PSPTO_4868	<i>retS</i>	Sensor histidine kinase/response regulator RetS	

Table 5.1 (Continued)

Tn5-68	R	PSPTO_3349	<i>ftsK</i>	DNA translocase FtsK	cell cycle [GO:0007049]; cell division [GO:0051301]; chromosome segregation [GO:0007059]
Tn5-05	E	PSPTO_3724	<i>lonI</i>	Lon protease	cellular response to stress [GO:0033554]; misfolded or incompletely synthesized protein catabolic process [GO:0006515]
Tn5-12	E	PSPTO_0965	<i>cbrB</i>	Sensor histidine kinase CbrB	regulation of transcription, DNA-templated [GO:0006355]; transmembrane transport [GO:0055085]
Tn5-23	E	PSPTO_0494	<i>bioH</i>	Biotin synthase	biotin biosynthetic process [GO:0009102]

Table 5.1 (Continued)

Tn5-26	E	PSPTO_0496	<i>bioB</i>	BioH protein	
				O-antigen ABC transporter, ATP-binding protein, putative	
Tn5-56	E	PSPTO_1075			
					tricarboxylic acid cycle [GO:0006099]
Tn5-30	A	PSPTO_2194	<i>gltA</i>	Citrate synthase	
					regulation of transcription, DNA-templated [GO:0006355]; transcription, DNA-templated [GO:0006351]
Tn5-38	A	PSPTO_3576	<i>tvrR</i>	TetR-like virulence regulator	
				Acetyltransferase component of pyruvate dehydrogenase complex (EC 2.3.1.12)	glycolytic process [GO:0006096]
Tn5-47	A	PSPTO_5006	<i>aceF</i>		

Table 5.1 (Continued)

Tn5-52	A	PSPTO_5483	<i>phoU</i>	Phosphate-specific transport system accessory protein PhoU	cellular phosphate ion homeostasis [GO:0030643]; negative regulation of phosphate metabolic process [GO:0045936]; phosphate ion transport [GO:0006817]
--------	---	------------	-------------	--	--

(Tn5-38 and Tn5-59) and did not appear different than WT *Pto* when grown on NB agar without supplemental Ca^{2+} added (Figures 5.17, 5.18). The phenotype of the $\text{p}\Omega::\text{tvrR}$ mutant when grown on NB supplemented with Ca^{2+} showed that the surface of the strain was stained by ARS (Figure 5.17A). This suggests that the opaque nature of this strain could be due to calcium precipitation on the colony surface. SEM of a $\text{p}\Omega::\text{tvrR}$ colony six days after spotting on NB supplemented with Ca^{2+} confirmed that calcium phosphate was accumulating on the surface of the colony (Figure 5.17B). In addition, calcium phosphate precipitate in the agar adjacent to the $\text{p}\Omega::\text{tvrR}$ cells was similar in morphology to the calcium phosphate particles found in the agar next to *P. syringae* pv. morsprunorum 5795 at 6 days of growth (Figure 5.17B). The $\text{p}\Omega::\text{retS}$ strain was not stained by ARS on the surface of the colony and very little of the agar surrounding the strain was stained (Figure 5.17A). SEM images of the $\text{p}\Omega::\text{retS}$ strain showed that there was no calcium precipitate on the cell surface. However, even though the phenotype of the $\text{p}\Omega::\text{retS}$ strain looked distinct compared to WT *Pto*, the agar adjacent to the cells had a precipitate with a morphology reminiscent of the amorphous apatite found in the agar adjacent to WT *Pto* (Figure 5.17B). SEM analysis of older samples of apatite found in agar adjacent to WT *Pto* looked like the samples from the $\text{p}\Omega::\text{retS}$ strain (Figure 5.17B). Overall, we confirmed that TvrR and RetS are involved in regulation of calcium precipitation in *Pto*.

Discussion

Here we report the ability of 14 different *Pseudomonas* strains to precipitate

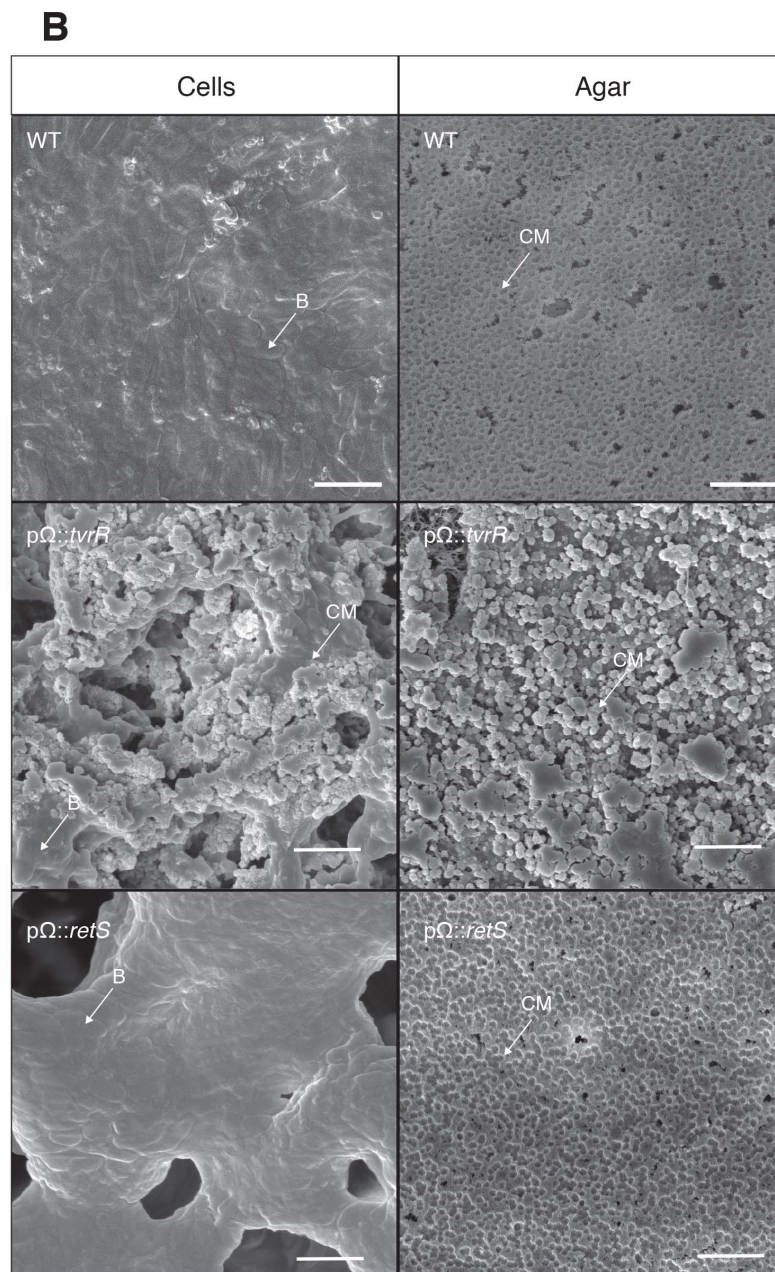
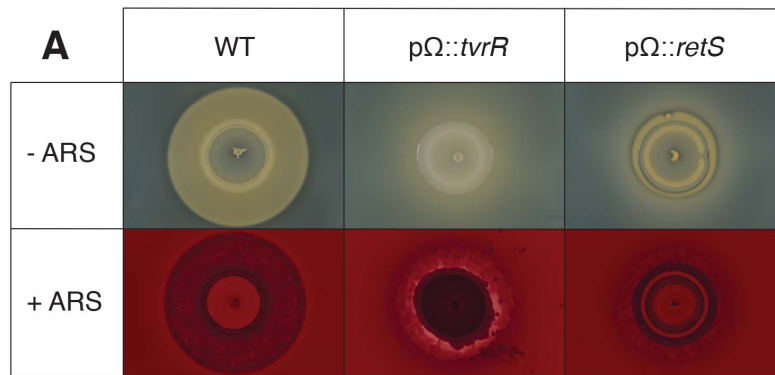


Figure 5.17: (A) Pictures of *P. syringae* pv. tomato DC3000, *P. syringae* pv. tomato DC3000 p Ω ::*tvrR*, and *P. syringae* pv. tomato DC3000 p Ω ::*retS* Pto grown on NB agar supplemented with calcium after four days of growth on plates. Pictures were taken of the same colony before and after staining of the colonies with 1.0% (w/v) ARS. These pictures are representative of the phenotype observed in each strain after four days of growth on NB agar supplemented with calcium. This assay was repeated three separate times and these pictures are representative of what was observed each time. (B) SEM images at 18,000x magnification of colony surface for *P. syringae* pv. tomato DC3000, agar adjacent to *P. syringae* pv. tomato DC3000, colony surface for *P. syringae* pv. tomato DC3000 p Ω ::*tvrR*, agar adjacent to *P. syringae* pv. tomato DC3000 p Ω ::*tvrR*, colony surface for *P. syringae* pv. tomato DC3000 p Ω ::*retS*, and agar adjacent to *P. syringae* pv. tomato DC3000 p Ω ::*retS* after six days of growth on NB supplemented with calcium. 2 μ m scale bars are indicated in the lower right-hand corner of the images. An arrow pointing to calcium phosphate (CM) on the surface of cells and at bacteria (B) are included on the *P. syringae* pv. tomato DC3000 p Ω ::*tvrR* image. Bacterial cells and agar were imaged with three different biological replicates. The images used are representative of what was observed each time.

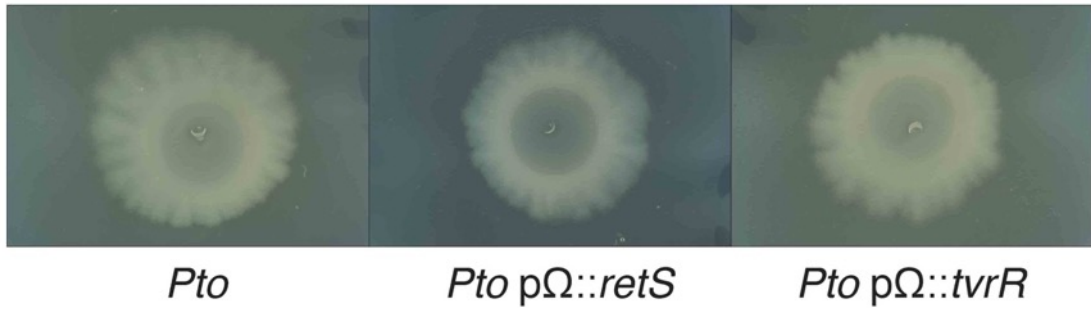


Figure 5.18: Pictures of *Pto*, *Pto pΩ::retS*, and *Pto pΩ::tvrR* after four days of growth on NB agar.

amorphous calcium phosphate or amorphous apatite when grown on NB agar supplemented with Ca^{2+} . We then identified several genes involved in calcium precipitation in *Pto*. Many of the genes encode for proteins with metabolic function, however approximately half of the genes have also been characterized as virulence genes. We further confirmed that the regulators TvrR and RetS regulate calcium phosphate precipitation in *Pto*.

Calcium precipitation was first assayed using ARS to stain calcium rich areas on the colonies and the agar around where the colonies grew. While this proved to be a quick and simple assay to test for the spatial distribution and the possibility of calcium precipitation, it also had several drawbacks. These included the fact that areas stained by ARS represent calcium rich areas that may not have any calcium precipitates present, since ARS stains calcium indiscriminately (240). Data obtained using Raman spectroscopy and SEM showed that ARS stained areas commonly represented areas where amorphous calcium phosphate or amorphous apatite was present. Interestingly, calcium carbonate was not precipitated by any of the *Pseudomonas* species assayed. Several *Pseudomonas* species have previously been shown to precipitate calcium carbonate under different conditions (62, 225, 226, 241). It is possible that the conditions we used to grow the *Pseudomonas* species facilitated the precipitation of calcium phosphate over calcium carbonate.

During MICP, bacterial cells act as nucleation points for calcium precipitation on the surface of bacterial colonies. Bacteria like *E. coli*, *Bacillus subtilis*, *C. matruchotii*, and *Chromohalobacter marismortui* all precipitate calcium on the surface of cells (215, 219, 242, 243). However, calcium phosphate precipitated only on the

colonies of seven of the *Pseudomonas* strains assayed. There was no set pattern to the surface-associated calcium precipitation phenotype among the strains assayed since strains within the same *Pseudomonas* species or strains that had similar lifestyles differed in the development of surface-associated calcium precipitation (Table 5.2). EPSs are thought to be a common nucleation point during MICP, however we did not detect alginate or cellulose on the surface of any *Pseudomonas* colonies assayed. It has recently been observed in *Bacillus* sp. JH7 and *P. aeruginosa* that EPS production does not always correlate with bacterial calcium precipitation (175, 244). Our findings suggest a similar trend. MICP is also thought to be associated with an increase in pH as calcium precipitation is more likely to spontaneously and rapidly occur at a higher pH (171, 179, 245, 246). While all the *Pseudomonas* strains assayed raised the pH of the surrounding media, the colonies for several *Pseudomonas* strains that precipitated calcium phosphate on the surface of cells became more acidic after two days of growth. MICP under acidic conditions would seem counterintuitive but appeared to occur in several *Pseudomonas* strains.

All the *Pseudomonas* strains assayed precipitated calcium phosphate as a white halo in the agar adjacent to the colonies. The calcium phosphate that precipitated in the white halo was amorphous, non-crystalline, and was likely precipitated through MICP (61). Among the *Pseudomonas* strains assayed, six of the seven *P. syringae* pathovars and *P. spp.* 92 precipitated a brown halo of amorphous apatite around the colonies. In the case of all the *Pseudomonas* where this occurred, the brown halo replaced a white halo that had been in the same location on the agar plate. This

Table 5.2: *Pseudomonas* species and strains used in this work.

a. In reference to the main life-style of the bacteria in relation to how it interacts with plants.

<i>Pseudomonas</i> species	Origin of isolation	Properties ^a	Calcium precipitation on cell surface	Calcium precipitation in agar/ (color)	Reference
<i>Pseudomonas putida</i> KT2440	Soil	Plant beneficial microbe	No	Yes/white	(247)
<i>Pseudomonas fluorescens</i> Pf0-1	Rif resistant mutant generated from a soil-borne isolate of <i>P. fluorescens</i>	Plant beneficial microbe	Yes	Yes/white	(248)
<i>Pseudomonas fluorescens</i> 55	Soil	Plant beneficial microbe	Yes	Yes/white	(17)
<i>Pseudomonas fluorescens</i> A506	Foliar	Plant beneficial microbe	Yes	Yes/white	(249)
<i>Pseudomonas fluorescens</i> SBW25	Soil	Plant beneficial microbe	No	Yes/white	(250)
<i>Pseudomonas</i> spp. 92	Phyllosphere	Plant beneficial microbe	No	Yes/brown	(251)
<i>Pseudomonas savastanoi</i> pv. <i>savastanoi</i> 4352	Foliar	Plant pathogen	Yes	Yes/brown	A. Collmer
<i>Pseudomonas syringae</i> pv. <i>tomato</i> DC3000	Foliar	Plant pathogen	No	Yes/brown	(60)
<i>Pseudomonas syringae</i> pv. <i>glycinea</i> 2159 Race 1	Foliar	Plant pathogen	No	Yes/brown	A. Collmer
<i>Pseudomonas syringae</i> pv. <i>morsprunorum</i> 5795	Foliar	Plant pathogen	Yes	Yes/white	A. Collmer
<i>Pseudomonas syringae</i> pv.	Foliar	Plant pathogen	Yes	Yes/brown	(252)

maculicola ES4326					
<i>Pseudomonas syringae</i> pv. tabaci ATCC11528	Foliar	Plant pathogen	Yes	Yes/brown	A. Collmer
<i>Pseudomonas syringae</i> pv. syringae B728a	Foliar	Plant pathogen	No	Yes/brown	(253)
<i>Pseudomonas viridiflava</i> NYS-1	Foliar	Plant pathogen	No	Yes/brown	A. Collmer

suggests that the *Pseudomonas* strains actively facilitate formation of this brown halo of amorphous apatite. Active formation of apatite is characteristic of M CCP (218). However, a couple characteristics of this amorphous apatite make it unlikely to be produced through M CCP. First, the morphology of the amorphous apatite was unordered and fibrous. Although these fibers displayed similarities with artificial bone precursors, they did not have an ordered crystalline structure expected during M CCP (218, 254). Second, bacteria produce an organic matrix during M CCP and our analyses did not identify anything that could be considered a bacterially produced organic matrix. As such, this apatite would likely be characterized as MICP even though it had several interesting characteristics. Further characterization of genes involved in this apatite formation could help determine the mechanism of its formation.

Biogenic apatite has applications in medical and conservation fields. *P. fluorescens* SBW25 produces apatite when grown on concrete in lysogeny broth (LB) supplemented with phosphate and could be used for preservation purposes (228). Although we did not perform our assays in LB supplemented with phosphate, we found that *P. fluorescens* SBW25 precipitated less calcium phosphate than other *P. fluorescens* strains assayed. Our results suggest that *P. fluorescens* strains, like *P. fluorescens* Pf0-1 or *P. fluorescens* 55, may be desirable *P. fluorescens* strains to use if biogenic apatite is needed for application purposes. Our results may aid in choosing or applying the appropriate *Pseudomonas* species for a particular application involving biogenic apatite.

Our Tn-mutant screen identified several global regulators and metabolic pathways involved in regulating calcium phosphate precipitation during growth of *Pto*. The Tn-mutant with an insertion in the gene *phoU* was one of the mutants that did not precipitate amorphous apatite in the agar adjacent to the colony. In *P. aeruginosa*, *phoU* regulates phosphate metabolism and deletion of *phoU* results in accumulation of ppGpp and polyphosphate in cells (255). Secretion of orthophosphate from stored polyphosphate is reported to be involved in MICP (65). The fact that the *phoU* mutant shows reduced and altered calcium precipitation suggests a link between polyphosphate accumulation and calcium precipitation in *Pto*. Further analysis of the link between *phoU* and calcium phosphate precipitation could provide a greater understanding into the role polyphosphates and phosphate metabolism play in this phenomenon.

Further analysis of the Tn-mutants showed that several genes linked to calcium precipitation, eight out of the 17 identified, have been assigned direct or indirect roles in virulence of *P. syringae*, another bacterial plant pathogen, or a related pathogenic *Pseudomonas* species (Table 5.3). Notably, the global regulators of virulence in *P. syringae*, *retS*, *tvrR*, and *cbrB*, were among the genes linked to calcium precipitation (117, 239, 256). Ca^{2+} is abundant within the leaf apoplast and is an important secondary messenger during the plant defense response (185, 257). Some bacterial plant pathogens chelate Ca^{2+} *in planta* with EPSs to reduce the defense response (187). Both alginate and cellulose chelate Ca^{2+} but are disposable during *Pto* virulence (95, 136). As such, there could be another mechanism through which *Pto* disables Ca^{2+} signaling *in planta* during infection. As calcium precipitation seems to correlate

Table 5.3: Genes found in Tn-mutant screen to be associated with virulence

- a. Reference that describes how that gene is involved in virulence of *P. syringae* pv. *tomato* DC3000, similar plant-pathogenic bacteria, or a related *Pseudomonas* species.

Gene Disrupted	Gene name	Reference ^a
PSPTO_5516	<i>uvrD</i>	(258)
PSPTO_0917	<i>ndh</i>	(259)
PSPTO_4868	<i>retS</i>	(117)
PSPTO_3724	<i>lonI</i>	(260)
PSPTO_3576	<i>tvrR</i>	(239)
PSPTO_0965	<i>cbrB</i>	(256)
PSPTO_3349	<i>fisK</i>	(261)
PSPTO_5483	<i>phoU</i>	(82)

with virulence related genes, investigation into whether *Pto* causes calcium precipitation to occur *in planta* could be worthwhile. If *Pto* does induce calcium precipitation *in planta*, it could be a novel mechanism that plant pathogens use to disrupt the plant immune response. A more thorough characterization of TvrR, RetS, and CbrB could identify the mechanism through which *Pto* regulates calcium phosphate precipitation and help determine whether calcium precipitation directly relates to virulence in *P. syringae*.

Materials and Methods

Growth and cultivation of *Pseudomonas* species: *Pseudomonas* (Table 5.2) were routinely cultivated on Kings B (KB) agar (147). Prior to inoculation, each strain was grown in KB medium for 10-12 hours and then washed twice in Nutrient Broth (NB) (Becton, Dickinson, and Company, Franklin Lakes, NJ) medium before being resuspended into NB medium at an optical density of 0.3 measured at 600 nm (OD₆₀₀). 5 µL of each bacterial suspension was then spotted onto individual NB agar plates and individual NB agar plates supplemented with 5 mM CaCl₂. For controls, individual NB agar plates supplemented with 5 mM CaCl₂ were spotted with 5 µL of autoclaved cells from each strain or left blank.

pH measurement of *Pseudomonas* cultures: Cultures were grown to stationary phase in KB medium and then washed twice in NB medium before being resuspended in NB medium at an OD₆₀₀ of 0.3. 5 µL of each bacterial suspension was spotted on an NB agar plate supplemented with 5 mM CaCl₂ and 0.1 % (w/v) BB and monitored for two days.

Alizarin red S staining: The method of ARS staining of calcium rich areas was modified from histological methods for the purposes of staining agar plates and bacterial colonies (240). NB agar plates and NB agar plates supplemented with 5 mM CaCl₂ spotted with bacterial colonies were flooded with 1.0% (w/v) ARS (Sigma-Aldrich, St. Louis, MO), pH 4.1. After five minutes, the dye was removed using a pipette and plates were washed with 1 mL of ddH₂O to remove excess ARS. The dark red areas were scored as calcium rich areas. ARS staining was repeated with five biological replicates for each strain.

Raman spectroscopy: Strains grown on NB agar plates supplemented with 5 mM CaCl₂ and uninoculated NB agar plates supplemented with 5 mM CaCl₂, were directly used for analysis. Raman spectroscopy was performed using a Renishaw InVia Confocal Raman Microscope (Renishaw, Illinois, IL) with a 785 nm laser. Spectra were taken at the center of each bacterial colony and on the agar directly adjacent to bacterial colonies every day for six days.

Scanning electron microscopy (SEM): One or six-day old bacterial colonies grown on NB agar plates supplemented with 5 mM CaCl₂ were frozen in nitrogen slush and freeze-dried. Freeze-dried bacterial colonies were removed from the agar and mounted directly on aluminum pegs using carbon tape. Subsequently, agar directly adjacent to the bacterial colonies was mounted on aluminum pegs using carbon tape. Mounted samples were then coated with gold-palladium in a Desk V sputter coater (Denton Vacuum, Moorestown, NJ). SEM was performed on a TESCAN Mira3 FESEM (Tescan, Czech Republic) using an In-Beam detector set at 5 kV.

Transposon Mutagenesis. Mutations were made using the EZ-Tn5TM <KAN-2> Tnp TransposomeTM Kit (Illumina, Madison, WI) following the manufacturer's protocol. Briefly, *P. syringae* pv. tomato DC3000 electrocompetent cells were prepared as described previously (262). For the mutagenesis reaction, 1 μ l of EZ-Tn5TM <KAN-2> Tnp TransposomeTM was added to 100 μ l of electrocompetent *P. syringae* pv. tomato DC3000 cells. Cells were immediately electroporated using the Bio-Rad (Hercules, CA) Gene Pulser XCellTM electroporation system with the following settings: 2 mm electroporation cuvette; 2.5 kV; 25 μ F; 200 Ω . Cells were immediately recovered in 1 ml of LM medium and incubated at 28°C for 3 hours (263). After recovery, the cell suspension was diluted 1:12 in LM medium and 100 μ l aliquots were plated onto a total of 120 NB agar plates supplemented with 50 μ g/ml of kanamycin and 5 mM CaCl₂. Plates were incubated at room temperature for 7 days and monitored for growth of colonies and calcium precipitation. Colonies that either had little or no visible halo of brown precipitate, colonies with white precipitate on the colony surface, and colonies with a halo of brown precipitate greater than WT were selected for further analysis.

Identification transposon insertion site. To identify the insertion site each transposon (Tn) mutant, was grown overnight in KB supplemented with 50 μ g/mL kanamycin at 28°C. Overnight cultures were used to extract genomic DNA using the Wizard® Genomic DNA Purification Kit (Promega, Madison, WI). Genomic DNA samples from each of the Tn5 mutant strains were used as templates for arbitrary PCR reactions. For each strain, two rounds of PCR were performed. Primers used to identify Tn insertions are found in Table 5.4. Round 1 used one primer specific to the

Table 5.4: Primers and plasmids used in this study

Primer name	Sequence (5' – 3')	Description
oSWC01139	GTAACACTGGCAGAGCATTACGC TG	1 st round of PCR 3' end of Tn
oSWC02330	CCTTTGCCATGTTTCAGAAACAA CT	1 st round of PCR 5' end of Tn
oSWC00141	GGCCACGCGTCGACTAGTACNNN NNNNNNNGAACG	Used during 1 st round of PCR
oSWC00142	GGCCACGCGTCGACTAGTAC	Primer specific to oSWC00141 tail seq.
oSWC02331	GGATCAGATCACGCATCTTCCCG ACA	2 nd round of PCR 3' end nested primer for Tn
oSWC02332	GCAATGTAACATCAGAGATTTTG AG	2 nd round of PCR 5' end nested primer for Tn
oSWC02209	ACCTACAACAAAGCTCTCATCAA CC	Fwd sequencing primer
oSWC02210	GCAATGTAACATCAGAGATTTTG AG	Rev sequencing primer
Plasmid	Description	Reference
pΩ:: <i>tvrR</i>	pΩ:: <i>tvrR</i> Sm ^R , Sp ^R	(239)
pAC1	pΩ:: <i>retS</i> Sm ^R , Sp ^R	(264)

Tn sequence (oSWC02330 for amplifying sequences adjacent to the 5' end of the Tn sequence, and oSWC01139 for amplifying sequences adjacent to the 3' end of the Tn) and one primer (oSWC0141) that contains the 5 bp sequence, GAACG, that is found to occur randomly at approximately every 400 nt in the *P. syringae* pv. tomato DC3000 genome and a specific tail sequence that is used in the second round of PCR reactions. Round 2 PCR reactions were carried out using a nested primer that is contained within the round 1 PCR amplicon and specific to the Tn sequence, but does not overlap the primer sequence used in round 1 (oSWC02332 5' end; oSWC02331 3' end) and a primer specific to the tail sequence of the oSWC0141 primer used in round 1 (oSWC0142). This allows for specific amplification of sequences immediately adjacent to the ends of the Tn for each mutant strain, and thus identification of the site of insertion. Tn insertion sites were considered correct only when sequencing results from both ends of the Tn could be mapped to the same locus in the genome of *P. syringae* pv. tomato DC3000. All PCR reactions were 25 μ l. Round 1 PCR reactions contained: 1 μ l gDNA (~ 500 ng); 12.5 μ l OneTaq® 2X Master Mix (New England Biolabs Inc., Ipswich, MA); 2 μ M of each primer; H₂O to 25 μ l. Thermocycling conditions: 94°C, 30s; (94°C, 30s; 42°C, 30s; 68°C, 3 min) for 6 cycles; (94°C, 30s; 52°C, 30s; 68°C, 3 min) for 25 cycles; 68° C for 7 minutes. After round 1 PCR, the reactions were cleaned to remove excess primers and gDNA using the QIAquick PCR Purification Kit (QIAGEN, Valencia, CA) following the manufacturer's protocol. Round 2 PCR reactions contained: 1.5 μ l of purified PCR product from round 1 as template; 0.2 μ M of oSWC0142 primer and 2 μ M of 2nd round nested primer (oSWC02332 or oSWC02331); H₂O to 25 μ l. Thermocycling conditions were similar

to round 1 PCRs with the exception that a touchdown PCR protocol was used where the annealing step started at a temperature of 63°C and decreased by 1°C each cycle for 13 cycles, and then remained at 50°C for an additional 17 cycles. After round 2 PCR, samples were cleaned using ExoSAP-IT™ PCR Product Cleanup Reagent (ThermoFisher Scientific, Waltham, MA) as per manufacturer's instructions. Cleaned PCR products were sequenced at the Cornell University Biotechnology Resource Center using an Applied Biosystems Automated 3730xl DNA Analyzer using sequencing primer oSWC2209 for 3' end products, and oSWC2210 for 5' end products.

Acknowledgements

We would like to thank Joyce Roper for sending us *P. fluorescens* A506. We would also like to thank Alan Collmer for providing us with all the other *Pseudomonas* strains used in this study. We would like to thank Barbara Kunkel for providing the pΩ::*tvrR* *Pto* strain and Alan Chambers for providing the pΩ::*retS* *Pto* strain. We would like to thank Jenny Russ Kunitake for helping perform initial Raman spectroscopy experiments. The U.S. Department of Agriculture (USDA) is an equal opportunity provider and employer. Mention of trade names or commercial products in this publication is solely for the purposes of providing specific information and does not imply recommendation or endorsement by the USDA. This work made use of the Cornell Center for Materials Research Facilities supported by the National Science Foundation under Award Number DMR-1719875. The authors declare no conflicts of interest.

CHAPTER 6

UNRAVELING THE INTERACTION BETWEEN *PSEUDOMONAS SYRINGAE* PV. TOMATO DC3000 AND *NICOTIANA BENTHAMIANA* USING DUAL-RNA SEQ⁷

Background.

Pseudomonas syringae is a hemibiotrophic bacterial plant pathogen that infects a multitude of species worldwide. *P. syringae* pv. *tomato* DC3000 (*Pto*) causes bacterial speck of tomato. Much is known about individual pathogenicity factors, such as type III secretions system effectors (T3Es), in *Pto*. However, not much is known about how *Pto* overcomes the initial plant defense response before it deploys effectors.

Transcriptome analysis (RNA-seq) during early stages of infection before and after effector deployment would help profile the overall changes occurring in *Pto* at early stages of infection and could lead to identifying new pathogenicity factors. In this study, we performed dual RNA-seq on *Pto* Δ *hopQ1-1* and *Nicotiana benthamiana* during a compatible interaction at one hour and six hours post inoculation (HPI) in order to profile changes in the host and pathogen genome during early stages of infection.

Results.

Transcriptome analysis of *N. benthamiana* and *Pto* Δ *hopQ1-1* revealed large changes in gene regulation in both the host and pathogen between 1 HPI and 6 HPI. Many

⁷ Maxwell R. Fishman, Paul V. Stodghill, Melanie J. Filiatrault. Unraveling the interaction between *Pseudomonas syringae* pv. *tomato* DC3000 and *Nicotiana benthamiana* using Dual-RNA Seq. in prep.

defense-related genes were differentially expressed between 1 HPI and 6 HPI in *N. benthamiana* with a large number of them being down-regulated at 6 HPI as compared to 1 HPI. In *Pto* Δ *hopQ1-1*, genes associated with many pathogenicity and virulence factors showed differential expression between 1 HPI and 6HPI. In particular, genes involved in flagellar motility, reactive oxygen species protection, coronatine biosynthesis, the type three secretion system and T3Es, general metabolic activity, and carbon catabolite repression were differentially expressed between 1 HPI and 6 HPI.

Conclusion.

Dual RNA-seq provides a detailed overview of both the pathogen and host response during the initial stages of pathogen infection. This allows for changes in metabolism, carbon uptake, and pathogenicity related genes in *Pto* Δ *hopQ1-1* to be assessed while assessing defense-related genes in *N. benthamiana*. It provides better insight into the unknown changes that occur during the initial hours after *Pto* infection of a host.

Background

Plants defend against hemibiotrophic pathogens in a two-step process according to the zig-zag model (5). Pathogen invasion is first recognized by the plant through pattern recognition receptors (PRRs) that identify microbial associated molecular patterns (MAMPs) and cause pattern-triggered immunity (PTI) (6). PTI is associated with a strong production of reactive oxygen species (ROS) 30 to 80 minutes after pathogen entry of the host apoplast (265). Pathogens deploy effectors into plant cells in order to stop PTI and override the plant defense response. However, this comes at the risk of activating the second line of the plant defense response called

effector-triggered immunity (ETI) (6). ETI occurs when, commonly a nucleotide binding leucine rich repeat (NLR) protein that is coded for by a resistance gene (R-gene) is activated by a single effector (5). NLR recognition of effectors can occur through direct binding with an effector or through indirect recognition where an NLR guards a host factor targeted by effectors or acts as bait for an effector (266).

Recognition of a type three secretion system effector (T3E) by an NLR results in the hypersensitive response (HR), plant cell death, and an incompatible interaction between the plant and the pathogen. If ETI does not occur, this is called a compatible interaction where the pathogen is able to grow and thrive within its host.

P. syringae pv. *tomato* DC3000 (*Pto*) is a well-characterized hemibiotrophic bacterial plant pathogen used extensively as a model in molecular plant-pathogen interactions. *Pto* causes bacterial speck of tomato and is a natural pathogen of *Solanum lycopersicum*, *Arabidopsis thaliana*, and several *Brassica* species (192). Much work in *Pto* has been devoted to understanding the mechanism involved in T3E deployment, the targets of T3Es, and how T3Es interact with various R-genes during ETI (192). In addition, a large amount of information is known about specific genes and factors necessary for virulence of *Pto* such as genes involved in resisting desiccation stress, sensing the plant environment, or metabolizing nutrients found within the apoplast (94, 121, 267). Even with all that is known about *Pto* pathogenicity factors, there is a black box around how *Pto* and other hemibiotrophic bacterial plant pathogens respond during infection to PTI prior to effector delivery and how that response in *Pto* changes after effector delivery. Time-points as early as one hour post inoculation (HPI) would likely be needed to study these changes and identification of

genes expressed at this time could identify unknown genes involved in defense that *Pto* employs during PTI.

Changes in gene expression within the pathogen during disease progression in the plant is a way to identify genes expressed by *Pto* during early stages of infection. Determining genes expressed by bacterial pathogens *in planta* was first characterized using *in vivo* expression technology (IVET) (268). This technique identifies positively expressed genes at a given time-point that are expressed by the pathogen during host-pathogen interactions, but is not able to decipher the complete transcriptional landscape of a pathogen. IVET has been used to successfully identify virulence factors in a number of plant pathogens including, *Xanthomonas campestris*, *Pectobacterium carotovorum*, *Dickeya dadantii*, *Pseudomonas syringae*, and *Erwinia amylovora* (269-273). More recent studies in *P. syringae* pv. *syringae* B728a, *Ralstonia solanacearum*, and *Xanthomonas oryzae* pv. *oryzae* used microarrays to assay bacterial gene expression during growth *in planta* and compared this gene expression to *in vitro* conditions, epiphytic conditions, or to different time points during infection (83, 274, 275). While these experiments lead to insight into plant-pathogen interactions, information about the overall transcriptomic profile could have been missed since microarrays are not able to detect low abundant transcripts as well as transcriptional analysis using next generation sequencing (RNA-seq). RNA-seq has been recently used to gain insight into *Xanthomonas glycine* infection of soybean and mapped changes in the transcriptional landscape of *X. glycine* during different time-points of infection (82). One drawback, however, for simultaneous RNA-seq of a host and pathogen (called dual RNA-seq) is that most of the RNA will belong to the host and

there are limited ways to enrich for the pathogen RNA. The difficulty involved in enriching bacterial RNA during host infection limited previous experiments investigating gene regulation in bacterial plant pathogens during growth *in planta* to time points typically starting at 24, 48, or 72 hours after inoculation.

Plant proteome, metabolome, and transcriptome data during the first few hours of infection show that drastic changes occur within the plant during bacterial infection (42, 276, 277). These changes are due to the plant response to the pathogen, and also due to the presence of pathogen secreted effectors that reprogram the host machinery for its own gain. Even though much is known about how the plant responds to *Pto*, it is still unclear how the transcriptional landscape of bacterial plant pathogens, such as *Pto*, changes during initial hours of infection. Determining the overall changes in gene regulation of *Pto* within the first few hours of plant pathogen inoculation could provide profound insight into genes necessary for the initial stages of colonization before T3E delivery when *Pto* encounters PTI.

Nicotiana benthamiana normally forms an incompatible interaction with *Pto* that results in the hypersensitive response (HR). However, a compatible interaction between *Pto* and *N. benthamiana* is possible by deleting the gene that codes for the T3E HopQ1-1 from *Pto* (4). This provides *Pto* with another host that can be used to assess host-pathogen interactions. As *N. benthamiana* is commonly a non-host plant, understanding how *Pto* interacts with it at initial stages of infection can be advantageous for several reasons. First, assessing changes in gene expression between a compatible interaction with *Pto* Δ *hopQ1-1* and *N. benthamiana* may give insight to differences between typical host and non-host interactions. Second, *N. benthamiana*

has become a model organism due to the ease at which genes can either be down-regulated using virus induced gene silencing (VIGS) or overexpressed through transient expression with *Agrobacterium tumefaciens*. This increases the scientific arsenal of tools that could be used to research plant-pathogen interactions and potentially increase knowledge about compatible and incompatible interactions.

In this manuscript, we developed a dual-RNA seq method to evaluate the interactions between *Pto ΔhopQ1-1* and *N. benthamiana* and report findings pertaining to initial hours of inoculation. By using dual RNA-seq, the response of the host and pathogen can be observed simultaneously. This was utilized to better understand the global transcriptional landscape and how it changes during the initial stages of *Pto ΔhopQ1-1* infection before and after effector deployment.

Results

Dual RNA-seq of during early stages of infection show a changing regulatory landscape for the plant and the pathogen. We monitored transcriptional changes in both *Pto ΔhopQ1-1* and *N. benthamiana* during 1 HPI and 6 HPI. Three biological replicates from each timepoint were used to evaluate differential gene expression of both *Pto ΔhopQ1-1* and *N. benthamiana*. cDNA libraries were run on individual flow cells and we initially obtained between 175 million and 277 million reads per cDNA library with 74% - 89% of the reads mapping back to either *Pto* or *N. benthamiana*. For the 1 HPI timepoint, 2.91% - 3.85% of the reads mapped to the *Pto* genome, while the remaining reads mapped to the *N. benthamiana* genome. For the 6 HPI timepoint, 5.54% - 8.96% of the reads mapped to the *Pto* genome, while the remaining reads mapped to the *N. benthamiana* genome. As expected, a majority of the sequenced

reads mapped back to the *N. benthamiana* genome at both timepoints. Reciprocal mapping verified that reads mapped back to the appropriate genome.

For this study, genes were considered differentially expressed if they showed a change in gene expression greater than or equal to 1.8-fold. In *Pto*, 2065 genes were differentially expressed between 1 HPI and 6 HPI with a fold change equal to or greater than 1.8 and with an FDR cutoff of < 0.05 . 1016 genes were up-regulated, while 1047 genes were down-regulated. The large number of genes differentially expressed between 1 HPI and 6 HPI showed that *Pto* was responding to a changing environment within the host. In *N. benthamiana*, 7,729 genes were differentially expressed between 1 HPI and 6 HPI with a fold change at or greater than 1.8 with an FDR cutoff of < 0.05 . 4,286 of those genes were up-regulated, while 3,433 of those genes were down-regulated. Such a large number of differentially expressed genes in the host during pathogen infection are thought to be a combination of both the plant defense response and pathogen hijacking of the plant.

Changes in bacterial transcriptional landscape during early stages of infection.

Gene ontology (GO) enrichment was performed on differentially expressed genes in *Pto* to map biological processes that significantly changed between 1 HPI and 6 HPI (Table 6.1)⁸. Following GO enrichment analysis, differentially expressed genes were annotated and genes of interest were grouped according to putative function (Tables 6.1-6.16)⁹. Several expected trends were observed within the dataset and are described below.

⁸ Table 6.1 is over 300 lines long and will be included in the supplementary data for this thesis.

⁹ Tables 6.16 is over and 2000 lines long and will be included in the supplementary data for this thesis.

Table 6.2: Differentially expressed motility genes between 1 HPI and 6 HPI

a. Major biological function category that genes fall under

b. The names and descriptions of proteins according to the Uniprot database (112).

Category ^a	Locus Number	Protein names ^b	Gene name	Fold Change
Flagellar motility				
	PSPTO_1939	Flagellar basal-body rod protein FlgF	<i>flgF</i>	-2.49
	PSPTO_1985	MotB protein		-2.53
	PSPTO_1984	Chemotaxis motA protein	<i>motA-1</i>	-2.68
	PSPTO_1941	Flagellar L-ring protein (Basal body L-ring protein)	<i>flgH</i>	-2.77
	PSPTO_1942	Flagellar P-ring protein (Basal body P-ring protein)	<i>flgI</i>	-2.86
	PSPTO_1940	Flagellar basal-body rod protein FlgG	<i>flgG</i>	-3.02
	PSPTO_1966	Flagellar hook-length control protein FliK	<i>fliK</i>	-3.17
	PSPTO_5230	Flagellar protein FliL, putative		-3.28
	PSPTO_4953	Chemotaxis motA protein	<i>motA-2</i>	-3.83
	PSPTO_1925	Negative regulator of flagellin synthesis FlgM		-4.17
	PSPTO_1950	Flagellin FlaG, putative		-4.61
	PSPTO_1933	Flagellar basal body rod protein FlgB	<i>flgB</i>	-6.33
	PSPTO_1934	Flagellar basal-body rod protein FlgC	<i>flgC</i>	-6.50
	PSPTO_1944	Flagellar hook-associated protein FlgK	<i>flgK</i>	-6.56
	PSPTO_1951	Flagellar hook-associated protein 2	<i>fliD</i>	-6.75
	PSPTO_4952	Chemotaxis motB protein	<i>motB</i>	-7.13
	PSPTO_1945	Flagellar hook-associated protein FlgL	<i>flgL</i>	-7.51
	PSPTO_1936	Flagellar hook protein FlgE	<i>flgE-1</i>	-8.24
	PSPTO_4156	Sodium-type flagellar protein MotY, putative		-8.37
	PSPTO_1952	Flagellar protein FliS	<i>fliS</i>	-9.13
	PSPTO_1949	Flagellin	<i>fliC</i>	-20.00

Table 6.2 (Continued)

Chemotaxis			
PSPTO_2254	Methyl-accepting chemotaxis protein		-1.89
PSPTO_0908	Chemotaxis response regulator protein-glutamate methylesterase of group 2 operon	<i>cheB2</i>	-2.22
PSPTO_0263	Methyl-accepting chemotaxis protein		-2.70
PSPTO_1988	Chemotaxis protein CheW	<i>cheW-2</i>	-2.74
PSPTO_5553	Methyl-accepting chemotaxis protein		-2.80
PSPTO_0117	Methyl-accepting chemotaxis protein		-2.91
PSPTO_1495	Chemotaxis protein methyltransferase CheR		-2.95
PSPTO_1493	Methyl-accepting chemotaxis protein		-3.15
PSPTO_3379	Methyl-accepting chemotaxis protein		-3.18
PSPTO_2475	Methyl-accepting chemotaxis protein		-3.21
PSPTO_1983	Chemotaxis response regulator protein-glutamate methylesterase of group 1 operon	<i>cheB1</i>	-3.28
PSPTO_1059	Methyl-accepting chemotaxis protein		-3.29
PSPTO_0910	Chemotaxis protein methyltransferase	<i>cheR-1</i>	-3.44
PSPTO_1066	Methyl-accepting chemotaxis protein		-3.64
PSPTO_0916	Methyl-accepting chemotaxis protein, putative		-3.65
PSPTO_4936	Methyl-accepting chemotaxis protein		-3.75
PSPTO_1008	Methyl-accepting chemotaxis protein		-4.07
PSPTO_3577	Methyl-accepting chemotaxis protein		-4.13
PSPTO_0912	Methyl-accepting chemotaxis protein		-4.22
PSPTO_0911	Chemotaxis protein CheW	<i>cheW-1</i>	-4.23
PSPTO_	Methyl-accepting chemotaxis protein		-4.26

Table 6.2 (Continued)

3480			
PSPTO_			
5159	Methyl-accepting chemotaxis protein		-4.39
PSPTO_			
3685	Methyl-accepting chemotaxis protein		-4.57
PSPTO_			
0915	Chemotaxis protein CheY	<i>cheY-1</i>	-4.62
PSPTO_			
1927	Chemotaxis protein CheV, putative		-4.67
PSPTO_			
1928	Chemotaxis protein methyltransferase CheR	<i>cheR-2</i>	-4.94
PSPTO_			
2480	Methyl-accepting chemotaxis protein		-5.26
PSPTO_			
2526	Methyl-accepting chemotaxis protein		-5.63
PSPTO_			
4531	Methyl-accepting chemotaxis protein, putative		-5.68
PSPTO_			
4624	Methyl-accepting chemotaxis protein		-5.92
PSPTO_			
0995	Methyl-accepting chemotaxis protein		-6.05
PSPTO_			
2997	Methyl-accepting chemotaxis protein		-6.09
PSPTO_			
3699	Methyl-accepting chemotaxis protein		-6.44
PSPTO_			
4541	Methyl-accepting chemotaxis protein		-6.49
PSPTO_			
1323	Chemotaxis protein CheV, putative		-6.75
PSPTO_			
2511	Methyl-accepting chemotaxis protein		-6.88
PSPTO_			
3524	Chemotaxis protein CheV, putative		-7.26
PSPTO_			
2448	Methyl-accepting chemotaxis protein		-7.34
PSPTO_			
2883	Methyl-accepting chemotaxis protein		-7.70
PSPTO_			
2441	Methyl-accepting chemotaxis protein		-8.21
PSPTO_			
1334	Methyl-accepting chemotaxis protein		-9.41
PSPTO_			
5352	Methyl-accepting chemotaxis protein		-9.88
PSPTO_			
	Methyl-accepting chemotaxis protein		-10.15

Table 6.2 (Continued)

5554		
PSPTO_		
3237	Methyl-accepting chemotaxis protein	-10.26
PSPTO_		
3098	Methyl-accepting chemotaxis protein	-10.98
PSPTO_		
2472	Methyl-accepting chemotaxis protein	-12.63
PSPTO_		
2616	Methyl-accepting chemotaxis protein	-14.19
PSPTO_		
3580	Methyl-accepting chemotaxis protein	-19.36

Table 6.3: Differentially expressed ROS protection genes between 1 HPI and 6 HPI

a. Major biological function category that genes fall under

b. The names and descriptions of proteins according to the Uniprot database (112).

Category^a	Locus Number	Protein names^b	Gene name	Fold Change
ROS protection				
	PSPTO_1767	Organic hydroperoxide resistance protein	<i>ohr</i>	7.80
	PSPTO_1338	Superoxide dismutase [Cu-Zn] (EC 1.15.1.1)	<i>sodC</i>	-5.66
	PSPTO_3108	Alkyl hydroperoxide reductase, subunit C	<i>ahpC</i>	-8.07
	PSPTO_5263	Catalase (EC 1.11.1.6)	<i>katE</i>	-9.71
	PSPTO_4530	Catalase-peroxidase (CP) (EC 1.11.1.21) (Peroxidase/catalase)	<i>katG</i>	-18.26
	PSPTO_3107	Alkyl hydroperoxide reductase, subunit F	<i>ahpF</i>	-28.38
	PSPTO_3582	Catalase (EC 1.11.1.6)	<i>katB</i>	-84.85

Table 6.4: Differentially expressed coronatine biosynthesis genes between 1 HPI and 6 HPI

a. Major biological function category that genes fall under

b. The names and descriptions of proteins according to the Uniprot database (112).

Category ^a	Locus Number	Protein names ^b	Gene name	Fold Change
Coronatine Biosynthesis				
	PSPTO_4685	Coronafacic acid synthetase, ligase component	<i>cfa5</i>	52.14
	PSPTO_4682	Coronafacic acid synthetase, dehydratase component	<i>cfa2</i>	49.57
	PSPTO_4686	Coronafacic acid polyketide synthase I	<i>cfa6</i>	46.24
	PSPTO_4684	Coronafacic acid synthetase component	<i>cfa4</i>	38.15
	PSPTO_4707	Coronamic acid synthetase CmaD	<i>cmaD</i>	36.95
	PSPTO_4710	Coronamic acid synthetase CmaB	<i>cmaB</i>	33.22
	PSPTO_4683	Coronafacic acid beta-ketoacyl synthetase component	<i>cfa3</i>	31.39
	PSPTO_4708	Coronamic acid synthetase CmaE	<i>cmaE</i>	28.83
	PSPTO_4680	Coronafacic acid synthetase, ligase component	<i>cfl</i>	28.50
	PSPTO_4712	Coronamic acid synthetase, thioesterase component	<i>cmaT</i>	28.44
	PSPTO_4709	Coronamic acid synthetase CmaA	<i>cmaA</i>	25.59
	PSPTO_4711	Coronamic acid synthetase CmaC	<i>cmaC</i>	21.45
	PSPTO_4687	Coronafacic acid polyketide synthetase II	<i>cfa7</i>	20.55

Table 6.5: Exopolysaccharide genes differentially expressed between 1 HPI and 6 HPI

a. Major biological function category that genes fall under

b. The names and descriptions of proteins according to the Uniprot database (112).

Category ^a	Locus Number	Protein names ^b	Gene name	Fold Change
Alginate Regulation and Biosynthesis				
	PSPTO_1240	Alginate biosynthesis protein AlgK	<i>algK</i>	31.66
	PSPTO_1242	Glycosyltransferase alg8	<i>alg8</i>	28.14
	PSPTO_1235	Probable alginate O-acetylase AlgI	<i>algI</i>	24.29
	PSPTO_1241	Alginate biosynthesis protein Alg44	<i>alg44</i>	23.41
	PSPTO_1236	Alginate lyase	<i>algL</i>	22.02
	PSPTO_1237	Alginate biosynthesis protein AlgX	<i>algX</i>	19.29
	PSPTO_1234	Probable alginate O-acetylase AlgJ	<i>algJ</i>	18.62
	PSPTO_1233	Alginate biosynthesis protein AlgF	<i>algF</i>	17.47
	PSPTO_1239	Alginate production protein AlgE	<i>algE</i>	16.98
	PSPTO_1232	Alginate biosynthesis protein AlgA	<i>algA</i>	11.64
	PSPTO_1541	Zinc metalloprotease	<i>mucP</i>	1.97
	PSPTO_0127	Alginate biosynthesis regulatory protein AlgR	<i>algR</i>	-2.44
	PSPTO_0136	Alginate regulatory protein AlgR3	<i>algR3</i>	-2.75
	PSPTO_0126	Alginate biosynthesis protein AlgZ/FimS	<i>algZ</i>	-3.72
Psl exopolysaccharide biosynthesis				
	PSPTO_3539	Membrane protein PslK	<i>pslK</i>	-3.04
	PSPTO_3533	Glycosyl transferase, group 1 family protein PslF	<i>pslF</i>	-3.24
	PSPTO_3536	Glycosyl transferase, group 1 family protein PslI	<i>pslI</i>	-3.45
	PSPTO_3535	Glycosyl transferase, group 1 family protein PslH	<i>pslH</i>	-4.08

PSPTO_3532	Exopolysaccharide biosynthesis protein PsIE	<i>pslE</i>	-4.31
PSPTO_3531	Lipoprotein PsID	<i>pslD</i>	-4.54
PSPTO_3537	Membrane protein PsIJ	<i>pslJ</i>	-4.63
PSPTO_3534	Glycosyl hydrolase, family 5 PsIG	<i>pslG</i>	-5.01
PSPTO_3529	Capsular polysaccharide biosynthesis protein PsIA	<i>pslA</i>	-5.37
PSPTO_3530	Mannose-1-phosphate guanylyltransferase/mannose-6-phosphate isomerase PsIB	<i>pslB</i>	-9.91

Table 6.6: Cyclic-di-GMP turnover genes differentially expressed between 1 HPI and 6 HPI

a. Major biological function category that genes fall under

b. The names and descriptions of proteins according to the Uniprot database (112).

Category^a	Locus Number	Protein names^b	Gene name	Fold Change
cyclic-di-GMP production/turnover				
	PSPTO_0306	Sensory box/GGDEF domain/EAL domain protein		2.96
	PSPTO_0114	GGDEF domain/EAL domain protein		2.18
	PSPTO_4365	GGDEF domain/EAL domain protein		-2.07
	PSPTO_1499	Response regulator/GGDEF domain protein		-2.31
	PSPTO_2171	Sensory box/GGDEF domain/EAL domain protein		-2.52
	PSPTO_2313	Sensory box/GGDEF domain protein Response regulator/sensory		-2.58
	PSPTO_5014	box/GGDEF domain/EAL domain protein		-2.61
	PSPTO_0505	GGDEF domain protein		-2.62
	PSPTO_1152	HD-GYP domain protein		-2.82
	PSPTO_3243	GGDEF domain protein		-3.24
	PSPTO_4639	Cyclic diguanosine monophosphate-binding protein		-3.31
	PSPTO_1483	Response regulator/EAL domain protein		-3.51
	PSPTO_0406	Sensory box/GGDEF domain/EAL domain protein		-3.68
	PSPTO_4106	GGDEF domain/EAL domain protein		-3.83
	PSPTO_2591	GGDEF domain protein		-4.19
	PSPTO_1004	GGDEF domain protein		-4.86
	PSPTO_4543	GAF domain/GGDEF domain/EAL domain protein		-6.24
	PSPTO_3886	EAL domain/GGDEF domain protein		-6.26

PSPTO_4208	HAMP domain/GGDEF domain/EAL domain protein	-7.01
PSPTO_2907	GGDEF domain/EAL domain protein	-7.57
PSPTO_0536	Sensory box/GGDEF domain/EAL domain protein	-9.08
PSPTO_1348	Sensory box/GGDEF domain/EAL domain protein	-9.83

Table 6.7: Iron uptake genes differentially expressed between 1 HPI and 6 HPI

a. Major biological function category that genes fall under

b. The names and descriptions of proteins according to the Uniprot database (112).

Category ^a	Locus Number	Protein names ^b	Gene name	Fold Change
Iron uptake				
	PSPTO_0760	Iron(III) dicitrate transport system, ATP-binding protein FecE	<i>fecE</i>	4.04
	PSPTO_0761	Iron(III) dicitrate transport system, permease protein FecD	<i>fecD</i>	3.44
	PSPTO_3257	Iron ABC transporter, permease protein, putative		3.01
	PSPTO_3256	Iron ABC transporter, periplasmic iron-binding protein, putative		2.91
	PSPTO_0762	Iron(III) dicitrate transport system, permease protein FecC	<i>fecC</i>	2.63
	PSPTO_0315	Iron ABC transporter, permease protein		2.63
	PSPTO_0763	Iron(III) dicitrate transport system, periplasmic iron-binding protein FecB	<i>fecB</i>	2.43
	PSPTO_1425	Iron-binding protein IscA	<i>iscA</i>	1.99
	PSPTO_1207	Iron(III) dicitrate transport protein fecA	<i>fecA</i>	-4.45
Siderophores				
	PSPTO_2597	Yersiniabactin synthetase, salicylate ligase component	<i>irp5</i>	-2.53
	PSPTO_2148	Pyoverdine sidechain peptide synthetase II, D-Asp-L-Thr component		-2.55
	PSPTO_2598	Yersiniabactin synthetase, thioesterase component	<i>irp4</i>	-2.61
	PSPTO_2602	Yersiniabactin non-ribosomal peptide synthetase		-2.92
	PSPTO_2153	Pyoverdine ABC transporter, ATP-binding/permease protein	<i>pvdE</i>	-2.98
	PSPTO_2146	Pyoverdine biosynthesis regulatory gene, putative		-3.03
	PSPTO_2135	Pyoverdine chromophore synthetase	<i>pvsA</i>	-3.04
	PSPTO_2150	Pyoverdine sidechain peptide synthetase IV, D-Asp-L-Ser component		-3.27
	PSPTO_2599	Yersiniabactin synthetase, thiazolanyl reductase component	<i>irp3</i>	-3.55

PSPTO_	Pyoverdine sidechain peptide	
2149	synthetase III, L-Thr-L-Ser component	-3.75
PSPTO_	Pyoverdine synthetase, thioesterase	
2134	component	-7.90
PSPTO_	Pyoverdine sidechain peptide	
2147	synthetase I, epsilon-Lys module	-10.85

Table 6.8: RNA polymerase and sigma factors genes differentially expressed between 1 HPI and 6 HPI

a. Major biological function category that genes fall under

b. The names and descriptions of proteins according to the Uniprot database (112).

Category^a	Locus Number	Protein names^b	Gene name	Fold Change
RNA polymerase and sigma factors				
	PSPTO_4104	RNA polymerase-associated protein RapA	<i>rapA</i>	4.02
	PSPTO_0651	DNA-directed RNA polymerase subunit alpha	<i>rpoA</i>	3.85
	PSPTO_0074	DNA-directed RNA polymerase subunit omega	<i>rpoZ</i>	3.34
	PSPTO_0619	DNA-directed RNA polymerase subunit beta	<i>rpoB</i>	3.22
	PSPTO_0537	RNA polymerase sigma factor RpoD	<i>rpoD</i>	3.20
	PSPTO_0620	DNA-directed RNA polymerase subunit beta'	<i>rpoC</i>	2.92
	PSPTO_0430	RNA polymerase sigma factor RpoH	<i>rpoH</i>	-1.88
	PSPTO_1565	RNA polymerase sigma factor RpoS	<i>rpoS</i>	-2.77
	PSPTO_1209	RNA polymerase sigma-70 family protein		-3.94
	PSPTO_5176	RNA polymerase sigma-70 family protein		-5.19
	PSPTO_2133	RNA polymerase sigma-70 family protein		-14.27

Table 6.9: Compatible solute genes differentially expressed between 1 HPI and 6 HPI

a. Major biological function category that genes fall under

b. The names and descriptions of proteins according to the Uniprot database (112).

Category ^a	Locus Number	Protein names ^b	Gene name	Fold Change
Compatible solute biosynthesis				
	PSPTO_2055	Polyamine aminopropyltransferase	<i>speE</i>	4.17
	PSPTO_2802	Proline/betaine transporter	<i>proP</i>	4.10
	PSPTO_0443	Oxygen-dependent choline dehydrogenase (CDH)	<i>betA</i>	2.77
	PSPTO_0441	NAD/NADP-dependent betaine aldehyde dehydrogenase (BADH)	<i>betB</i>	2.31
	PSPTO_0463	Glycine/betaine/L-proline ABC transporter, permease protein		2.23
	PSPTO_3060	Glycine betaine/L-proline ABC transporter, ATP-binding protein		-2.97
	PSPTO_1622	Glycine betaine-binding protein, putative		-3.73
	PSPTO_3880	Polyamine ABC transporter, permease protein, putative		-3.79
	PSPTO_3881	Polyamine ABC transporter, permease protein, putative		-6.04
	PSPTO_0565	Polyamine ABC transporter, permease protein		-9.80
	PSPTO_0564	Polyamine ABC transporter, permease protein		-19.94
	PSPTO_0562	Polyamine-transporting ATPase		-36.11

Table 6.10: LPS biosynthesis genes differentially expressed between 1 HPI and 6 HPI

a. Major biological function category that genes fall under

b. The names and descriptions of proteins according to the Uniprot database (112).

Category^a	Locus Number	Protein names^b	Gene name	Fold Change
LPS Biosynthesis				
	PSPTO_2767	Lipopolysaccharide core biosynthesis domain protein		5.02
	PSPTO_4990	Uncharacterized protein		4.52
	PSPTO_4992	Carbamoyltransferase family protein		3.98
	PSPTO_4988	Uncharacterized protein		3.68
	PSPTO_4987	Uncharacterized protein		3.55
	PSPTO_4989	Uncharacterized protein		3.55
	PSPTO_4986	Membrane protein, putative		3.50
	PSPTO_4998	Lipopolysaccharide biosynthesis protein, putative		3.35
	PSPTO_4991	Glycosyl transferase, group 1 family protein		3.22
	PSPTO_5002	Lipopolysaccharide heptosyltransferase	waaC	3.08
	PSPTO_4984	Lipid A export ATP-binding/permease protein MsbA	msbA	2.90
	PSPTO_5001	Lipopolysaccharide core biosynthesis protein WaaG	waaG	2.79
	PSPTO_5000	Lipopolysaccharide core heptose(I) kinase	waaP	2.53
	PSPTO_5003	ADP-heptose--LPS heptosyltransferase II	rfaF	2.51
	PSPTO_4997	Uncharacterized protein		2.37
	PSPTO_4983	Bifunctional protein HldE	hldE	2.31
	PSPTO_4999	Lipopolysaccharide core biosynthesis protein, putative		2.22

Table 6.11: Efflux pump genes differentially expressed between 1 HPI and 6 HPI

a. Major biological function category that genes fall under

b. The names and descriptions of proteins according to the Uniprot database (112).

Category ^a	Locus Number	Protein names ^b	Gene name	Fold Change
Efflux Pumps				
	PSPTO_0999	Probable sugar efflux transporter	<i>sotB</i>	3.91
	PSPTO_3101	Outer membrane efflux protein		2.93
	PSPTO_2593	Multidrug resistance protein, AcrA/AcrE family		2.78
	PSPTO_2592	Aliphatic isothiocyanate resistance protein SaxG AcrB/AcrD/AcrF family	<i>saxG</i>	2.71
	PSPTO_3748	Multidrug resistance protein		2.52
	PSPTO_3100	Aliphatic isothiocyanate resistance protein SaxF AcrB/AcrD/AcrF family	<i>saxF</i>	2.21
	PSPTO_4304	Isothiocyanate resistance protein SaxB isochorismatase family	<i>saxB</i>	2.12
	PSPTO_4303	Efflux transporter, RND family, MFP subunit		2.07
	PSPTO_3099	Multidrug efflux RND membrane fusion protein MexE	<i>mexE</i>	1.98
	PSPTO_2355	Glutathione-regulated potassium-efflux system protein		1.92
	PSPTO_0376	Cation efflux family protein		-2.73
	PSPTO_0377	Metal ion efflux outer membrane protein, putative		-4.37

Table 6.12: T3SS genes and T3E genes differentially expressed between 1 HPI and 6 HPI

a. Major biological function category that genes fall under

b. The names and descriptions of proteins according to the Uniprot database (112).

Category ^a	Locus Number	Protein names ^b	Gene name	Fold Change
T3SS regulators				
	PSPTO_1380	Type III transcriptional regulator HrpS	<i>hrpS</i>	-2.26
	PSPTO_1404	RNA polymerase sigma factor HrpL	<i>hrpL</i>	-3.76
T3SS pilus and T3SS machinery				
	PSPTO_1381	Hrp pili protein HrpA (TTSS pilin HrpA)	<i>hrpA</i>	-2.00
	PSPTO_1402	Type III secretion protein HrcV	<i>hrcV</i>	-2.59
	PSPTO_1400	Type III secretion ATP synthase HrcN (EC 3.6.3.14)	<i>hrcN</i>	-2.73
T3SS harpins and transglycosylases				
	PSPTO_1405	Type III helper protein HrpK1	<i>hrpK1</i>	-1.94
	PSPTO_1387	Type III secretion protein HrpF	<i>hrpF</i>	-2.00
	PSPTO_1382	Harpin HrpZ (Harpin-Pst) (HrpZ-Pst protein)	<i>hrpZ</i>	-2.07
	PSPTO_1398	Type III secretion protein HrpP	<i>hrpP</i>	-2.31
	PSPTO_1403	Type III secretion protein HrpJ	<i>hrpJ</i>	-2.73
	PSPTO_1388	Type III secretion protein HrpG	<i>hrpG</i>	-2.87
	PSPTO_1401	Type III secretion protein HrpQ	<i>hrpQ</i>	-2.95
	PSPTO_0905	Type III effector HopAH1	<i>hopAH1</i>	-2.12
	PSPTO_3292	Type III effector HopAH2-1	<i>hopAH2-1</i>	-3.08
	PSPTO_1378	Membrane-bound lytic murein transglycosylase D	<i>hrpH</i>	-2.11
	PSPTO_2678	Type III helper protein HopP1	<i>hopP1</i>	-3.15
	PSPTO_4101	Type III helper protein HopAK1	<i>hopAK1</i>	-3.53

T3SS chaperones				
PSPTO_4599	Type III chaperone ShcS1	<i>shcS1</i>		-1.91
PSPTO_5353	Type III chaperone protein ShcA	<i>shcA</i>		-2.38
PSPTO_1376	Type III chaperone ShcE	<i>shcE</i>		-4.23
PSPTO_1374	Type III chaperone ShcM	<i>shcM</i>		-4.88
PSPTO_4589	Type III chaperone ShcS2	<i>shcS2</i>		-7.99
T3SS Effectors				
PSPTO_4722	Effector protein hopD2	<i>hopD2</i>		6.64
PSPTO_0474	Type III effector HopAS1	<i>hopAS1</i>		4.22
PSPTO_4724	Type III effector HopD	<i>hopD</i>		2.94
PSPTO_1568	Type III effector HopAF1	<i>hopAF1</i>		2.45
PSPTO_0501	Type III effector HopU1	<i>hopU1</i>		2.45
PSPTO_0876	Effector protein hopD1	<i>hopD1</i>		2.05
PSPTO_4001	Type III effector protein AvrPto1	<i>avrPto1</i>		1.91
PSPTO_4691	Effector protein hopAD1	<i>hopAD1</i>		1.89
PSPTO_4727	Type III effector HopG1	<i>hopG1</i>		-1.98
PSPTO_4597	Type III effector HopS1	<i>hopS1</i>		-2.09
PSPTO_1377	Type III effector protein AvrE1	<i>avrE1</i>		-2.59
PSPTO_5354	Type III effector HopA1	<i>hopA1</i>		-2.61
PSPTO_4718	Type III effector HopAA1-2	<i>hopAA1</i>		-2.82
PSPTO_4776	Type III effector HopI1	<i>hopI1</i>		-2.85
PSPTO_1375	Effector protein HopM1	<i>hopM1</i>		-4.37
PSPTO_4588	Type III effector HopS2	<i>hopS2</i>		-5.81

Table 6.13: Metabolism-related genes differentially expressed between 1 HPI and 6 HPI

- a. Major biological function category that genes fall under
- b. The names and descriptions of proteins according to the Uniprot database (112).

Category ^a	Locus Number	Protein names ^b	Gene name	Fold Change
Ribosomal Proteins and ribosome biosynthesis				
	PSPTO_1103	50S ribosomal protein L25	<i>rplY</i>	8.08
	PSPTO_1775	ATP-dependent RNA helicase DeaD	<i>deaD</i>	7.39
	PSPTO_0635	30S ribosomal protein S17	<i>rpsQ</i>	5.87
	PSPTO_0089	50S ribosomal protein L28	<i>rpmB</i>	5.70
	PSPTO_0631	50S ribosomal protein L22	<i>rplV</i>	5.58
	PSPTO_4930	50S ribosomal protein L9	<i>rplI</i>	5.38
	PSPTO_4487	30S ribosomal protein S15	<i>rpsO</i>	5.36
	PSPTO_0638	50S ribosomal protein L5	<i>rplE</i>	5.32
	PSPTO_4425	30S ribosomal protein S9	<i>rpsI</i>	5.31
	PSPTO_0645	50S ribosomal protein L15	<i>rplO</i>	5.30
	PSPTO_0644	50S ribosomal protein L30	<i>rpmD</i>	5.25
	PSPTO_0630	30S ribosomal protein S19	<i>rpsS</i>	5.19
	PSPTO_0802	30S ribosomal protein S20	<i>rpsT</i>	5.18
	PSPTO_0634	50S ribosomal protein L29	<i>rpmC</i>	5.03
	PSPTO_0798	50S ribosomal protein L27	<i>rpmA</i>	4.85
	PSPTO_0637	50S ribosomal protein L24	<i>rplX</i>	4.81
	PSPTO_4426	50S ribosomal protein L13	<i>rplM</i>	4.77
	PSPTO_0618	50S ribosomal protein L7/L12	<i>rplL</i>	4.75
	PSPTO_0642	50S ribosomal protein L18	<i>rplR</i>	4.71
	PSPTO_0797	50S ribosomal protein L21	<i>rplU</i>	4.70
	PSPTO_0643	30S ribosomal protein S5	<i>rpsE</i>	4.60

Table 6.13 (Continued)

PSPTO_0090	50S ribosomal protein L33	<i>rpmG</i>	4.59
PSPTO_0633	50S ribosomal protein L16	<i>rplP</i>	4.57
PSPTO_0627	50S ribosomal protein L4	<i>rplD</i>	4.57
PSPTO_0649	30S ribosomal protein S11	<i>rpsK</i>	4.53
PSPTO_0650	30S ribosomal protein S4	<i>rpsD</i>	4.42
PSPTO_0615	50S ribosomal protein L11	<i>rplK</i>	4.39
PSPTO_0628	50S ribosomal protein L23	<i>rplW</i>	4.38
PSPTO_0641	50S ribosomal protein L6	<i>rplF</i>	4.33
PSPTO_0640	30S ribosomal protein S8	<i>rpsH</i>	4.27
PSPTO_0539	30S ribosomal protein S21	<i>rpsU</i>	4.18
PSPTO_3835	50S ribosomal protein L32	<i>rpmF</i>	4.14
PSPTO_0652	50S ribosomal protein L17	<i>rplQ</i>	3.98
PSPTO_0626	50S ribosomal protein L3	<i>rplC</i>	3.86
PSPTO_0617	50S ribosomal protein L10	<i>rplJ</i>	3.74
PSPTO_1473	30S ribosomal protein S16	<i>rpsP</i>	3.71
PSPTO_5136	50S ribosomal protein L31	<i>rpmE</i>	3.68
PSPTO_5615	50S ribosomal protein L34	<i>rpmH</i>	3.58
PSPTO_4019	Ribosomal protein S12 methylthiotransferase	<i>rimO</i>	3.50
PSPTO_0639	30S ribosomal protein S14	<i>rpsN</i>	3.44
PSPTO_1750	30S ribosomal protein S1	<i>rpsA</i>	3.31
PSPTO_0622	30S ribosomal protein S7	<i>rpsG</i>	3.25
PSPTO_0648	30S ribosomal protein S13	<i>rpsM</i>	3.18

Table 6.13 (Continued)

PSPTO_	1534	30S ribosomal protein S2	<i>rpsB</i>	3.12
PSPTO_	4862	Ribosomal protein L11 methyltransferase	<i>prmA</i>	2.71
PSPTO_	0647	50S ribosomal protein L36	<i>rpmJ</i>	2.69
PSPTO_	2381	50S ribosomal protein L20	<i>rplT</i>	2.50
PSPTO_	2380	50S ribosomal protein L35	<i>rpmI</i>	2.06
PSPTO_	4183	50S ribosomal protein L31 type B	<i>rpmE2</i>	-2.45
ATP synthase				
PSPTO_	5598	ATP synthase epsilon chain	<i>atpC</i>	6.45
PSPTO_	5603	ATP synthase subunit b	<i>atpF</i>	5.48
PSPTO_	5599	ATP synthase subunit beta	<i>atpD</i>	4.76
PSPTO_	5605	ATP synthase subunit a	<i>atpB</i>	4.59
PSPTO_	5602	ATP synthase subunit delta	<i>atpH</i>	4.51
PSPTO_	5600	ATP synthase gamma chain	<i>atpG</i>	3.93
PSPTO_	5601	ATP synthase subunit alpha	<i>atpA</i>	3.86
PSPTO_	5604	ATP synthase subunit c	<i>atpE</i>	3.37
Chromosome replication and cell division				
PSPTO_	4428	Cell division protein ZapE	<i>zapE</i>	4.15
PSPTO_	1472	Signal recognition particle protein	<i>ffh</i>	3.50
PSPTO_	0469	Cell division protein ZapA	<i>zapA</i>	3.48
PSPTO_	0001	Chromosomal replication initiator protein DnaA	<i>dnaA</i>	2.56
PSPTO_	0003	DNA replication and repair protein RecF	<i>recF</i>	2.52
PSPTO_	4405	Cell division protein FtsQ	<i>ftsQ</i>	2.07
PSPTO_	1555	Cell division protein FtsB	<i>ftsB</i>	1.92

Table 6.13 (Continued)

PSPTO_3511	Cell division inhibitor SulA		-2.10
Electron transport chain			
PSPTO_3376	NADH dehydrogenase I, M subunit	<i>nuoM</i>	5.68
PSPTO_3365	NADH-quinone oxidoreductase subunit A	<i>nuoA</i>	4.96
PSPTO_3373	NADH dehydrogenase I, J subunit	<i>nuoJ</i>	4.70
PSPTO_3374	NADH-quinone oxidoreductase subunit K	<i>nuoK</i>	4.59
PSPTO_3368	NADH dehydrogenase I, E subunit	<i>nuoE</i>	3.57
PSPTO_3372	NADH-quinone oxidoreductase subunit I	<i>nuoI</i>	3.44
PSPTO_3369	NADH dehydrogenase I, F subunit	<i>nuoF</i>	3.20
PSPTO_3366	NADH-quinone oxidoreductase subunit B	<i>nuoB</i>	2.81
PSPTO_3370	NADH-quinone oxidoreductase subunit G	<i>nuoG</i>	2.80
PSPTO_3367	NADH-quinone oxidoreductase subunit C/D	<i>nuoC</i>	2.65
PSPTO_1326	Cytochrome o ubiquinol oxidase, subunit I	<i>cyoB</i>	2.46
PSPTO_1327	Cytochrome o ubiquinol oxidase, subunit III	<i>cyoC</i>	2.34
PSPTO_1328	Cytochrome o ubiquinol oxidase, subunit IV	<i>cyoD</i>	2.22
Trehalose and alpha-glucan biosynthesis			
PSPTO_2762	1,4-alpha-glucan branching enzyme GlgB	<i>glgB</i>	-4.88
PSPTO_3128	Glycosyl hydrolase, family 13		-5.53
PSPTO_3133	Methyltransferase, putative		-5.66
PSPTO_2761	Alpha-amylase family protein		-6.34
PSPTO_3131	Uncharacterized protein		-6.51
PSPTO_2760	alpha-amylase family protein glgZ	<i>glgZ</i>	-7.43

Table 6.13 (Continued)

PSPTO_3125	Glycogen synthase	<i>glgA</i>	-7.55
PSPTO_3130	Glycogen operon protein GlgX homolog	<i>glgX</i>	-7.95
PSPTO_3132	Conserved domain protein		-8.33
PSPTO_3134	Glycosyl transferase, group 2 family protein		-8.98
PSPTO_3126	Malto-oligosyltrehalose trehalohydrolase		-9.36
PSPTO_3127	4-alpha-glucanotransferase	<i>malQ</i>	-11.92
PSPTO_3129	Uncharacterized protein		-12.54

Table 6.14: small RNAs differentially expressed between 1 HPI and 6 HPI
a. Major biological function category that genes fall under

Category^a	Locus Number	Gene name	Fold Change
small RNAs			
	PSPTO_5653	<i>cob-1</i>	5.59
	PSPTO_5662	<i>S15</i>	5.35
	PSPTO_5655	<i>cob-2</i>	4.93
	PSPTO_5673	<i>rsmX-3</i>	-2.34
	PSPTO_5670	<i>spf</i>	-3.10
	PSPTO_5668	<i>crcZ</i>	-3.30
	PSPTO_5669	<i>crcX</i>	-4.16
	PSPTO_5652	<i>rsmZ</i>	-7.46
	PSPTO_5664	<i>p24</i>	-9.49
	PSPTO_5660	<i>P16</i>	-10.13
	PSPTO_5671	<i>rsmX-1</i>	-10.57
	PSPTO_5672	<i>rsmX-2</i>	-10.60
	PSPTO_5649	<i>prrf1</i>	-24.39

Table 6.15: Carbon uptake and metabolism genes differentially expressed between 1 HPI and 6 HPI

- a. Major biological function category that genes fall under
- b. The names and descriptions of proteins according to the Uniprot database (112).

Category ^a	Locus Number	Protein names ^b	Gene name	Fold Change
Trehalose uptake				
	PSPTO_3735	ABC transporter		-2.68
Fructose Metabolism				
	PSPTO_0956	Phosphotransferase system, fructose-specific IIBC component		3.32
	PSPTO_0955	Phosphofructokinase	<i>fruK</i>	2.52
	PSPTO_0953	Fructose repressor FruR, putative		-2.07
	PSPTO_2701	Fructokinase		-2.38
Maltose uptake				
	PSPTO_0886	Maltose/maltodextrin ABC transporter, ATP-binding protein	<i>malkK</i>	2.82
	PSPTO_0887	Sugar ABC transporter, permease protein		2.93
	PSPTO_0889	Sugar ABC transporter, periplasmic sugar-binding protein		2.84
	PSPTO_0888	Sugar ABC transporter, permease protein		2.18
Sucrose metabolism/uptake				
	PSPTO_0885	Invertase		4.30
	PSPTO_0890	Sucrose porin	<i>scrY</i>	3.09
Glucose uptake				
	PSPTO_1294	Glucose ABC transporter, permease protein, putative		-2.29
	PSPTO_1293	Glucose ABC transporter, permease protein, putative		-2.45
	PSPTO_1295	Glucose ABC transporter, ATP-binding protein	<i>gltK</i>	-2.56
	PSPTO_1292	Glucose ABC transporter, periplasmic glucose-binding protein, putative		-4.17
Xylose uptake				
	PSPTO_3005	D-xylose ABC transporter, permease protein	<i>xylH</i>	-3.29
	PSPTO_3003	D-xylose ABC transporter, periplasmic D xylose binding protein	<i>xylF</i>	-5.68
	PSPTO_3003	Xylose isomerase	<i>xylA</i>	-4.50

Table 6.15 (Continued)

3002	PSPTO_	Xylose operon regulatory protein	<i>xylR</i>	-3.63
3001				
Gluconate uptake/metabolism				
3565	PSPTO_	Gluconate permease		5.60
3563	PSPTO_	Gluconate utilization system GNT-I transcriptional repressor	<i>gntR</i>	3.10
Ribose uptake				
2995	PSPTO_	Ribose ABC transporter, ATP-binding protein, putative		4.01
2368	PSPTO_	Ribose ABC transporter, ATP-binding protein	<i>rbsA-1</i>	2.71
2398	PSPTO_	Ribose ABC transporter, ATP-binding protein	<i>rbsA-2</i>	-4.34
2399	PSPTO_	Ribose ABC transporter, periplasmic ribose-binding protein	<i>rbsB-2</i>	-8.99
2400	PSPTO_	Ribose ABC transporter, permease protein	<i>rbsC-2</i>	-25.39
Arabinose uptake				
2640	PSPTO_	L-arabinose ABC transporter, permease protein	<i>araH</i>	-7.23
2639	PSPTO_	Arabinose import ATP-binding protein AraG	<i>araG</i>	-8.00
2638	PSPTO_	L-arabinose-binding periplasmic protein (ABP)	<i>abP</i>	-11.68
Rhizopine uptake				
3488	PSPTO_	Sugar ABC transporter, permease protein		-13.48
3490	PSPTO_	Sugar ABC transporter, periplasmic sugar-binding protein		-68.67
TCA cycle				
1302	PSPTO_	4-hydroxy-2-oxoglutarate aldolase/2-dehydro-3-deoxyphosphogluconate	<i>eda-1</i>	2.90
2195	PSPTO_	Succinate dehydrogenase, cytochrome b556 subunit	<i>sdhC</i>	2.23
2202	PSPTO_	Succinyl-CoA synthetase subunit beta	<i>sucC</i>	2.12
4339	PSPTO_	Fumarate hydratase, class I, putative		2.12
2203	PSPTO_	Succinyl-CoA ligase [ADP-forming] subunit alpha	<i>sucD</i>	1.91
	PSPTO_	Malate synthase G 1	<i>glcB1</i>	-2.03

Table 6.15 (Continued)

0480				
PSPTO_1731	Fumarate hydratase class II (Fumarase C)	<i>fumC</i>	-3.25	
PSPTO_3559	Malate synthase G 2	<i>glcB2</i>	-3.68	
PSPTO_0062	Citrate transporter		-4.23	
PSPTO_3364	Isocitrate lyase	<i>aceA</i>	-4.34	
PSPTO_2287	Methylisocitrate lyase (2-MIC) (MICL)	<i>prpB</i>	-12.32	
PSPTO_2288	Citrate synthase	<i>prpC</i>	-16.58	
PSPTO_2178	4-hydroxy-2-oxoglutarate aldolase/2-dehydro-3-deoxyphosphogluconate	<i>eda-2</i>	-69.04	
GABA metabolism/uptake				
PSPTO_0301	4-aminobutyrate aminotransferase	<i>gabT-2</i>	-1.89	
PSPTO_5356	Gamma-aminobutyrate permease	<i>gabP</i>	-2.27	
PSPTO_2136	2,4-diaminobutyrate 4-transaminase	<i>daT</i>	-3.22	
Pentose phosphate pathway				
PSPTO_1301	6-phosphogluconolactonase	<i>pgl</i>	3.30	
PSPTO_1300	Glucose-6-phosphate 1-dehydrogenase (G6PD)	<i>zwf-1</i>	3.11	
PSPTO_1288	6-phosphogluconate dehydratase	<i>edd</i>	2.73	
PSPTO_3121	Glucose-6-phosphate 1-dehydrogenase (G6PD)	<i>zwf-2</i>	-1.97	

Pto down-regulates flagellar biosynthesis and motility from 1 HPI to 6 HPI. Among down-regulated genes, the only GO terms significantly enriched were associated with locomotion and chemotaxis (Table 6.1). All flagellar and chemotaxis genes that showed differential expression between 1 HPI and 6 HPI were down-regulated (Table 6.2). It is well known that flagella is PAMP in bacterial plant pathogens that causes significant PTI in plants (7). Down-regulation of motility genes is expected in *Pto* in order to evade PTI. Thus, throughout the course of early host colonization, *Pto* was repressing expression of genes related to motility.

Pto experiences reactive oxygen species stress after initial inoculation. Plants initially react to pathogen invasion with a temporary reactive oxygen species (ROS) burst. This ROS burst is thought to mainly play a role in signaling within the plant since plant pathogens, including *Pto*, have ample ways to defend against ROS (278). Bacterial plant-pathogens make use of catalase and superoxide dismutase to detoxify ROS (12, 279). By 6 HPI, *Pto* down-regulated the gene that encodes catalase and the gene for *sodC* (Table 6.3). This is understandable given the fact that the initial ROS burst peaks is over by 6 HPI and no other ROS burst has been observed during a compatible interaction (265). This suggests that ROS detoxification was most important during the initial hours of plant colonization and becomes less important even by 6 HPI. One ROS detoxification gene, *ohr*, was upregulated at 6 HPI as compared to 1 HPI (Table 6.3). *ohr* has been characterized in *Sinorhizobium melliloti* and is necessary for organic peroxide detoxification (280). Plants can produce organic peroxides and they are considered quite toxic. It is possible that *Pto* encounters organic peroxides at later stages of infection.

Pto up-regulates genes involved in coronatine biosynthesis during infection. Genes that code for proteins involved in or associated with coronatine biosynthesis were up-regulated at 6 HPI compared to 1 HPI by 20 to 58-fold (Table 6.4). This was not unexpected as coronatine is known to be produced during *Pto* infection and plays an important role in pathogenesis (281). The tremendous increase in expression between 1 HPI and 6 HPI for the coronatine biosynthesis locus highlighted its importance for *Pto* pathogenicity as only a putative drug or metabolite transporter (PSPTO_0210) showed a greater increase in expression than the most differentially expressed coronatine biosynthesis genes at 6 HPI (Table 6.16). This signifies that coronatine may be secreted by *Pto* at a later phase than effectors during endophytic growth.

Pto up-regulates alginate biosynthesis genes and down-regulates Psl exopolysaccharide biosynthesis genes during infection of N. benthamiana. Alginate is known to be produced by *P. syringae* during pathogenesis (282). Indeed, many genes involved in alginate biosynthesis showed an increase in expression from 10 to 28-fold between 1 HPI and 6 HPI (Table 6.5). The extracytoplasmic function (ECF) sigma-factor AlgU regulates transcription of alginate biosynthesis genes but was not differentially expressed between 1 HPI and 6 HPI. However, it did appear to be expressed at both timepoints (Table 6.17). This suggests that even though *algU* was not differentially expressed between both timepoints, it was likely still active. The genes for the alginate positive transcriptional regulators, *algR*, *algR3*, and *algZ*, were all down-regulated at 6 HPI as compared to 1 HPI (Table 6.5). All three of these genes are necessary for alginate biosynthesis in *P. aeruginosa* and *algR* has been characterized as an essential positive regulator of alginate biosynthesis in *P. syringae*

Table 6.17: Average gene expression of a select number of genes in *Pto* during growth *in planta*

- Major functional category that genes fall under
- Base mean refers to the normalized number of reads associated with each gene at 1 HPI and 6 HPI. Base mean was calculated using DeSeq2 (283).

Category ^a	locus number	gene name	Base mean ^b
Sigma-factor			
	PSPTO_2298	<i>sigX</i>	39333.4
	PSPTO_4224	<i>algU</i>	18381.7
	PSPTO_0537	<i>rpoD</i>	5651.4
	PSPTO_1979	<i>fliA</i>	2137.2
	PSPTO_4453	<i>rpoN</i>	1623.9
	PSPTO_0430	<i>rpoH</i>	909.0
	PSPTO_1565	<i>rpoS</i>	648.0
	PSPTO_1043		174.4
Effectors			
	PSPTO_4001	<i>avrPtoI</i>	57730.5
	PSPTO_0589	<i>hopC1</i>	12086.1
	PSPTO_4331	<i>hopE1</i>	10712.0
	PSPTO_3087	<i>avrPtoB</i>	9808.0
	PSPTO_5354	<i>hopA1</i>	6584.6
	PSPTO_0876	<i>hopD1</i>	5883.3
	PSPTO_1406	<i>hopB1</i>	4004.5
	PSPTO_4722	<i>hopAO1</i>	3989.4
	PSPTO_4776	<i>hopI1</i>	3096.0
	PSPTO_0883	<i>hopR1</i>	2439.1
	PSPTO_1377	<i>avrE1</i>	2282.8
	PSPTO_1375	<i>hopM1</i>	2149.4
	PSPTO_1370	<i>hopN1</i>	2114.8
	PSPTO_0061	<i>hopY1</i>	2081.0
	PSPTO_4720	<i>hopV1</i>	1957.5
	PSPTO_4724	<i>hopD</i>	1837.2
	PSPTO_4718	<i>hopAA1-2</i>	1794.8
	PSPTO_4727	<i>hopG1</i>	1721.7
	PSPTO_4691	<i>hopAD1</i>	1198.1
	PSPTO_4597	<i>hopS1</i>	924.0
	PSPTO_1372	<i>hopAA1-1</i>	704.7
	PSPTO_0502	<i>hopF2</i>	573.2

PSPTO_1568	<i>hopAF1</i>	557.6
PSPTO_5618	<i>hopAT1</i>	474.0
PSPTO_4703	<i>hopAQ1</i>	444.7
PSPTO_0501	<i>hopU1</i>	379.1
PSPTO_4588	<i>hopS2</i>	331.8
PSPTO_4593	<i>hopT1-2</i>	259.1
PSPTO_0473	<i>hopAS1</i>	134.4
PSPTO_0906	<i>hopA11</i>	111.2
PSPTO_4594	<i>hopO1-2</i>	86.6
PSPTO_0901	<i>hopAG1</i>	76.3
PSPTO_0474	<i>hopAS1</i>	56.9
PSPTO_4590	<i>hopT2</i>	38.7
PSPTO_4592	<i>hopO1-3</i>	28.7
PSPTO_4732	<i>hopQ1-2</i>	17.7
PSPTO_4591	<i>hopO1-3</i>	13.6
PSPTO_1022	<i>hopAM1-1</i>	0.0

(284-287). The down-regulation of these genes at 6 HPI while genes involved in alginate biosynthesis were up-regulated suggests that another mechanism that positively regulates alginate production was active in *Pto* during growth *in planta*.

In addition to alginate, *Pto* can also produce the EPSs cellulose, Psl, and levan (60). When comparing 1 HPI to the 6 HPI timepoint, genes involved in Psl biosynthesis were down-regulated (Table 6.5). Psl is essential for biofilm development in *P. aeruginosa* (288). *Pto* forms microcolonies during endophytic growth, but the downregulation of Psl biosynthesis genes suggests that Psl is not a major component of these microcolonies. Genes involved in cellulose biosynthesis were expressed at a lower level than Psl biosynthesis genes during growth *in planta*, suggesting that cellulose does not form a major component of *Pto* microcolonies either. Cellulose is regulated through c-di-GMP production and through the transcriptional repressor AmrZ in *Pto* (116, 136). *Pto* has a total of 22 annotated diguanylate cyclases in its genome and one HD-GYP domain protein. A majority of the diguanylate cyclases and the single HD-GYP domain protein in *Pto* were down-regulated at 6 HPI as compared to 1 HPI (Table 6.6). At the same time, there is no difference in *amrZ* expression between 1 HPI and 6 HPI. This further suggests that cellulose is not produced in abundance by *Pto* during growth *in planta* from 1 HPI to 6 HPI.

Pto considers the plant apoplast to be iron rich. *Pto* uses pyoverdine, yersiniabactin, and citrate as siderophores (289). Plants store iron as Fe (III) dicitrate in the leaf apoplast and *Pto* is able to take up iron chelated to citrate (290). We found that genes coding for pyoverdine and yersiniabactin were down-regulated between 1 HPI and 6

HPI, while genes for iron citrate uptake were up-regulated (Table 6.7). Thus, the leaf apoplast does seem to be considered iron-rich for *Pto*.

Pto experiences osmotic stress during initial growth in planta. The plant apoplast is water-limited and *Pto* uses compatible solutes as well as several effectors to cope with hyperosmotic conditions (291, 292). *Pto* is thought to primarily use four different compatible solutes, betaine, choline, N-acetylglutaminylglutamine amide (NAGGN), and trehalose (291). Our data suggests that at 6 HPI *Pto* was primarily producing the compatible solute betaine or choline, as genes involved in betaine synthesis and choline metabolism were up-regulated at 6 HPI as compared to 1 HPI (Table 6.8). In comparison, genes involved in NAGGN biosynthesis and trehalose biosynthesis were down-regulated at 6 HPI as compared to 1 HPI (Table 6.8). Plants produce quite a bit of choline and it is thought that *Pto* uses host choline during pathogenesis (267). Our data supports this finding as the gene that codes for BetI was upregulated along with choline oxidase at 6 HPI. BetI is a transcriptional repressor that is inhibited by the presence of choline (267). This leads to increased transcription of *betI* and a choline oxidase. Since we observed increased expression of *betI* and a choline oxidase, this suggested that choline is likely being taken up by *Pto* during growth *in planta* (Table 6.8).

Changes in sigma-factor expression. Overall changes in gene expression are directed by sigma-factors. Identifying sigma-factors that are differentially expressed or highly expressed *in planta* would hint at the overall change in gene expression patterns occurring in *Pto* during early stages of infection and provide regulons that are considered important for initial colonization of a host. Among sigma factors in *Pto*,

only *rpoD* increased in expression between 1 HPI and 6 HPI, while *rpoH*, *rpoS*, *hrpL*, and several sigma-70 family proteins showed a decrease in expression (Table 6.9).

Looking at overall expression of *Pto* genes during growth *in planta* it became apparent that several sigma factors were expressed at 1 HPI and 6 HPI, but not differentially expressed. This included *sigX*, *algU*, *fliA*, *rpoN*, and PSPTO_1043 (Table 6.17). Of note, *sigX* and *algU* appeared to be highly expressed at 1 HPI and 6HPI, suggesting that they may be important during the initial stages of *Pto* growth *in planta*.

Lipopolysaccharide production in planta. Genes that code for proteins involved in Lipopolysaccharide (LPS) biosynthesis were up-regulated between 1 HPI and 6 HPI (Table 6.10). Lipid A is a known MAMP however LPS is needed for virulence in *P. syringae* (293, 294). As the genes for LPS biosynthesis are up-regulated at 6 HPI as compared to 1 HPI, it would suggest that LPS is essential for *Pto* during growth *in planta*.

Efflux pump activity suggests Pto encounters antimicrobial metabolites. *Pto* produces several characterized multidrug efflux pumps. The most well characterized are the Sax efflux pumps involved in efflux of isothiocyanate during growth in *A. thaliana* (295). Several multidrug efflux pumps, including *saxB*, *saxF*, and *saxG* increase in expression between 1 HPI and 6 HPI (Table 6.11). Upregulation of these efflux pumps would suggest that *Pto* is encountering an antimicrobial during growth *in planta*.

Effector gene regulation *in planta.* Effector delivery by *Pto* is thought to occur around 3 to 4 HPI (296). One would expect effectors to be delivered in a coordinated fashion and that they would be delivered by 6 HPI. However, we found that at 6 HPI some effector genes were up-regulated and others were down-regulated (Figure 6.1,

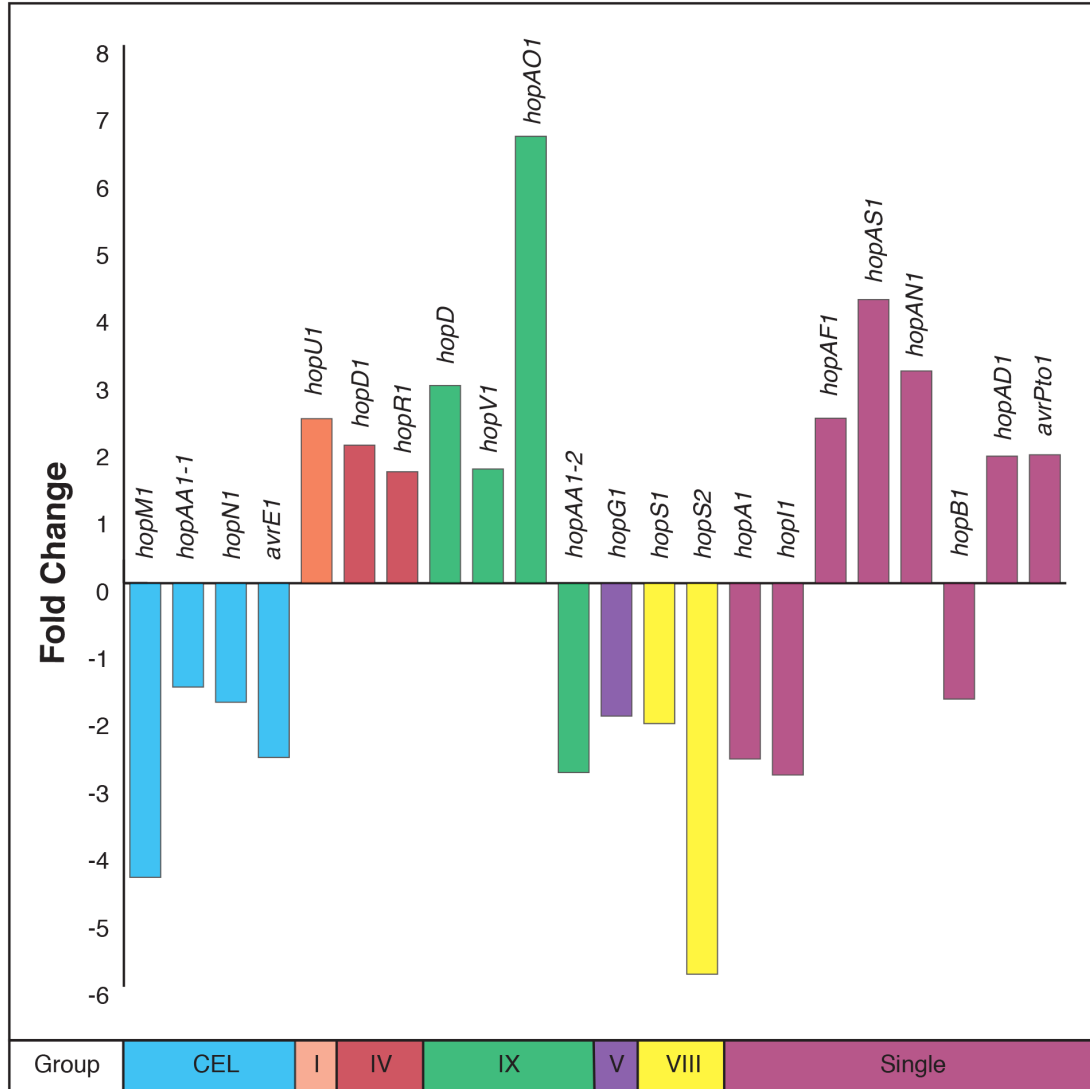


Figure 6.1: Changes in gene expression of various effectors at 6 HPI as compared to 1 HPI. The y-axis is the fold-change in expression for each effector at 6 HPI as compared to 1 HPI. The effectors are color coded according to the group they have been assigned. The key at the bottom of the figure shows the corresponding group assigned to each color. The group labelled as single corresponds to effectors that do not cluster with other effectors in the genome.

Table 6.12). This does not hold true for the T3SS machinery, harpins, or T3SS regulators (HrpL, HrpR, and HrpS) as genes in all three of these categories were down-regulated by 6 HPI (Table 6.12). The fact that certain effectors showed increased transcription at 6 HPI while *hrpL* was down-regulated, suggests complex regulation of effector genes *in planta*.

There are 36 known effectors in *Pto* and only 22 of them were differentially expressed between 1 HPI and 6 HPI. Effectors are grouped into clusters according to location in the genome of *Pto* (297). There are also several effectors that are found individually throughout the genome. Effectors from clusters I, IV, V, VIII, IX, and the conserved effector locus (CEL) all showed differential expression between 1 HPI and 6 HPI (Figure 6.1, Table 6.12). In addition, eight effectors found individually throughout the genome also showed differential expression between 1 HPI and 6 HPI. All four effectors in the CEL cluster showed decreased expression between 1 HPI and 6 HPI, with *hopAAI-1* and *hopNI* showing a weak decrease in expression. *hopDI* and *hopRI* from cluster IV showed increased expression between 1 HPI and 6 HPI. *hopQI-1* did not show differential expression since this is the Δ *hopQI-1* *Pto* strain. In cluster IX, *hopD* showed an increase in expression, *hopVI* showed a slight increase in expression, *hopAOI* showed an increase in expression and *hopAAI-2* showed a decrease in expression. This was the only cluster with multiple effectors expressed that did not have similar expression patterns among effectors. The increased expression of *hopD* was somewhat unexpected as an ISPsy5 element is inserted the middle of the effector and is thought to render the effector inactive. The differential expression,

along with the relatively high expression of *hopD* as compared to other effectors, begs the question if this was an artifact or if *hopD* was transcribed and translated. Several effectors are accompanied by a chaperone. Of the differentially expressed effectors, AvrE1, HopM1, HopN1, HopS1, HopS2, and HopV1 all have chaperones and all, except for *hopV1*, showed decreased expression between 1 HPI and 6 HPI. The gene *hopANI* showed increased in expression between 1 HPI and 6 HPI. *hopANI* is considered a pseudogene but is found in a putative operon with several other genes, including a putative class II aldolase (PSPTO_5062). The orthologous proteins for HopAN1 and for the aldolase are virulence factors in *Pectobacterium carotovorum* (298). PSPTO_5062 was up-regulated at 6 HPI as compared to 1 HPI and may be worth investigating in the future.

The range at which effectors were expressed varied widely. The most highly expressed effector with a base mean of 55,000 was *avrPto* while the least expressed effector was *hopOI-3* with a base mean of 13 (Table 6.17). The next most highly expressed effectors were *hopHI*, *hopE1*, *hopC1*, and *avrPtoB*. It was interesting that *hopHI*, *hopE1*, and *hopC1* were more highly expressed *in planta* as compared to the expression level of other effectors as deletion of *hopHI*, *hopE1*, or *hopC1*, does not significantly affect virulence of *Pto* in *N. benthamiana* (146). AvrPto and AvrPtoB are considered important for virulence. One might expect effectors known to be involved in virulence and symptom development, like HopM1, AvrE1, HopAA1-1, or HopG1, to be more highly expressed than most other effectors. However, the opposite was true. Among viable effectors, the CEL effectors had lower base means. Only effectors with truncations or known to be weakly expressed had lower base means than the CEL

effectors. *hopG1* was also weakly expressed compared to other effectors. HopM1, AvrE1, and HopAA1-1, can all individually elicit cell death in *N. benthamiana* (4, 125). It is possible that by keeping by expression levels low, *Pto* may be attempting to discreetly evade the plant immune system and not elicit cell death while reprogramming plant cells. One thing to note about the five highly expressed effectors are that all of them except HopH1 are known to be involved in suppressing PTI (145, 299, 300). It could be that the high expression of these effectors is necessary to subvert the immune system and allow effectors like HopM1 and AvrE1 to do their job.

***Pto* is metabolically active at 6 HPI.** The metabolic state of *Pto* during early stages of infection is currently unknown. One way to determine the metabolic state of cells is to examine changes in ribosomal biosynthesis, ATP production, the electron transfer chain, cell replication, and glycogen biosynthesis. A proxy to determining ribosome biosynthesis can be determined by looking at changes gene expression of ribosomal proteins and the ATP dependent RNA helicase *DeaD*. There was increased expression of genes involved in ribosomal protein production and increased expression of *deaD* at 6 HPI as compared to 1 HPI (Table 6.13). This suggests that proteins were being actively produced by *Pto* at 6 HPI. *Pto* gene expression showed signs of replication at 6 HPI. Protein biosynthesis and replication would use a significant amount of energy that would require respiration to be active and energy storage mechanisms to be inactive. At 6 HPI, genes involved in ATP synthesis and the electron transport chain were both up-regulated, while genes involved in glycogen biosynthesis were down-regulated (Table 6.13). In addition, several genes involved in replication were up-regulated at 6 HPI as compared to 1 HPI (Table 6.13). Taken together, *Pto* appeared to

be actively replicating and growing within the plant by 6 HPI. If there was any period during the initial stages of infection where *Pto* was attempting to mask its presence or remain in a dormant, protective state, it had already come and gone by 6 HPI.

***Pto* is using preferred carbon sources by 6 HPI.** *Pto* uses carbon catabolite repression (CCR) to make use of preferred carbon sources in its environment (301). In *Pto*, like all other *Pseudomonas*, CCR is regulated post-translationally by the protein Crc (256). Increased activity of Crc results in the use of preferred carbon sources by *Pto* (256). The activity of Crc can be determined by the transcription of the two Crc binding sRNAs *crcX* and *crcZ* (301). Increased transcription of these sRNAs results in sequestration of Crc and the use of less preferred carbon sources by *Pto*. Expression of *crcX* and *crcZ* was down-regulated when comparing 6 HPI to 1 HPI, suggesting that Crc was active and *Pto* was making use of preferred carbon sources (Table 6.14). To further support this hypothesis, 77 of the 91 predicted Crc targets in *Pto* were down-regulated at 6 HPI as compared to 1 HPI (Table 6.18). Many of these genes are involved in carbon metabolism and give insight into what carbon sources *Pto* makes use of during pathogenesis (Table 6.18, Figure 6.2). Glucose, trehalose, and arabinose are among the carbon sources less preferred by *Pto* at 6 HPI. On the other hand, gluconate, sucrose, maltose, fructose, arginine/ornithine, and glutamate appeared to all to be among preferred carbon sources for *Pto* at 6 HPI. In addition, the gene encoding citrate synthase was down-regulated at 6 HPI as compared to 1 HPI (Table 6.7). This is not to say that citrate was not being taken up by *Pto* as genes involved in the transport of ferric citrate were up-regulated at 6 HPI and it is possible that exogenous citrate was used by *Pto in planta* when it was taken up with iron. It is thought that *Pto*

Table 6.18: Genes that are differentially expressed in *Pto* between 1 HPI and 6 HPI and are also putatively regulated by Crc

- a. Protein description as determined by the Uniprot database (112).

Locus Number	Protein Description^a	Fold-Change
PSPTO_3490	Sugar ABC transporter, periplasmic sugar-binding protein	-68.67
PSPTO_2722	Oxidoreductase, Gfo/Idh/MocA family	-40.63
PSPTO_1623	Uncharacterized protein	-33.92
PSPTO_3500	IolC protein	-28.92
PSPTO_3499	xanthine phosphoribosyltransferase (XPRTase) (EC 2.4.2.22)	-28.06
PSPTO_3494	Inositol 2-dehydrogenase (EC 1.1.1.18)	-23.91
PSPTO_3495	IolD protein	-22.43
PSPTO_3496	IolI protein	-20.83
PSPTO_1825	Acetyl-coenzyme A synthetase (AcCoA synthetase) (Acs)	-19.39
PSPTO_2288	Citrate synthase	-16.58
PSPTO_2143	Uncharacterized protein	-15.28
PSPTO_3488	Sugar ABC transporter, permease protein	-13.48
PSPTO_0993	Uncharacterized protein	-13.04
PSPTO_2472	Methyl-accepting chemotaxis protein	-12.63
PSPTO_2638	L-arabinose-binding periplasmic protein (ABP)	-11.68
PSPTO_2739	Acyl-CoA dehydrogenase, putative	-11.45
PSPTO_0728	Aldehyde dehydrogenase family protein	-11.32
PSPTO_1953	Uncharacterized protein	-11.18
PSPTO_3155	Pyruvate ferredoxin/flavodoxin oxidoreductase family protein	-10.46
PSPTO_5352	Methyl-accepting chemotaxis protein	-9.88
PSPTO_2636	Aldose 1-epimerase (EC 5.1.3.3) (Galactose mutarotase)	-9.85
PSPTO_1149	Uncharacterized protein	-9.78
PSPTO_3126	Malto-oligosyltrehalose trehalohydrolase (MTHase)	-9.36
PSPTO_2338	Protocatechuate 3,4-dioxygenase, beta subunit	-8.91
PSPTO_2765	Uncharacterized protein	-8.13
PSPTO_3771	Major facilitator family transporter	-7.87
PSPTO_2640	L-arabinose ABC transporter, permease protein	-7.23
PSPTO_4296	Metabolite-proton symporter, putative	-7.18
PSPTO_0743	Oxidoreductase, short chain dehydrogenase/reductase family	-6.58
PSPTO_3699	Methyl-accepting chemotaxis protein	-6.44
PSPTO_0518	Tryptophan 2-monooxygenase, putative	-5.97
PSPTO_3003	D-xylose ABC transporter, periplasmic-D xylose binding protein	-5.68

Table 6.18 (Continued)

PSPTO_1296	Porin B	-5.58
PSPTO_3284	Major facilitator family transporter	-5.50
PSPTO_5087	Malonate decarboxylase, alpha subunit	-5.50
PSPTO_3569	Uncharacterized protein	-5.28
PSPTO_4232	TctC protein, putative	-4.63
PSPTO_2637	Senescence marker protein-30 family protein	-4.58
PSPTO_3002	Xylose isomerase (EC 5.3.1.5)	-4.50
PSPTO_2340	4-hydroxybenzoate transporter	-4.25
PSPTO_1292	Glucose ABC transporter, periplasmic glucose-binding protein, putative	-4.17
PSPTO_3741	Sigma-54 dependent transcriptional regulator	-4.09
PSPTO_1274	Cold shock domain family protein	-3.89
PSPTO_2707	Mannitol ABC transporter, periplasmic mannitol-binding protein	-3.83
PSPTO_3164	Acetyl-CoA acetyltransferase	-3.82
PSPTO_0312	Uncharacterized protein	-3.75
PSPTO_3740	ABC transporter, ATP-binding protein	-3.65
PSPTO_1720	Outer membrane protein	-3.65
PSPTO_3001	Xylose operon regulatory protein	-3.63
PSPTO_1051	TRAP dicarboxylate transporter, DctP subunit	-3.56
PSPTO_1054	Outer membrane porin, OprD family	-3.41
PSPTO_1906	Major facilitator family transporter	-3.35
PSPTO_3501	Transcriptional regulator, RpiR family	-3.26
PSPTO_1800	Uncharacterized protein	-3.02
PSPTO_4082	Oxidoreductase, short chain dehydrogenase/reductase family	-2.99
PSPTO_4638	Carbon starvation protein CstA	-2.93
PSPTO_5553	Methyl-accepting chemotaxis protein	-2.80
PSPTO_0136	Alginate regulatory protein AlgR3	-2.75
PSPTO_0376	Cation efflux family protein	-2.73
PSPTO_3456	3-oxoacid CoA-transferase, subunit B family	-2.70
PSPTO_3735	ABC transporter, periplasmic substrate-binding protein, putative	-2.68
PSPTO_3555	Glycolate oxidase, subunit GlcD	-2.59
PSPTO_2703	D-mannonate oxidoreductase	-2.57
PSPTO_3705	Enol-CoA hydratase/isomerase family protein	-2.53
PSPTO_3777	Membrane protein, putative	-2.47
PSPTO_1053	Uronate dehydrogenase (EC 1.1.1.203)	-2.41
PSPTO_2949	Oxidoreductase, short-chain	-2.40

Table 6.18 (Continued)

	dehydrogenase/reductase family	
PSPTO_4548	MFS transporter, phthalate permease family	-2.35
PSPTO_0107	Uncharacterized protein	-2.31
PSPTO_5147	Polyhydroxyalkanoate granule-associated protein PhaF	-2.27
PSPTO_5080	Malonate transporter, MadL subunit	-2.22
PSPTO_2944	p-hydroxycinnamoyl CoA hydratase/lyase	-2.14
PSPTO_5219	MFS transporter, phthalate permease family	-2.10
PSPTO_5216	Lipoprotein, NLPA family	-2.07
PSPTO_0957	Acetyl-CoA acetyltransferase	-2.07
PSPTO_4427	Transcriptional regulator, AraC family	-1.97
PSPTO_1127	Uncharacterized protein	-1.88
PSPTO_1290	DNA-binding response regulator	2.07
PSPTO_0308	Sulfate-binding protein	2.22
PSPTO_3654	Acetyltransferase, GNAT family	2.77
PSPTO_5500	Sodium/alanine transporter	2.81
PSPTO_5060	Oxidoreductase, acting on the CH-OH group of donors, NAD or NADP as acceptor	2.84
PSPTO_0889	Sugar ABC transporter, periplasmic sugar- binding protein	2.84
PSPTO_4495	Phosphoglucosamine mutase (EC 5.4.2.10)	3.01
PSPTO_1287	Glyceraldehyde-3-phosphate dehydrogenase (EC 1.2.1.-)	3.10
PSPTO_0956	Phosphotransferase system, fructose-specific IIBC component	3.32
PSPTO_0954	Phosphoenolpyruvate-protein phosphotransferase, EI/HPr/EIIA components	3.81
PSPTO_0633	50S ribosomal protein L16	4.57
PSPTO_0642	50S ribosomal protein L18	4.71
PSPTO_3565	Gluconate permease	5.60
PSPTO_1239	Alginate production protein AlgE	16.98

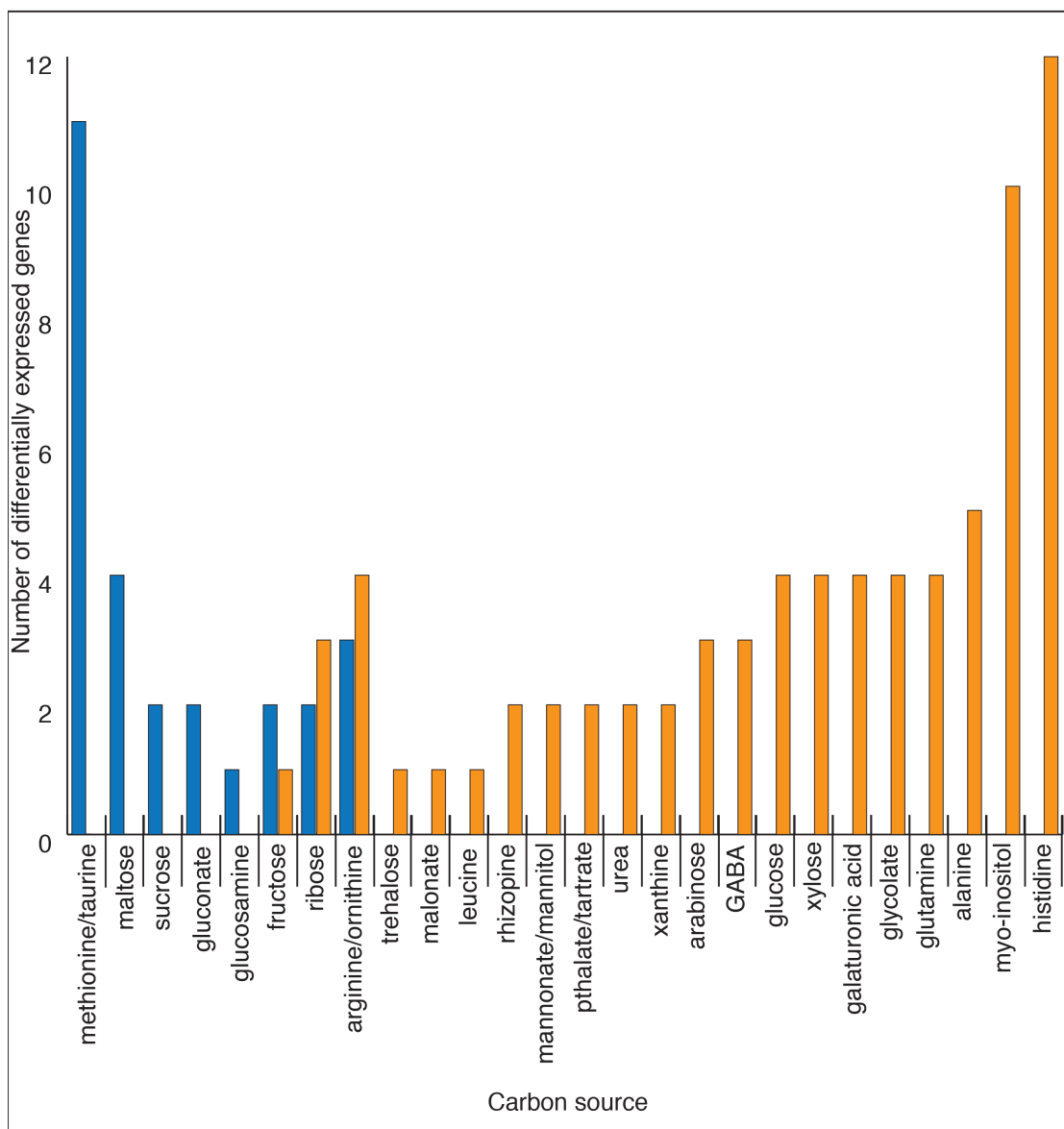


Figure 6.2: Number of genes differentially expressed in the genome of *Pto* related to metabolite uptake. Bars in blue correspond to up-regulated genes, while bars in orange correspond to down-regulated genes.

uses glucose, GABA, and myo-inositol as carbon sources *in planta* (91, 302). Genes involved in uptake of these carbon sources were all down-regulated by 6 HPI as compared to 1 HPI, suggesting that those carbon sources were not preferred by *Pto* after effector delivery (Table 6.15). A set of genes putatively involved in galactose or galacturonic acid metabolism were among the most highly down-regulated genes at 6 HPI as compared to 1 HPI (Table 6.15). This suggests that galactose or galacturonic acid could be an initial carbon source *Pto* uses during pathogenesis, but not used after effector delivery.

Known *N. benthamiana* ETI and PTI marker genes respond to high *Pto* inocula titer as expected during compatible interactions. *N. benthamiana* is typically inoculated with *Pto* at 1×10^4 cfu/mL (4). However, we determined that *Pto* inoculated at 5×10^8 cfu/mL was needed in order to collect enough bacterial RNA at 1 HPI and 6 HPI to profile changes in gene expression. As such high inocula is not normally used during a compatible interaction and there was the chance this amount of inocula could overwhelm *N. benthamiana* plants, *N. benthamiana* response to $\Delta hopQ1-1$, $\Delta hrcQb-U$, and WT *Pto* inoculated at 5×10^8 cfu/mL was compared in order to determine whether ETI or PTI occurred in the plants inoculated with the $\Delta hopQ1-1$ *Pto* strain. The gene *HINI* has previously been used as a marker gene for ETI in tobacco while *acre31* has previously been used as a PTI marker gene for tobacco plants inoculated with *P. syringae* (303, 304). Expression levels of *HINI* and *acre31* were compared between the *N. benthamiana* plants inoculated with the different *Pto* strains at 6 HPI and a mock inoculated *N. benthamiana* plant. *N.*

benthamiana tissue inoculated with the $\Delta hopQ1-1$ strain expressed lower levels of *HIN1* and *acre31* at 6 HPI than *N. benthamiana* tissue inoculated with the $\Delta hrcQb-U$ strain or WT (Figure 6.3). One would expect expression of *HIN1* to be the same between WT and $\Delta hopQ1-1$ *Pto* inoculated *N. benthamiana* plants if ETI was occurring in the $\Delta hopQ1-1$ *Pto* inoculated *N. benthamiana* plant. At the same time, one would expect the expression of *acre31* to be similar between the $\Delta hrcQb-U$ and the $\Delta hopQ1-1$ strain inoculated *N. benthamiana* plants if PTI was occurring in the $\Delta hopQ1-1$ strain inoculated *N. benthamiana* plant. Since this was not the case, we concluded that initial inocula at 5×10^8 cfu/mL allowed for a compatible interaction between *Pto* and *N. benthamiana* to occur.

HIN1 from *Nicotiana tabacum* is homologous to the gene Niben101Scf08020g06001 in *N. benthamiana*, while *acre31* from *N. tabacum* is homologous to the gene Niben101Scf07586g00004 in *N. benthamiana*. According to RNA-seq data, gene Niben101Scf08020g06001 and Niben101Scf07586g00004 were down-regulated between 1 HPI and 6 HPI (29-fold and 175-fold, respectively). Thus, it appeared that the $\Delta hopQ1-1$ strain lowered the defense response of *N. benthamiana*.

Changes in *N. benthamiana* defense genes during early stages of infection.

Differentially expressed genes were annotated and genes of interest were grouped according to putative function and GO annotation (Table 6.19)¹⁰. During a compatible interaction, *Pto* will dampen the defense response in plants using effector delivery.

Genes involved in defense signaling during biotic stress commonly fall into certain

¹⁰ Table 6.19 is over 7000 lines long. Due to the length of this table it has been included in the supplementary data for this thesis.

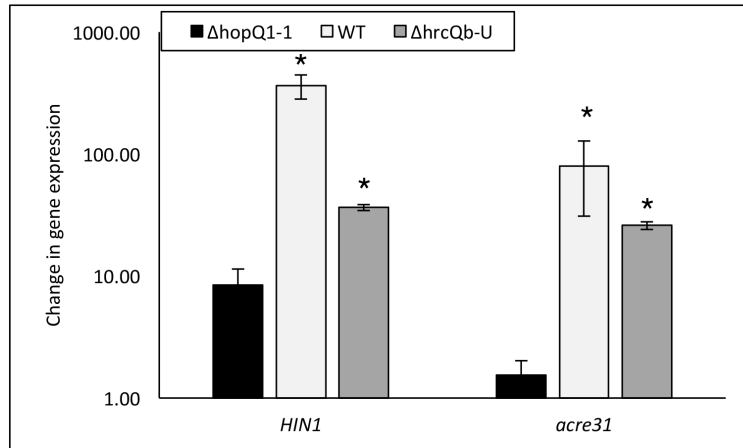


Figure 6.3: Change in expression of *HIN1* and *acre31* in *N. benthamiana* infected with 5×10^8 cfu/mL of the $\Delta hopQ1-1$, WT, or $\Delta hrcQb-U$ strain at 6 HPI as compared to a mock inoculated *N. benthamiana* plant. The error bars represent standard error between samples. A * represents a significant difference between expression of that particular gene in either WT or the $\Delta hrcQb-U$ strain as compared to the $\Delta hopQ1-1$ strain.

categories, including mitogen-activated kinases (MAP kinases), Ankyrin domain proteins, ethylene sensitive transcription factors, WRKY domain transcription factors, NB-LRRs, calcium and calmodulin binding proteins, and serine/threonine protein kinases (305-310). Differential expression of genes involved in defense signaling occurred and are listed Table 6.21¹¹. While certain putative defense genes were down-regulated one hundred-fold or more between 1 HPI and 6 HPI, other putative defense-related genes showed a noticeable increase in expression. Among the most highly down-regulated genes between 1 HPI and 6 HPI, were a WRKY transcription factor and an ethylene responsive transcription factor. The strong down regulation of both transcription factors suggests that they were resistance genes important in plant defense that *Pto* inactivated during infection.

Discussion

In this paper, we describe a method through which one can capture gene expression in both *Pto* and a host during the initial hours of pathogen inoculation. This allowed us to get a glimpse into the mechanism through which *Pto* overcomes PTI before T3E delivery and also observe how *Pto* interacts with the plant soon after T3E deployment. The ability to visualize *Pto* gene expression *in planta* allows for future experiments where *Pto* can be used to probe changes in the apoplastic environment under different conditions. For example, many questions still remain about PTI and how priming a plant allows for it to become at least partially resistant to a pathogen. Dual RNA-seq would allow for one to compare differentially expressed genes in *Pto*

¹¹ Table 6.21 is over 500 lines long. Due to its length it has been included in the supplementary data of this thesis.

and the host when inoculated in a PTI primed versus a PTI naïve plant. In addition, *Pto* gene expression data *in planta* can be compared to *in vitro* gene expression data sets in order to understand how well the conditions used for those datasets replicate the apoplast. It can also be used to compare how *in vitro* RNA-seq data for a mutant strain compares to gene expression in the plant. These concepts have been put to use with *P. syringae* pv. *syringae* B728a using microarrays and gave insightful information of regulatory networks in *P. syringae* pv. *syringae* B728a (83, 311).

Overall trends in expression of genes involved in flagellar motility, ROS protection, iron uptake, compatible solute biosynthesis, and alginate production between 1 HPI and 6 HPI corresponded well to known interactions between *Pto* and its hosts (7, 12, 267, 282, 289). At the same time, several new insights into *Pto* gene regulation during initial stages of host colonization were observed. Most notable was how strongly up-regulated genes involved in coronatine biosynthesis were at 6 HPI as compared to 1 HPI. Coronatine is involved in symptom development by *Pto* in *N. benthamiana* and other hosts and, while it was known to be secreted *in planta*, it was unclear as to the exact timing of coronatine deployment *in planta* (143, 144, 281). It is now clear that even though coronatine is necessary for *Pto* to open stomata during invasion into the apoplast, it is also deployed *in planta* after T3Es are delivered (312). Another new insight is that Psl exopolysaccharide is likely not produced by *Pto* in planta. It was already known that cellulose production and alginate production were not essential for *Pto* pathogenesis during endophytic growth, but little was known about Psl exopolysaccharide (95, 136). Initial assays of a Psl exopolysaccharide

deficient *Pto* strain suggests that it is also not essential for *Pto* pathogenesis during endophytic growth (Data not shown).

In general, it is thought that plant pathogenic bacteria hide or reduce production of MAMPs during endophytic growth so as to not elicit PTI. Flagella is the classic example of a MAMP that *Pto* reduces production of during growth *in planta*. This is possible because flagella are not essential to bacteria for survival. However, unlike flagella other MAMPs, like LPS, are essential for survival *in planta* (294). Plants produce a series of antimicrobial peptides in response to pathogens, including defensins. (313, 314). Several genes that code for defensin-like proteins were up-regulated in *N. benthamiana* at 6 HPI as compared to 1 HPI, suggesting that *N. benthamiana* may deploy antimicrobial peptides to defend against *Pto* even after effector delivery (Table S3). Bacteria are known to modify LPS in order to combat antimicrobial peptides (315). Thus, the very nature of the environment *in planta* likely dictates that *Pto* modify LPS and produce cold-shock proteins as was reflected in the transcriptomic data (Table 6.1).

Deployment of effectors during pathogenesis is tantamount for *Pto* to be a successful pathogen during a compatible interaction (192). Systematic removal of groups of effectors in *Pto* have found many effectors to be dispensable for growth and virulence in *N. benthamiana* (146, 297). While this systematic approach has identified the core effectors necessary for *Pto* to be virulent, extensive work still needs to be performed in order to understand the interactions between different effectors. Our RNA-seq data suggests that effectors are not all produced at the same time or in the same amount even though they are all HrpL regulated. The differences in gene

expression of various effectors *in planta* suggest that unknown regulators other than HrpL may regulate expression of effectors. Effectors in the CEL cluster are expressed during the initial hours of infection and then decrease expression by 6 HPI. Other effectors, like those in group IV, show an increase in expression at 6 HPI as compared to 1 HPI. Then there are effectors that seemed to be expressed at somewhat constant levels at 1 HPI and 6 HPI, like *avrPtoB*. Effectors in the CEL cluster are important for virulence but can also elicit the HR if expressed constitutively (4, 125). Alternatively, effectors like AvrPtoB are known to safeguard *Pto* against the HR caused by other effectors, like HopAD1 (13). Dispensable effectors like HopC1, HopH1, and HopAO1 have a limited effect in suppressing ETI or PTI during plant pathogen interactions (145, 299, 300, 316). The regulatory profile of effector gene expression during early stages of infection may reflect the potential toxicity of various effectors *Pto* deploys or the role the effectors play in defending against the HR or PTI. Timing of effector deployment and action has been found to be necessary for successful pathogenesis in *Salmonella enterica* serovar Typhimurum and this may also hold true in *Pto* (317).

One role that effectors play during *Pto* pathogenesis, is reprogramming the host to provide preferred nutrients (318, 319). Since *crcZ* and *crcX* are down-regulated at 6 HPI compared to 1 HPI, it appears that preferred carbon sources are being made available to *Pto* soon after effector deployment. According to changes in gene expression, gluconate, sucrose, maltose, and fructose are among the carbon sources that *Pto* may be taking up from the surrounding environment at 6 HPI. This transcriptional response by *Pto* Δ *hopQ1-1* to sucrose and fructose reflects the concentrations of those sugars found in the apoplast of *Phaseolus vulgaris* during

early timepoints of a compatible interaction with *P. syringae* pv. *phaeseolicola* (42). While gluconate was not found in abundance in *P. vulgaris*, the relative abundance of gluconate increased starting at 6 HPI and *Pseudomonas* will commonly oxidize glucose to gluconate or α -keto gluconate prior to uptake (320). C₄-dicarboxylic acids are thought to be among the most preferred carbon source for *Pto*, yet they do not appear to be one of the carbon sources *Pto* utilizes *in planta* according to changes in gene expression between 1 HPI and 6 HPI (302). Deletion of *crc* reduces the ability for *Pto* to elicit the HR and be virulent (256). Decreased expression of *crcZ* and *crcX* at 6 HPI as compared to 1 HPI seems to point to Crc being active *in planta* and provides insight into why Crc is involved in virulence of *Pto*.

While our analysis mainly focused on interpreting differential gene expression in *Pto* between 1 HPI and 6 HPI, aspects of differential gene expression in *N. benthamiana* suggest that *Pto* is dampening the plant immune response. Many defense-related genes are down-regulated in *N. benthamiana* at 6 HPI as compared to 1 HPI. Typically, the more strongly down-regulated genes are crucial to the plant defense network. The ease at which *N. benthamiana* can be manipulated with VIGS makes future endeavors into investigating these genes relatively easy. Thus, this highlights a strength in using *N. benthamiana* as a host when investigating *Pto*-host interactions.

In conclusion, dual RNA-seq proved to be a powerful method through which one can understand the changes *Pto* undergoes during initial stages of infection while simultaneously understanding changes the host undergoes as well. This can lead to identifying new virulence genes or virulence regulators and also pointing out gaps in

current knowledge on gene regulation in *Pto* and identifying new defense genes in the host. It also allows for the opportunity to use *Pto* as a probe to map changes in the apoplastic environment and compare those changes to known *in vitro* conditions. Further studies using dual RNA-seq could begin to unravel some of the more mysterious unknowns in plant-pathogen interactions.

Methods

Bacterial growth and culture conditions. *Pto* Δ *hopQ1-1* (4) was routinely grown on Kings B (KB) agar prior to inoculation (147).

***N. benthamiana* inoculation.** *Pto* Δ *hopQ1-1* was streaked from a glycerol stock onto KB agar two days prior to the inoculation and placed in a 28°C incubator. Four-week-old *N. benthamiana* plants were transferred from the greenhouse to the lab two days prior to inoculation. One day prior to inoculation, the bacterial culture was spread on the plate using 200 μ L of KB medium and then allowed to grow at 28°C. On the day of inoculation, bacteria were resuspended in 10 mM MgCl₂ at 5×10^8 cfu/mL. Bacterial cultures were then infiltrated into *N. benthamiana* leaves using a blunt-tip syringe. Three *N. benthamiana* plants were used for each time point.

Tissue sampling for RNA extraction. Tissue was sampled at one hour post inoculation and six hours post inoculation. Approximately 200 mg of tissue was punched or excised using a 1.5 mm hole punch from each *N. benthamiana* plant. Tissue was immediately frozen using liquid nitrogen upon sampling and stored at -80°C until RNA was extracted. Tissue was also taken from each plant and used for cell counts.

RNA extraction. RNA was extracted in a similar manner as was described by Schenk et. al. (321). *N. benthamiana* tissue was ground up in liquid nitrogen using a pre-chilled mortar and pestle. Tissue was transferred to a 2.0 mL microfuge tube. 750 μ L of BPEX buffer (0.35 M glycine; 0.7 M NaCl; 2% (w/v) polyethylene glycol 20000 (Sigma-Aldrich, St. Louis, MO); 40 mM EDTA (0.5 M EDTA stock solution, pH 8.0); 50 mM NaOH (10 M NaOH stock solution); 4% (w/v) SDS) was added to the tissue samples. Samples were mixed for 90 seconds at 1,400 rpm and 95°C using a Thermomixer (Eppendorf, Haupage, NY). Samples were centrifuged for one minute at 16,000 x g in a microfuge (Eppendorf) to remove plant debris. Supernatant was then transferred to a new 2.0 mL microfuge tube. 750 μ L of water-saturated acid phenol (ThermoFisher) was added to the samples and mixed for 5 minutes. Samples were then centrifuged at 16,000 x g for seven minutes. 675 μ L of the aqueous layer was removed and loaded into a 2.0 mL microfuge tube preloaded with 675 μ L of water-saturated acid phenol. Samples were mixed for 5 minutes and then centrifuged at 16,000 x g in a microfuge for seven minutes. 575 μ L of the aqueous layer from each sample was then loaded into a 2.0 mL microfuge tube preloaded with 575 μ L of water-saturated acid phenol. Samples were mixed for five minutes and then centrifuged at 16,000 x g in a microfuge for seven minutes. 435 μ L of the aqueous layer from each sample was then loaded into a 2.0 mL microfuge tube preloaded with chloroform:isoamyl alcohol (24:1) (Sigma). 55 μ L of warmed CTAB:NaCl solution (10% (w/v) CTAB; 0.7 M NaCl) was layered on top. The samples were then mixed for five minutes and then centrifuged at 16,000 x g in a microfuge for seven minutes. 435 μ L of the aqueous phase from each sample were loaded into 1.7 mL microfuge tubes

preloaded with 145 μ L of 8 M LiCl (Sigma). Samples mixed by inversion and then placed in a -20°C freezer overnight to precipitate RNA. The following day, the samples were centrifuged at 16,000 x g in a microfuge at 4°C for 30 minutes. Supernatant was then decanted and the samples were washed 2x with 1.0 mL of ice-cold 75% ethanol. Following the second wash, ethanol was decanted and samples were allowed to dry. RNA was resuspended in 20 μ L of nuclease-free water (ThermoFisher). Concentration and purity of the RNA was determined using a Qubit (ThermoFisher).

qRT-PCR. 1 μ g of extracted RNA was converted to cDNA using qScript cDNA supermix (Quanta, Beverly, MA). A reaction mixture that consisted of 10 μ L Sso-Advanced SYBR Green Supermix (Bio-Rad, Hercules, CA), 1 μ L of a 1:10 dilution of the cDNA, 5 μ L water, 2 μ L of each primer at 2 μ M was run on a Bio-Rad CFX Connect. Gene expression for *HINI* (forward primer - AGTTGTCTCTTTGGATGCCTCTGC, reverse primer - ACTGAGTCAACGTAGCATCGGTCA) and *acre31* (forward primer - AATTCGGCCATCGTGATCTTGGTC, reverse primer - GAGAAACTGGGATTGCCTGAAGGA) was determined for each sample. The reference gene *eflalpha* (forward primer – CAACTACCAGCCTCCAAC, reverse primer - TGCCTTCACCAACATACC) was used to normalize expression between samples. Experiments were performed three times. Averages and standard deviations from each biological replicate were generated from the experiments.

Library preparation and RNA sequencing. 2.5 μ g of RNA was simultaneously treated with Ribo-zero for gram negative bacteria (Illumina, San Diego, Ca) and with

Ribo-zero for plant leaves (Illumina) to remove ribosomal RNA (rRNA). cDNA libraries were made using Scriptseq V2 (Illumina) using 10 to 20 ng of RNA according to the manufacturer's protocol and sent to the Cornell core facility for sequencing on an Illumina HiSeq 2500. Each sample was run on a single lane of a flow cell.

Analysis of RNA-seq data. RNA-seq data was analyzed using a method similar to a published method for RNA-seq analysis of mixed infections (322). Initially, both the *Pto* and *N. benthamiana* genomes were indexed separately by Bowtie2 (156). Raw reads were then mapped to the *N. benthamiana* genome using Tophat set on default parameters (323). Raw reads were separately mapped to the *Pto* genome using Bowtie2 set to the default parameters in addition to the parameters `-k5 -end-to-end` (156). Reads that did not align to the *N. benthamiana* genome or the *Pto* genome were then reciprocally aligned to the genome they had not been analyzed against previously using the program and parameters described above. The reads that mapped to the *N. benthamiana* and *Pto* genome from the previously unmapped reads were then used to examine differential expression between one hour post inoculation (HPI) and six hours post inoculation (HPI). For *N. benthamiana*, Cufflinks was used to determine genes that demonstrated differential expression for reads that mapped to *N. benthamiana* (324). Following this, Cuffdiff was run using the default parameters with an FDR set to < 0.05 to determine differentially expressed genes between 1 HPI and 6 HPI. For *Pto*, DeSeq2 was then used as previously described to determine differentially expressed genes between 1 HPI and 6 HPI (95, 283).

Acknowledgements

We would like to thank Katherine D'Amico for helping with initial pilot experiments.

The U.S. Department of Agriculture (USDA) is an equal opportunity provider and employer. Mention of trade names or commercial products in this publication is solely for the purposes of providing specific information and does not imply recommendation or endorsement by the USDA. The authors declare no conflicts of interest.

CHAPTER 7

CONCLUSIONS AND FUTURE DIRECTIONS

Introduction

The major conclusions on CvsSR, PSPTO_5255, *Pseudomonas* calcium precipitation regulation, and dual RNA-seq of *Pto* and a host during early timepoints of a compatible interaction have been presented in the previous chapters. This chapter will be a conclusion that will focus on synthesizing data that was presented throughout this thesis and attempt to suggest future experiments of interest.

Direct activators of CvsR

When characterizing CvsSR, only inducers of the two-component system (TCS) were identified. Unfortunately, a direct activator of CvsSR that binds CvsS remained elusive. Two criteria typically need to be met in order for a compound or ion to be considered an activator of a TCS. First, the activator must directly interact to a portion of the signaling domain of the histidine kinase (HK). Second, the TCS should become active upon the activator and HK interacting. The gold standard for this phenomenon can be found in the characterization of PhoPQ in *Salmonella enterica* (325). While not shown in this thesis, addition of Ca^{2+} to *Pto* pBS59::P_{cvsSR} after nine hours of growth in MG induced transcription of *cvsS* and *cvsR* within 45 minutes (M.F. unpublished data). This data could be used as proof that Ca^{2+} can quickly induce CvsSR, but additional experiments would need to be performed to show that CvsS binds to Ca^{2+} . Fe^{2+} was found to be the activator of the orthologous TCS to CvsSR in *Pseudomonas aeruginosa*, BqsSR, that bound to an REXXE motif in BqsS (169). CvsS does not have an REXXE motif but does have an NXXE motif in the signaling domain of CvsS. NXXE motifs in ribokinases can bind a variety of divalent cations, including Ca^{2+} and Zn^{2+} (326, 327). Mutation of this NXXE domain in CvsS would be a

plausible first step for showing that Ca^{2+} , Fe^{3+} , Zn^{2+} , and Cd^{2+} are activators of CvsSR. One of the notable things about NXXE binding domains in ribokinases is that the metal cations coordinate with a phosphate anion (327). Unpublished data suggests that the strength of induction of *cvsS* and *cvsR* is dependent not only on the concentration of Ca^{2+} in the medium, but also PO_4^- (M.F. unpublished results). This was not observed with any of the other metal cations that induce CvsSR. It is possible that if Ca^{2+} does bind to the NXXE motif in CvsS, CvsSR activation by Ca^{2+} may require coordination of Ca^{2+} with PO_4^- in the NXXE motif of CvsS. Expression and purification of CvsS would allow for one to test these hypotheses by using techniques such as surface plasmon resonance, nuclear magnetic resonance, or x-ray crystallization. While these techniques would remove any biological noise that could occur from attempting to perform these experiments *in vivo* they are technically challenging techniques that could prove difficult.

Identifying the role of CvsSR *in planta*

In the second chapter of this thesis, it was determined that *in planta* Ca^{2+} can induce *cvsS* and *cvsR* expression. It was partially for this reason that supplemental Ca^{2+} was added to medium when determining the regulon of CvsR. There were several interesting genes from the ChIP-seq data that looked to be regulated by CvsR that did not show any differential regulation in the RNA-seq data. This included several type III effectors (T3Es). Given the fact that CvsSR may regulate several T3Es and differential regulation of these T3Es was not determined *in vitro*, a dual RNA-seq experiment comparing WT and the ΔcvsS and ΔcvsR strains may be useful. A dual RNA-seq protocol was described in chapter six of this thesis that allowed for identification of transcriptional changes in *Pto* during growth *in planta*. This protocol that could be used to compare gene regulation of WT and the ΔcvsS and ΔcvsR strains during growth *in planta*. By performing this type of experiment, one would hopefully

see differential regulation between the CvsR-regulated T3Es when comparing the WT and the $\Delta cvsS$ and $\Delta cvsR$ strains. This type of data could help in deciphering how much of a role CvsSR plays in regulating these T3Es and other genes associated with the type III secretion system.

Identifying the function of PSPTO_5255 in *Pto*

Chapters three and four of this thesis explored the transcriptional regulation of PSPTO_5255 (5255) and the role 5255 plays in *Pseudomonas syringae* pv. tomato DC3000 (*Pto*). The phenotypes that were observed in the Δ PSPTO_5255 strain of *Pseudomonas syringae* pv. tomato DC3000 (*Pto*) provides a good foundation for identifying the function of PSPTO_5255 (5255) in *Pto*. The phenotypes of increased cellulose production and decreased dissolution of calcium phosphate in medium surrounding bacterial colonies in the Δ 5255 strain are particularly helpful in dictating the next steps one might take in characterizing 5255. Increased cellulose production is commonly indicative of internal increased cyclic-di-GMP (cdG) concentration in *Pto* and decreased calcium dissolution in the Δ 5255 strain could indicate a decrease in carbonic acid and bicarbonate production by this strain as compared to WT (116). Thus, it would be helpful to quantify the amount of cdG and the amount of bicarbonate made by WT and the Δ 5255 strain. An increase in internal cdG concentration and a decrease in bicarbonate production in the Δ 5255 strain could hint at a role of bicarbonate in being a signaling molecule in *Pto* that can cause changes in cdG concentration. Bicarbonate being a signaling molecule in *Pto* is not a far stretch given the fact that environmental bicarbonate is a signaling molecule for many bacteria (200-202, 205). What would be unique about this situation with *Pto* is that bicarbonate that *Pto* produced would be used as a signaling molecule. This could potentially be a novel regulatory mechanism.

Calcium precipitation and its role in *Pto*

Of all the chapters in this thesis, the ones that involve *Pseudomonas* mediated calcium precipitation are in some ways the most frustrating. Part of my original thesis proposal was to investigate whether *Pto* induced calcium precipitation *in planta*. However, this was technically quite difficult. The *in vitro* experiments described in chapters three and five were the closest I came to investigating *Pseudomonas* induced calcium precipitation *in planta*. As most can guess, an agar plate is a very different environment from the interior of a plant leaf. These experiments did identify several genes that are involved in calcium precipitation in *Pto* and also involved in virulence. Both *cvsS* and *cvsR* were among the identified genes and could prove the most useful for investigating whether calcium precipitation occurs *in planta*. Based on data presented in chapters three and five, environmental calcium precipitation may be a transient phenotype in *Pto*. This could also be the case *in planta*. If so, it may be difficult to find a time-point after infection when *Pto* actually precipitates calcium. However, the $\Delta cvsS$ and $\Delta cvsR$ strains never performed calcium dissolution *in vitro* and may show a similar behavior *in planta*. This suggests that these strains may be useful for investigating whether *Pto* induces calcium precipitation *in planta*. Techniques that would prove to be useful for investigating *in planta* calcium precipitation would be SEM and TEM. SEM has previously been used to study calcium oxalate and calcium sulfate production in plant tissues (328). An alternative method to performing SEM and TEM for investigating calcium precipitation *in planta* could be to extract apoplastic washing fluid (AWF) and look for signs of calcium minerals in the AWF.

Dual RNA-seq

Chapter 6 of this thesis described a method for performing dual RNA-seq with the $\Delta hopQ1-1$ strain of *Pto* and *Nicotiana benthamiana*. The technique relied on infiltrating high titers of the $\Delta hopQ1-1$ strain into *N. benthamiana* and extracting RNA

at one hour post inoculation and six hours post inoculation (HPI). With the high concentration of bacteria present in the samples, bacterial transcript made up between 1% and 3% of the reads from RNA-sequencing runs. There are several drawbacks to this method. First, the method was costly as each sample required a single lane on an Illumina HiSeq flow cell in order to recover enough reads to make inferences about the *Pto* transcriptional landscape *in planta*. The high cost could be inhibitory to performing large experiments that require many time-points and biological replicates. Second, the high titer of the inocula was four orders of magnitude higher than the normal titer levels of inocula used when syringe infiltrating *N. benthamiana* in the lab. This could cause some to be skeptical when assessing the data from this experiment because the initial inocula could be overwhelming the host and is far from the concentration of inocula found in a natural setting. Our data suggests that the plant still mounts a normal response to the amount of inocula that it was presented with during the dual RNA-seq experiment (Figure 6.3). Lastly, the high levels of inocula that were used cap 6 HPI or a few hours after as the last timepoint one can take because the cells in the inoculated regions begin to collapse at that time. Thus, in order to perform a time course beyond 6 HPI, the initial inocula would have to be optimized. Even with these drawbacks, the data generated from the dual RNA-seq experiment proved to be exciting and could lead to new findings. For example, around 500 genes within the dataset were up-regulated at 1 HPI as compared to an RNA-seq dataset that was collected *in vitro* and at the same time were down-regulated at 6 HPI compared to 1 HPI (Table 7.1)¹² (157). Among the genes within this group are genes that defend against PAMP-triggered immunity, like *katB*, and genes that regulate the T3SS, like *hrpL* and *hrpS*. Thus, it is possible that some of the other genes found within this set

¹² Table 7.1 is over 500 rows in length. Due to the size of this table, it will be included in the supplementary data of this thesis and not within the text of the thesis.

may be unidentified or uncharacterized genes that *Pto* needs to be a successful pathogen. This list includes 10 uncharacterized transcriptional regulators and six uncharacterized histidine kinase/response regulators (Table 7.2). While it is unclear whether these uncharacterized regulators would be important for pathogenesis, their presence in this list makes them potential targets for further evaluation *in planta*.

A recent paper was just published on *in planta* transcriptomics of *Pto* that used lower initial inocula than was used in chapter 6, was able to get good data at a 6 HPI timepoint, and allowed for multiplexing of samples (84). The method used in Nobori et al. overcomes the drawbacks to the dual RNA-seq method described in chapter 6 of this thesis. Given these recent findings, it could make sense to update or change the method described in chapter 6 to allow for better enrichment of bacterial RNA at lower titer. One method would be copying the method from Nobori et al. with slight modifications to allow for extraction of plant and bacterial RNA in any future *Pto* based dual RNA-seq experiments. An alternative approach for enriching *Pto* transcripts *in planta* could be to perform ribosome profiling. Ribosome profiling can be utilized to identify transcripts that are currently being translated into proteins and can give a snapshot of the translome (similar to the proteome) (329). The one drawback of ribosome profiling is that it would not capture any small regulatory RNAs. Ribosome profiling was recently used to identify the translational landscape in *Arabidopsis thaliana* (330). Knowing that tagged bacterial ribosomes are still functional one could tag a ribosomal protein in *Pto* and then enrich for *Pto* ribosomes from ribosomes extracted during *Pto* growth *in planta* (331). In addition, it could be possible to simultaneously perform ribosome profiling on plant tissue as well using this method if that was so desired.

Table 7.2: Transcriptional regulators in *Pto* that are up-regulated at 1 HPI *in planta* as compared to *in vitro* growth conditions and down-regulated at 6 HPI as compared to 1 HPI.

- a. The locus number for the gene as annotated
- b. The description of the protein coded for by the designated gene as found in the Uniprot database (112)
- c. Fold-change is in reference to the fold-change between 1 HPI and 6 HPI

Locus ^a	Description of protein ^b	Fold-change ^c
PSPTO_1870	Sensory box histidine kinase/response regulator	-8.0
PSPTO_2717	Sensory box histidine kinase/response regulator	-3.9
PSPTO_2129	Sensory box histidine kinase/response regulator	-2.6
PSPTO_0353	Histidine kinase (EC 2.7.13.3)	-2.7
PSPTO_1490	Sensory box histidine kinase/response regulator	-3.5
PSPTO_4079	Sensor histidine kinase/response regulator	-2.5
PSPTO_4528	Transcriptional regulator, AraC family	-4.1
PSPTO_2181	Transcriptional regulator, IclR family	-4.2
PSPTO_2286	Transcriptional regulator, GntR family	-12.5
PSPTO_3501	Transcriptional regulator, RpiR family	-3.3
PSPTO_2505	Transcriptional regulator, AraC family	-5.7
PSPTO_4427	Transcriptional regulator, AraC family	-2.0
PSPTO_3050	Transcriptional regulator, AraC family	-2.9
PSPTO_2743	Transcriptional regulator, MerR family	-2.3
PSPTO_1502	Transcriptional regulator, TetR family	-1.9
PSPTO_2945	Transcriptional regulator, MarR family	-2.0
PSPTO_4080	DNA-binding response regulator, LuxR family	-2.9

REFERENCES

1. **Hirano SS, Upper CD.** 1990. Population Biology and Epidemiology of *Pseudomonas syringae*. Annual Review of Phytopathology **28**:155-177.
2. **Kennelly MM, Cazorla FM, de Vicente A, Ramos C, Sundin GW.** 2007. *Pseudomonas syringae* Diseases of Fruit Trees: Progress Toward Understanding and Control. Plant Disease **91**:4-17.
3. **Xin XF, He SY.** 2013. *Pseudomonas syringae* pv. tomato DC3000: a model pathogen for probing disease susceptibility and hormone signaling in plants. Annual Review of Phytopathology **51**:473-498.
4. **Wei CF, Kvitko BH, Shimizu R, Crabill E, Alfano JR, Lin NC, Martin GB, Huang HC, Collmer A.** 2007. A *Pseudomonas syringae* pv. tomato DC3000 mutant lacking the type III effector HopQ1-1 is able to cause disease in the model plant *Nicotiana benthamiana*. The Plant Journal **51**:32-46.
5. **Jones JDG, Dangl JL.** 2006. The plant immune system. Nature **444**:323-329.
6. **Spoel SH, Dong X.** 2012. How do plants achieve immunity? Defence without specialized immune cells. Nature Reviews Immunology **12**:89-100.
7. **Felix G, Duran JD, Volko S, Boller T.** 1999. Plants have a sensitive perception system for the most conserved domain of bacterial flagellin. The Plant Journal **18**:265-276.

8. **Kunze G, Zipfel C, Robatzek S, Niehaus K, Boller T, Felix G.** 2004. The N-Terminus of Bacterial Elongation Factor Tu Elicits Innate Immunity in *Arabidopsis* Plants. *The Plant Cell* **16**:3496-3507.
9. **Ranf S.** 2016. Immune sensing of lipopolysaccharide in plants and animals: same but different. *PLoS pathogens* **12**:e1005596.
10. **Felix G, Boller T.** 2003. Molecular sensing of bacteria in plants: the highly conserved RNA-binding motif RNP-1 of bacterial cold shock proteins is recognized as an elicitor signal in tobacco. *Journal of Biological Chemistry* **278**:6201-6208.
11. **Bigeard J, Colcombet J, Hirt H.** 2015. Signaling mechanisms in pattern-triggered immunity (PTI). *Molecular Plant* **8**:521-539.
12. **Guo M, Block A, Bryan CD, Becker DF, Alfano JR.** 2012. *Pseudomonas syringae* Catalases Are Collectively Required for Plant Pathogenesis. *Journal of Bacteriology* **194**:5054-5064.
13. **Wei H-L, Chakravarthy S, Mathieu J, Helmann TC, Stodghill P, Swingle B, Martin GB, Collmer A.** 2015. *Pseudomonas syringae* pv. tomato DC3000 type III secretion effector polymutants reveal an interplay between HopAD1 and AvrPtoB. *Cell Host & Microbe* **17**:752-762.
14. **Xiao Y, Hutcheson SW.** 1994. A single promoter sequence recognized by a newly identified alternate sigma factor directs expression of pathogenicity and host range determinants in *Pseudomonas syringae*. *Journal of Bacteriology* **176**:3089-3091.

15. **Hutcheson SW, Bretz J, Sussan T, Jin S, Pak K.** 2001. Enhancer-Binding Proteins HrpR and HrpS Interact To Regulate hrp-Encoded Type III Protein Secretion in *Pseudomonas syringae* Strains. *Journal of Bacteriology* **183**:5589-5598.
16. **Bronstein PA, Filiatrault MJ, Myers CR, Rutzke M, Schneider DJ, Cartinhour SW.** 2008. Global transcriptional responses of *Pseudomonas syringae* DC3000 to changes in iron bioavailability in vitro. *BMC Microbiology* **8**:209.
17. **Huang HC, Schuurink R, Denny TP, Atkinson MM, Baker CJ, Yucel I, Hutcheson SW, Collmer A.** 1988. Molecular cloning of a *Pseudomonas syringae* pv. *syringae* gene cluster that enables *Pseudomonas fluorescens* to elicit the hypersensitive response in tobacco plants. *Journal of Bacteriology* **170**:4748-4756.
18. **Hu W, Yuan J, Jin Q-L, Hart P, He SY.** 2001. Immunogold labeling of Hrp pili of *Pseudomonas syringae* pv. tomato assembled in minimal medium and *in planta*. *Molecular Plant-Microbe Interactions* **14**:234-241.
19. **Stock AM, Robinson VL, Goudreau PN.** 2000. Two-component signal transduction. *Annual Review of Biochemistry* **69**:183-215.
20. **Bernardini ML, Fontaine A, Sansonetti PJ.** 1990. The two-component regulatory system OmpR-EnvZ controls the virulence of *Shigella flexneri*. *Journal of Bacteriology* **172**:6274-6281.
21. **Fiedler T, Mix M, Meyer U, Mikkat S, Glocker MO, Bahl H, Fischer R-J.** 2008. The two-component system PhoPR of *Clostridium acetobutylicum* is

- involved in phosphate-dependent gene regulation. *Journal of Bacteriology* **190**:6559-6567.
22. **Groisman EA.** 2001. The pleiotropic two-component regulatory system PhoP-PhoQ. *Journal of Bacteriology* **183**:1835-1842.
 23. **Ainsaar K, Mumm K, Ilves H, Hõrak R.** 2014. The ColRS signal transduction system responds to the excess of external zinc, iron, manganese, and cadmium. *BMC Microbiology* **14**:162.
 24. **Galperin MY.** 2006. Structural classification of bacterial response regulators: diversity of output domains and domain combinations. *Journal of Bacteriology* **188**:4169-4182.
 25. **Cameron ADS, Dorman CJ.** 2012. A Fundamental Regulatory Mechanism Operating through OmpR and DNA Topology Controls Expression of *Salmonella* Pathogenicity Islands SPI-1 and SPI-2. *PLoS Genetics* **8**:e1002615.
 26. **Rampersaud A, Norioka S, Inouye M.** 1989. Characterization of OmpR binding sequences in the upstream region of the *ompF* promoter essential for transcriptional activation. *Journal of Biological Chemistry* **264**:18693-18700.
 27. **Lavin JL, Kiil K, Resano O, Ussery DW, Oguiza JA.** 2007. Comparative genomic analysis of two-component regulatory proteins in *Pseudomonas syringae*. *BMC Genomics* **8**:397.
 28. **Chatterjee A, Cui Y, Yang H, Collmer A, Alfano JR, Chatterjee AK.** 2003. GacA, the response regulator of a two-component system, acts as a master

- regulator in *Pseudomonas syringae* pv. tomato DC3000 by controlling regulatory RNA, transcriptional activators, and alternate sigma factors. *Molecular Plant-Microbe Interactions* **16**:1106-1117.
29. **Sreedharan A, Penaloza-Vazquez A, Kunkel BN, Bender CL.** 2006. CorR Regulates Multiple Components of Virulence in *Pseudomonas syringae* pv. tomato DC3000. *Molecular Plant-Microbe Interactions* **19**:768-779.
 30. **Moriconi V, Sellaro R, Ayub N, Soto G, Rugnone M, Shah R, P Pathak G, Gärtner W, Casal JJ.** 2013. LOV-domain photoreceptor, encoded in a genomic island, attenuates the virulence of *Pseudomonas syringae* in light-exposed *Arabidopsis* leaves. *The Plant Journal* **76**:322-331.
 31. **Xiao Y, Lan L, Yin C, Deng X, Baker D, Zhou J-M, Tang X.** 2007. Two-Component Sensor RhpS Promotes Induction of *Pseudomonas syringae* Type III Secretion System by Repressing Negative Regulator RhpR. *Molecular Plant-Microbe Interactions* **20**:223-234.
 32. **Dominguez DC.** 2004. Calcium signalling in bacteria. *Molecular Microbiology* **54**:291-297.
 33. **Dominguez DC, Guragain M, Patrauchan M.** 2015. Calcium binding proteins and calcium signaling in prokaryotes. *Cell Calcium* **57**:151-165.
 34. **Jones HE, Holland IB, Campbell AK.** 2002. Direct measurement of free Ca²⁺ shows different regulation of Ca²⁺ between the periplasm and the cytosol of *Escherichia coli*. *Cell Calcium* **32**:183-192.

35. **Tisa LS, Adler J.** 1995. Cytoplasmic free-Ca²⁺ level rises with repellents and falls with attractants in *Escherichia coli* chemotaxis. Proceedings of the National Academy of Sciences **92**:10777-10781.
36. **Herbaud M-L, Guiseppi A, Denizot F, Haiech J, Kilhoffer M-C.** 1998. Calcium signalling in *Bacillus subtilis*. Biochimica et Biophysica Acta (BBA) - Molecular Cell Research **1448**:212-226.
37. **Gode-Potratz CJ, Chodur DM, McCarter LL.** 2010. Calcium and iron regulate swarming and type III secretion in *Vibrio parahaemolyticus*. Journal of Bacteriology **192**:6025-6038.
38. **Bartra SS, Jackson MW, Ross JA, Plano GV.** 2006. Calcium-Regulated Type III Secretion of Yop Proteins by an *Escherichia coli hha* Mutant Carrying a *Yersinia pestis* pCD1 Virulence Plasmid. Infection and Immunity **74**:1381-1386.
39. **Dasgupta N, Ashare A, Hunninghake GW, Yahr TL.** 2006. Transcriptional induction of the *Pseudomonas aeruginosa* type III secretion system by low Ca²⁺ and host cell contact proceeds through two distinct signaling pathways. Infection and Immunity **74**:3334-3341.
40. **Sarkisova S, Patrauchan MA, Berglund D, Nivens DE, Franklin MJ.** 2005. Calcium-induced virulence factors associated with the extracellular matrix of mucoid *Pseudomonas aeruginosa* biofilms. Journal of Bacteriology **187**:4327-4337.

41. **Stael S, Wurzinger B, Mair A, Mehlmer N, Vothknecht UC, Teige M.** 2012. Plant organellar calcium signalling: an emerging field. *Journal of Experimental Botany* **63**:1525-1542.
42. **O'Leary BM, Neale HC, Geilfus C-M, Jackson RW, Arnold DL, Preston GM.** 2016. Early changes in apoplast composition associated with defence and disease in interactions between *Phaseolus vulgaris* and the halo blight pathogen *Pseudomonas syringae* pv. phaseolicola. *Plant, Cell & Environment* **39**:2172-2184.
43. **De La Fuente L, Parker JK, Oliver JE, Granger S, Brannen PM, van Santen E, Cobine PA.** 2013. The Bacterial Pathogen *Xylella fastidiosa* Affects the Leaf Ionome of Plant Hosts during Infection. *PLoS one* **8**:e62945.
44. **Lindskog S.** 1997. Structure and mechanism of carbonic anhydrase. *Pharmacology & Therapeutics* **74**:1-20.
45. **McKenna R, Frost SC.** 2014. Overview of the Carbonic Anhydrase Family, p 3-5. *In* Frost SC, McKenna R (ed), *Carbonic Anhydrase: Mechanism, Regulation, Links to Disease, and Industrial Applications* doi:10.1007/978-94-007-7359-2_1. Springer Netherlands, Dordrecht.
46. **Del Prete S, Vullo D, Fisher GM, Andrews KT, Poulsen S-A, Capasso C, Supuran CT.** 2014. Discovery of a new family of carbonic anhydrases in the malaria pathogen *Plasmodium falciparum*—The η -carbonic anhydrases. *Bioorganic & Medicinal Chemistry Letters* **24**:4389-4396.

47. **Capasso C, Supuran CT.** 2015. An overview of the alpha-, beta- and gamma-carbonic anhydrases from Bacteria: can bacterial carbonic anhydrases shed new light on evolution of bacteria? *Journal of Enzyme Inhibition and Medicinal Chemistry* **30**:325-332.
48. **Merlin C, Masters M, McAteer S, Coulson A.** 2003. Why is carbonic anhydrase essential to *Escherichia coli*? *Journal of Bacteriology* **185**:6415-6424.
49. **Kusian B, Sültemeyer D, Bowien B.** 2002. Carbonic anhydrase is essential for growth of *Ralstonia eutropha* at ambient CO₂ concentrations. *Journal of Bacteriology* **184**:5018-5026.
50. **Rae BD, Long BM, Badger MR, Price GD.** 2013. Functions, compositions, and evolution of the two types of carboxysomes: polyhedral microcompartments that facilitate CO₂ fixation in cyanobacteria and some proteobacteria. *Microbiology and Molecular Biology Reviews* **77**:357-379.
51. **Cannon GC, Heinhorst S, Kerfeld CA.** 2010. Carboxysomal carbonic anhydrases: structure and role in microbial CO₂ fixation. *Biochimica et Biophysica Acta (BBA)-Proteins and Proteomics* **1804**:382-392.
52. **Lotlikar SR, Hnatusko S, Dickenson NE, Choudhari SP, Picking WL, Patrauchan MA.** 2013. Three functional β -carbonic anhydrases in *Pseudomonas aeruginosa* PAO1: role in survival in ambient air. *Microbiology* **159**:1748-1759.
53. **Burghout P, Cron LE, Gradstedt H, Quintero B, Simonetti E, Bijlsma JJ, Bootsma HJ, Hermans PW.** 2010. Carbonic anhydrase is essential for

- Streptococcus pneumoniae* growth in environmental ambient air. Journal of Bacteriology **192**:4054-4062.
54. **Buchieri MV, Riafrecha LE, Rodríguez OM, Vullo D, Morbidoni HR, Supuran CT, Colinas PA.** 2013. Inhibition of the β -carbonic anhydrases from *Mycobacterium tuberculosis* with C-cinnamoyl glycosides: Identification of the first inhibitor with anti-mycobacterial activity. Bioorganic & Medicinal Chemistry Letters **23**:740-743.
55. **Guilloton MB, Lamblin AF, Kozliak EI, Gerami-Nejad M, Tu C, Silverman D, Anderson PM, Fuchs JA.** 1993. A physiological role for cyanate-induced carbonic anhydrase in *Escherichia coli*. Journal of Bacteriology **175**:1443-1451.
56. **Bury-Mone S, Mendz GL, Ball GE, Thibonnier M, Stingl K, Ecobichon C, Ave P, Huerre M, Labigne A, Thiberge JM, De Reuse H.** 2008. Roles of alpha and beta carbonic anhydrases of *Helicobacter pylori* in the urease-dependent response to acidity and in colonization of the murine gastric mucosa. Infection and Immunity **76**:497-509.
57. **Abuaita BH, Withey JH.** 2009. Bicarbonate induces *Vibrio cholerae* virulence gene expression by enhancing ToxT activity. Infection and Immunity **77**:4111-4120.
58. **Bell KS, Sebahia M, Pritchard L, Holden MTG, Hyman LJ, Holeva MC, Thomson NR, Bentley SD, Churcher LJC, Mungall K, Atkin R, Bason N, Brooks K, Chillingworth T, Clark K, Doggett J, Fraser A, Hance Z, Hauser H, Jagels K, Moule S, Norbertczak H, Ormond D, Price C, Quail**

- MA, Sanders M, Walker D, Whitehead S, Salmond GPC, Birch PRJ, Parkhill J, Toth IK.** 2004. Genome sequence of the enterobacterial phytopathogen *Erwinia carotovora* subsp. *atroseptica* and characterization of virulence factors. Proceedings of the National Academy of Sciences **101**:11105-11110.
59. **Raffaele S, Win J, Cano LM, Kamoun S.** 2010. Analyses of genome architecture and gene expression reveal novel candidate virulence factors in the secretome of *Phytophthora infestans*. BMC Genomics **11**:637-637.
60. **Buell CR, Joardar V, Lindeberg M, Selengut J, Paulsen IT, Gwinn ML, Dodson RJ, Deboy RT, Durkin AS, Kolonay JF, Madupu R, Daugherty S, Brinkac L, Beanan MJ, Haft DH, Nelson WC, Davidsen T, Zafar N, Zhou L, Liu J, Yuan Q, Khouri H, Fedorova N, Tran B, Russell D, Berry K, Utterback T, Van Aken SE, Feldblyum TV, D'Ascenzo M, Deng W-L, Ramos AR, Alfano JR, Cartinhour S, Chatterjee AK, Delaney TP, Lazarowitz SG, Martin GB, Schneider DJ, Tang X, Bender CL, White O, Fraser CM, Collmer A.** 2003. The complete genome sequence of the *Arabidopsis* and tomato pathogen *Pseudomonas syringae* pv. *tomato* DC3000. Proceedings of the National Academy of Sciences **100**:10181-10186.
61. **Frankel RB, Bazylinski DA.** 2003. Biologically induced mineralization by bacteria. Reviews in Mineralogy and Geochemistry **54**:95-114.

62. **Boquet E, Boronat A, Ramos-Cormenzana A.** 1973. Production of Calcite (Calcium Carbonate) Crystals by Soil Bacteria is a General Phenomenon. *Nature* **246**:527.
63. **Hammes F, Boon N, de Villiers J, Verstraete W, Siciliano SD.** 2003. Strain-Specific Ureolytic Microbial Calcium Carbonate Precipitation. *Applied and Environmental Microbiology* **69**:4901-4909.
64. **Achal V, Pan X.** 2014. Influence of calcium sources on microbially induced calcium carbonate precipitation by *Bacillus* sp. CR2. *Applied Biochemistry and Biotechnology* **173**:307-317.
65. **Nathan Y, Bremner JM, Loewenthal RE, Monteiro P.** 1993. Role of bacteria in phosphorite genesis. *Geomicrobiology Journal* **11**:69-76.
66. **Cosmidis J, Benzerara K, Guyot F, Skouri-Panet F, Duprat E, Férard C, Guigner J-M, Babonneau F, Coelho C.** 2015. Calcium-phosphate biomineralization induced by alkaline phosphatase activity in *Escherichia coli*: localization, kinetics and potential signatures in the fossil record. *Frontiers in Earth Science* **3**.
67. **Thackray AC, Sammons RL, Macaskie LE, Yong P, Lugg H, Marquis PM.** 2004. Bacterial biosynthesis of a calcium phosphate bone-substitute material. *Journal of Materials Science: Materials in Medicine* **15**:403-406.
68. **Rodríguez H, Fraga R.** 1999. Phosphate solubilizing bacteria and their role in plant growth promotion. *Biotechnology Advances* **17**:319-339.

69. **Kucey RMN, Janzen HH, Leggett ME.** 1989. Microbially Mediated Increases in Plant-Available Phosphorus, p 199-228. *In* Brady NC (ed), Advances in Agronomy, vol 42. Academic Press.
70. **Gyaneshwar P, Parekh LJ, Archana G, Poole PS, Collins MD, Hutson RA, Kumar GN.** 1999. Involvement of a phosphate starvation inducible glucose dehydrogenase in soil phosphate solubilization by *Enterobacter asburiae*. FEMS Microbiology Letters **171**:223-229.
71. **Babu-Khan S, Yeo TC, Martin WL, Duron MR, Rogers RD, Goldstein AH.** 1995. Cloning of a mineral phosphate-solubilizing gene from *Pseudomonas cepacia*. Applied and Environmental Microbiology **61**:972-978.
72. **Van Schie B, De Mooy O, Linton J, Van Dijken J, Kuenen J.** 1987. PQQ-dependent production of gluconic acid by *Acinetobacter*, *Agrobacterium* and *Rhizobium* species. Microbiology **133**:867-875.
73. **de Werra P, Péchy-Tarr M, Keel C, Maurhofer M.** 2009. Role of gluconic acid production in the regulation of biocontrol traits of *Pseudomonas fluorescens* CHA0. Applied and Environmental Microbiology **75**:4162-4174.
74. **Li W, Zhou PP, Jia LP, Yu LJ, Li XL, Zhu M.** 2009. Limestone dissolution induced by fungal mycelia, acidic materials, and carbonic anhydrase from fungi. Mycopathologia **167**:37-46.
75. **Jacobson AD, Wu L.** 2009. Microbial dissolution of calcite at T=28°C and ambient pCO₂. Geochimica et Cosmochimica Acta **73**:2314-2331.

76. **Zhu Y, Ma N, Jin W, Wu S, Sun C.** 2017. Genomic and Transcriptomic Insights into Calcium Carbonate Biomineralization by Marine Actinobacterium *Brevibacterium linens* BS258. *Frontiers in Microbiology* **8**:602.
77. **Xiao L, Hao J, Wang W, Lian B, Shang G, Yang Y, Liu C, Wang S.** 2014. The Up-regulation of Carbonic Anhydrase Genes of *Bacillus mucilaginosus* under Soluble Ca²⁺ Deficiency and the Heterologously Expressed Enzyme Promotes Calcite Dissolution. *Geomicrobiology Journal* **31**:632-641.
78. **Westermann AJ, Barquist L, Vogel J.** 2017. Resolving host–pathogen interactions by dual RNA-seq. *PLoS Pathogens* **13**:e1006033.
79. **Humphrys MS, Creasy T, Sun Y, Shetty AC, Chibucos MC, Drabek EF, Fraser CM, Farooq U, Sengamalay N, Ott S, Shou H, Bavoil PM, Mahurkar A, Myers GSA.** 2013. Simultaneous Transcriptional Profiling of Bacteria and Their Host Cells. *PLoS ONE* **8**:e80597.
80. **Baddal B, Muzzi A, Censini S, Calogero RA, Torricelli G, Guidotti S, Taddei AR, Covacci A, Pizza M, Rappuoli R, Soriani M, Pezzicoli A.** 2015. Dual RNA-seq of Nontypeable *Haemophilus influenzae* and Host Cell Transcriptomes Reveals Novel Insights into Host-Pathogen Cross Talk. *mBio* **6**:e01765-01715.
81. **Westermann AJ, Förstner KU, Amman F, Barquist L, Chao Y, Schulte LN, Müller L, Reinhardt R, Stadler PF, Vogel J.** 2016. Dual RNA-seq unveils noncoding RNA functions in host–pathogen interactions. *Nature* **529**:496.

82. **Chatnaparat T, Prathuangwong S, Lindow SE.** 2016. Global Pattern of Gene Expression of *Xanthomonas axonopodis* pv. *glycines* Within Soybean Leaves. *Molecular Plant-Microbe Interactions* **29**:508-522.
83. **Yu X, Lund SP, Scott RA, Greenwald JW, Records AH, Nettleton D, Lindow SE, Gross DC, Beattie GA.** 2013. Transcriptional responses of *Pseudomonas syringae* to growth in epiphytic versus apoplastic leaf sites. *Proceedings of the National Academy of Sciences* **110**:E425-E434.
84. **Nobori T, Velásquez AC, Wu J, Kvitko BH, Kremer JM, Wang Y, He SY, Tsuda K.** 2018. Transcriptome landscape of a bacterial pathogen under plant immunity. *Proceedings of the National Academy of Sciences* doi:10.1073/pnas.1800529115.
85. **Baltrus DA, Nishimura MT, Romanchuk A, Chang JH, Mukhtar MS, Cherkis K, Roach J, Grant SR, Jones CD, Dangl JL.** 2011. Dynamic evolution of pathogenicity revealed by sequencing and comparative genomics of 19 *Pseudomonas syringae* isolates. *PLoS Pathogens* **7**:e1002132.
86. **Green S, Laue B, Fossdal CG, A'Hara SW, Cottrell JE.** 2009. Infection of horse chestnut (*Aesculus hippocastanum*) by *Pseudomonas syringae* pv. *aesculi* and its detection by quantitative real-time PCR. *Plant Pathology* **58**:731-744.
87. **McCann HC, Rikkerink EHA, Bertels F, Fiers M, Lu A, Rees-George J, Andersen MT, Gleave AP, Haubold B, Wohlers MW, Guttman DS, Wang PW, Straub C, Vanneste J, Rainey PB, Templeton MD.** 2013. Genomic

- Analysis of the Kiwifruit Pathogen *Pseudomonas syringae* pv. actinidiae Provides Insight into the Origins of an Emergent Plant Disease. *PLoS Pathogens* **9**:e1003503.
88. **Gill US, Lee S, Mysore KS.** 2015. Host Versus Nonhost Resistance: Distinct Wars with Similar Arsenals. *Phytopathology* **105**:580-587.
89. **Lindeberg M, Stavrinides J, Chang JH, Alfano JR, Collmer A, Dangl JL, Greenberg JT, Mansfield JW, Guttman DS.** 2005. Proposed guidelines for a unified nomenclature and phylogenetic analysis of type III Hop effector proteins in the plant pathogen *Pseudomonas syringae*. *Molecular Plant-Microbe Interactions* **18**:275-282.
90. **Lam HN, Chakravarthy S, Wei H-L, BuiNguyen H, Stodghill PV, Collmer A, Swingle BM, Cartinhour SW.** 2014. Global Analysis of the HrpL Regulon in the Plant Pathogen *Pseudomonas syringae* pv. tomato DC3000 Reveals New Regulon Members with Diverse Functions. *PLoS one* **9**:e106115.
91. **Ferreira AO, Myers CR, Gordon JS, Martin GB, Vencato M, Collmer A, Wehling MD, Alfano JR, Moreno-Hagelsieb G, Lamboy WF, DeClerck G, Schneider DJ, Cartinhour SW.** 2006. Whole-genome expression profiling defines the HrpL regulon of *Pseudomonas syringae* pv. tomato DC3000, allows de novo reconstruction of the Hrp cis element, and identifies novel coregulated genes. *Molecular Plant-Microbe Interactions* **19**:1167-1179.
92. **Jovanovic M, James EH, Burrows PC, Rego FGM, Buck M, Schumacher J.** 2011. Regulation of the co-evolved HrpR and HrpS AAA+ proteins

- required for *Pseudomonas syringae* pathogenicity. Nature Communications **2**:177.
93. **Lan L, Deng X, Zhou J, Tang X.** 2006. Genome-wide gene expression analysis of *Pseudomonas syringae* pv. *tomato* DC3000 reveals overlapping and distinct pathways regulated by *hrpL* and *hrpRS*. Molecular Plant-Microbe Interactions **19**:976-987.
94. **Deng X, Liang H, Chen K, He C, Lan L, Tang X.** 2014. Molecular mechanisms of two-component system RhpRS regulating type III secretion system in *Pseudomonas syringae*. Nucleic Acids Research **42**:11472-11486.
95. **Markel E, Stodghill P, Bao Z, Myers CR, Swingle B.** 2016. AlgU Controls Expression of Virulence Genes in *Pseudomonas syringae* pv. *tomato* DC3000. Journal of Bacteriology **198**:2330-2344.
96. **Moll S, Schneider DJ, Stodghill P, Myers CR, Cartinhour SW, Filiatrault MJ.** 2010. Construction of an *rsmX* co-variance model and identification of five *rsmX* non-coding RNAs in *Pseudomonas syringae* pv. *tomato* DC3000. RNA Biology **7**:508-516.
97. **Kong HS, Roberts DP, Patterson CD, Kuehne SA, Heeb S, Lakshman DK, Lydon J.** 2012. Effect of overexpressing *rsmA* from *Pseudomonas aeruginosa* on virulence of select phytotoxin-producing strains of *P. syringae*. Phytopathology **102**:575-587.
98. **Hershberger CD, Ye RW, Parsek MR, Xie ZD, Chakrabarty AM.** 1995. The *algT* (*algU*) gene of *Pseudomonas aeruginosa*, a key regulator involved

in alginate biosynthesis, encodes an alternative sigma factor (sigma E).
Proceedings of the National Academy of Sciences **92**:7941-7945.

99. **Norris V, Chen M, Goldberg M, Voskuil J, McGurk G, Holland B.** 1991. Calcium in bacteria: a solution to which problem? *Molecular Microbiology* **5**:775-778.
100. **Werthen M, Lundgren T.** 2001. Intracellular Ca(2+) mobilization and kinase activity during acylated homoserine lactone-dependent quorum sensing in *Serratia liquefaciens*. *Journal of Biological Chemistry* **276**:6468-6472.
101. **Guragain M, Lenaburg DL, Moore FS, Reutlinger I, Patrauchan MA.** 2013. Calcium homeostasis in *Pseudomonas aeruginosa* requires multiple transporters and modulates swarming motility. *Cell Calcium* **54**:350-361.
102. **Cruz LF, Cobine PA, De La Fuente L.** 2012. Calcium increases *Xylella fastidiosa* surface attachment, biofilm formation, and twitching motility. *Applied and Environmental Microbiology* **78**:1321-1331.
103. **Patrauchan MA, Sarkisova S, Sauer K, Franklin MJ.** 2005. Calcium influences cellular and extracellular product formation during biofilm-associated growth of a marine *Pseudoalteromonas* sp. *Microbiology* **151**:2885-2897.
104. **Bilecen K, Yildiz FH.** 2009. Identification of a calcium-controlled negative regulatory system affecting *Vibrio cholerae* biofilm formation. *Environmental Microbiology* **11**:2015-2029.

105. **Parker JK, Chen H, McCarty SE, Liu LY, De La Fuente L.** 2016. Calcium transcriptionally regulates the biofilm machinery of *Xylella fastidiosa* to promote continued biofilm development in batch cultures. *Environmental Microbiology* **18**:1620-1634.
106. **Flego D, Pirhonen M, Saarilahti H, Palva TK, Palva ET.** 1997. Control of virulence gene expression by plant calcium in the phytopathogen *Erwinia carotovora*. *Molecular Microbiology* **25**:831-838.
107. **Butcher BG, Bronstein PA, Myers CR, Stodghill PV, Bolton JJ, Markel EJ, Filiatrault MJ, Swingle B, Gaballa A, Helmann JD, Schneider DJ, Cartinhour SW.** 2011. Characterization of the Fur regulon in *Pseudomonas syringae* pv. tomato DC3000. *Journal of Bacteriology* **193**:4598-4611.
108. **Guragain M, King MM, Williamson KS, Perez-Osorio AC, Akiyama T, Khanam S, Patrauchan MA, Franklin MJ.** 2016. The *Pseudomonas aeruginosa* PAO1 Two-Component Regulator CarSR Regulates Calcium Homeostasis and Calcium-Induced Virulence Factor Production through Its Regulatory Targets CarO and CarP. *Journal of Bacteriology* **198**:951-963.
109. **Filiatrault MJ, Stodghill PV, Myers CR, Bronstein PA, Butcher BG, Lam H, Grills G, Schweitzer P, Wang W, Schneider DJ, Cartinhour SW.** 2011. Genome-wide identification of transcriptional start sites in the plant pathogen *Pseudomonas syringae* pv. tomato str. DC3000. *PLoS one* **6**:e29335.

110. **Kreamer NN, Wilks JC, Marlow JJ, Coleman ML, Newman DK.** 2012. BqsR/BqsS constitute a two-component system that senses extracellular Fe(II) in *Pseudomonas aeruginosa*. *Journal of Bacteriology* **194**:1195-1204.
111. **Perkins TT, Davies MR, Klemm EJ, Rowley G, Wileman T, James K, Keane T, Maskell D, Hinton JCD, Dougan G, Kingsley RA.** 2013. ChIP-seq and transcriptome analysis of the OmpR regulon of *Salmonella enterica* serovars Typhi and Typhimurium reveals accessory genes implicated in host colonization. *Molecular Microbiology* **87**:526-538.
112. **Consortium TU.** 2017. UniProt: the universal protein knowledgebase. *Nucleic Acids Research* **45**:D158-D169.
113. **Hay ID, Remminghorst U, Rehm BH.** 2009. MucR, a novel membrane-associated regulator of alginate biosynthesis in *Pseudomonas aeruginosa*. *Applied and Environmental Microbiology* **75**:1110-1120.
114. **Kaplan JB.** 2010. Biofilm Dispersal: Mechanisms, Clinical Implications, and Potential Therapeutic Uses. *Journal of Dental Research* **89**:205-218.
115. **Daniels R, Vanderleyden J, Michiels J.** 2004. Quorum sensing and swarming migration in bacteria. *FEMS Microbiology Reviews* **28**:261-289.
116. **Pérez-Mendoza D, Aragón IM, Prada-Ramírez HA, Romero-Jiménez L, Ramos C, Gallegos M-T, Sanjuán J.** 2014. Responses to Elevated c-di-GMP Levels in Mutualistic and Pathogenic Plant-Interacting Bacteria. *PLoS one* **9**:e91645.

117. **Records AR, Gross DC.** 2010. Sensor kinases RetS and LadS regulate *Pseudomonas syringae* type VI secretion and virulence factors. *Journal of Bacteriology* **192**:3584-3596.
118. **Byrd MS, Sadovskaya I, Vinogradov E, Lu H, Sprinkle AB, Richardson SH, Ma L, Ralston B, Parsek MR, Anderson EM, Lam JS, Wozniak DJ.** 2009. Genetic and biochemical analyses of the *Pseudomonas aeruginosa* Psl exopolysaccharide reveal overlapping roles for polysaccharide synthesis enzymes in Psl and LPS production. *Molecular Microbiology* **73**:622-638.
119. **Ude S, Arnold DL, Moon CD, Timms-Wilson T, Spiers AJ.** 2006. Biofilm formation and cellulose expression among diverse environmental *Pseudomonas* isolates. *Environmental Microbiology* **8**:1997-2011.
120. **Vinatzer BA, Jelenska J, Greenberg JT.** 2005. Bioinformatics Correctly Identifies Many Type III Secretion Substrates in the Plant Pathogen *Pseudomonas syringae* and the Biocontrol Isolate *P. fluorescens* SBW25. *Molecular Plant-Microbe Interactions* **18**:877-888.
121. **McCraw SL, Park DH, Jones R, Bentley MA, Rico A, Ratcliffe RG, Kruger NJ, Collmer A, Preston GM.** 2016. GABA (γ -Aminobutyric Acid) Uptake Via the GABA Permease GabP Represses Virulence Gene Expression in *Pseudomonas syringae* pv. *tomato* DC3000. *Molecular Plant-Microbe Interactions* **29**:938-949.

122. **Fraser KR, Tuite NL, Bhagwat A, O'Byrne CP.** 2006. Global effects of homocysteine on transcription in *Escherichia coli*: induction of the gene for the major cold-shock protein, CspA. *Microbiology* **152**:2221-2231.
123. **Kashyap DR, Rompca A, Gaballa A, Helmann JD, Chan J, Chang CJ, Hozo I, Gupta D, Dziarski R.** 2014. Peptidoglycan Recognition Proteins Kill Bacteria by Inducing Oxidative, Thiol, and Metal Stress. *PLoS Pathogens* **10**:e1004280.
124. **Ortiz-Martín I, Thwaites R, Macho AP, Mansfield JW, Beuzón CR.** 2010. Positive Regulation of the Hrp Type III Secretion System in *Pseudomonas syringae* pv. *phaseolicola*. *Molecular Plant-Microbe Interactions* **23**:665-681.
125. **Badel JL, Shimizu R, Oh H-S, Collmer A.** 2006. A *Pseudomonas syringae* pv. tomato *avrE1/hopM1* Mutant Is Severely Reduced in Growth and Lesion Formation in Tomato. *Molecular Plant-Microbe Interactions* **19**:99-111.
126. **Prost LR, Miller SI.** 2008. The *Salmonellae* PhoQ sensor: mechanisms of detection of phagosome signals. *Cellular Microbiology* **10**:576-582.
127. **Yoshida T, Qin L, Egger LA, Inouye M.** 2006. Transcription regulation of *ompF* and *ompC* by a single transcription factor, OmpR. *Journal of Biological Chemistry* **281**:17114-17123.
128. **Ogasawara H, Teramoto J, Hirao K, Yamamoto K, Ishihama A, Utsumi R.** 2004. Negative Regulation of DNA Repair Gene (*ung*) Expression by the CpxR/CpxA Two-Component System in *Escherichia coli* K-12 and

- Induction of Mutations by Increased Expression of CpxR. *Journal of Bacteriology* **186**:8317-8325.
129. **Weatherspoon-Griffin N, Yang D, Kong W, Hua Z, Shi Y.** 2014. The CpxR/CpxA two-component regulatory system up-regulates the multidrug resistance Cascade to facilitate *Escherichia coli* resistance to a model antimicrobial peptide. *The Journal of Biological Chemistry* **289**:32571-32582.
 130. **Martínez-Granero F, Navazo A, Barahona E, Redondo-Nieto M, Rivilla R, Martín M.** 2012. The Gac-Rsm and SadB Signal Transduction Pathways Converge on AlgU to Downregulate Motility in *Pseudomonas fluorescens*. *PLoS one* **7**:e31765.
 131. **Wood LF, Ohman DE.** 2009. Use of cell wall stress to characterize σ_{22} (AlgT/U) activation by regulated proteolysis and its regulon in *Pseudomonas aeruginosa*. *Molecular Microbiology* **72**:183-201.
 132. **Verstraeten N, Braeken K, Debkumari B, Fauvart M, Fransaer J, Vermant J, Michiels J.** 2008. Living on a surface: swarming and biofilm formation. *Trends in Microbiology* **16**:496-506.
 133. **Dong YH, Zhang XF, An SW, Xu JL, Zhang LH.** 2008. A novel two-component system BqsS-BqsR modulates quorum sensing-dependent biofilm decay in *Pseudomonas aeruginosa*. *Communicative & Integrative Biology* **1**:88-96.
 134. **Burch AY, Shimada BK, Mullin SW, Dunlap CA, Bowman MJ, Lindow SE.** 2012. *Pseudomonas syringae* coordinates production of a motility-

- enabling surfactant with flagellar assembly. *Journal of Bacteriology* **194**:1287-1298.
135. **Zorraquino V, Garcia B, Latasa C, Echeverz M, Toledo-Arana A, Valle J, Lasa I, Solano C.** 2013. Coordinated cyclic-di-GMP repression of *Salmonella* motility through YcgR and cellulose. *Journal of Bacteriology* **195**:417-428.
136. **Prada-Ramirez HA, Perez-Mendoza D, Felipe A, Martinez-Granero F, Rivilla R, Sanjuan J, Gallegos MT.** 2016. AmrZ regulates cellulose production in *Pseudomonas syringae* pv. tomato DC3000. *Molecular Microbiology* **99**:960-977.
137. **Kuchma SL, Delalez NJ, Filkins LM, Snavely EA, Armitage JP, O'Toole GA.** 2015. Cyclic di-GMP-mediated repression of swarming motility by *Pseudomonas aeruginosa* PA14 requires the MotAB stator. *Journal of Bacteriology* **197**:420-430.
138. **Toutain CM, Zegans ME, O'Toole GA.** 2005. Evidence for two flagellar stators and their role in the motility of *Pseudomonas aeruginosa*. *Journal of Bacteriology* **187**:771-777.
139. **Terashima H, Kojima S, Homma M.** 2008. Flagellar Motility in Bacteria. *International Review of Cell and Molecular Biology* **270**:39-85.
140. **Cardenal-Muñoz E, Ramos-Morales F.** 2013. DsbA and MgrB Regulate steA Expression through the Two-Component System PhoQ/PhoP in *Salmonella enterica*. *Journal of Bacteriology* **195**:2368-2378.

141. **Gao R, Stock AM.** 2013. Evolutionary Tuning of Protein Expression Levels of a Positively Autoregulated Two-Component System. *PLoS Genetics* **9**:e1003927.
142. **Munkvold KR, Russell AB, Kvitko BH, Collmer A.** 2009. *Pseudomonas syringae* pv. tomato DC3000 type III effector HopAA1-1 functions redundantly with chlorosis-promoting factor PSPTO4723 to produce bacterial speck lesions in host tomato. *Molecular Plant-Microbe Interactions* **22**:1341-1355.
143. **Worley JN, Russell AB, Wexler AG, Bronstein PA, Kvitko BH, Krasnoff SB, Munkvold KR, Swingle B, Gibson DM, Collmer A.** 2013. *Pseudomonas syringae* pv. tomato DC3000 CmaL (PSPTO4723), a DUF1330 Family Member, Is Needed To Produce l-allo-Isoleucine, a Precursor for the Phytotoxin Coronatine. *Journal of Bacteriology* **195**:287-296.
144. **Chakravarthy S, Worley JN, Montes-Rodriguez A, Collmer A.** 2017. *Pseudomonas syringae* pv. tomato DC3000 polymutants deploying coronatine and two type III effectors produce quantifiable chlorotic spots from individual bacterial colonies in *Nicotiana benthamiana* leaves. *Molecular Plant Pathology* doi:10.1111/mpp.12579.
145. **Guo M, Kim P, Li G, Elowsky Christian G, Alfano James R.** 2016. A Bacterial Effector Co-opts Calmodulin to Target the Plant Microtubule Network. *Cell Host & Microbe* **19**:67-78.
146. **Kvitko BH, Park DH, Velásquez AC, Wei C-F, Russell AB, Martin GB, Schneider DJ, Collmer A.** 2009. Deletions in the Repertoire of

- Pseudomonas syringae* pv. *tomato* DC3000 Type III Secretion Effector Genes Reveal Functional Overlap among Effectors. *PLoS Pathogens* **5**:e1000388.
147. **King EO, Ward MK, Raney DE.** 1954. Two simple media for the demonstration of pyocyanin and fluorescin. *Journal of Laboratory and Clinical Medicine* **44**:301-307.
148. **Schafer A, Tauch A, Jager W, Kalinowski J, Thierbach G, Puhler A.** 1994. Small mobilizable multi-purpose cloning vectors derived from the *Escherichia coli* plasmids pK18 and pK19: selection of defined deletions in the chromosome of *Corynebacterium glutamicum*. *Gene* **145**:69-73.
149. **Markel E, Maciak C, Butcher BG, Myers CR, Stodghill P, Bao Z, Cartinhour S, Swingle B.** 2011. An extracytoplasmic function sigma factor-mediated cell surface signaling system in *Pseudomonas syringae* pv. *tomato* DC3000 regulates gene expression in response to heterologous siderophores. *Journal of Bacteriology* **193**:5775-5783.
150. **Choi KH, Schweizer HP.** 2006. mini-Tn7 insertion in bacteria with single attTn7 sites: example *Pseudomonas aeruginosa*. *Nature Protocols* **1**:153-161.
151. **Swingle B, Thete D, Moll M, Myers CR, Schneider DJ, Cartinhour S.** 2008. Characterization of the PvdS-regulated promoter motif in *Pseudomonas syringae* pv. *tomato* DC3000 reveals regulon members and insights regarding PvdS function in other pseudomonads. *Molecular Microbiology* **68**:871-889.

152. **O'Leary BM, Rico A, McCraw S, Fones HN, Preston GM.** 2014. The Infiltration-centrifugation Technique for Extraction of Apoplastic Fluid from Plant Leaves Using *Phaseolus vulgaris* as an Example. Journal of Visualized Experiments doi:10.3791/52113:52113.
153. **Park SH, Butcher BG, Anderson Z, Pellegrini N, Bao Z, D'Amico K, Filiatrault MJ.** 2013. Analysis of the small RNA P16/RgsA in the plant pathogen *Pseudomonas syringae* pv. tomato strain DC3000. Microbiology **159**:296-306.
154. **Lelliott RA, Billing E, Hayward AC.** 1966. A determinative scheme for the fluorescent plant pathogenic pseudomonads. Journal of Applied Bacteriology **29**:470-489.
155. **Aronesty E.** 2013. Comparison of sequencing utility programs. The Open Bioinformatics Journal **7**:1-8.
156. **Langmead B, Salzberg SL.** 2012. Fast gapped-read alignment with Bowtie 2. Nature Methods **9**:357-359.
157. **Filiatrault MJ, Stodghill PV, Bronstein PA, Moll S, Lindeberg M, Grills G, Schweitzer P, Wang W, Schroth GP, Luo S, Khrebtukova I, Yang Y, Thannhauser T, Butcher BG, Cartinhour S, Schneider DJ.** 2010. Transcriptome analysis of *Pseudomonas syringae* identifies new genes, noncoding RNAs, and antisense activity. Journal of Bacteriology **192**:2359-2372.

158. **Bailey TL, Boden M, Buske FA, Frith M, Grant CE, Clementi L, Ren J, Li WW, Noble WS.** 2009. MEME Suite: tools for motif discovery and searching. *Nucleic Acids Research* **37**:W202-W208.
159. **Vencato M, Tian F, Alfano JR, Buell CR, Cartinhour S, DeClerck GA, Guttman DS, Stavrinides J, Joardar V, Lindeberg M, Bronstein PA, Mansfield JW, Myers CR, Collmer A, Schneider DJ.** 2006. Bioinformatics-enabled identification of the HrpL regulon and type III secretion system effector proteins of *Pseudomonas syringae* pv. phaseolicola 1448A. *Molecular Plant-Microbe Interactions* **19**:1193-1206.
160. **Knutson CA, Jeanes A.** 1968. A new modification of the carbazole analysis: application to heteropolysaccharides. *Analytical Biochemistry* **24**:470-481.
161. **Deziel E, Lepine F, Milot S, Villemur R.** 2003. rhlA is required for the production of a novel biosurfactant promoting swarming motility in *Pseudomonas aeruginosa*: 3-(3-hydroxyalkanoyloxy)alkanoic acids (HAAs), the precursors of rhamnolipids. *Microbiology* **149**:2005-2013.
162. **Rashid MH, Kornberg A.** 2000. Inorganic polyphosphate is needed for swimming, swarming, and twitching motilities of *Pseudomonas aeruginosa*. *Proceedings of the National Academy of Sciences* **97**:4885-4890.
163. **Tremblay J, Richardson AP, Lepine F, Deziel E.** 2007. Self-produced extracellular stimuli modulate the *Pseudomonas aeruginosa* swarming motility behaviour. *Environmental Microbiology* **9**:2622-2630.

164. **Merritt JH, Kadouri DE, O'Toole GA.** 2005. Growing and analyzing static biofilms. *Curr Protoc Microbiol* **Chapter 1**:Unit 1B 1.
165. **Fishman MR, Zhang J, Bronstein PA, Stodghill P, Filiatrault MJ.** 2018. Ca²⁺-induced two-component system CvsSR regulates the type III secretion system and the extracytoplasmic function sigma factor AlgU in *Pseudomonas syringae* pv. tomato DC3000. *Journal of Bacteriology* **200**:e00538-00517.
166. **Bader MW, Navarre WW, Shiau W, Nikaido H, Frye JG, McClelland M, Fang FC, Miller SI.** 2003. Regulation of *Salmonella typhimurium* virulence gene expression by cationic antimicrobial peptides. *Molecular Microbiology* **50**:219-230.
167. **Choi J, Groisman EA.** 2016. Acidic pH sensing in the bacterial cytoplasm is required for *Salmonella* virulence. *Molecular Microbiology* **101**:1024-1038.
168. **Steele KH, O'Connor LH, Burpo N, Kohler K, Johnston JW.** 2012. Characterization of a Ferrous Iron-Responsive Two-Component System in Nontypeable *Haemophilus influenzae*. *Journal of Bacteriology* **194**:6162-6173.
169. **Kreamer NN, Costa F, Newman DK.** 2015. The Ferrous Iron-Responsive BqsRS Two-Component System Activates Genes That Promote Cationic Stress Tolerance. *MBio* **6**.
170. **Kearns DB.** 2010. A field guide to bacterial swarming motility. *Nature reviews Microbiology* **8**:634-644.

171. **Konhauser K, Riding R.** 2012. Bacterial Biomineralization, p 105-130, Fundamentals of Geobiology doi:10.1002/9781118280874.ch8. John Wiley & Sons, Ltd.
172. **Knorre Hv, Krumbein WE.** 2000. Bacterial calcification, p 25-31, Microbial sediments. Springer.
173. **Ercole C, Cacchio P, Botta AL, Centi V, Lepidi A.** 2007. Bacterially induced mineralization of calcium carbonate: the role of exopolysaccharides and capsular polysaccharides. Microscopy and Microanalysis **13**.
174. **Arias JL, Fernández MS.** 2008. Polysaccharides and Proteoglycans in Calcium Carbonate-based Biomineralization. Chemical Reviews **108**:4475-4482.
175. **Kim HJ, Shin B, Lee YS, Park W.** 2017. Modulation of calcium carbonate precipitation by exopolysaccharide in *Bacillus* sp. JH7. Applied Microbiology and Biotechnology **101**:6551-6561.
176. **Sharma SB, Sayyed RZ, Trivedi MH, Gobi TA.** 2013. Phosphate solubilizing microbes: sustainable approach for managing phosphorus deficiency in agricultural soils. SpringerPlus **2**:587.
177. **Rodríguez H, Fraga R, Gonzalez T, Bashan Y.** 2006. Genetics of phosphate solubilization and its potential applications for improving plant growth-promoting bacteria. Plant and Soil **287**:15-21.
178. **Felce J, Saier MH, Jr.** 2004. Carbonic anhydrases fused to anion transporters of the SulP family: evidence for a novel type of bicarbonate

- transporter. *Journal of Molecular Microbiology and Biotechnology* **8**:169-176.
179. **Mekmene O, Quillard S, Rouillon T, Bouler J-M, Piot M, Gaucheron F.** 2009. Effects of pH and Ca/P molar ratio on the quantity and crystalline structure of calcium phosphates obtained from aqueous solutions. *Dairy Science & Technology* **89**:301-316.
180. **Sato T, Fujihashi M, Miyamoto Y, Kuwata K, Kusaka E, Fujita H, Miki K, Atomi H.** 2013. An uncharacterized member of the Ribokinase family in *Thermococcus kodakarensis* exhibits myo-Inositol kinase activity. *Journal of Biological Chemistry* **288**:20856-20867.
181. **Merino F, Rivas-Pardo JA, Caniuguir A, García I, Guixé V.** 2012. Catalytic and regulatory roles of divalent metal cations on the phosphoryl-transfer mechanism of ADP-dependent sugar kinases from hyperthermophilic archaea. *Biochimie* **94**:516-524.
182. **Braissant O, Cailleau G, Dupraz C, Verrecchia EP.** 2003. Bacterially induced mineralization of calcium carbonate in terrestrial environments: the role of exopolysaccharides and amino acids. *Journal of Sedimentary Research* **73**:485-490.
183. **Pan HB, Darvell BW.** 2009. Calcium Phosphate Solubility: The Need for Re-Evaluation. *Crystal Growth & Design* **9**:639-645.
184. **Ke W-J, Hsueh Y-H, Cheng Y-C, Wu C-C, Liu S-T.** 2015. Water surface tension modulates the swarming mechanics of *Bacillus subtilis*. *Frontiers in Microbiology* **6**.

185. **O'Leary BM, Neale HC, Geilfus CM, Jackson RW, Arnold DL, Preston GM.** 2016. Early changes in apoplast composition associated with defence and disease in interactions between *Phaseolus vulgaris* and the halo blight pathogen *Pseudomonas syringae* Pv. *phaseolicola*. *Plant, Cell & Environment* **39**:2172-2184.
186. **Lecourieux D, Ranjeva R, Pugin A.** 2006. Calcium in plant defence-signalling pathways. *New Phytologist* **171**:249-269.
187. **Aslam SN, Newman M-A, Erbs G, Morrissey KL, Chinchilla D, Boller T, Jensen TT, De Castro C, Ierano T, Molinaro A, Jackson RW, Knight MR, Cooper RM.** 2008. Bacterial Polysaccharides Suppress Induced Innate Immunity by Calcium Chelation. *Current Biology* **18**:1078-1083.
188. **Rowlett RS.** 2010. Structure and catalytic mechanism of the β -carbonic anhydrases. *Biochimica et Biophysica Acta (BBA) - Proteins and Proteomics* **1804**:362-373.
189. **Chegwidden WR, Dodgson SJ, Spencer IM.** 2000. The roles of carbonic anhydrase in metabolism, cell growth and cancer in animals, p 343-363, *The Carbonic Anhydrases*. Springer.
190. **Henry RP.** 1996. Multiple roles of carbonic anhydrase in cellular transport and metabolism. *Annual Review of Physiology* **58**:523-538.
191. **DiMario RJ, Clayton H, Mukherjee A, Ludwig M, Moroney JV.** 2017. Plant Carbonic Anhydrases: Structures, Locations, Evolution, and Physiological Roles. *Molecular Plant* **10**:30-46.

192. **Xin X-F, He SY.** 2013. *Pseudomonas syringae* pv. *tomato* DC3000: A Model Pathogen for Probing Disease Susceptibility and Hormone Signaling in Plants. *Annual Review of Phytopathology* **51**:473-498.
193. **Moscoso JA, Mikkelsen H, Heeb S, Williams P, Filloux A.** 2011. The *Pseudomonas aeruginosa* sensor RetS switches Type III and Type VI secretion via c-di-GMP signalling. *Environmental Microbiology* **13**:3128-3138.
194. **Ueda A, Wood TK.** 2009. Connecting Quorum Sensing, c-di-GMP, Pel Polysaccharide, and Biofilm Formation in *Pseudomonas aeruginosa* through Tyrosine Phosphatase TpbA (PA3885). *PLoS Pathogens* **5**:e1000483.
195. **Lo Y-L, Shen L, Chang C-H, Bhuwan M, Chiu C-H, Chang H-Y.** 2016. Regulation of Motility and Phenazine Pigment Production by FliA Is Cyclic-di-GMP Dependent in *Pseudomonas aeruginosa* PAO1. *PLoS one* **11**:e0155397.
196. **Pukatzki S, McAuley SB, Miyata ST.** 2009. The type VI secretion system: translocation of effectors and effector-domains. *Current Opinion in Microbiology* **12**:11-17.
197. **Haapalainen M, Mosorin H, Dorati F, Wu RF, Roine E, Taira S, Nissinen R, Mattinen L, Jackson R, Pirhonen M, Lin NC.** 2012. Hcp2, a secreted protein of the phytopathogen *Pseudomonas syringae* pv. *tomato* DC3000, is required for fitness for competition against bacteria and yeasts. *J Bacteriol* **194**:4810-4822.

198. **House BL, Mortimer MW, Kahn ML.** 2004. New recombination methods for *Sinorhizobium meliloti* genetics. *Applied and Environmental Microbiology* **70**:2806-2815.
199. **Aguilera J, Van Dijken JP, De Winde JH, Pronk JT.** 2005. Carbonic anhydrase (Nce103p): an essential biosynthetic enzyme for growth of *Saccharomyces cerevisiae* at atmospheric carbon dioxide pressure. *Biochemical Journal* **391**:311-316.
200. **Koestler BJ, Waters CM.** 2014. Bile acids and bicarbonate inversely regulate intracellular cyclic di-GMP in *Vibrio cholerae*. *Infection and immunity* **82**:3002-3014.
201. **Rose SJ, Bermudez LE.** 2016. Identification of Bicarbonate as a Trigger and Genes Involved with Extracellular DNA Export in Mycobacterial Biofilms. *mBio* **7**:e01597-01516.
202. **Wilton M, Charron-Mazenod L, Moore R, Lewenza S.** 2016. Extracellular DNA acidifies biofilms and induces aminoglycoside resistance in *Pseudomonas aeruginosa*. *Antimicrobial Agents and Chemotherapy* **60**:544-553.
203. **Pfeilmeier S, Saur IML, Rathjen JP, Zipfel C, Malone JG.** 2016. High levels of cyclic-di-GMP in plant-associated *Pseudomonas* correlate with evasion of plant immunity. *Molecular Plant Pathology* **17**:521-531.
204. **Delwiche EA, Fukui GM, Andrews AW, Surgalla MJ.** 1959. Environmental conditions affecting the population dynamics and the

- retention of virulence of *Pasturella pestis*: the role of carbon dioxide.
Journal of Bacteriology **77**:355-360.
205. **Morgan JK, Vendura KW, Stevens SM, Riordan JT.** 2013. RcsB determines the locus of enterocyte effacement (LEE) expression and adherence phenotype of *Escherichia coli* O157:H7 spinach outbreak strain TW14359 and coordinates bicarbonate-dependent LEE activation with repression of motility. Microbiology **159**:2342-2353.
206. **Kenny B, Abe A, Stein M, Finlay BB.** 1997. Enteropathogenic *Escherichia coli* protein secretion is induced in response to conditions similar to those in the gastrointestinal tract. Infection and Immunity **65**:2606-2612.
207. **Martínez H, Buhse T, Rivera M, Parmananda P, Ayala G, Sánchez J.** 2012. Endogenous CO₂ may inhibit bacterial growth and induce virulence gene expression in enteropathogenic *Escherichia coli*. Microbial Pathogenesis **53**:49-55.
208. **Wolfgang MC, Lee VT, Gilmore ME, Lory S.** 2003. Coordinate Regulation of Bacterial Virulence Genes by a Novel Adenylate Cyclase-Dependent Signaling Pathway. Developmental Cell **4**:253-263.
209. **Topal H, Fulcher NB, Bitterman J, Salazar E, Buck J, Levin LR, Cann MJ, Wolfgang MC, Steegborn C.** 2012. Crystal structure and regulation mechanisms of the CyaB adenylyl cyclase from the human pathogen *Pseudomonas aeruginosa*. Journal of Molecular Biology **416**:271-286.
210. **Holtsmark I, Eijsink VGH, Brurberg MB.** 2008. Bacteriocins from plant pathogenic bacteria. FEMS Microbiology Letters **280**:1-7.

211. **Broder UN, Jaeger T, Jenal U.** 2016. LadS is a calcium-responsive kinase that induces acute-to-chronic virulence switch in *Pseudomonas aeruginosa*. *Nature Microbiology* **2**:16184.
212. **Soscia C, Hachani A, Bernadac A, Filloux A, Bleves S.** 2007. Cross talk between type III secretion and flagellar assembly systems in *Pseudomonas aeruginosa*. *Journal of Bacteriology* **189**:3124-3132.
213. **Streckfuss JL, Smith WN, Brown LR, Campbell MM.** 1974. Calcification of selected strains of *Streptococcus mutans* and *Streptococcus sanguis*. *Journal of Bacteriology* **120**:502-506.
214. **van Dijk S, Dean DD, Liu Y, Zhao Y, Chirgwin JM, Schwartz Z, Boyan BD.** 1998. Purification, Amino Acid Sequence, and cDNA Sequence of a Novel Calcium-Precipitating Proteolipid Involved in Calcification of *Corynebacterium matruchotii*. *Calcified Tissue International* **62**:350-358.
215. **Ennever J, Vogel J, Streckfuss J.** 1974. Calcification by *Escherichia coli*. *Journal of Bacteriology* **119**:1061.
216. **Benzerara K, Menguy N, Guyot F, Skouri F, de Luca G, Barakat M, Heulin T.** 2004. Biologically controlled precipitation of calcium phosphate by *Ramlibacter tataouinensis*. *Earth and Planetary Science Letters* **228**:439-449.
217. **Khanafari A, Akbari T, Sohrabi MR.** 2014. Comparison of nano-hydroxyapatite productivity by *Pseudomonas aeruginosa* and *Serratia marcescense* through encapsulation method. *Nanomedicine Journal* **1**:276-284.

218. **Bazylnski DA, Frankel RB.** 2003. Biologically controlled mineralization in prokaryotes. *Reviews in Mineralogy and Geochemistry* **54**:217-247.
219. **Vogel JJ, Smith WN.** 1976. Calcification of Membranes Isolated from: *Bacterionema matruchotii*. *Journal of Dental Research* **55**:1080-1083.
220. **Rainey PB.** 1999. Adaptation of *Pseudomonas fluorescens* to the plant rhizosphere. *Environmental Microbiology* **1**:243-257.
221. **Molina L, Ramos C, Duque E, Ronchel MC, García JM, Wyke L, Ramos JL.** 2000. Survival of *Pseudomonas putida* KT2440 in soil and in the rhizosphere of plants under greenhouse and environmental conditions. *Soil Biology and Biochemistry* **32**:315-321.
222. **Mariano RL, McCarter SM.** 1993. Epiphytic survival of *Pseudomonas viridiflava* on tomato and selected weed species. *Microbial Ecology* **26**:47-58.
223. **Penyalver R, García A, Ferrer A, Bertolini E, López MM.** 2000. Detection of *Pseudomonas savastanoi* pv. *savastanoi* in olive plants by enrichment and PCR. *Applied and Environmental Microbiology* **66**:2673-2677.
224. **Sarkar SF, Guttman DS.** 2004. Evolution of the core genome of *Pseudomonas syringae*, a highly clonal, endemic plant pathogen. *Applied and Environmental Microbiology* **70**:1999-2012.
225. **Hammes F, Boon N, de Villiers J, Verstraete W, Siciliano SD.** 2003. Strain-specific ureolytic microbial calcium carbonate precipitation. *Applied and Environmental Microbiology* **69**:4901-4909.

226. **Connolly J, Kaufman M, Rothman A, Gupta R, Redden G, Schuster M, Colwell F, Gerlach R.** 2013. Construction of two ureolytic model organisms for the study of microbially induced calcium carbonate precipitation. *Journal of Microbiological Methods* **94**:290-299.
227. **Li X, Chopp DL, Russin WA, Brannon PT, Parsek MR, Packman AI.** 2015. Spatial patterns of carbonate biomineralization in biofilms. *Applied and Environmental Microbiology* **81**:7403-7410.
228. **Turner RJ, Renshaw JC, Hamilton A.** 2017. Biogenic Hydroxyapatite: A New Material for the Preservation and Restoration of the Built Environment. *ACS Applied Materials and Interfaces* doi:10.1021/acsami.7b07927.
229. **Moghim A, Lewis D, Oades J.** 1978. Release of phosphate from calcium phosphates by rhizosphere products. *Soil Biology and Biochemistry* **10**:277-281.
230. **Miller T, Schroth M.** 1972. Monitoring the epiphytic population of *Erwinia amylovora* on pear with a selective medium. *Phytopathology* **62**:1175-1182.
231. **Koutsopoulos S.** 2002. Synthesis and characterization of hydroxyapatite crystals: A review study on the analytical methods. *Journal of Biomedical Materials Research* **62**:600-612.
232. **de Aza PN, Guitián F, Santos C, de Aza S, Cuscó R, Artús L.** 1997. Vibrational Properties of Calcium Phosphate Compounds. 2. Comparison

- between Hydroxyapatite and β -Tricalcium Phosphate. *Chemistry of Materials* **9**:916-922.
233. **Zimmermann KA, LeBlanc JM, Sheets KT, Fox RW, Gatenholm P.** 2011. Biomimetic design of a bacterial cellulose/hydroxyapatite nanocomposite for bone healing applications. *Materials Science and Engineering: C* **31**:43-49.
234. **Luo Y, Lode A, Wu C, Chang J, Gelinsky M.** 2015. Alginate/Nanohydroxyapatite Scaffolds with Designed Core/Shell Structures Fabricated by 3D Plotting and in Situ Mineralization for Bone Tissue Engineering. *ACS Applied Materials & Interfaces* **7**:6541-6549.
235. **Heinemann M, Meinberg H, Büchs J, Koß H-J, Ansorge-Schumacher MB.** 2005. Method for Quantitative Determination of Spatial Polymer Distribution in Alginate Beads Using Raman Spectroscopy. *Applied Spectroscopy* **59**:280-285.
236. **Szymańska-Chargot M, Cybulska J, Zdunek A.** 2011. Sensing the Structural Differences in Cellulose from Apple and Bacterial Cell Wall Materials by Raman and FT-IR Spectroscopy. *Sensors (Basel, Switzerland)* **11**:5543-5560.
237. **Campos-Vallette MM, Chandía NP, Clavijo E, Leal D, Matsuhira B, Osorio-Román IO, Torres S.** 2010. Characterization of sodium alginate and its block fractions by surface-enhanced Raman spectroscopy. *Journal of Raman Spectroscopy* **41**:758-763.

238. **Czamara K, Majzner K, Pacia MZ, Kochan K, Kaczor A, Baranska M.** 2015. Raman spectroscopy of lipids: a review. *Journal of Raman Spectroscopy* **46**:4-20.
239. **Preiter K, Brooks DM, Penaloza-Vazquez A, Sreedharan A, Bender CL, Kunkel BN.** 2005. Novel virulence gene of *Pseudomonas syringae* pv. tomato strain DC3000. *Journal of Bacteriology* **187**:7805-7814.
240. **Puchtler H, Meloan SN, Terry MS.** 1969. On the history and mechanism of alizarin and alizarin red S stains for calcium. *Journal of Histochemistry and Cytochemistry* **17**:110-124.
241. **Daskalakis MI, Magoulas A, Kotoulas G, Catsikis I, Bakolas A, Karageorgis AP, Mavridou A, Doulia D, Rigas F.** 2013. *Pseudomonas, Pantoea* and *Cupriavidus* isolates induce calcium carbonate precipitation for bioremediation of ornamental stone. *Journal of Applied Microbiology* **115**:409-423.
242. **Barabesi C, Galizzi A, Mastromei G, Rossi M, Tamburini E, Perito B.** 2007. *Bacillus subtilis* gene cluster involved in calcium carbonate biomineralization. *Journal of Bacteriology* **189**:228-235.
243. **Rivadeneira MA, Martin-Algarra A, Sanchez-Roman M, Sanchez-Navas A, Martin-Ramos JD.** 2010. Amorphous Ca-phosphate precursors for Ca-carbonate biominerals mediated by *Chromohalobacter marismortui*. *ISME Journal* **4**:922-932.

244. **Bai Y, Guo X-j, Li Y-z, Huang T.** 2017. Experimental and visual research on the microbial induced carbonate precipitation by *Pseudomonas aeruginosa*. *AMB Express* **7**:57.
245. **Ferguson JF, Jenkins D, Eastman J.** 1973. Calcium Phosphate Precipitation at Slightly Alkaline pH Values. *Journal (Water Pollution Control Federation)* **45**:620-631.
246. **Song Y, Hahn HH, Hoffmann E.** 2002. Effects of solution conditions on the precipitation of phosphate for recovery: A thermodynamic evaluation. *Chemosphere* **48**:1029-1034.
247. **Nelson KE, Weinel C, Paulsen IT, Dodson RJ, Hilbert H, Martins dos Santos VA, Fouts DE, Gill SR, Pop M, Holmes M, Brinkac L, Beanan M, DeBoy RT, Daugherty S, Kolonay J, Madupu R, Nelson W, White O, Peterson J, Khouri H, Hance I, Chris Lee P, Holtzapple E, Scanlan D, Tran K, Moazzez A, Utterback T, Rizzo M, Lee K, Kosack D, Moestl D, Wedler H, Lauber J, Stjepandic D, Hoheisel J, Straetz M, Heim S, Kiewitz C, Eisen JA, Timmis KN, Dusterhoft A, Tumbler B, Fraser CM.** 2002. Complete genome sequence and comparative analysis of the metabolically versatile *Pseudomonas putida* KT2440. *Environmental Microbiology* **4**:799-808.
248. **Compeau G, Al-Achi BJ, Platsouka E, Levy SB.** 1988. Survival of rifampin-resistant mutants of *Pseudomonas fluorescens* and *Pseudomonas putida* in soil systems. *Applied and Environmental Microbiology* **54**:2432-2438.

249. **Wilson M, Lindow S.** 1993. Interactions between the biological control agent *Pseudomonas fluorescens* A506 and *Erwinia amylovora* in pear blossoms. *Phytopathology* **83**:117-123.
250. **Jackson RW, Preston GM, Rainey PB.** 2005. Genetic characterization of *Pseudomonas fluorescens* SBW25 *rsp* gene expression in the phytosphere and *in vitro*. *Journal of Bacteriology* **187**:8477-8488.
251. **Boivin R, Lebeuf H, Dion P.** 1987. Octopine and octopinic acid utilization in a nonfluorescent *Pseudomonas* sp.: enhancement by spontaneous mutation and lack of effect from curing of a plasmid. *Canadian Journal of Microbiology* **33**:534-540.
252. **Preston GM.** 2000. *Pseudomonas syringae* pv. *tomato*: the right pathogen, of the right plant, at the right time. *Molecular Plant Pathology* **1**:263-275.
253. **Loper JE, Lindow SE.** 1987. Lack of evidence for the *in situ* fluorescent pigment production by *Pseudomonas syringae* pv. *syringae* on bean leaf surfaces. *Phytopathology* **77**:1449-1454.
254. **Li P, Ohtsuki C, Kokubo T, Nakanishi K, Soga N, Nakamura T, Yamamuro T.** 1993. Process of formation of bone-like apatite layer on silica gel. *Journal of Materials Science: Materials in Medicine* **4**:127-131.
255. **de Almeida LG, Ortiz JH, Schneider RP, Spira B.** 2015. *phoU* Inactivation in *Pseudomonas aeruginosa* Enhances Accumulation of ppGpp and Polyphosphate. *Applied and Environmental Microbiology* **81**:3006-3015.
256. **Chakravarthy S, Butcher BG, Liu Y, D'Amico K, Coster M, Filiatrault MJ.** 2017. Virulence of *Pseudomonas syringae* pv. *tomato* DC3000 Is

- Influenced by the Catabolite Repression Control Protein Crc. *Molecular Plant-Microbe Interactions* **30**:283-294.
257. **Lecourieux D, Ranjeva R, Pugin A.** 2006. Calcium in plant defence-signalling pathways. *New Phytologist* **171**:249-269.
258. **Choi JY, Sifri CD, Goumnerov BC, Rahme LG, Ausubel FM, Calderwood SB.** 2002. Identification of virulence genes in a pathogenic strain of *Pseudomonas aeruginosa* by representational difference analysis. *Journal of Bacteriology* **184**:952-961.
259. **Granato LM, Picchi SC, de Oliveira Andrade M, Takita MA, de Souza AA, Wang N, Machado MA.** 2016. The ATP-dependent RNA helicase HrpB plays an important role in motility and biofilm formation in *Xanthomonas citri* subsp. *citri*. *BMC Microbiology* **16**:55.
260. **Lan L, Deng X, Xiao Y, Zhou JM, Tang X.** 2007. Mutation of Lon protease differentially affects the expression of *Pseudomonas syringae* type III secretion system genes in rich and minimal media and reduces pathogenicity. *Mol Plant Microbe Interact* **20**:682-696.
261. **Kinscherf TG, Hirano SS, Willis DK.** 2000. Transposon insertion in the *ftsK* gene impairs *in planta* growth and lesion-forming abilities in *Pseudomonas syringae* pv. *syringae* B728a. *Molecular Plant-Microbe Interactions* **13**:1263-1265.
262. **Choi KH, Kumar A, Schweizer HP.** 2006. A 10-min method for preparation of highly electrocompetent *Pseudomonas aeruginosa* cells:

- application for DNA fragment transfer between chromosomes and plasmid transformation. *Journal of Microbiological Methods* **64**:391-397.
263. **Hanahan D.** 1983. Studies on transformation of *Escherichia coli* with plasmids. *Journal of Molecular Biology* **166**:557-580.
264. **Chambers A.** 2010. Characterization Of The *Pseudomonas syringae* Pathovar *tomato* DC3000 Rets Hybrid Two Component Sensor For Induction Of The Type Three Secretion System And Motility.
265. **Smith JM, Heese A.** 2014. Rapid bioassay to measure early reactive oxygen species production in *Arabidopsis* leave tissue in response to living *Pseudomonas syringae*. *Plant Methods* **10**:6-6.
266. **Cui H, Tsuda K, Parker JE.** 2015. Effector-Triggered Immunity: From Pathogen Perception to Robust Defense. *Annual Review of Plant Biology* **66**:487-511.
267. **Chen C, Li S, McKeever DR, Beattie GA.** 2013. The widespread plant-colonizing bacterial species *Pseudomonas syringae* detects and exploits an extracellular pool of choline in hosts. *The Plant Journal* **75**:891-902.
268. **Angelichio MJ, Camilli A.** 2002. In Vivo Expression Technology. *Infection and Immunity* **70**:6518-6523.
269. **Osbourn A, Barber C, Daniels M.** 1987. Identification of plant-induced genes of the bacterial pathogen *Xanthomonas campestris* pathovar *campestris* using a promoter-probe plasmid. *The EMBO journal* **6**:23.

270. **Boch J, Joardar V, Gao L, Robertson TL, Lim M, Kunkel BN.** 2002. Identification of *Pseudomonas syringae* pv. tomato genes induced during infection of *Arabidopsis thaliana*. *Molecular Microbiology* **44**:73-88.
271. **Chuang DY, Kyeremeh AG, Gunji Y, Takahara Y, Ehara Y, Kikumoto T.** 1999. Identification and cloning of an *Erwinia carotovora* subsp. *carotovora* bacteriocin regulator gene by insertional mutagenesis. *Journal of Bacteriology* **181**:1953-1957.
272. **Kazemi-Pour N, Condemine G, Hugouvieux-Cotte-Pattat N.** 2004. The secretome of the plant pathogenic bacterium *Erwinia chrysanthemi*. *Proteomics* **4**:3177-3186.
273. **Zhao Y, Blumer SE, Sundin GW.** 2005. Identification of *Erwinia amylovora* genes induced during infection of immature pear tissue. *Journal of Bacteriology* **187**:8088-8103.
274. **Jacobs JM, Babujee L, Meng F, Milling A, Allen C.** 2012. The *In Planta* Transcriptome of *Ralstonia solanacearum*: Conserved Physiological and Virulence Strategies during Bacterial Wilt of Tomato. *mBio* **3**:e00114-00112.
275. **Soto-Suárez M, Bernal D, González C, Szurek B, Guyot R, Tohme J, Verdier V.** 2010. *In planta* gene expression analysis of *Xanthomonas oryzae* pathovar *oryzae*, African strain MAI1. *BMC Microbiology* **10**:170.
276. **Rosli HG, Zheng Y, Pombo MA, Zhong S, Bombarely A, Fei Z, Collmer A, Martin GB.** 2013. Transcriptomics-based screen for genes induced by

- flagellin and repressed by pathogen effectors identifies a cell wall-associated kinase involved in plant immunity. *Genome Biology* **14**:R139.
277. **De-la-Peña C, Lei Z, Watson BS, Sumner LW, Vivanco JM.** 2008. Root-Microbe Communication through Protein Secretion. *Journal of Biological Chemistry* **283**:25247-25255.
278. **Sewelam N, Kazan K, Schenk PM.** 2016. Global Plant Stress Signaling: Reactive Oxygen Species at the Cross-Road. *Frontiers in Plant Science* **7**.
279. **Santos R, Franza T, Laporte M-L, Sauvage C, Touati D, Expert D.** 2001. Essential Role of Superoxide Dismutase on the Pathogenicity of *Erwinia chrysanthemi* Strain 3937. *Molecular Plant-Microbe Interactions* **14**:758-767.
280. **Fontenelle C, Blanco C, Arrieta M, Dufour V, Trautwetter A.** 2011. Resistance to organic hydroperoxides requires *ohr* and *ohrR* genes in *Sinorhizobium meliloti*. *BMC Microbiology* **11**:100-100.
281. **Zheng XY, Spivey NW, Zeng W, Liu PP, Fu ZQ, Klessig DF, He SY, Dong X.** 2012. Coronatine promotes *Pseudomonas syringae* virulence in plants by activating a signaling cascade that inhibits salicylic acid accumulation. *Cell Host Microbe* **11**:587-596.
282. **Keith RC, Keith LMW, Hernández-Guzmán G, Uppalapati SR, Bender CL.** 2003. Alginate gene expression by *Pseudomonas syringae* pv. tomato DC3000 in host and non-host plants. *Microbiology* **149**:1127-1138.
283. **Love MI, Huber W, Anders S.** 2014. Moderated estimation of fold change and dispersion for RNA-seq data with DESeq2. *Genome Biology* **15**:550.

284. **Baynham PJ, Brown AL, Hall LL, Wozniak DJ.** 1999. *Pseudomonas aeruginosa* AlgZ, a ribbon-helix-helix DNA-binding protein, is essential for alginate synthesis and *algD* transcriptional activation. *Molecular Microbiology* **33**:1069-1080.
285. **Lizewski SE, Schurr JR, Jackson DW, Frisk A, Carterson AJ, Schurr MJ.** 2004. Identification of AlgR-Regulated Genes in *Pseudomonas aeruginosa* by Use of Microarray Analysis. *Journal of Bacteriology* **186**:5672-5684.
286. **Kato J, Misra TK, Chakrabarty AM.** 1990. AlgR3, a protein resembling eukaryotic histone H1, regulates alginate synthesis in *Pseudomonas aeruginosa*. *Proceedings of the National Academy of Sciences* **87**:2887-2891.
287. **Penaloza-Vazquez A, Fakhr MK, Bailey AM, Bender CL.** 2004. AlgR functions in *algC* expression and virulence in *Pseudomonas syringae* pv. *syringae*. *Microbiology* **150**:2727-2737.
288. **Ma L, Jackson KD, Landry RM, Parsek MR, Wozniak DJ.** 2006. Analysis of *Pseudomonas aeruginosa* conditional *psl* variants reveals roles for the *psl* polysaccharide in adhesion and maintaining biofilm structure postattachment. *Journal of Bacteriology* **188**:8213-8221.
289. **Jones AM, Wildermuth MC.** 2011. The Phytopathogen *Pseudomonas syringae* pv. *tomato* DC3000 Has Three High-Affinity Iron-Scavenging Systems Functional under Iron Limitation Conditions but Dispensable for Pathogenesis. *Journal of Bacteriology* **193**:2767-2775.

290. **Bienfait HF, Scheffers M.** 1992. Some properties of ferric citrate relevant to the iron nutrition of plants. *Plant and Soil* **143**:141-144.
291. **Freeman BC, Chen C, Yu X, Nielsen L, Peterson K, Beattie GA.** 2013. Physiological and transcriptional responses to osmotic stress of two *Pseudomonas syringae* strains that differ in epiphytic fitness and osmotolerance. *Journal of Bacteriology* **195**:4742-4752.
292. **Xin X-F, Nomura K, Aung K, Velásquez AC, Yao J, Boutrot F, Chang JH, Zipfel C, He SY.** 2016. Bacteria establish an aqueous living space in plants crucial for virulence. *Nature* **539**:524-529.
293. **Ranf S, Gisch N, Schaffer M, Illig T, Westphal L, Knirel YA, Sanchez-Carballo PM, Zahringer U, Huckelhoven R, Lee J, Scheel D.** 2015. A lectin S-domain receptor kinase mediates lipopolysaccharide sensing in *Arabidopsis thaliana*. *Nature Immunology* **16**:426-433.
294. **Deng W-L, Lin Y-C, Lin R-H, Wei C-F, Huang Y-C, Peng H-L, Huang H-C.** 2010. Effects of *galU* Mutation on *Pseudomonas syringae*-plant interactions. *Molecular Plant-Microbe Interactions* **23**:1184-1196.
295. **Fan J, Crooks C, Creissen G, Hill L, Fairhurst S, Doerner P, Lamb C.** 2011. *Pseudomonas sax* Genes Overcome Aliphatic Isothiocyanate-Mediated Non-Host Resistance in *Arabidopsis*. *Science* **331**:1185-1188.
296. **Mysore KS, Crasta OR, Tuori RP, Folkerts O, Swirsky PB, Martin GB.** 2002. Comprehensive transcript profiling of Pto- and Prf-mediated host defense responses to infection by *Pseudomonas syringae* pv. tomato. *The Plant Journal* **32**:299-315.

297. **Cunnac S, Chakravarthy S, Kvitko BH, Russell AB, Martin GB, Collmer A.** 2011. Genetic disassembly and combinatorial reassembly identify a minimal functional repertoire of type III effectors in *Pseudomonas syringae*. *Proceedings of the National Academy of Sciences* **108**:2975-2980.
298. **Mole B, Habibi S, Dangl JL, Grant SR.** 2010. Gluconate metabolism is required for virulence of the soft-rot pathogen *Pectobacterium carotovorum*. *Molecular Plant-Microbe Interactions* **23**:1335-1344.
299. **Li X, Lin H, Zhang W, Zou Y, Zhang J, Tang X, Zhou J-M.** 2005. Flagellin induces innate immunity in nonhost interactions that is suppressed by *Pseudomonas syringae* effectors. *Proceedings of the National Academy of Sciences of the United States of America* **102**:12990-12995.
300. **He P, Shan L, Lin N-C, Martin GB, Kemmerling B, Nürnberger T, Sheen J.** 2006. Specific Bacterial Suppressors of MAMP Signaling Upstream of MAPKKK in *Arabidopsis* Innate Immunity. *Cell* **125**:563-575.
301. **Filiatrault MJ, Stodghill PV, Wilson J, Butcher BG, Chen H, Myers CR, Cartinhour SW.** 2013. CrcZ and CrcX regulate carbon source utilization in *Pseudomonas syringae* pathovar tomato strain DC3000. *RNA Biology* **10**:245-255.
302. **Rico A, Preston GM.** 2008. *Pseudomonas syringae* pv. tomato DC3000 Uses Constitutive and Apoplast-Induced Nutrient Assimilation Pathways to Catabolize Nutrients That Are Abundant in the Tomato Apoplast. *Molecular Plant-Microbe Interactions* **21**:269-282.

303. **Takahashi Y, Berberich T, Yamashita K, Uehara Y, Miyazaki A, Kusano T.** 2004. Identification of tobacco *HIN1* and two closely related genes as spermine-responsive genes and their differential expression during the Tobacco mosaic virus -induced hypersensitive response and during leaf- and flower-senescence. *Plant Molecular Biology* **54**:613-622.
304. **Nguyen HP, Chakravarthy S, Velásquez AC, McLane HL, Zeng L, Nakayashiki H, Park D-H, Collmer A, Martin GB.** 2010. Methods to study PAMP-triggered immunity using tomato and *Nicotiana benthamiana*. *Molecular Plant-Microbe Interactions* **23**:991-999.
305. **Dong J, Chen C, Chen Z.** 2003. Expression profiles of the *Arabidopsis* WRKY gene superfamily during plant defense response. *Plant Molecular Biology* **51**:21-37.
306. **Romeis T, Piedras P, Jones JDG.** 2000. Resistance Gene-Dependent Activation of a Calcium-Dependent Protein Kinase in the Plant Defense Response. *The Plant Cell* **12**:803-815.
307. **Lorenzo O, Piqueras R, Sánchez-Serrano JJ, Solano R.** 2003. ETHYLENE RESPONSE FACTOR1 Integrates Signals from Ethylene and Jasmonate Pathways in Plant Defense. *The Plant Cell* **15**:165-178.
308. **Singh KB, Foley RC, Oñate-Sánchez L.** 2002. Transcription factors in plant defense and stress responses. *Current Opinion in Plant Biology* **5**:430-436.
309. **Zhang S, Klessig DF.** 2001. MAPK cascades in plant defense signaling. *Trends in Plant Science* **6**:520-527.

310. **Afzal AJ, Wood AJ, Lightfoot DA.** 2008. Plant receptor-like serine threonine kinases: roles in signaling and plant defense. *Molecular Plant-Microbe Interactions* **21**:507-517.
311. **Yu X, Lund SP, Greenwald JW, Records AH, Scott RA, Nettleton D, Lindow SE, Gross DC, Beattie GA.** 2014. Transcriptional analysis of the global regulatory networks active in *Pseudomonas syringae* during leaf colonization. *MBio* **5**:e01683-01614.
312. **Melotto M, Underwood W, He SY.** 2008. Role of Stomata in Plant Innate Immunity and Foliar Bacterial Diseases. *Annual review of phytopathology* **46**:101-122.
313. **Broekaert WF, Terras F, Cammue B, Osborn RW.** 1995. Plant defensins: novel antimicrobial peptides as components of the host defense system. *Plant physiology* **108**:1353.
314. **Nawrot R, Barylski J, Nowicki G, Broniarczyk J, Buchwald W, Goździcka-Józefiak A.** 2014. Plant antimicrobial peptides. *Folia microbiologica* **59**:181-196.
315. **Gunn JS.** 2001. Bacterial modification of LPS and resistance to antimicrobial peptides. *Journal of Endotoxin Research* **7**:57-62.
316. **Guo M, Tian F, Wamboldt Y, Alfano JR.** 2009. The majority of the type III effector inventory of *Pseudomonas syringae* pv. tomato DC3000 can suppress plant immunity. *Molecular Plant-Microbe Interactions* **22**:1069-1080.

317. **Galán JE, Zhou D.** 2000. Striking a balance: modulation of the actin cytoskeleton by *Salmonella*. Proceedings of the National Academy of Sciences **97**:8754-8761.
318. **Chen L-Q, Hou B-H, Lalonde S, Takanaga H, Hartung ML, Qu X-Q, Guo W-J, Kim J-G, Underwood W, Chaudhuri B, Chermak D, Antony G, White FF, Somerville SC, Mudgett MB, Frommer WB.** 2010. Sugar transporters for intercellular exchange and nutrition of pathogens. Nature **468**:527-532.
319. **Wang K, Senthil-Kumar M, Ryu C-M, Kang L, Mysore KS.** 2012. Phytosterols Play a Key Role in Plant Innate Immunity against Bacterial Pathogens by Regulating Nutrient Efflux into the Apoplast. Plant Physiology **158**:1789-1802.
320. **del Castillo T, Ramos JL, Rodriguez-Herva JJ, Fuhrer T, Sauer U, Duque E.** 2007. Convergent peripheral pathways catalyze initial glucose catabolism in *Pseudomonas putida*: genomic and flux analysis. J Bacteriol **189**:5142-5152.
321. **Schenk A, Weingart H, Ullrich MS.** 2008. Extraction of high-quality bacterial RNA from infected leaf tissue for bacterial in planta gene expression analysis by multiplexed fluorescent Northern hybridization. Molecular Plant Pathology **9**:227-235.
322. **Kawahara Y, Oono Y, Kanamori H, Matsumoto T, Itoh T, Minami E.** 2012. Simultaneous RNA-Seq Analysis of a Mixed Transcriptome of Rice and Blast Fungus Interaction. PLoS one **7**:e49423.

323. **Kim D, Pertea G, Trapnell C, Pimentel H, Kelley R, Salzberg S.** 2013. TopHat2: accurate alignment of transcriptomes in the presence of insertions, deletions and gene fusions. *Genome Biology* **14**.
324. **Trapnell C, Roberts A, Goff L, Pertea G, Kim D, Kelley DR, Pimentel H, Salzberg SL, Rinn JL, Pachter L.** 2012. Differential gene and transcript expression analysis of RNA-seq experiments with TopHat and Cufflinks. *Nature Protocols* **7**:562-578.
325. **Shin D, Lee EJ, Huang H, Groisman EA.** 2006. A positive feedback loop promotes transcription surge that jump-starts *Salmonella* virulence circuit. *Science* **314**:1607-1609.
326. **Park J, Gupta RS.** 2008. Adenosine kinase and ribokinase--the RK family of proteins. *Cell Molecular Life Sciences* **65**:2875-2896.
327. **Parducci RE, Cabrera R, Baez M, Guixe V.** 2006. Evidence for a catalytic Mg²⁺ ion and effect of phosphate on the activity of *Escherichia coli* phosphofructokinase-2: regulatory properties of a ribokinase family member. *Biochemistry* **45**:9291-9299.
328. **He H, Bleby TM, Veneklaas EJ, Lambers H, Kuo J.** 2012. Precipitation of calcium, magnesium, strontium and barium in tissues of four *Acacia* species (*Leguminosae: Mimosoideae*). *PLoS one* **7**:e41563.
329. **Ingolia NT.** 2016. Ribosome footprint profiling of translation throughout the genome. *Cell* **165**:22-33.
330. **Hsu PY, Calviello L, Wu H-YL, Li F-W, Rothfels CJ, Ohler U, Benfey PN.** 2016. Super-resolution ribosome profiling reveals unannotated

translation events in *Arabidopsis*. Proceedings of the National Academy of Sciences **113**:E7126-E7135.

331. **Ederth J, Mandava CS, Dasgupta S, Sanyal S.** 2009. A single-step method for purification of active His-tagged ribosomes from a genetically engineered *Escherichia coli*. Nucleic Acids Research **37**:e15-e15.